

**Selective Catalytic Reduction of NO_x by Hydrocarbons
over Fe/ZSM5 Prepared by Sublimation of FeCl₃**

Characterization and Catalysis

**Selective Catalytic Reduction of NO_x by Hydrocarbons
over Fe/ZSM5 Prepared by Sublimation of FeCl₃**

Characterization and Catalysis

Selectieve Katalytische Reductie van NO_x door Koolwaterstoffen
over Fe/ZSM5 Bereid door Sublimatie van FeCl₃

Karakterisering en Katalyse

(met een samenvatting in het Nederlands)

Proefschrift

ter verkrijging van de graad van doctor aan de Universiteit Utrecht op gezag van de Rector
Magnificus, Prof. Dr. W. H. Gispen, ingevolge het besluit van het College voor Promoties in
het openbaar te verdedigen op woensdag 12 februari 2003 des middags te 12:45 uur
door

Andrea Antonio Battiston

geboren op 13 november 1970, te Milaan, Italië

Promotor: Prof. Dr. Ir. D. C. Koningsberger

Co-promotor: Dr. J. H. Bitter

Verbonden aan de Sectie Anorganische Chemie en Katalyse, Debye Instituut, Faculteit Scheikunde, Universiteit Utrecht

Het in dit proefschrift beschreven onderzoek werd mede mogelijk gemaakt met financiële steun van de Nederlandse Organisatie voor Wetenschappelijk Onderzoek (NWO)

ISBN 90-393-3239-8

Cover lay-out by Jan den Boesterd, Ingrid van Rooijen en Aloys Lurvink, AV-dienst, Faculteit Scheikunde, Universiteit Utrecht

Drukkerij Ponsen & Looijen bv, Wageningen

For you, dear mum and dad

Contents

<i>Chapter 1</i>	Introduction	1
<i>Chapter 2</i>	Evolution of the Fe-Species During the Synthesis of Over-Exchanged Fe/ZSM5, Prepared by Sublimation of FeCl ₃	17
<i>Chapter 3</i>	Reactivity of the Fe-Binuclear Complexes in Over-Exchanged Fe/ZSM5, Studied by <i>In situ</i> XAFS Spectroscopy: Heat Treatment in He and O ₂	61
<i>Chapter 4</i>	Reactivity of the Fe-Binuclear Complexes in Over-Exchanged Fe/ZSM5, Studied by <i>In situ</i> XAFS Spectroscopy: Selective Catalytic Reduction of NO with Isobutane	97
<i>Chapter 5</i>	Accessibility of the Fe-Species in Over-Exchanged Fe/ZSM5, Prepared by Sublimation of FeCl ₃	131
<i>Chapter 6</i>	Combining Pt/ZSM5 and Over-Exchanged Fe/ZSM5 for the Selective Catalytic Reduction of NO _x by Hydrocarbons: a Dual-bed Configuration	149
<i>Chapter 7</i>	Summary	175
	Samenvatting	179
	List of Publications and Presentations	183
	Acknowledgements	187
	<i>Curriculum Vitae</i>	191

Introduction

Air pollution

Air pollution is the most important environmental problem for human health. This was recently confirmed in 1999 by the consolidation of 39 regional, state and local comparative risk analysis studies (1).

There are many forms of air pollution, but the most dangerous are:

1. Particles (smoke, soot)
2. Sulfur dioxide
3. Ozone (O₃)
4. Lead
5. Nitrogen oxides (NO and NO₂, lumped together as NO_x).

Particles and Sulfur dioxide

The presence of particles in highly populated areas is mostly due to motor vehicle engines, power stations and industry, SO₂ being one of the most important sources. Depending on their dimension, particles can cause irritation to the bronchi and seriously affect the function of the lungs. The most dangerous particles are those with an average dimension smaller than 2.5 μm (PM_{2.5}), since they can force their way into the very part of the lungs where oxygen is absorbed.

The concentration of particles in urban areas of the most developed countries has fallen dramatically in the last decades (1). This result has been achieved by reducing consumption of high-sulfur coal, by limiting the sulfur content in diesel oil, by using smoke scrubbing equipments and, in general, by increasing energy efficiency.

Besides being responsible for the formation of particles, SO₂ is converted in the atmosphere to sulfuric acid (H₂SO₄). This is one of the main causes for the phenomenon of acid rain, responsible of damaging forests and of the corrosion of metallic structures, buildings and cultural objects.

SO₂ emissions in the United States and in the European Union have been declining steadily since 1980, as a result of agreements signed in Helsinki (1979) in the Long-Range Transboundary Air Pollution convention. In the U.S. new regulations were introduced by the Clean Air Act Amendment in 1990, cutting emissions from power plants by about 50 percent. Statistics from the U.K. and the U.S. show a decline of almost 80% in the SO₂ average daily intake of the population from 1960 to 1997 (1).

Ozone

Ozone is generated by a complex interplay between NO_x and hydrocarbons. Close to the earth ozone is harmful to humans and affects plant growth. Together with NO_x it is one of the major players in the formation of brown (photochemical) smog. The most evident effect of ozone is irritation of the respiratory organs. Also for ozone a decreasing concentration has been measured in the last decade in the urban areas of the European Union and of the United States (1).

Lead

Lead is extremely toxic. High concentrations of lead in the bloodstream can cause cramps, coma and death. Even very small concentrations of lead can be extremely dangerous for unborn children, resulting in a rise of miscarriages and birth of retarded children. Lead also reduces men's fertility and can cause hypertension (2).

Around 90 percent of lead emissions come from lead added to petrol. The U.S. eliminated lead from petrol, starting in 1973 and completing the task in 1986. All U.S. gasoline is since then unleaded. In 2001 more than 75 percent of gasoline consumed in the U.K. was unleaded as well. The results of the imposed regulations have been a decrease of lead of 85 percent in U.K. air and of 97 percent in the U.S. air in the period 1977-1999. Over the same period the lead content measured in the blood of U.S. citizens has decreased, on average from 14.5 to 2.8 µg/dl (1).

Nitrogen oxides

Nitrogen oxides (NO and NO₂) are generated primarily from motor vehicles and stationary sources like power stations and industrial heaters. They contribute to acid rain and, together with ozone, they form the main component of brown smog. NO_x can cause respiratory problems and lung infections in children and other vulnerable groups, such as asthmatics. They can also work as overfertilizers, causing algae to flourish. In late summer this can increase the risk of oxygen depletion and fish death (1).

In contrast to the well-established dramatic diminution realized for lead, SO₂ and particles concentrations the decrease in concentration of NO and NO₂ has been less important. In Fig. 1 the annual average NO₂ concentration in the U.S. and in central London from 1976 to 1998 is depicted (3,4).

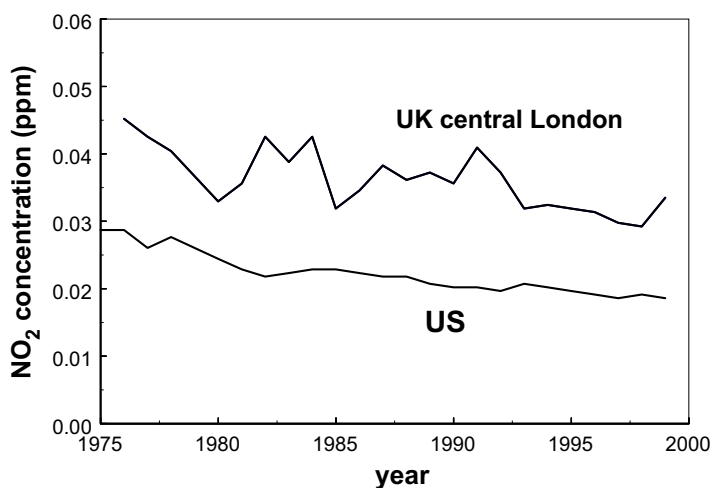


Figure 1: Annual average NO₂ concentration in the US and in central London (3,4).

While nation-wide data from the U.S. show a clear diminishing trend in NO₂ concentration, data from an extremely dense populated as London appear to be less comforting.

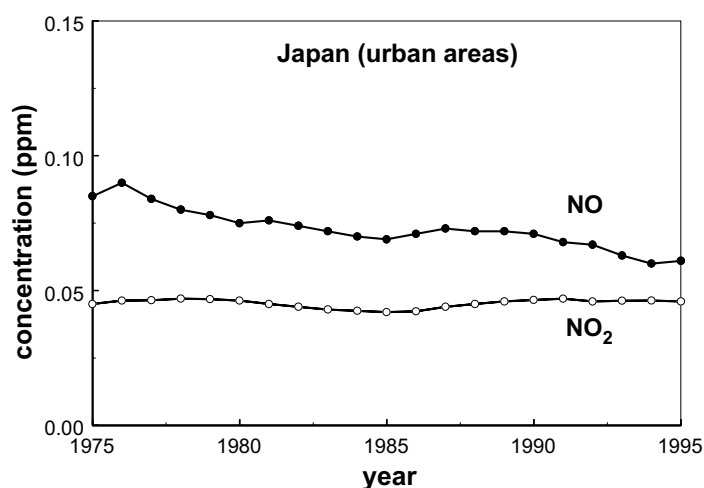


Figure 2: Annual average concentration of NO and NO₂ in Japan (urban areas) (5).

Figure 2 (5) shows annual changes in the concentration of NO and NO₂ in Japan, measured from 1975 to 1995 by road-side monitoring stations in urban areas.

While a decrease is visible in the atmospheric levels of NO, the concentration of NO₂, mostly generated by reaction of NO in the atmosphere with oxygen and ozone, appears to be stable. Data obtained nation-wide from Spain and Germany account for an average decrease of NO₂ in the last 10-15 years of approximately 15-20 percent (1).

Thermodynamic stability of nitrogen oxides

The conversion of NO₂ to NO and O₂ is thermodynamically highly favored at high temperature and kinetically relatively easy (6). For this reason, NO accounts for the majority (>90%) of the NO_x emissions from combustion sources.

From a thermodynamic point of view also NO is unstable, the decomposition to N₂ and O₂ being favored up to 1000°C. Nevertheless, due to its high energy of dissociation (364 kJ/mol, (6)), NO is kinetically stable. Therefore, conversion of NO to N₂ requires the use of a catalyst and, preferably, of an appropriate reductant. Compared to direct decomposition, reduction of NO displays significantly lower Gibbs free energy values (7), further reduced by the presence of oxygen.

These observations have been used to design technologies for treating NO_x-containing exhausts. Catalytic Techniques that make use of additional reductants for the conversion of NO_x to N₂ in the presence of excess oxygen are usually denoted as Selective Catalytic Reducing (SCR) techniques. The term selective refers to the ability of the reductants to selectively react with oxygen from the NO_x, instead of being oxidized by molecular oxygen (O₂) present in the feed.

Selective catalytic reduction of NO from stationary sources: NH₃-SCR

Among flue gas treatment methods, the Selective Catalytic Reduction using NH₃ is best developed and used world-wide for the control of NO_x emissions in fuel combustion (8). In addition to the most common applications in coal-, oil-, and gas-fired power stations and industrial heaters, NH₃-SCR is widely applied to industrial and municipal waste incinerators, chemical plants, and in the glass, steel and cement industries. The success of this technique is due to its efficiency (9-11). Nevertheless, due to the potential risk related to the transport of ammonia, NH₃-SCR is applied only for the treatment of exhaust gases from stationary sources.

The NH₃-SCR process is based on the following reactions:





In particular reaction [1] occurs very rapidly on the catalyst in the temperature range 250-450°C and accounts for the overall stoichiometry of the process ($\text{NH}_3/\text{NO}=1$).

Three main classes of catalysts have been developed for NH_3 -SCR systems: supported noble metals, metal oxides and zeolites.

Noble metals are very active in the selective reduction of NO_x but they present the major drawback of NH_3 direct oxidation. For this reason they have soon been replaced by metal oxide catalysts and are now considered for low temperature and natural gas applications (12).

Among the various investigated metal oxide mixtures those based on vanadia supported on titania, and promoted with tungsta or molybdena present great advantages, not only due to their high activity and selectivity but also because of their resistance towards poisoning by SO_2 (13-18). They are used in conventional NH_3 -SCR applications between 300°C and 400°C. V_2O_5 based catalysts with high vanadia loading have also been proposed for natural gas applications at low temperature.

Zeolite catalysts in the acidic form with transition metal ions (*e.g.* iron) are potential candidates for applications at high temperature (up to a maximum of 600°C (8)), prohibitive for metal oxides.

Catalytic treatment of exhausts from automotive sources

Since the original clear air act of the 1970s, the application of catalyst technologies have led to substantial improvements in reducing the engine out and the tailpipe emissions. At the moment over 700 millions passenger cars and trucks are used, with an annual worldwide production of new cars approaching 60 millions/year (19). Vehicles make use of a spark ignited gasoline or a diesel engine. The majority of these vehicles in the most developed countries are provided with catalytic systems for the abatement of the most dangerous emissions.

Spark ignited gasoline engines

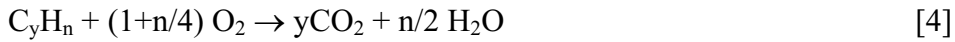
Typical exhaust gas composition from a spark ignited gasoline engine at normal operating conditions is (19):

- Carbon monoxide (CO , 0.5 vol%)
- Unburned hydrocarbons (HC , 350 vppm)
- Nitrogen oxides (NO_x , 900 vppm)
- Hydrogen (H_2 , 0.17 vol%)

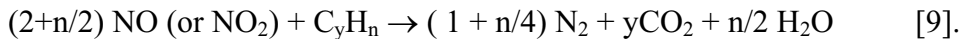
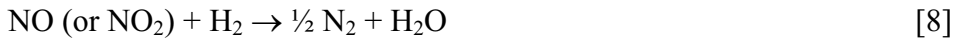
- Water (H₂O, 10 vol%)
- Carbon dioxide (CO₂, 10 vol%)
- Oxygen (O₂, 0.5 vol%).

By catalytically treating the gas exhaust, oxidative and reductive reactions are made possible, resulting in the contemporary decrease in the emission of CO, HC and NO_x.

The oxidation reactions are:



The reduction reaction are:



Typically, at increasing temperatures (the light off temperature depends on the catalyst applied) reactions of CO begin, followed by those of HC and NO_x. When all the three reactions occur, the term three way catalyst (TWC) is used. The typical response of a TWC catalyst as a function of the air-to-fuel ratio of the engine feed is shown in Fig. 3.

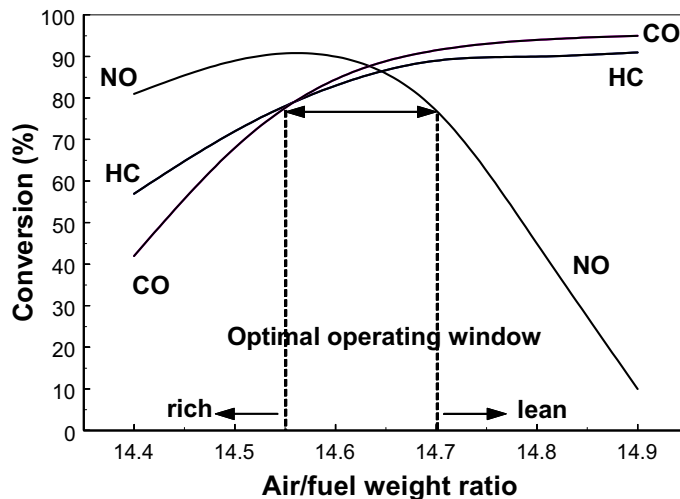


Figure 3: Influence of the air/fuel ratio of the engine feed on the performance of a TWC catalyst (lean conditions: stoichiometric excess of O₂; rich conditions: stoichiometric defect of O₂).

Oxidation of hydrocarbons and CO is highly favoured in the presence of excess oxygen (lean conditions). This condition is fulfilled when feeding the engine with an air/fuel ratio exceeding the stoichiometric value of 14.6 wgt/wgt. Below this value (rich conditions), conversion of NO to N₂ are favored, whereas the oxidation reactions are strongly inhibited. As can be seen in the figure, in order to balance oxidation and reduction reactions, the air to fuel ratio supplied to the engine has to be strictly confined between an optimal operating window. This is obtained by a computer-controlled feedback, activated by a zirconia-based electrochemical O₂ sensor. During fuel rich/lean perturbations a temporary compensation can be provided by the catalyst itself by alternatively storing and releasing oxygen. This function is obtained by adding to the catalyst combinations of CeO₂ and ZrO₂ (20). Composition of the TWC catalyst and supporting technology have widely changed in the last years. Modern three way catalysts make use of precious metals. They can exist in combination. They primarily consist of Pt and Rh combinations or only Pd, deposited on high surface area alumina. In each case, proprietary base-metal oxides are used to promote the activity and the stability of the catalyst. A complete overview on the subject can be found in Ref. (21).

(Direct injection) lean-burn gasoline engines

Operating an engine under lean burn conditions (stoichiometric excess of oxygen) is very attractive, primarily for fuel-efficiency reasons. Nevertheless, as shown in Fig. 3, the TWC catalyst is not effective in reducing NO_x under such conditions. The most promising solution appears to be so called TWC/TRAP catalytic system (19). This system requires that the engine is operated alternatively under fuel lean and rich conditions. In this system an alkaline metal oxide trap is used in order to adsorb the NO_x during lean-burn operation (22-24). This operation mode can be maintained during steady state driving, leading to an improved fuel economy up to 15-20% when compared to continuous stoichiometric operation. In order to be adsorbed, NO must first be converted to NO₂ over Pt during the lean burn operation of the catalyst:



At temperatures above 500°C NO₂ is not thermodynamically favored. Nevertheless, the equilibrium of [10] is shifted towards NO₂ by its adsorption on the alkaline trap (BaO or K₂CO₃), incorporated in the precious metal washcoat of the TWC:



The engine is operated in the fuel economy mode for around 60 seconds, after which a fuel rich mode is commanded. Under these conditions, NO_2 desorbed from the trap will be reduced by the TWC catalyst and the trap will be regenerated. In order to prevent deactivation of the trap by SO_x poisoning, the sulfur content of the gasoline should be less than 10 ppm.

The operation of a TWC/TRAP system is shown in Fig. 4.

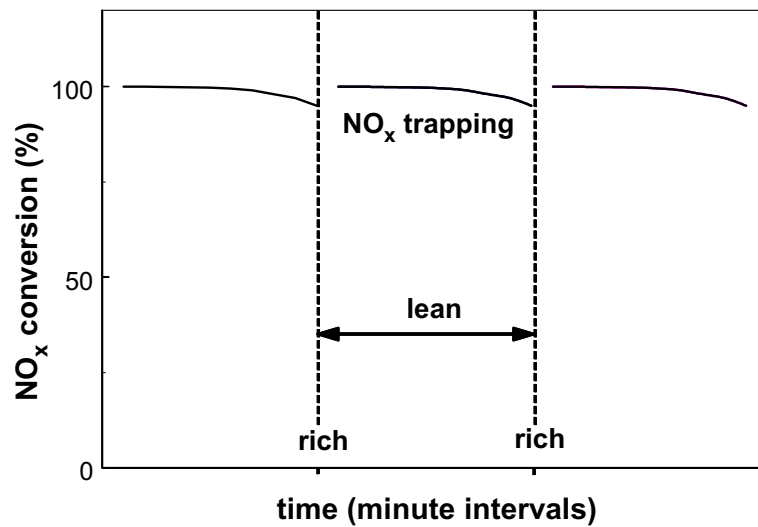


Figure 4: NO_x trapping for gasoline engines (TWC/TRAP system).

Diesel engines

When compared to spark ignited gasoline engines, diesel engines allow economy of operation and a decrease in CO_2 emissions. Therefore, the number of diesel vehicles is expected to increase dramatically in the next years (19).

In a diesel engine, the fuel is injected in a highly compressed charge of air, where the sufficiently high temperature allows its combustion. Since the engine is typically operated under continuous lean-burn conditions (excess of oxygen), the temperature of the exhausts is lower than in the gasoline counterpart.

Diesel emissions typically consist of soot, liquid sulfates, liquid unburned fuel and lubricating oil (collectively, SOF), gaseous hydrocarbons (HC), carbon monoxide (CO) and nitrogen oxides (NO_x). Reduction of NO_x in the presence of excess oxygen with the present

technology is not possible, therefore the role of the catalyst is limited to the oxidation of SOF, HC and CO. Contemporarily it should be able to minimize oxidation of SO₂ to SO₃ (H₂SO₄).

Catalytic metals such as Pt and Pd were considered early due to their low temperature oxidation properties. However, they are also very active for the SO₂ oxidation reaction. The most successful approach is the use of a monolithic catalyst, composed of high surface area bulk CeO₂ in combination with γ -Al₂O₃. This catalyst combines high conversion of SOF (a somewhat lower oxidation of HC and CO) with very little formation of SO₃ (25).

Such Diesel oxidation catalysts are now commonly used for medium to heavy-duty trucks in the US (26), Japan (27), and Europe (28). For a cooler running passenger car a higher metal loaded catalyst is still preferred (19).

Fuel cells

Fuel cells hold promise as an alternative to hydrocarbons combustion for power generation in stationary and mobile sources in the future. They are about twice as fuel efficient as the internal combustion engine and do not produce pollution (CO, HC or NO_x) (19). These goals can be achieved by directly converting chemical energy into electrical energy, avoiding the mechanical steps and thermodynamic limitations of combustion energy cycles. Hydrogen gas is electrocatalytically oxidized to hydrogen ions at the anode of the cell. The ions pass through an electrolyte to the cathode (29), where they combine with electrocatalytically reduced O₂ (obtained from the air), producing H₂O. The electrons flow in the external circuit and do work.

Although storage on board of H₂ would be the preferred solution, still significant technological breakthroughs are needed. Furthermore, there is no infrastructure yet for obtaining hydrogen at the local gas station or at home. A different approach would be to reform liquid fuels such as gasoline to H₂ continuously on board (30). Several studies are now directed also to the use of methanol (19).

Daimler Chrysler executives estimate the current fuel cell costs about 30000 US\$. According to the same source, in order to obtain a competitive system, the price should be reduced to about 3000 US\$ (31).

Selective Catalytic Reduction of NO_x using hydrocarbons (HC-SCR)

The solutions applied at the moment for the removal of nitrogen oxides present significant drawbacks. Drawbacks related to the widespread removal of NO_x from stationary sources using ammonia (NH₃-SCR) are the still considerably high costs of operation, problems

related to the transport and storage of anhydrous ammonia, slips of unreacted ammonia to the atmosphere and possible plugging by ammonium-sulfates (32).

However, more significant problems are related to the treatment of exhaust from mobile sources. As already discussed, the reduction of NO_x by the three way catalysts (spark ignited engines) can not be accomplished under lean-burn conditions. This is paid in terms of energy efficiency by the use of additional gasoline. Catalysts systems for diesel engines, on the other hand, which have to reduce pollution emissions from lean-burn streams, are not able to accomplish reduction of NO_x to N_2 and are designed for the solely oxidation of SOF, HC and CO.

Besides using N-containing reductants, the reduction of the NO_x content under lean burn conditions can be accomplished by using hydrocarbons as “selective” reducing agents. On adequate catalysts, hydrocarbons preferentially react with the nitrogen oxides rather than with oxygen. This process is the so-called HydroCarbon Selective Catalytic Reduction (HC-SCR) of nitrogen oxides. HC-SCR therefore represents a promising cleaning alternative.

Hydrocarbons are usually not available in sufficient quantities in the exhaust stream to allow a complete reduction of the nitrogen oxides. A solution would be an additional feed. In their absence, the cheapest and simplest method would be the direct decomposition of NO into N_2 and O_2 . Therefore, the finding of Iwamoto and coworkers that decomposition of NO_x takes place at an appreciable rate over Cu-exchanged zeolites, in particular over Cu/ZSM5 (33,34), caused considerable scientific and industrial interest in the 80's. However, tests under more realistic conditions (NO_x concentration of around 1000 ppm, 5% O_2 and an adequate gas space velocity) showed only little NO conversion (35). In addition, water and sulfur dioxide, omnipresent in diesel exhausts gases, were found to poison the catalyst (36). For these reasons there it is general belief that Cu/ZSM5 and, more in general, direct decomposition of NO_x in the presence of excess oxygen will fail in offer practical applications. Nevertheless, Cu/ZSM5 showed increased activity in the reduction of NO_x under lean-burn conditions when hydrocarbons were added to the feed (37-40). This finding opened the way to an impressive number of scientific studies, devoted to the development of active and stable HC-SCR catalysts. The most interesting results have been obtained sofar over noble- and transition-metal loaded zeolites, in particular with Pt, Co and Fe. A comprehensive review on the subject can be found in the work of Y. Traa *et al.* (41).

At first glance, platinum-containing zeolite, in particular Pt/ZSM5, seem to be promising catalysts. On this material small paraffins are less reactive than olefins, ethylene and propene being the most active NO_x reductants. Pt/ZSM5 shows considerable activity at low temperature (200-300°C, depending on the reactant applied). Anyhow, it possesses deficits

as well. Firstly, the deactivation problem, although not as serious as with Cu/ZSM5, has not been overcome (42). Secondly, it shows a low selectivity towards N_2 . Indeed, N_2O is formed in comparable amounts during HC-SCR operation (43-47). This represents a major problem since N_2O is a strong greenhouse gas and contributes to stratospheric ozone destruction.

The unique feature of cobalt-containing zeolites, in particular Co/ZSM5 and Co/beta, is their ability to reduce NO_x with methane (41,48,49). Since methane is inexpensive and readily available, its use is highly desired. However, the reaction temperature necessary to activate methane is by far too high for treating mobile exhaust gases (application could be possible for engines powered by natural gas). Main drawback for Co-zeolites are the low activity and especially their sensitivity towards water and sulfur dioxide (41).

Fe/ZSM5

Until 1996 little attention was paid to the HC-SCR properties of iron-loaded zeolites. Nevertheless, the situation changed rapidly upon two publications by Feng and Hall (50,51), reporting on the exceptional activity and stability of Fe/ZSM5 towards the selective catalytic reduction of NO by isobutane. A N_2 yield of nearly 100% could be obtained in the temperature range 400-500°C at the relatively high gas hourly space velocity of 42000 h^{-1} . This high NO conversion could be maintained for 2500 hours even upon injection of 20 vol.% H_2O and 150 vppm of SO_2 . The catalyst was prepared by ion-exchange in aqueous solution from FeC_2O_4 (ferrous oxalate), the exchange procedure being performed under exclusion of air. By this method an extremely high iron exchange could be obtained ($n_{Fe}/n_{Al}=0.90$), contemporarily avoiding formation of catalytically inactive Fe_2O_3 clusters. Unfortunately, the authors failed in reproducing their result, which could be obtained from a single batch of commercial ZSM5 (Si/Al molar ratio = 19). The reason was ascribed to the difficulty in preventing precipitation of ferrous oxalate and bulky iron hydroxide complexes in the pores of the zeolite (52,53). Upon washing and calcination, iron was mainly present as Fe-oxide clusters.

An important breakthrough was obtained in 1998 by Chen and Sachtler. Upon failing to reproduce an active catalyst by the Fe-oxalate technique, they proposed a different synthesis procedure, consisting in subliming $FeCl_3$ into the cavities of an acidic H/ZSM5 support. Over the as-obtained Fe/ZSM5, at reaction conditions identical to those adopted by Feng and Hall, a NO conversion of approximately 75% could be obtained in the temperature range 350-400°C, with a complete selectivity towards N_2 (54,55). Similar performances could be achieved when using n-butane or propane as reductant (56). In the presence of 10 vol% of water the activity of the catalyst appeared to be almost unaffected.

Differently from the results of Feng and Hall, a decrease in the activity of approximately 10% was detected upon 100 h on stream. This deactivation was reversible: initial activity could be restored by treatment with 10 vol% of O₂ in He at 500°C for 2h.

Fe/ZSM5 obtained by the FeCl₃ CVD technique has recently been demonstrated to be also extremely active in the direct decomposition of N₂O (57).

A typical result of the sublimation and chemical vapor deposition (CVD) of FeCl₃ in the pores of H/ZSM5 is that a complete exchange of Fe for the acidic Brønsted sites can be obtained. In the Si/Al range of 15-20 a n_{Fe}/n_{Al} of 1.0 is achieved, this result being highly reproducible, thanks to the simplicity of the technique.

The nature of the active phase is Fe/ZSM5 obtained by CVD is currently under debate in the literature. Although no conclusive evidence has been found yet, most of the studies assign the outstanding properties of this catalyst to the presence of binuclear Fe-oxo/hydroxo complexes, anchored at the ion exchange positions of the zeolite. The suggestion that the active phase consists of binuclear Fe-oxo/hydroxo complexes is based on results obtained by H₂/ and CO-Temperature Programmed Reduction, Fourier Transform-Infrared Spectroscopy, Electron Spin Resonance and Isotopic Exchange with ¹⁸O₂ (54,55,57-59). The binuclear Fe-complexes are believed to be responsible for both the decomposition of N₂O (57) and the selective reduction of NO by hydrocarbons in the presence of excess oxygen (54,55,58).

Scope and structure of this thesis

At the moment, Fe/ZSM5 obtained by chemical vapor deposition of FeCl₃ represents one of the most promising catalyst for the selective catalytic reduction (SCR) of NO_x and for the decomposition of N₂O. Although the outstanding catalytic properties of this material are well established, several questions remain unanswered. These questions concern mainly the influence of the different synthesis steps on the evolution of the Fe-species, the nature, the structure and the reactivity of the resulting Fe active phase, and its accessibility for the reactants during catalysis.

In **Chapter 2** the evolution of Fe/ZSM5 (Si/Al=17) prepared via chemical vapor deposition of FeCl₃ is studied at each stage of the synthesis, *i.e.* introduction of iron via sublimation of FeCl₃, washing and calcination. The influence of calcination is monitored upon application of two different procedures. The first one, denoted as “severe calcination”, corresponds to the one described in the work of most of other researchers. The second one, “mild calcination”, is introduced in order to suppress agglomeration phenomena occurring to iron, and resulting in the formation of catalytically inactive Fe-oxidic particles. By doing so, it was possible to obtain a material in which the concentration of spectators (Fe inactive

phase) was minimized. The presence of a large amount of spectators would make impossible to study the catalytically active sites. Characterization has been performed by using the widest possible range of significative techniques. The evolution of the ZSM5 support has been studied by combining N₂ physisorption, X-ray Diffraction (XRD), Fourier Transform-Infrared Spectroscopy (FT-IR), ²⁷Al Nuclear Magnetic Resonance (²⁷Al NMR) and Al K-edge X-ray Absorption Spectroscopy (Al XAS). Fe species have been studied using Extended X-Ray Absorption Fine Structure Spectroscopy (EXAFS), High Resolution X-Ray Absorption Near Edge Spectroscopy (HR-XANES), ⁵⁷Fe Mössbauer spectroscopy, Electron Energy Loss Spectroscopy (EELS) and High Resolution Transmission Electron Microscopy (HR-TEM).

In **Chapter 3** the structure of the iron species in mildly calcined Fe/ZSM5 (see Chapter 2) has been studied during heat treatments in He and in the presence of oxygen. This study has been performed by coupling *in situ* Fe K-edge HR-XANES and EXAFS. From the information obtained a model is proposed for the structure of the Fe active phase and for the reactivity of oxygen (auto-reduction of Fe) in different temperature ranges.

Chapter 4 represents the continuation of the *in situ* EXAFS study presented in Chapter 3. The aim of the investigation presented in this chapter is to determine the active coordination-sites in Fe/ZSM5 for the HC-SCR reaction of NO. The local environment of iron has been studied *in situ* during reaction with typical HC-SCR reactants (NO, i-C₄H₁₀, O₂), fed separately or in combination. The catalytic activity of Fe/ZSM5 for the decomposition of NO, the oxidation of NO to NO₂ and for the selective catalytic reduction of NO with isobutane has been monitored (via chemiluminescence analysis of the gas outlet) during the collection of the XAFS data.

In **Chapter 5** the accessibility of the iron species in Fe/ZSM5 has been studied using a Tapered Element oscillating Microbalance (TEOM). Uptake measurements using n-hexane as probe molecule have been performed over ZSM5 prior to and after loading iron (via the FeCl₃ CVD technique). The effect of the calcination procedure on the accessibility of the Fe species has also been investigated by comparing the uptake of n-hexane on a mildly and a severely calcined Fe/ZSM5 sample. The catalytic activity of the two samples has been tested towards the SCR of NO with isobutane. The results obtained are discussed on the basis of the characterization study presented in Chapter 2.

In **Chapter 6** a dual-bed catalytic system for the SCR of NO is studied. The aim is to couple the catalytic properties of two different catalysts, *i.e.* Fe/ZSM5, obtained through the FeCl₃ CVD technique, and Pt/ZSM5, obtained via liquid ion exchange from Pt(NH₃)₄(NO₃)₂. Pt/ZSM5 is an active material for HC-SCR. Compared to Fe/ZSM5, it has the advantage of being able to operate at a lower temperature (225-300°C) and that no CO

is produced. Nevertheless, it displays a low selectivity towards N_2 . Large amounts of N_2O are formed together with N_2 during the HC-SCR. Fe/ZSM5 (positioned in a subsequent bed, operated at a higher temperature) has been used to convert the N_2O formed by the Pt/ZSM5 to harmless N_2 . It will be shown that, depending on the amount of hydrocarbons present, this conversion can occur on Fe/ZSM5 via the direct catalytic decomposition of N_2O and/or via the selective reduction of N_2O by the hydrocarbons (de N_2O). With this respect, the influence of an extra injection of isobutane between the Pt/ZSM5 and the Fe/ZSM5 bed has also been explored.

Reference list

1. Lomborg B., "The Skeptical Environmentalist", Cambridge University Press, Cambridge, U.K., (2001), and references therein.
2. Chiras, D.D., "Environmental Science: A Systems Approach to Sustainable Development", Wadsworth Publishing Company, Belmont, CA, (1998).
3. The UK National Air Quality Information Archive, <http://www.aeat.co.uk/netcen/airqual/>.
4. National Air Quality and Emissions Trends Report 1996. US Environmental Protection Agency. EPA Document Number EPA-820-F-97-002.
5. Misono, M., *Cattech* June, 53 (1998).
6. Fritz, A., Pitchon, V., *Appl. Catal. B* **13**, 1 (1997).
7. Pârvulescu, V.I., Grange, P., Delmon, B., *Catal. Today* **46**, 233 (1998).
8. Forzatti, P., *Appl. Catal. A* **222**, 221 (2001).
9. Bosch, H., and Janssen, F., *Catal. Today* **2**, 369 (1988).
10. Nakajima, F., Hamada, I., *Catal. Today* **29**, 109 (1996).
11. Matsuda, S., Kamo, T., Kato, A., and Nakajima F., *Ind. Eng. Chem. Prod. Res. Develop.* **21**, 48 (1982).
12. Pereira, C.J., Plumlee, K.W., and Evans, M., in: Proceedings of the 2nd International Symposium on Turbomachinery, Combined Cycle Technologies and Cogeneration, Vol.3, IGTI, p. 131, Serovy, G.K., and Fransson T.H. editions.
13. Kartte, K., and Nonnenmaker, H., US Patent 3,279,884 (1966).
14. Kunichi, M., Sakurada, H., Onuma, K., and Fujii, S., Ger. Offen. 2,443,262 (1975).
15. Nakajima, F., Tacheuci, M., Matsuda, S., Uno, S., Moti, T., Watanabe Y., and Inamuri M., US Patent 4,085,193 (1978).
16. Amiridis, M.D., Duevel, R.V., and Wachs, I.E., *Appl. Catal. B* **20**, 111 (2001).
17. Lietti, L., Forzatti, P., and Bregani F., *Ind. Eng. Chem. Res.* **35** (11) 3884 (1996).

18. Lietti, L., Nova, G., Ramis, L., Dall'Acqua, L., Busca, G., Giamello, E., Forzatti, P., and Gregani, F., *J. Catal.* **187**, 419 (1999).
19. Heck, R.M., and Farrauto, R.J., *Appl. Catal. A* **221**, 443 (2001).
20. Heck, R.M., and Farrauto, R.J., *Catal. Today* **55**, 179 (2000).
21. Heck, R.M., and Farrauto, R.J. "Catalytic Air Pollution Control: Commercial Technology, Van Nostrand Reinhold, New York, (1995).
22. Nishizawa, K., Momoshima, S., Koga, M., Tsuchida, H., and Yamamoto, S., SAE 2000-01-0890 (2000).
23. Miyoshi, M., Matsumoto, S., Katoh, K., Tanaka, T., Harada, J., Takahashi, N., Yokato, K., Sigiura, M., and Kasahara, K., SAE 950809 (1995).
24. Hodjati, S., Vaezzadeh, K., Petit, C., Pitchon, V., and Kiennemann, A., *Catal. Today* **59**, 323 (2000).
25. Farrauto, R.J., Voss, K.E., *Appl. Catal. B* **10 (1-3)**, 29 (1996).
26. Clerc, J., *Appl. Catal. B* **10 (1-3)**, 99 (1996).
27. Hosoya, M., and Shimoda, M., *Appl. Catal. B* **10 (1-3)**, 83 (1996).
28. Stein, H., *Appl. Catal. B* **10 (1-3)**, 69 (1996).
29. Voss, D., *Science* **285**, 683 (1999).
30. Farrauto, R.J., C.R. Acad. Sci. Paris, Serie IIc Chim./chem. **3**, 573 (2000).
31. *New York Times*, 2 April 1999.
32. Shelef, M., *Chem. Rev.* **95**, 209 (1995).
33. Iwamoto, M., Yokoo, S., Sakai, S., and Kagawa, S., *J. Chem. Soc., Faraday Trans. 1* **1** 1629 (1981).
34. Iwamoto, M., Furukawa, H., Mine, Y., Uemura, F., Mikurija, S., and Kagawa, S., *J. Chem. Soc., Chem. Commun.* **94** 6145 (1981).
35. Truex, T.J., Searles, R.A., and Sun, D.C. *Platinum Met. Rev.* **36**, 2 (1992).
36. Gilot, P., Guyon, M., and Stanmore, B.R., *Fuel* **76** 507 (1997).
37. Held, W., König, A., Richter, T., and Puppe, L., SAE Trans., Section 4 No. 900496, 209 (1990).
38. Held, W., and König, A, German Patent Application3642018, assigned to Volkswagen AG, (1987).
39. Iwamoto, M., Yahiro, H., Yu-u, Y., Shundo, S., Mizuno, N., *Shokubai* **32**, 430 (1990).
40. Ritscher, J.S., and Sandner, M.R., US Patent 4297328, assigned to Union Carbide Corporation, (1981).
41. Traa, Y., Burger, B., and Weitkamp, J., *Micropor. Macropor. Mater.* **30**, 3 (1999).
42. Kharas, K.C.C., Robota, H.J., Liu, D.-J., and Datye, A.K., *Prepr. Am. Chem. Soc. Div. Fuel Chem.* **40**, 1668 (1995).

43. Obuchi, A., Ohi, A., Nakamura, M., Ogata, A., Mizuno, K., and Ohuchi, H., *Appl. Catal. B* **2**, 71 (1993).
44. Iwamoto, M., Yahiro, H., Shin, H.K., Watanabe, M., Guo, J., Konno, M., Chikahisa, T., and Murayama T., *Appl. Catal. B* **5** L1-L5 (1994).
45. Captain, D.K., Roberts, K.L., Amiridis, M.D., *Catal. Today* **42**, 93, (1998).
46. Xin, M., Hwang, I.C., and Woo, S.I., *Catal. Today* **38**, 187 (1997).
47. Bamwenda, G.R., Obuki, A., Ogata, A., Oi, J., Kushiya, S., and Mizuno, K., *J. Molec. Catal. A* **126** 151, (1997).
48. Burch, R., and Scire, S., *Appl. Catal. B* **3**, 295 (1994).
49. Li, Y., and Armor, J.N., US Patent 5149512, assigned to Air Products and Chemicals Inc., (1992).
50. Feng, X., and Hall, W.K., *Catal. Lett.* **41**, 45 (1996).
51. Feng, X., and Hall, W.K., *J. Catal.* **166**, 368 (1997).
52. Hall, W.K., Feng, X., Dumesic, J., and Watwe, R., *Catal. Lett.* **52**, 13 (1998).
53. Marturano, P., Kogelbauer, A., and Prins, R., *J. Catal.* **190**, 460 (2000).
54. Chen, H.-Y., and Sachtler, W.M.H., *Catal. Today* **42**, 73 (1998).
55. Chen, H.-Y., Voskoboinikov, T., and Sachtler, W.M.H., *J. Catal.* **180**, 171 (1998).
56. Chen, H.-Y., Voskoboinikov, T., and Sachtler, W.M.H., *Catal. Today* **54**, 483 (1999).
57. El-Malki, E.-M., van Santen, R.A., and Sachtler, W.M.H., *J. Catal.* **196**, 212 (2000).
58. Voskoboinikov, T.V., Chen, H.-Y., and Sachtler, W.M.H., *J. Molec. Catal. A* **155**, 155 (2000).
59. Chen, H.-Y., El-Malki, E.M., Wang, X., van Santen, R.A., and Sachtler, W.M.H., *J. Molec. Catal. A* **162**, 159 (2000).

Evolution of the Fe-Species During the Synthesis of Over-Exchanged Fe/ZSM5, Prepared by Sublimation of FeCl₃

Abstract

The evolution of iron in over-exchanged Fe/ZSM5 prepared via chemical vapor deposition (sublimation) of FeCl₃ was studied at each stage of the synthesis. Different characterization techniques (EXAFS, HR-XANES, ⁵⁷Fe Mössbauer spectroscopy, ²⁷Al NMR, EELS, HR-TEM, XRD, N₂ physisorption and FTIR spectroscopy) were applied in order to correlate the changes occurring in the local environment of the Fe atoms with migration and aggregation phenomena of iron at micro- and macroscopic scale. Mononuclear isolated Fe-species are formed upon FeCl₃ sublimation, which are transformed into binuclear Fe-complexes during washing. During calcination, iron detached from the Brønsted sites migrates to the external surface of the zeolite, finally leading to significant agglomeration. Nevertheless, agglomeration of Fe can be strongly suppressed by adequately tuning the conditions of the calcination. No significant damage occurs to the framework of the zeolite, even applying a severe calcination procedure.

Introduction

Iron loaded zeolites have recently attracted renewed attention due to their outstanding catalytic properties (1-14). In particular, over-exchanged Fe/ZSM5 (Fe/Al molar ratio > 0.5) obtained through the Chemical Vapor Deposition (CVD) of anhydrous iron trichloride has been reported to be very efficient in the Selective Catalytic Reduction of nitrogen oxides using HydroCarbons (HC-SCR). The high activity of this material has been demonstrated in a wide oxygen concentration window (2-10%) and in the presence of water (10%) when using isobutane as the reductant (1,2). A similar performance has been achieved when using n-butane or propane (3). Furthermore, high activity on Fe/ZSM5 obtained through CVD of FeCl₃ has been claimed also for the conventional selective catalytic reduction of NO using ammonia (4-6) and for the catalytic decomposition of N₂O (7).

Besides CVD of anhydrous FeCl₃, alternative methods with the aim of synthesizing highly iron loaded ZSM5 have been reported in the literature. These include aqueous ion-exchange from ferrous oxalate, performed under exclusion of air (8), and solid-state ion-exchange using Fe(II)chloride (9,10), Fe(III)chloride (11-14) or FeSO₄·7H₂O (15). The synthesis in aqueous solution with ferrous oxalate as precursor has led to results comparable to those obtained through the CVD of FeCl₃, with respect to both the iron loading and the catalytic activity towards HC-SCR with isobutane. Nevertheless, the oxalate technique has shown lack of reproducibility, the reason being the difficulty in preventing the precipitation, during the synthesis, of neutral FeC₂O₄ complexes onto the pores mouth of the zeolite (16,17). Via solid-state ion-exchange the amount of iron loaded on the ZSM5 can easily be tuned during the synthesis. The solid-state ion-exchanged Fe/ZSM5 has shown high activity in the catalytic decomposition of N₂O (12) and in the HC-SCR of NO with isobutane (13). However, the use of FeCl₃ in its gaseous form has a clear advantage: by avoiding the contact between the ZSM5 support and the moisture always present in the precursor, it prevents the formation of large iron hydroxide and oxide clusters (11). The result of the CVD is the highest possible dispersion of extra-framework iron at the acidic exchange positions of the lattice, coupled with a very high reproducibility of the synthesis.

The remarkable catalytic properties have made the over-exchanged Fe/ZSM5 one of the most investigated materials in the last years. Several characterization studies have been performed in order to unravel the nature of the active phase (1,2,11,12,18-23). Binuclear iron oxo-hydroxo clusters at the ion-exchange positions of the ZSM5 lattice have been proposed earlier as the active phase for both the HC-SCR of NO (1,2,18) and the catalytic decomposition of N₂O (12). This model is based on results obtained by characterization with H₂ and CO TPR, XRD, FTIR, and EPR. X-ray Absorption Fine Structure spectroscopy (XAFS) studies performed independently by our group (19) and by Marturano *et al.* (20,21)

confirmed the presence of Fe binuclear oxo-hydroxo clusters in the over-exchanged Fe/ZSM5 obtained through CVD. Nevertheless, binuclear complexes are not the only Fe-species present in over-exchanged Fe/ZSM5. In addition to binuclear Fe-oxocations, EPR has revealed the presence of oxo/hydroxo ions, such as $(\text{Fe}(\text{OH})_2)^+$ or $(\text{Fe}=\text{O})^+$. Also the presence of a minor amount of iron oxide particles has been suggested (12,18,22).

While it is generally believed that the CVD of FeCl_3 is able to produce the most homogeneous and reproducible over-exchanged Fe/ZSM5 material possible, the nature of the active sites is still under debate. Furthermore, the processes occurring to iron and to the ZSM5 support during the different steps of the synthesis are not satisfactorily described. A lack of information regards especially the influence of the calcination treatment.

In the present work a comprehensive characterization is presented, with the aim of tracking the evolution of iron and of the support after each step of the synthesis: sublimation of the FeCl_3 into the zeolite pores; hydrolysis and washing of the residual chlorine; calcination. Different characterization techniques have been applied, including X-ray Absorption Spectroscopy (XAS), X-Ray Diffraction (XRD), N_2 physisorption, Electron Energy Loss Spectroscopy (EELS), High-Resolution Transmission Electron Microscopy (HR-TEM), Fourier Transform Infra-Red Spectroscopy (FTIR), Aluminum-Nuclear Magnetic Resonance (Al-NMR) and Mössbauer Spectroscopy. The goals of this study are: (i) to elucidate the pathway by which the Fe binuclear complexes, *i.e.* the suggested catalytic active phase, are formed; (ii) to study the structure of these complexes; (iii) to identify and to control the processes responsible for their undesired further aggregation towards larger and presumably inactive clusters. With this respect, a modified calcination procedure is presented by which the agglomeration of iron can be significantly suppressed.

Experimental

Preparation of the samples

Over-exchanged Fe/ZSM5 was prepared via the FeCl_3 CVD method described by Chen and Sachtler (1). $\text{NH}_4/\text{ZSM5}$ (Si/Al atomic ratio = 17) obtained by Zeolyst, further referred to as $\text{NH}_4/\text{ZSM5-17}$, was converted into the acidic form by calcination under O_2 at 550°C for 3 hrs. For the CVD exchange a dedicated U-shaped quartz reactor was used. The reactor was built with a porous frit in each of the legs, allowing a separate loading of the H/ZSM5 support and the FeCl_3 precursor. Furthermore, it could be isolated by closing two Pyrex valves mounted on its inlet and outlet. In order to remove absorbed moisture, 1.5 g of the H/ZSM5 (sieve fraction between 212 and 450 μm) were loaded onto one frit and flushed overnight under He (40 ml/min) at 300°C . The temperature was then lowered to 30°C under

the same He flow. The reactor was sealed and moved to a glove bag (under N₂), where 0.45 g of anhydrous FeCl₃ (98%, Acros Organics) were loaded on its second frit. After being reconnected to the He line (30 ml/min), the reactor was heated (5°C/min) to 330°C and kept at this temperature for 30 minutes. The HCl formed during the reaction of the sublimed FeCl₃ with the Brønsted sites of the support was absorbed in 100 ml of 0.05 M NaOH solution for titration. After completion of the iron loading, the temperature was lowered to 30°C, the Pyrex valves were closed and the isolated reactor was moved to the N₂ atmosphere of the glove bag. There, the synthesized Fe/ZSM5 was carefully extracted from the reactor, part of it being sealed and stored under N₂ for characterization (sample further denoted as Fe/ZSM5-17-Cl). The remaining Fe/ZSM5 was washed under stirring in 1000 ml doubly deionized H₂O for 30 minutes and dried overnight in air at 70°C. Part of the dried sample was isolated and stored under air (Fe/ZSM5-17-H₂O). The rest was pressed to obtain a sieve fraction between 150 and 212 μm, and divided into two batches which were subjected to two different calcination procedures. The first batch was heated under flowing oxygen in a tubular oven (5°C/min, 120 ml/min) and calcined at 550°C for 3hrs. The sample deriving from this relatively severe calcination procedure will be denoted as Fe/ZSM5-17-s.c. (severely calcined). For the calcination of the second batch a Plug Flow Reactor (PFR) was used (I.D.=1.2 cm). Under a He flow of 800 ml/min, the sample was heated with an extremely low temperature ramp (0.5°C/min) to 200°C. At this temperature, 200 ml/min of O₂ were added to the He flow while, under the same temperature ramp, heating was continued to 550°C. After 3 hrs at 550°C the temperature was decreased to 30°C. The resulting sample, stored in air, will be referred to as Fe/ZSM5-17-m.c. (mildly calcined).

Characterization

ICP, HCl titration, N₂ physisorption

The elemental composition of the starting H/ZSM5 support and of the obtained over-exchanged Fe/ZSM5 was determined by using Inductively Coupled Plasma emission spectroscopy (ICP). The amount of HCl formed during the Fe loading was measured by acid-base titration. The derived H⁺ removal efficiency was calculated as the molar ratio between the released HCl and the aluminum of the support, according to the exchange reaction: $\downarrow\text{FeCl}_{3(g)} + \text{H}^+ \rightarrow \text{FeCl}_2^+ + \text{HCl}_{(g)}\uparrow$. The micropore volume of the ZSM5 crystals was determined by N₂ physisorption, using a Micromeritics ASAP 2010. The measurements were performed at 77 K, in the pressure range 0-1 bars, after de-gassing the samples in vacuo at 200°C for 16 hrs. N₂ physisorption data obtained on the Fe-loaded samples were corrected for the additional metal loading for comparison with the support.

FTIR spectroscopy

Interaction of the iron species with the Brønsted and the silanol sites of the support was investigated using Fourier Transform Infrared Spectroscopy. Samples, pressed into self-supporting wafers, were heated *in situ* under helium with a temperature ramp of 2°C/min to 350°C. Transmission infrared spectra were recorded under helium at 350°C on a Perkin Elmer 2000 spectrometer using a DTGS detector. One hundred scans were recorded at a resolution of 4 cm⁻¹ and averaged. Data were baseline-corrected and the intensity of each spectrum was normalized at the zeolite overtones (1850-1950 cm⁻¹).

XRD

The crystalline fingerprint of the zeolitic support was compared after each synthesis step to visualize significant lattice damage or formation of large particles of iron oxidic or oxo-hydroxidic crystalline phases. X-Ray Diffraction (XRD) patterns were recorded by means of a Nonius PDS 120 powder diffractometer equipped with a curved position-sensitive INEL detector. The radiation used was Co K α 1 ($\lambda=1.78897$ Å). In order to optimize the signal-to-noise ratio XRD patterns were averaged after measuring for 24 hrs.

HR-TEM/EDX

Imaging of the samples was obtained through High-Resolution Transmission Electron Microscopy (HR-TEM). For this purpose a Philips CM30UT electron microscope was used with a field-emission gun operated at 300 kV as the source of electrons. Measurements were performed also with a Philips CM200FEG operated at 200 kV. Samples were positioned on a carbon microgrid, supported on copper, by placing a few droplets of a suspension of ground sample in ethanol. The grid was dried at ambient conditions. When possible, identification of visible Fe-containing crystalline aggregates was performed on the basis of the observed lattice d-spacings. These were derived from high-resolution images and compared with literature XRD data. Elemental composition was obtained by Energy Dispersive analysis of X-rays (EDX) performed through a LINK EDX system.

EELS/STEM

Spatial distribution, migration and clustering of iron occurring during the synthesis were monitored by Electron Energy Loss Spectroscopy (EELS), at the Fe L_{2,3}-edges and the O K-edge. EELS was coupled with Scanning Transmission Electron Microscopy (STEM). The combination of these techniques provides very detailed morphological and spectroscopic information (including chemical composition) at the nanometer scale. The data were recorded with a scanning transmission electron microscope VGHB501, equipped with a field-emission source and a parallel Gatan 666 EELS spectrometer. This instrument

produced EELS spectra, with a typical 0.7 eV resolution, recorded from subnanometer areas (24,25). In the line spectrum mode spectra were recorded while moving the probe with given steps across the specimen. Acquisition times required for achieving a satisfactory signal-to-noise level on core edges were in the order of 0.1-1.0 s. The data recorded at the Fe L_{2,3} and at the O K-edges were corrected by the corresponding elemental crossover sections. To obtain information on the concentration of iron in the ZSM5 crystals, the Fe intensity was divided by that of oxygen. By doing so, a homogeneous distribution of oxygen in the ZSM5 matrix was assumed at the scale of the investigation. Data obtained from local sub-areas were coupled to obtain information on larger areas. Data were analyzed by means of Savantic Spim Doctor 5.3 and Digital Micrograph 5.3 software.

⁵⁷Fe Mössbauer spectroscopy

Agglomeration of iron was studied with Mössbauer spectroscopy. ⁵⁷Fe Mössbauer spectra were measured on a constant acceleration spectrometer in a triangular mode with a ⁵⁷Co:Rh source. Mössbauer spectra were recorded at 300, 77 and 4.2 K in a closed cell with the sample in contact with He gas. The overall spectra were deconvoluted with calculated Mössbauer spectra consisting of Lorentzian-shaped lines. In the case of quadrupole doublets the line widths and the adsorption areas of the constituent lines were constrained equally. Positional parameters were not constrained in the fitting process. Isomer shift values are reported relatively to sodium nitroprusside. The estimated accuracy of the positional parameters is ±0.03 mm/s.

²⁷Al MAS NMR, Al K-edge XAFS

²⁷Al Magic Angle Spinning Nuclear Magnetic Resonance (²⁷Al MAS NMR) and Al K-edge X-ray Absorption Spectroscopy (Al K XAS) were combined to study the coordination of the Al atoms in the starting ZSM5 support and to track their evolution along the synthesis of Fe/ZSM5.

²⁷Al magic-angle spinning (MAS) NMR experiments were performed to determine the aluminum coordination in the ZSM5 support (ammonium and acidic form). The experiments were carried out on a Chemagnetics Infinity 600 (14.1 T, corresponding to 156.3 MHz ²⁷Al resonance), using a 2.5 mm HX MAS probe head. Magic angle spinning (MAS) was performed at a rotation speed higher than 25 kHz. To allow a quantitative evaluation of the single pulse excitation, $\pi/18$ pulses using a rf field strength of ~35 kHz were used. Chemical shifts were referenced relatively to a 1 M aqueous Al(NO₃)₃ solution. The relaxation delays were 0.5 s, determined to be adequate for a quantitative analysis using saturation recovery experiments. Samples were fully hydrated overnight in a controlled environment before measuring.

X-ray absorption measurements of the Al K-edge (Al K XAS) were performed on the starting ZSM5 support (ammonium and acidic form) and on the Fe/ZSM5 sample after severe calcination. The coordination of aluminum was deduced from the X-ray absorption near edge (XANES) by identification of characteristic features in the spectra (26). Data were collected at station 3.4 of the SRS Daresbury (U.K.), using a double crystal monochromator equipped with YB66 crystals. A recently developed *in situ* Low Energy X-ray Absorption Fine Structure Spectroscopy set-up (ILEXAFS) was used (27,28). The samples were pressed into self-supporting wafers and measured at room temperature under high vacuum ($P < 10^{-5}$ bar). Fluorescence detection, via a gas proportional counter (GPC), was used. Normalization of the data was performed through standard procedures (38).

Fe K-edge HR-XANES

Experimental set-up

High-Resolution X-ray Absorption Near Edge Spectroscopy (HR-XANES) was used to study the oxidation state and the local coordination geometry of Fe. The HR-XANES measurements at the Fe K-edge were carried out at the inelastic X-ray scattering undulator beamline ID16 at the European Synchrotron Radiation Facility (ESRF). The set-up of the beamline has been described in detail elsewhere (29). The white beam is monochromatized by a Si(111) double crystal device. The fluorescence signal is detected by a 1m Rowland circle spectrometer consisting of a spherically bent Si (531) single-crystal wafer. The analyzer is operated at the Fe $K\beta$ emission line, with a typical resolution of 0.4 eV. Using this high-resolution fluorescence detector yields a spectral sharpening of the XANES spectrum below its lifetime broadening of 2 eV (30, 31). Hematite was used as internal reference for the energy calibration of the monochromator.

HR-XANES data collection and processing.

Samples were pressed to obtain self-supporting wafers and placed in an *in situ* fluorescence cell (32) at 45° with respect to the beam. After flushing with He at 30°C and atmospheric pressure, the cell was closed and the spectra were collected.

The fluorescence Fe K XANES spectra were normalized using the average absorption coefficient in the 7200-7300 eV region. In order to isolate the pre-edge feature, the contribution of the edge jump to the pre-edge was calculated using a cubic spline function obtained by interpolating the data several eVs before and after the pre-edge.

The influence of fluorescence saturation effects was checked using the procedure as outlined in Ref. (33). These effects were revealed in particular on α -Fe₂O₃. Nevertheless, numerical comparison showed that as far as the pre-edge is concerned, it was possible to correct for the them by dividing the maximum intensity of the background subtracted

fluorescence pre-edge by that of the corresponding transmission spectrum. For this purpose XANES spectra measured in transmission on each sample at beamline X1.1 at Hasylab (*vide infra*) were used as internal standard.

The normalized height, centroid position, half-width and integrated intensity of the obtained pre-edge features were obtained using the software Grams. Prior to calculations, the pre-edge of α -Fe₂O₃ was deconvoluted into pseudo-Voigt components (50% Gaussian, 50% Lorentzian peaks shape). Contribution to the centroid position and to the integrated intensity from components centered above 7115.0 eV was ignored (34, 35). The estimated accuracy in the energy determination for the HR-XANES spectra presented in this study is ± 0.05 eV.

Fe K-edge XAFS

XAFS data collection

Fe K-edge XAFS was applied in combination with Fe K-edge HR-XANES in order to study the atomic environment around iron. X-ray absorption spectra of the Fe K-edge were collected at Hasylab (Hamburg, Germany) Wiggler Station X1.1, using a Si (111) double crystal monochromator. The monochromator was detuned to 50% of the maximum intensity to avoid higher harmonics in the X-ray beam. The measurements were performed in transmission mode using ion chambers filled with Ar to have a X-ray absorbance of 20% in the first ion chamber and of 80% of the remaining radiation in the second one. In all the experiments a Fe foil was measured using a third ionization chamber. The edge position was determined for each scan by calibrating the monochromator with the iron foil. The samples were pressed into self-supporting wafers and placed in a controlled atmosphere cell (32). Spectra were recorded at liquid nitrogen temperature after flushing the cell with He at 30°C.

XAFS data-processing

Extraction of the EXAFS data from the measured absorption spectra was performed with the XDAP code developed by Vaarkamp *et al.* (36). Three scans were averaged and the pre-edge was subtracted using a modified Victoreen curve (37). The background was subtracted employing cubic spline routines with a continuously adjustable smooth parameter (38,39). Normalization was performed by dividing the data by the intensity of the absorption spectrum at 50 eV above the Fe K-edge.

EXAFS phase-shifts and backscattering amplitudes

The Fe-O reference was obtained directly from experimental EXAFS data of ferric acetylacetonate. Table 1a gives the crystallographic data (40) and the forward and inverse

Fourier transform ranges used to create the Fe-O reference.

Table 1a: Crystallographic data and forward/inverse Fourier Transform ranges used to produce the EXAFS Fe-O reference file.

Atom pair	Ref compd	Ref	N	R(Å)	k weighting	Forward FT	Inverse FT
						Δk (Å ⁻¹)	ΔR (Å)
Fe-O	Ferric(acac)	(40)	6	1.99	k ³	2.5-13.3	0.7-2.2

The Fe-Fe and Fe-Cl phase shifts and backscattering amplitudes were calculated using the software FEFF7 (41). The Fe-Fe and the Fe-Cl references were calibrated on the EXAFS data obtained from Fe₂O₃ (hematite) and FeCl₃·6H₂O, respectively, by fitting in R-space (see Tables 1b and 1c).

Table 1b: Crystallographic data and input parameters for FEFF 7 used to produce the EXAFS Fe-Fe and Fe-Cl reference files.

Atom pair	Ref compd	Ref	N	R(Å)	$\Delta\sigma^2$	V _r (eV)	V _i (eV)	S ₀ ²
Fe-Fe	α -Fe ₂ O ₃	(42)	4	2.95	0.013	-16.0	3	0.53
Fe-Cl	FeCl ₃ ·6H ₂ O	(43)	2	2.31	0.002	1.0	3	0.91

The following average crystallographic parameters were used for the R-space fit of hematite: Fe-O₁ (N=3, R=1.95 Å); Fe-O₂ (N=3, R=2.12 Å); Fe-Fe₁ (N=4, R=2.95 Å); Fe-Fe₂ (N=3, R=3.36 Å); Fe-Fe₃ (N=7, R=3.74 Å) (42). The crystallographic parameters adopted for the fit of the closest shells in FeCl₃·(6H₂O) were: Fe-Cl (N=2, R=2.31 Å); Fe-O (N=4, R=2.07 Å) (43). Both the reference spectra and the samples were measured at liquid nitrogen temperature. This means that temperature effects (dynamic disorder) can be ruled out in the difference of the Debye-Waller factor ($\Delta\sigma^2$) between the samples and the reference.

Table 1c: Structural parameters (closest Fe-Fe shell in hematite and closest Fe-Cl shell in ferric chloride hexahydrate), as obtained from the R-space fit by using the theoretical references.

Atom pair	k ¹ Fourier Transform		Structural Parameters				Variance	
	Δk (Å ⁻¹)	ΔR (Å)	N	R(Å)	$\Delta\sigma^2$ (Å ²)	ΔE_0 (eV)	Im.	Abs.
Fe-Fe	3.0-13.0	1.0-3.5	4.0	2.95	0	0	0.62	0.38
Fe-Cl	3.0-13.0	1.0-2.2	2.0	2.31	0	0	0.13	0.07

EXAFS data-analysis

The EXAFS data-analysis was performed by applying multiple-shell fitting in R-space. R-space fitting has important advantages compared to the usually applied fitting in k-space and is extensively discussed in a recent paper by Koningsberger *et al.* (38). The difference file technique was applied together with phase-corrected Fourier Transforms to resolve the different contributions in the EXAFS data (38). The EXAFS fits were checked by applying k^1 , k^2 and k^3 weightings.

The number of independent data points (N_{indp}) was determined as outlined in the ‘Reports on Standard and Criteria in XAFS Spectroscopy’(44):

$$N_{\text{indp}} = \frac{2\Delta k\Delta R}{\pi} + 2 \quad [1].$$

Errors in the numerical values obtained by the EXAFS data analysis are estimated to be $\pm 10\%$ in the coordination number (N), $\pm 1\%$ in the distance (R), $\pm 5\%$ in the Debye Waller factor ($\Delta\sigma^2$) and $\pm 10\%$ in the inner potential correction (ΔE_0) (45). In this study the statistical significance of each contribution has been checked by comparing the amplitude of (Fit)_j with the noise level present in the experimental data.

Results

ICP, H⁺ removal efficiency, N₂ physisorption

The elemental composition of the parent H/ZSM5 support and of the Fe/ZSM5 samples is presented in Table 2. In the same table the H⁺ removal efficiency (calculated from the

titrated HCl) is compiled, together with the evolution of the micropore volume of the support.

Table 2: Elemental composition (ICP), H⁺ removal efficiency and micropore volume (N₂ physisorption).

Samples	Si/Al (atomic ratio)	Fe/Al (atomic ratio)	H ⁺ removal efficiency (%)	Micropore volume (cm ³ /g)
H/ZSM5-17	17.0	0.0	--	0.15
Fe/ZSM5-17-H ₂ O	17.4	1.0	100	0.12
Fe/ZSM5-17-m.c.	17.2	1.0	--	0.12
Fe/ZSM5-17-s.c.	17.2	1.0	--	0.13

The Si/Al ratio of the parent H/ZSM5 was maintained after the ion-exchange and the subsequent washing procedure, indicating that no significant amount of aluminum was leached out during the synthesis. The FeCl₃ CVD procedure led to an iron content of Fe/Al=1.0 as a result of the complete exchange with the Brønsted protons. Completion of the H⁺ removal was confirmed by titration of the HCl released during the synthesis. After the loading of iron, a decrease of around 20% in the micropore volume was detected by N₂ physisorption (Fe/ZSM5-17-H₂O). While applying a mild calcination procedure resulted in no significant change of the micropore volume (Fe/ZSM5-17-m.c.), the latter was partially regained (re-increase between 5 and 10%) after a severe calcination (Fe/ZSM5-17-s.c.).

FTIR spectroscopy

The normalized spectra of the hydroxyl stretching region (3900-3000 cm⁻¹) are depicted in Fig. 1.

For H/ZSM5-17 two intense bands were observed at 3590 and 3740 cm⁻¹. They are assigned respectively to Brønsted acid groups (associated with framework aluminum (Si(OH)Al)) and to terminal silanol groups (located inside the zeolite channels and on the external surface of the crystals (46-48)). A small shoulder detected at 3650 cm⁻¹ is attributed to hydroxyl groups of extra-framework aluminum species (49). Following FeCl₃ CVD and washing (Fe/ZSM5-17-H₂O, Fig.1), the intensity of the band at 3590 cm⁻¹ decreased significantly, as a result of the exchange of the Brønsted protons by iron, while the signal from the silanol groups remained unchanged. In addition, a new band appeared at 3715 cm⁻¹. This band is ascribable to the stretching vibration of hydrolyzed Fe species

formed upon washing of the residual chlorine (20), and disappeared after calcination (Fe/ZSM5-17-m.c., Fe/ZSM5-17-s.c.). No clear changes were detected upon calcination in the intensity of the silanol and of the Al-Brønsted signal. It should nevertheless be noted that, due to differences in the broadening of the Al-OH Brønsted and Si-OH silanol bands, a quantitative comparison between washed and calcined sample is not possible.

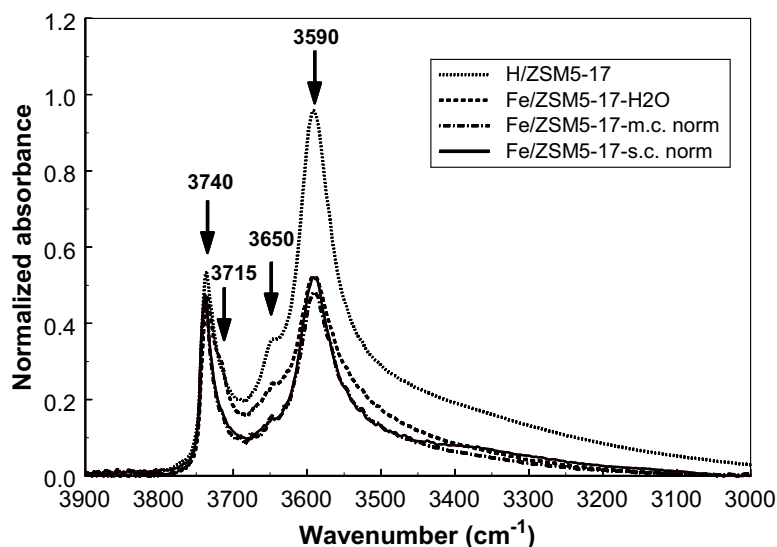


Figure 1: Infrared spectra of the hydroxyl stretching region for H/ZSM5-17 and Fe/ZSM5-17, measured at 350°C in helium (heating ramp of 2°C/min).

XRD

X-ray diffractograms (not shown) were collected after each synthesis step and compared to that of the parent H/ZSM5. All patterns appeared to be identical, indicating no detectable damage to the ZSM5 structure. In addition, no contribution in the XRD patterns was detected from reflections ascribable to Fe oxidic or oxo-hydroxidic crystalline phases.

HR-TEM/EDX

High-resolution transmission electron micrographs of the over-exchanged Fe/ZSM5, collected in Fig. 2, were taken upon sublimation and washing (Fe/ZSM5-17-H₂O), and after the different calcination procedures.

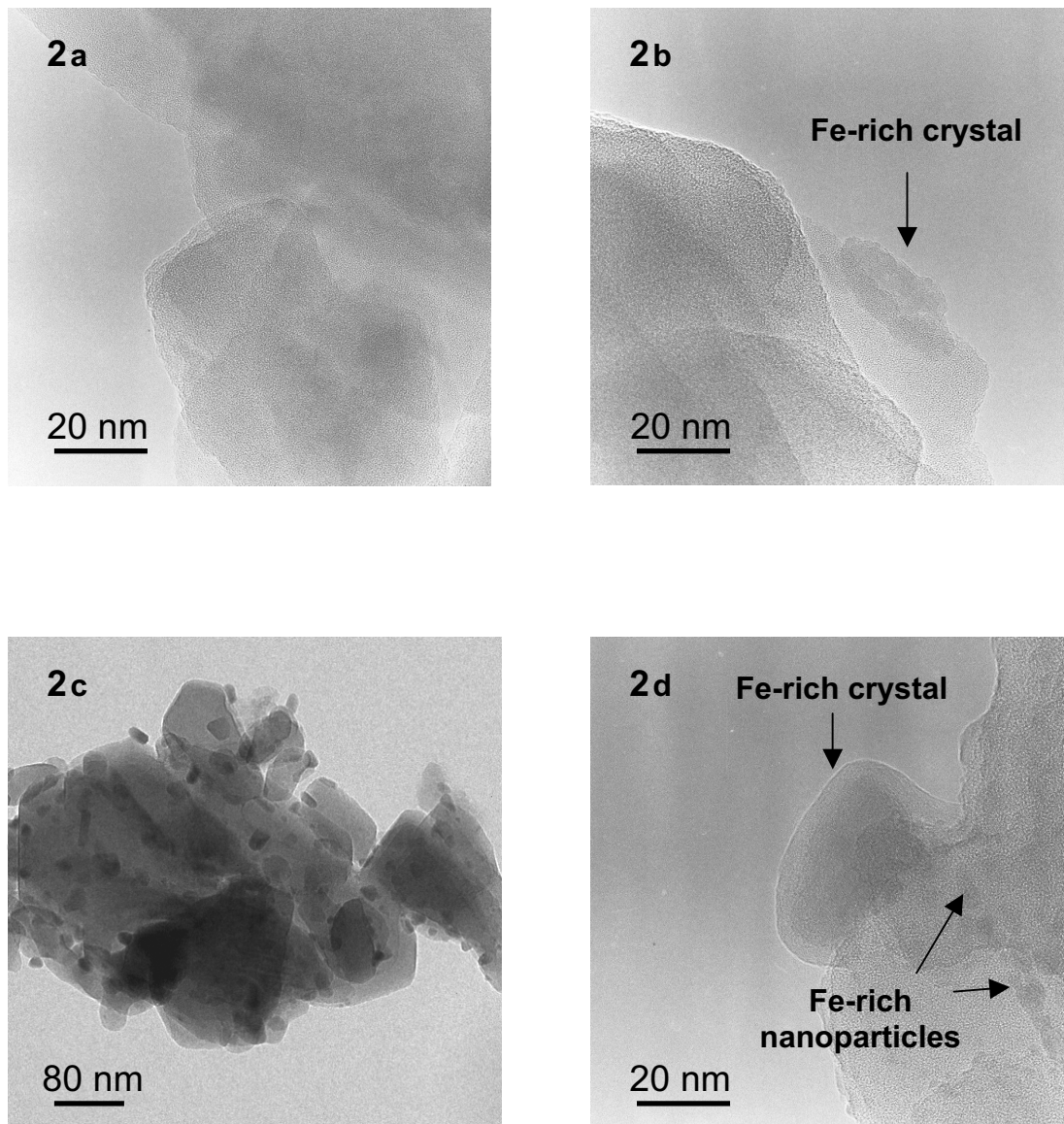


Figure 2: TEM micrographs of Fe/ZSM5-H₂O (2a), Fe/ZSM5-17-m.c. (2b), Fe/ZSM5-17-s.c. (2c, 2d).

As expected, no particles were visible on the Fe/ZSM5-17-H₂O (Fig. 2a), suggesting that no agglomeration of iron occurred during the Fe-exchange process and the following washing. At this stage of the synthesis Fe is highly dispersed within the zeolite channels. The uniform distribution of iron was confirmed by elemental analysis performed on local areas (D~100 nm) by EDX. In a few EDX measurements traces of residual chlorine were found.

TEM images collected from the sample upon mild calcination (not shown here) did not reveal significant changes when compared to those obtained after washing. Nevertheless, when HR-TEM was applied in combination with EDX, some coalescing iron was revealed on the external surface of the Fe/ZSM5-m.c. crystals. This was visible as infrequent dark spots with sizes between 2 and 5 nm. In addition, very few crystalline particles were detected. In Fig. 2b one of these Fe-containing crystals is depicted. From the largest Fe-containing particles detected on Fe/ZSM5-17-m.c. the following d-spacings could be determined: 2.85, 2.66 and 2.53 Å (estimated margin of error equal to ± 0.05 Å). By comparison with XRD data obtained from the literature (50), these Fe-containing particles are identified as oxo-hydroxides like α -goethite (2.53 and 2.69 Å) or β -goethite (2.55 and 2.63 Å), and possibly hematite (2.52 and 2.70 Å).

Severe calcination, on the other hand, leads to considerable aggregation of iron in the Fe/ZSM5 material. This can clearly be seen when observing the micrographs obtained from the severely calcined Fe/ZSM5 (Figs. 2c and 2d). Already at medium magnification (Fig. 2c) clustering into iron-rich particles is clearly visible. When compared to the Fe/ZSM5-17-m.c., the number of particles is drastically increased, together with their average dimension and degree of crystallization. A HR-TEM picture (Fig 2d) shows one large crystalline Fe-containing particle of around 40 nm, together with some Fe-rich clusters of 1-2 nm. D-spacings obtained from this sample are 3.33, 3.26 and 2.53 Å. While the d-spacing at 2.53 Å can be attributed to either α -goethite or hematite, those at ~ 3.3 Å are typical only of goethite-like oxo-hydroxo crystalline structures (50).

EELS/STEM

In Fig. 3a the oxygen map of a Fe/ZSM5-17-H₂O crystal is shown. The picture, produced from EELS O K-edge absorption spectra recorded with spatial step increments of 2.5 nm and a probe diameter of 0.5 nm, is plotted in grayscale (oxygen in white). In this image luminosity is proportional to the number of oxygen atoms encountered in each sub-area by the electron beam. In Fig. 3b the Fe/O map (atomic ratio) of the same region is depicted. In the Fe/O map brightness is proportional to the concentration of iron. Due to the uniform distribution of oxygen in the ZSM5 support, the Fe/O ratio provides information on the local concentration of iron in the crystal. From Fig. 3b it can be concluded that, after FeCl₃ CVD and washing, iron was homogeneously distributed across the crystal. In particular, no gradient in the iron concentration was detected when approaching the crystal surface. Furthermore, the calculated Fe/O ratio, obtained by integration over the whole sampling area, was 0.028, in good agreement with the Fe content detected by bulk ICP elemental analysis.

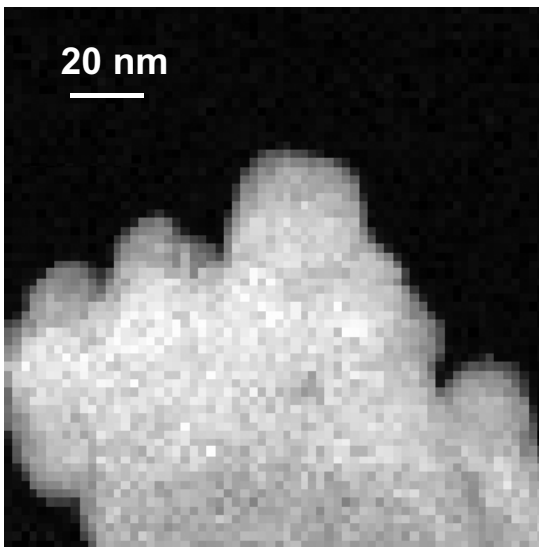


Figure 3(a)

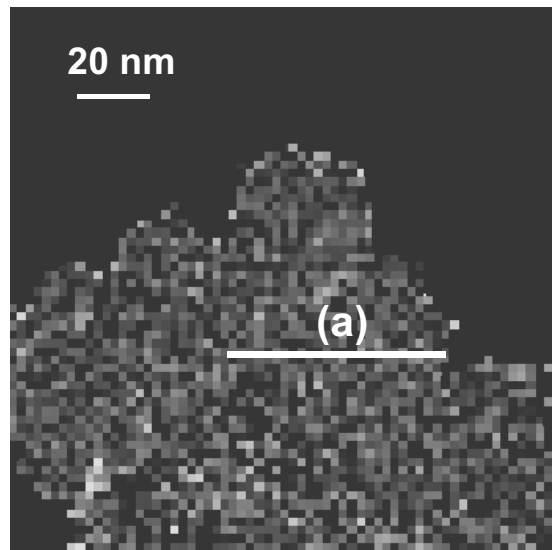


Figure 3(b)

Figure 3(a): Grayscale EELS (O K-edge) oxygen map of Fe/ZSM5-17-H₂O (oxygen depicted in white); 3(b): Grayscale EELS Fe/O map (atomic ratio) of Fe/ZSM5-17-H₂O (iron depicted in white).

The O and Fe/O map of the edge of a Fe/ZSM5 crystal after mild calcination are collected in Figs. 3c and 3d, respectively.

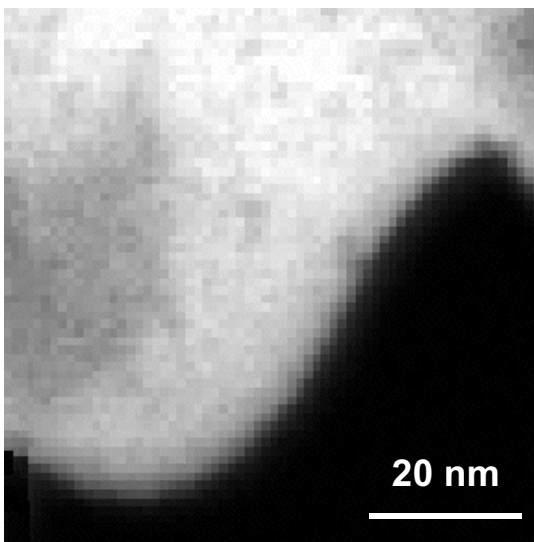


Figure 3(c)

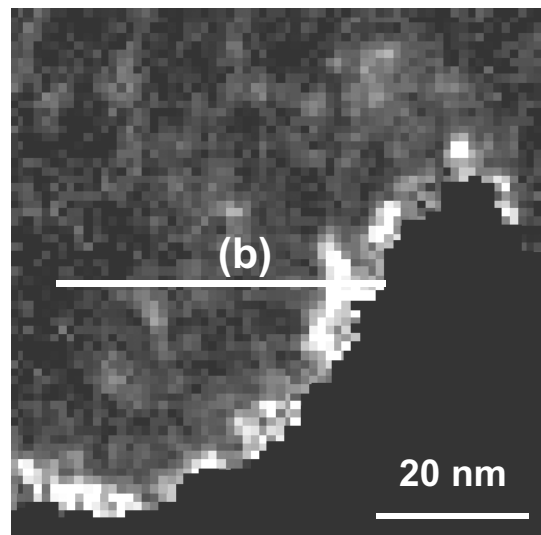


Figure 3(d)

Figure 3(c): Grayscale EELS (O K-edge) oxygen map of Fe/ZSM5-17-m.c.; 3(d): Grayscale EELS Fe/O map (atomic ratio) of Fe/ZSM5-17-m.c..

The pictures were produced from spectra recorded with a spatial step increment of 1.25 nm (the probe diameter was kept at 0.5 nm). In this case the Fe concentration appeared to be higher in the proximity of the external surface. Furthermore, the Fe/O ratio integrated over the whole area was 0.054, thus showing a clear increase in the Fe content when compared to that of the sample after washing. This is ascribed to the migration towards the edge of the crystal of iron, which prior to the mild calcination procedure, was still located well inside the crystal. This migration was nevertheless not accompanied by the formation of clearly visible particles on the surface.

The formation of well defined Fe-rich particles, on the contrary, was clearly visible on the external surface of the severely calcined sample, as shown in Figs. 3e and 3f.

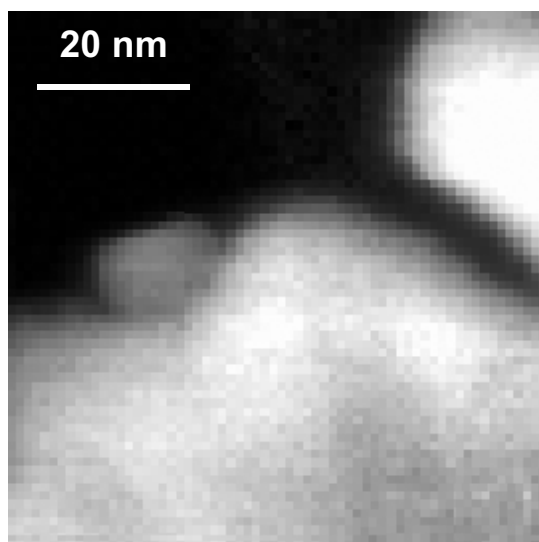


Figure 3(e)

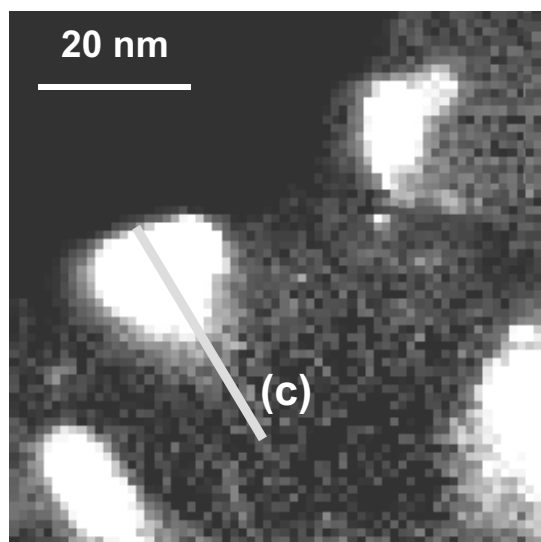


Figure 3(f)

Figure 3(e): Grayscale EELS (O K-edge) oxygen map of Fe/ZSM5-17-s.c.; 3(f): Grayscale EELS Fe/O map (atomic ratio) of Fe/ZSM5-17-s.c..

Four Fe-containing clusters with an average dimension of 20 nm are visible (Fig. 3f). One of them is recognizable also in the upper-left part of the corresponding O map (Fig. 3e). This indicates that the cluster was located on the external surface of the ZSM5. As a consequence, its chemical composition could be obtained, avoiding misleading information from the ZSM5 support. The result is shown in Figure 4. In this figure three Fe/O line-scans are plotted, measured along the lines (a), (b) and (c), selected respectively from the Fe/O maps of Figs. 3b, 3d and 3f. These line-scans show the concentration of iron in the different samples as a function of the distance from the crystal surface.

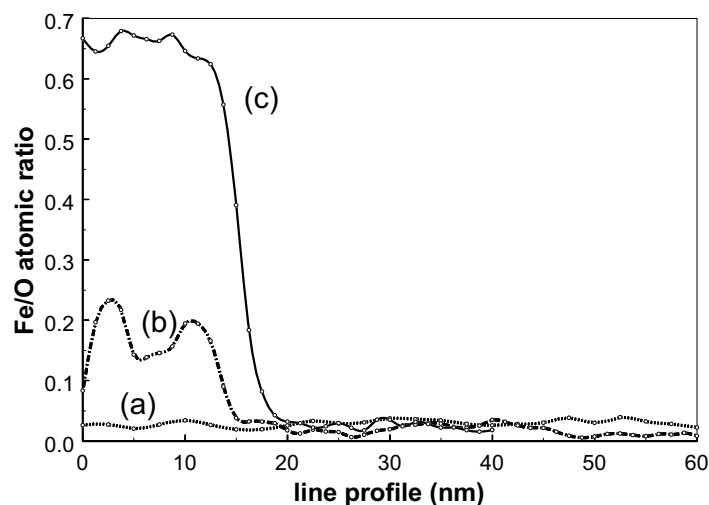


Figure 4: Fe/O scans (atomic ratio) measured along lines: (a), Fe/ZSM5-17-H₂O, from Fig. 3b; (b), Fe/ZSM5-17-m.c., from Fig. 3d; (c), Fe/ZSM5-17-s.c., from Fig. 3f.

Line (a) (Fe/ZSM5-17-H₂O) shows a homogeneous Fe/O profile over the whole distance, confirming the homogeneous dispersion of iron within the zeolite channels after CVD and washing. After applying a mild calcination (line (b)), a clear increase in the Fe signal was visible when approaching the crystal surface (0-15 nm). Quantification of the Fe/O ratio in the Fe-rich phase alone was not possible due to its overlap with the ZSM5. It should be noted that the Fe concentration of line (b) in the region 20-60 nm is somewhat lower than that of line (a). This shows that the agglomeration at the crystal surface was produced by migration of iron from inside the crystal. Prior to calcination this iron was still homogeneously distributed in the zeolite channels. Line (c) shows the influence on the Fe agglomeration of a severe calcination procedure. The data-points in the 0-15 nm region of line (c) are of the EELS scan across the Fe-containing cluster mentioned above. The Fe/O ratio in this region is 0.67. By coupling this result with that of HR-TEM, this particle is identified as α -Fe₂O₃. Also for line (c) a decrease in the Fe concentration was visible when scanning the internal region of the ZSM5 crystal (20-40 nm). In this case the decrease appears less pronounced than for the mildly calcined sample. This is probably due to the presence of some additional Fe aggregation in the vicinity of the hematite crystal.

⁵⁷Fe Mössbauer spectroscopy

⁵⁷Fe Mössbauer spectra were recorded under He at 300, 77 and 4.2 K. In Fig. 5a the spectra of the Fe/ZSM5-17-H₂O are shown.

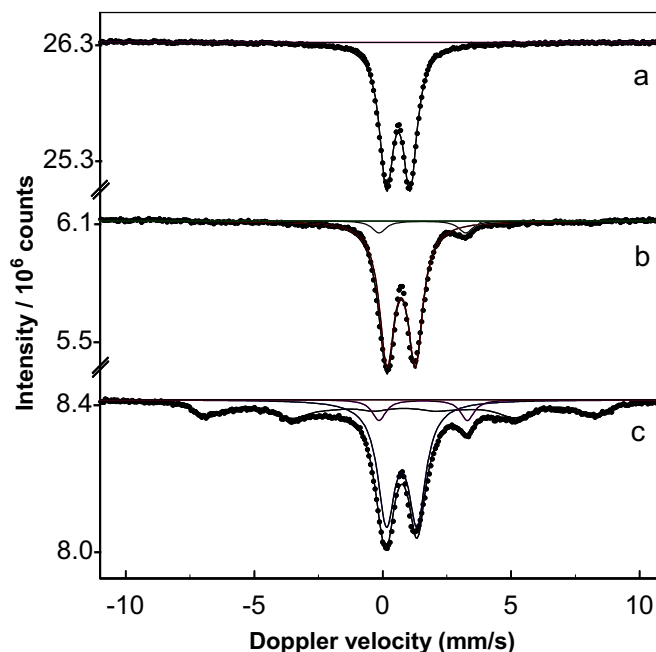


Figure 5a: ^{57}Fe Mössbauer spectra of Fe/ZSM5-17- H_2O recorded in He at 300K (a), 77K (b) and 4.2K (c).

At 300 K (spectrum a) a doublet was detected with an isomer shift (IS) of 0.61 mm/s and a quadrupole splitting (QS) equal to 1.02 mm/s. The presence of this well resolved paramagnetic doublet is the result of high electron spin relaxation rates due to the mutual magnetic interaction of Fe^{3+} neighboring atoms. This shows that, after CVD and washing, Fe was not present as monoatomic species at the Al-exchange position of the lattice. By lowering the temperature to 77 K (spectrum b) an additional doublet was detected with a QS of 3.37 mm/s, assigned to Fe^{2+} . The Fe^{2+} doublet accounts for around 8% of the overall signal. At 4.2 K (spectrum c), together with the doublets, also the contribution of a weak sextet became visible, with an average Hyperfine Field (HF) of 46.7 T. The presence of the sextet is ascribed to the magnetic ordering of a fraction of iron (51). This indicates the presence of some Fe agglomeration occurring already after washing. The extreme width of the sextet is an indication for the amorphous character of the aggregated phase. The hyperfine parameters of the Fe/ZSM5-17- H_2O , together with the relative integrated intensity of the different Fe species are collected in Table 3a.

Table 3a: ⁵⁷Fe Mössbauer Hyperfine Parameters and Relative Integrated Intensities of the iron species in Fe/ZSM5-17-H₂O.

Conditions	Isomer Shift (mm/s)	Quadrupole Splitting (mm/s)	Hyperfine Field (T)	Relative Intensity (%)	Identification
300K, He	0.61	1.02	--	100	Doublet, Fe(III)
77K, He	0.72	1.10	--	92	Doublet, Fe(III)
	1.55	3.37	--	8	Doublet, Fe(II)
4.2K, He	0.74	1.19	--	53	Doublet, Fe(III)
	1.58	3.44	--	8	Doublet, Fe(II)
	0.78	--	46.7	39	Sextet, Fe(III)

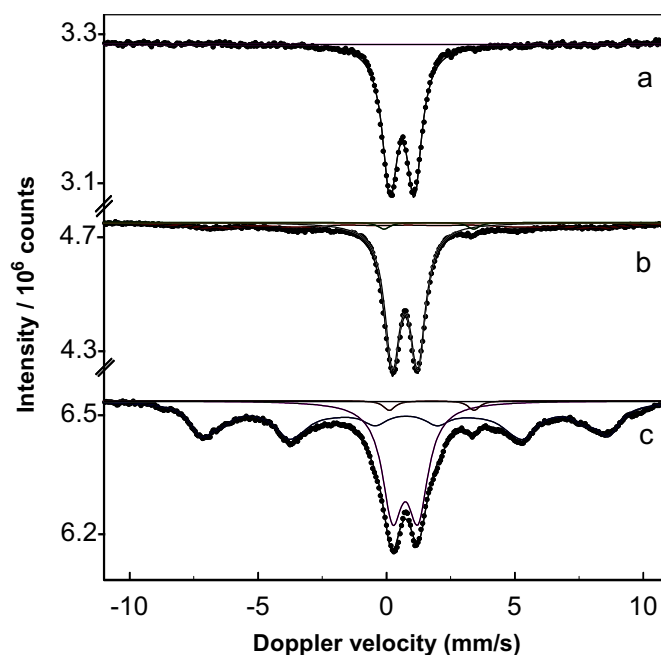


Figure 5b: ⁵⁷Fe Mössbauer spectra of Fe/ZSM5-17-m.c. recorded in He at 300K (a), 77K (b) and 4.2K (c).

Fig. 5b shows the spectra of the Fe/ZSM5 sample after the mild calcination procedure. No significant differences are visible when comparing the Fe/ZSM5-17-m.c. spectra recorded at 300 and 77 K (a and b) with those of the Fe/ZSM5-17-H₂O. Nevertheless, when measuring at 4.2 K, an increase was detected in the intensity of the sextet signal. This is ascribed to further agglomeration of Fe. The corresponding average hyperfine field at 4.2 K was 48.0 T. The complete list of the hyperfine parameters of the Fe/ZSM5-17-m.c. as a function of the temperature are shown in Table 3b.

Table 3b: ⁵⁷Fe Mössbauer Hyperfine Parameters and Relative Integrated Intensities of the iron species in Fe/ZSM5-17-m.c.

Conditions	Isomer Shift (mm/s)	Quadrupole Splitting (mm/s)	Hyperfine Field (T)	Relative Intensity (%)	Identification
300K, He	0.61	0.94	--	100	Doublet, Fe(III)
77K, He	0.73	0.99	--	76	Doublet, Fe(III)
	1.65	3.49	--	3	Doublet, Fe(II)
	0.79		46.6	21	Sextet, Fe(III)
4.2K, He	0.73	0.99	--	41	Doublet, Fe(III)
	1.76	3.30	--	2	Doublet, Fe(II)
	0.73	--	48.0	57	Sextet, Fe(III)

Significant changes were detected when a severe calcination procedure was applied (Fe/ZSM5-17-s.c.) (Figure 5c, Tab. 3c). The detection of the sextet already at room temperature is the result of the increased average size of the Fe-containing clusters formed during the severe calcination. By lowering the temperature, the signal of the sextet increased considerably. The Fe²⁺ doublet became visible as well. As can be seen from spectrum c, at 4.2 K the dominant component is that of the sextet (HF=50.0 T). When comparing the present spectrum with spectra c recorded at 4.2 K on the washed and on the mildly calcined samples, the sextet appears enhanced and significantly sharper. This is ascribed to a higher concentration and a higher average size of the agglomerated Fe-containing phase caused by the severe calcination procedure.

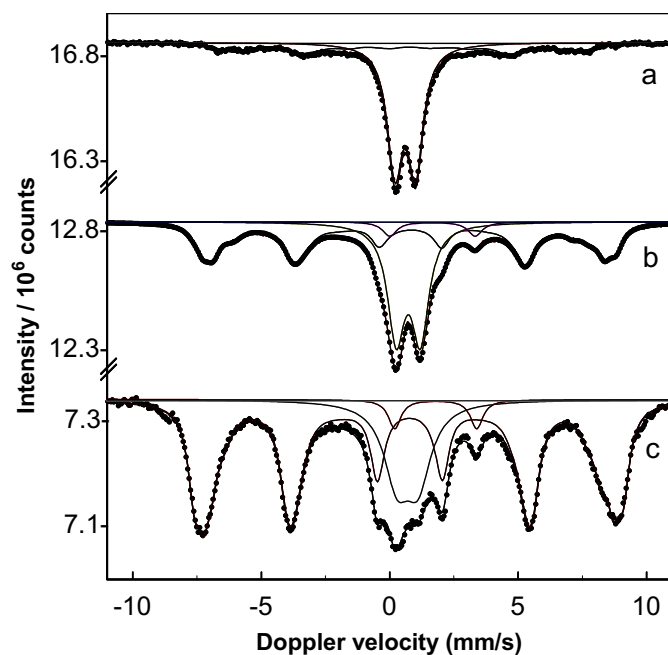


Figure 5c: ⁵⁷Fe Mössbauer spectra of Fe/ZSM5-17-s.c. recorded in He at 300K (a), 77K (b) and 4.2K (c).

Table 3c: ⁵⁷Fe Mössbauer Hyperfine Parameters and Relative Integrated Intensities of the iron species in Fe/ZSM5-17-s.c.

Conditions	Isomer Shift (mm/s)	Quadrupole Splitting (mm/s)	Hyperfine Field (T)	Relative Intensity (%)	Identification
300K, He	0.62	0.83	--	69	Doublet, Fe(III)
	0.59		40.7	31	
77K, He	0.72	0.94	--	41	Doublet, Fe(III)
	1.66	3.34	--	4	Doublet, Fe(II)
	0.75	--	48.6	55	Sextet, Fe(III)
4.2K, He	0.70	0.82	--	21	Doublet, Fe(III)
	1.79	3.19	--	4	Doublet, Fe(II)
	0.76	--	50.0	75	Sextet, Fe(III)

²⁷Al MAS NMR, Al K-edge XAFS

²⁷Al MAS NMR spectroscopy was carried out on the original zeolite provided by Zeolyst (NH₄/ZSM5-17) and on its acidic form (H/ZSM5-17) obtained by calcination. The spectra are reported in Fig. 6.

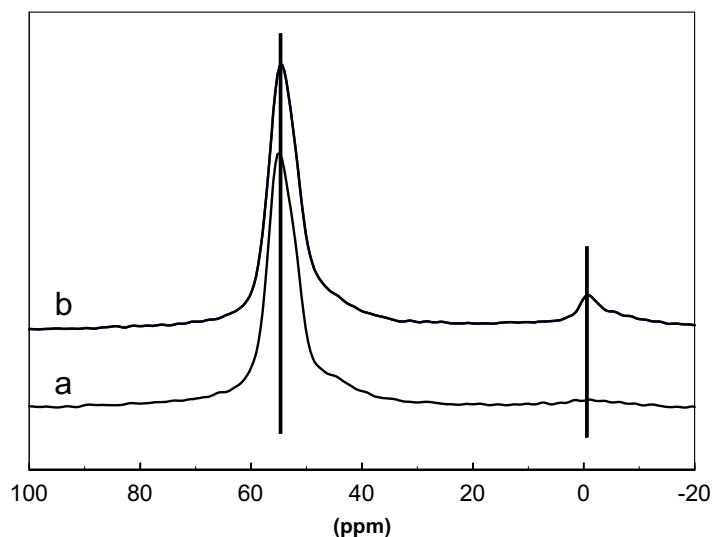


Figure 6: ²⁷Al MAS NMR spectra of NH₄/ZSM5-17 (a) and H/ZSM5-17 (b).

For both samples a dominating resonance was detected at 55 ppm, attributed to tetrahedrally coordinated framework Al atoms (52). The shape of the resonance is asymmetric. This is ascribed to variations in the chemical shift arising from the Si-O-Al angles of the different crystallographic T sites. An additional signal was recorded at 0 ppm and is assigned to octahedrally coordinated extra-framework Al. While in the NH₄/ZSM5 this peak was present as a hardly visible weak broad component, its intensity increased upon calcination to about 7% of the total aluminum. The existence of octahedrally coordinated aluminum attached to the framework has frequently been reported for acidic zeolites (53).

Al K-edge XANES spectra of the support (NH₄/ZSM5-17, H/ZSM5-17) and of the over-exchanged Fe/ZSM5-17 after severe calcination (Fe/ZSM5-17-s.c.) are depicted in Fig. 7. As can be seen in this picture, all spectra overlap, pointing to an identical aluminum coordination in all the samples. A sharp whiteline is visible, followed by a fine structure in the region 4-11 eV above the edge (1569-1576 eV). A broad peak is also present, centered

at around 20 eV above the edge (1584 eV). These features are typical of tetrahedrally coordinated aluminum (26).

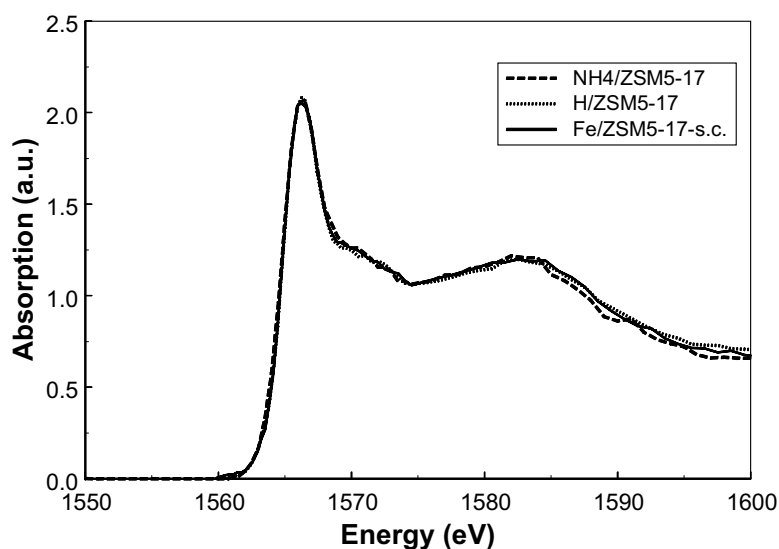


Figure 7: XAS Al K-edge spectra of NH₄/ZSM5-17, H/ZSM5-17 and Fe/ZSM5-17 s.c..

The octahedrally coordinated aluminum, measured by ²⁷Al MAS NMR in H/ZSM5-17 is not visible in the Al K-edge spectra. This is ascribed to the differences in the measurements conditions, *i.e.* high vacuum (Al XAS) versus strongly hydrated state (²⁷Al MAS NMR). When water is removed from the pores of the zeolite, only tetrahedral aluminum is present (28). From the results presented it is concluded that no significant changes occurred to the aluminum coordination during the synthesis, even after applying a severe calcination procedure.

Fe K-edge HR-XANES

Fig. 8 shows the normalized high-resolution fluorescence pre-edge spectrum of the hematite reference and its calculated deconvolution peaks. Four different contributions are visible. Peaks 1 and 2, centered respectively at 7112.65 and 7114.05 eV, are related to 1s→3d (quadrupolar) and/or 1s→4p (dipolar) metal electronic transitions (35,54,55). Contributions 3 and 4, centered above 7115.0 eV (7115.34 and 7116.88 eV), are due to extra transitions involving 3d orbitals of distant iron neighbors (35). Contributions 3 and 4 were not included in the determination of the reference pre-edge area and centroid position.

The pre-edge area and the centroid position of the hematite reference were used as standard to analyze the data of the Fe/ZSM-5 samples (34).

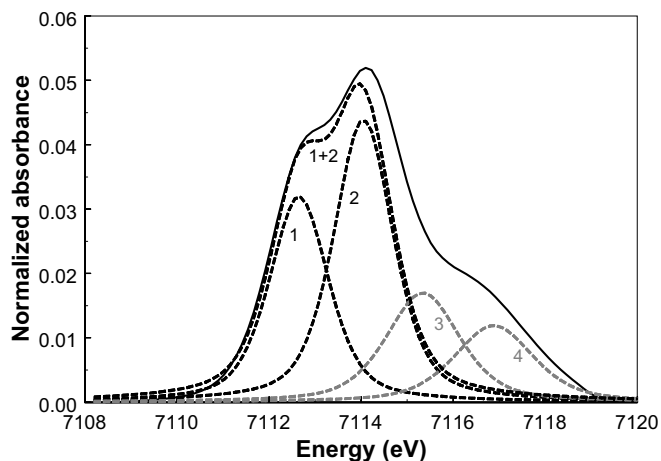


Figure 8: Normalized high-resolution fluorescence pre-edge spectrum of hematite (measured in He at 30°C, 1bar) and best deconvolution calculated with GRAMS.

In Fig. 9 the experimental normalized pre-edge spectra of the Fe/ZSM5 samples are presented together with that of hematite.

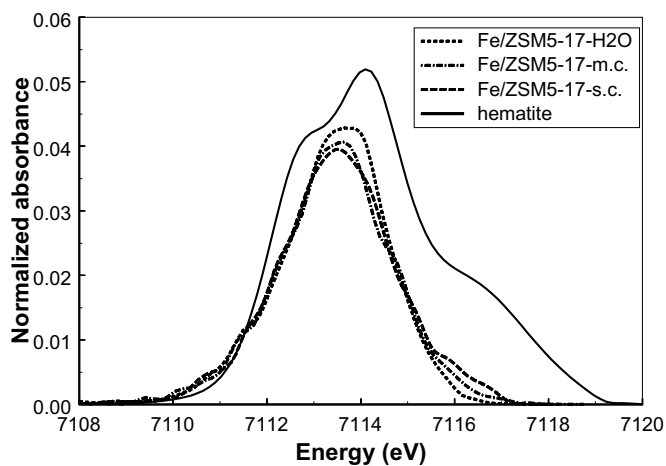


Figure 9: Normalized high-resolution fluorescence pre-edge spectra of Fe/ZSM5-17-H₂O, Fe/ZSM5-17-m.c., Fe/ZSM5-17-s.c. and hematite (measured in He at 30°C).

The Fe K pre-edges of all samples are significantly different from that of the reference oxide. They hardly show contributions centered at high energy (>7115.0 eV), ascribable to distant Fe neighbors. When comparing the pre-edges of the calcined samples (Fe/ZSM5-17-m.c. and Fe/ZSM5-17-s.c.) with that of Fe/ZSM5-17-H₂O, only minor changes are visible. After calcination the overall height appears to be slightly decreased and some tailing are visible at around 7116 eV. This contribution, more evident in the severely calcined sample (Fe/ZSM5-17-s.c.), can be attributed to agglomeration processes of iron occurred during calcination. The pre-edge features of the measured samples are collected in Table 4, together with that of averaged Fe(II) and Fe(III) reference materials with known coordination and geometry, obtained from the literature (34).

Table 4: Pre-edge characteristics of Fe/ZSM5-17-H₂O, Fe/ZSM5-17-m.c., Fe/ZSM5-17-s.c., α -Fe₂O₃, and of reference model coordinations (34).

Sample	Normalized height	Total area	Centroid position (eV)
Fe/ZSM5-17-H ₂ O	0.043	0.119	7113.41
Fe/ZSM5-17-m.c.	0.040	0.120	7113.42
Fe/ZSM5-17-s.c.	0.039	0.119	7113.48
α -Fe ₂ O ₃ *	0.049	0.138	7113.50
α -Fe ₂ O ₃	0.052	0.204	7114.29

*After subtraction of spectral contributions 3 and 4 (FIG. 8)

Reference model	Total area	Centroid position (eV)
Fe(II) in tetrahedral coordination	0.22 (± 0.02)	7112.1
Fe(II) in octahedral coordination	0.06 (± 0.02)	7112.1
Fe(III) in tetrahedral coordination	0.34 (± 0.02)	7113.5
Fe(III) in octahedral coordination	0.08 (± 0.02)	7113.5

Typically, a separation of 1.4 ± 0.1 eV is present in the pre-edge centroid position of Fe(II) (7112.1 eV) and Fe(III) (7113.5 eV) compounds, irrespective to their coordination. On the contrary, the pre-edge area is depending on both the oxidation state and the geometry of the iron coordination. As appears in Table 4, the centroid position of the pre-edges of the Fe/ZSM5 samples and of hematite corresponds, within the margin of error, to that of Fe(III) reference compounds. Furthermore, the integrated intensity of the Fe/ZSM5 pre-edges,

which appear to be lower than that of the reference hematite, is closer to that of a perfectly symmetric octahedrally coordinated reference. It is therefore concluded that in the Fe/ZSM5 measured under ambient conditions iron is present as Fe^{3+} octahedra with a slightly distorted symmetry. No significant differences in the local geometry of iron was visible upon calcination.

Fe K-edge XAFS

In Figure 10 the near edge (XANES) spectra of the Fe/ZSM5 samples, are presented, together with that of the Fe(III) hematite reference.

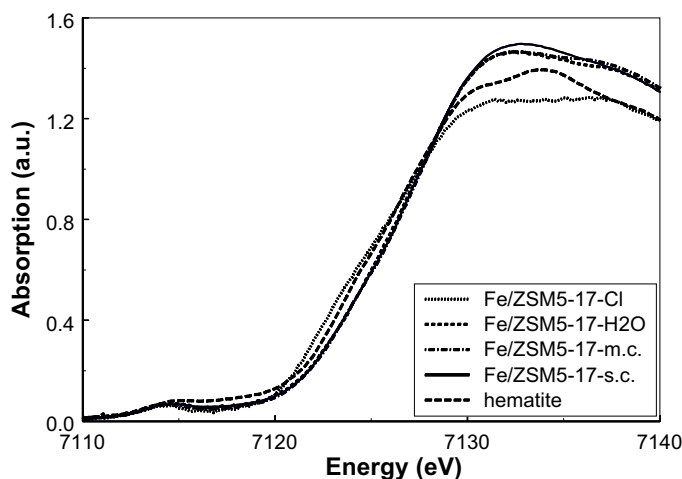


Figure 10: Normalized XANES spectra of Fe/ZSM5-17-Cl, Fe/ZSM5-17-H₂O, Fe/ZSM5-17-m.c., Fe/ZSM5-17-s.c. and hematite (measured in He at 77 K).

As can be seen, the edge position of all the Fe/ZSM5 samples, including that of Fe/ZSM5-17-Cl, corresponds to that of the reference. It is therefore concluded that, also after sublimation of FeCl_3 , the oxidation state of iron is Fe^{3+} .

Figure 11a shows the experimental EXAFS data of Fe/ZSM5-17-Cl. The corresponding k^1 Fourier Transformed spectrum (uncorrected) is depicted in Figure 11b, together with the best fit obtained.

In the Fourier spectrum one major asymmetric peak is visible at around 1.6 Å, followed by a second weak contribution at 2.5 Å. The best fit for the major peak was obtained by using two separate shells: a Fe-Cl and a closer Fe-O shell.

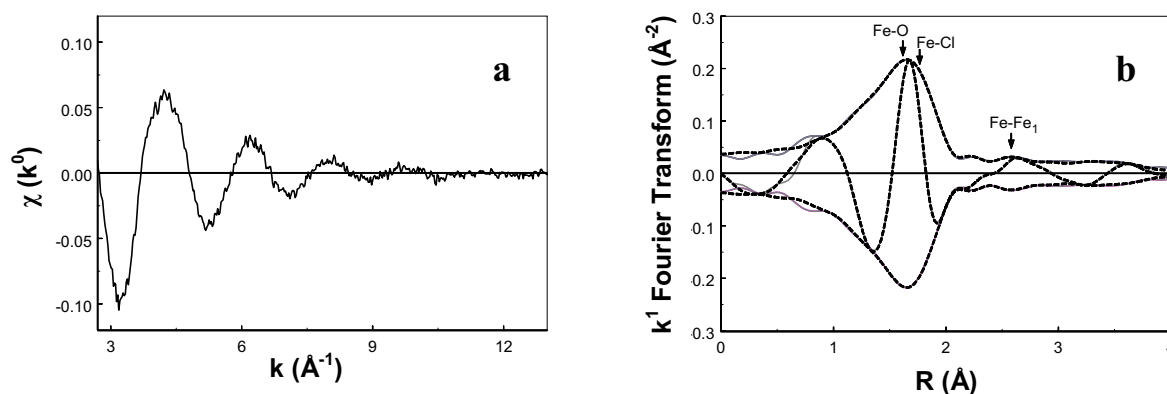


Figure 11: a) $\chi(k^0)$ experimental data of Fe/ZSM5-17-Cl, measured in He at 77 K; b) k^1 Fourier transformed experimental (gray solid line) and fitted (black dashed line, $1 < R(\text{Å}) < 4$, $\Delta k = 2.7-13.0$) data of Fe/ZSM5-17-Cl, measured in He at 77 K.

A k^3 weighing of the Fourier Transform showed that the contribution at 2.5 Å was ascribable to a heavy scatterer. Therefore this contribution was fitted with a Fe-Fe shell. The total fit was further optimized by including the contribution of distant O-neighbors, ascribable to oxygen of the zeolite lattice (Fe-O_z). The results of the EXAFS analysis are collected in Table 6 (*vide infra*). These show that upon sublimation of FeCl₃ the majority of the iron atoms in the Fe/ZSM5 consist of isolated Fe³⁺ species. These species contain on average two chlorine atoms and are bound to the zeolite via two oxygen atoms (21). The Fe-Fe contribution, however, suggests that a minor fraction of iron is present, already at this stage of the synthesis, as binuclear or oligomeric chlorinated Fe-complexes.

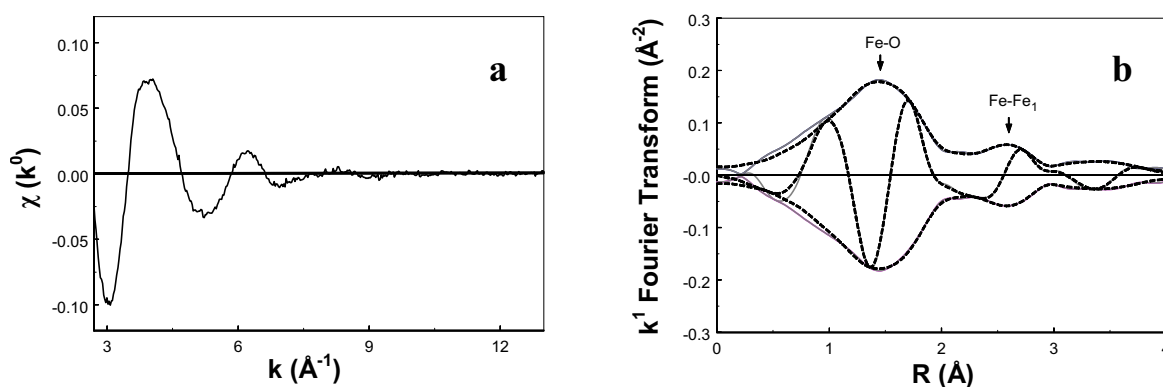


Figure 12: a) $\chi(k^0)$ experimental data of Fe/ZSM5-17-H₂O, measured in He at 77 K; b) k^1 Fourier transformed experimental (gray solid line) and fitted (black dashed line, $1 < R(\text{Å}) < 4$, $\Delta k = 2.7-13.0$) data of Fe/ZSM5-17-H₂O, measured in He at 77 K.

The EXAFS data of the Fe/ZSM5 after washing are plotted in Figure 12a. The k^1 Fourier transformation is presented together with the best total fit in Fig. 12b. A very broad peak is present in the Fourier Transform of the Fe/ZSM5-17-H₂O at 1.5 Å (\downarrow Fe-O in the picture), together with a second one at around 2.5 Å (\downarrow Fe-Fe₁). No satisfactory fit could be obtained by using a Fe-Cl contribution. The peak at 1.5 Å was therefore entirely fitted with the Fe-O reference. The results of the EXAFS analysis are shown in Table 5.

Table 5: Fits of different models obtained by multiple shells analysis of the EXAFS data from Fe/ZSM5-17-H₂O.

Shells	N ($\pm 10\%$)	R (Å) ($\pm 1\%$)	$\Delta\sigma^2$ (10^{-3} Å ²) ($\pm 5\%$)	ΔE_0 (eV) ($\pm 10\%$)	k^1 -variance (%)	
					Im. part	Abs. part
Fe/ZSM5-17-H ₂ O (model 2:4)					0.33	0.17
Fe-O ₁	2.1	1.93	6.5	12.0		
Fe-O ₂	4.0	2.03	8.7	-6.5		
Fe-Fe ₁	1.0	3.03	1.1	0.5		
Fe-O _Z	4.8	4.18	11.4	-8.8		
Fe/ZSM5-17-H ₂ O (model 2:2:2)					0.13	0.07
Fe-O ₁	1.9	1.85	0.5	7.2		
Fe-O ₂	2.0	1.99	0.1	11.1		
Fe-O ₃	2.1	2.09	3.0	-10.5		
Fe-Fe ₁	1.0	3.05	0.8	-2.5		
Fe-O _Z	4.5	4.02	9.4	-3.0		
Fe/ZSM5-17-H ₂ O (model 3:3)					0.13	0.08
Fe-O ₁	3.1	1.91	9.1	12.0		
Fe-O ₂	3.0	2.05	5.9	-8.1		
Fe-Fe ₁	1.0	3.05	0.7	-3.0		
Fe-O _Z	4.4	3.99	10.5	-1.9		

The analysis of the Fe-O contribution was performed on the basis of the information obtained by the HR-XANES experiments, *i.e.* a total amount of six oxygen neighbors was always fitted. Different possibilities for the distribution of the six oxygen neighbors were

explored, *i.e.* two separate Fe-O shells with a 2:4 or a 3:3 oxygen distribution and three separate Fe-O shells with a 2:2:2 distribution (Table 5). Even though all the models present acceptable statistics, the best fit could be obtained with the models 2:2:2 and 3:3. The second peak of the Fourier Transform (\downarrow Fe-Fe₁, Fig. 12b) could be satisfactorily fitted with one single Fe-Fe shell centered at 3.05 Å. Also for the washed sample oxygen from the lattice was fitted at higher distance (Fe-O_z). As can be seen from Table 5, in Fe/ZSM5-17-H₂O iron is organized in binuclear Fe-clusters (Fe-Fe coordination is 1.0).

Figure 13a shows the EXAFS data of the Fe/ZSM5 sample after mild calcination. The corresponding k^1 Fourier transformation is presented together with the best total fit in Fig. 13b.

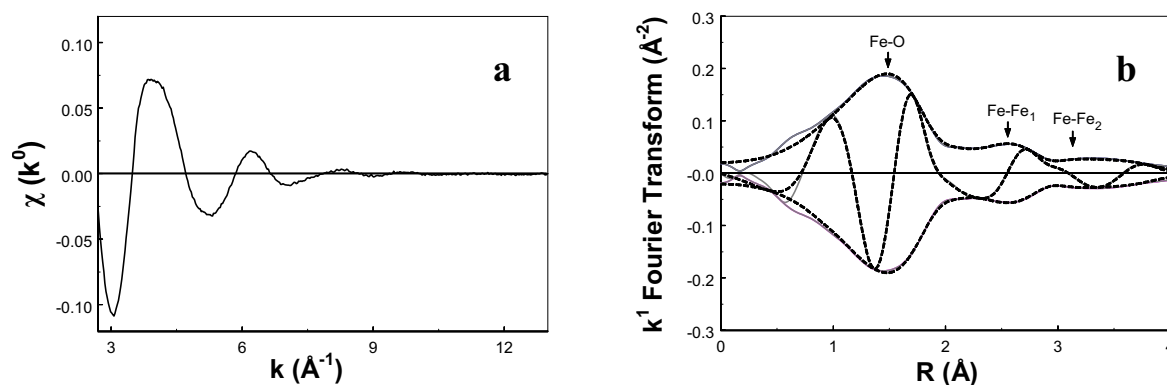


Figure 13: a) $\chi(k^0)$ experimental data of Fe/ZSM5-17-m.c., measured in He at 77 K; b) k^1 Fourier transformed experimental (gray solid line) and fitted (black dashed line, $1 < R(\text{Å}) < 4$, $\Delta k = 2.7-13.0$) data of Fe/ZSM5-17-m.c., measured in He at 77 K.

By comparing Figs 12b and 13b it is evident that the Fourier Transform of the mildly calcined sample resembles very closely that of the sample after washing. Minor changes are visible in the imaginary part of the Fourier Transformation at 3.0 Å. The same procedure used for the Fe/ZSM5-17-H₂O was applied for fitting the distribution of the oxygen atoms in this sample. Also for the mildly calcined sample the best fit could be obtained with both the 3:3 and the 2:2:2 models, *i.e.* with a symmetrical distribution of the six oxygen atoms in two or three separate Fe-O shells. The EXAFS coordination parameters for the model 3:3 (this model is chosen since it makes use of less free parameters than the 2:2:2) are summarized in Table 6. Slight changes were revealed in the Fe-Fe contribution. The use of a single Fe-Fe shell could not produce a satisfactory fit. A second shell had to be introduced (\downarrow Fe-Fe₂ in Fig. 13b). The coordination number of the Fe-Fe₁ shell is increased to 1.2.

Furthermore a second Fe-Fe shell (Fe-Fe₂) with N equal to 0.4 appears at higher distance. These changes are ascribed to further agglomeration of iron.

Table 6: Best fits obtained by multiple shells analysis of the EXAFS data: Fe/ZSM5-17-Cl, Fe/ZSM5-17-H₂O, Fe/ZSM5-17-m.c., Fe/ZSM5-17-s.c..

Shells	N (±10%)	R (Å) (±1%)	$\Delta\sigma^2$ (10^{-3} Å ²) (±5%)	ΔE_0 (eV) (±10%)	k ¹ -variance (%)	
					Im. part	Abs. part
Fe/ZSM5-17-Cl					0.08	0.04
Fe-O	1.8	1.99	-1.0	-5.9		
Fe-Cl	2.1	2.20	1.4	4.5		
Fe-Fe	0.3	2.94	0.0	8.5		
Fe-O _Z	4.4	3.97	10.5	-5.5		
Fe/ZSM5-17-H ₂ O (model 3:3)					0.13	0.08
Fe-O ₁	3.1	1.91	9.1	12.0		
Fe-O ₂	3.0	2.05	5.9	-8.1		
Fe-Fe ₁	1.0	3.05	0.7	-3.0		
Fe-O _Z	4.4	3.99	10.5	-1.9		
Fe/ZSM5-17-m.c. (model 3:3)					0.10	0.06
Fe-O ₁	3.0	1.90	9.6	12.0		
Fe-O ₂	3.1	2.04	4.3	-7.3		
Fe-Fe ₁	1.2	3.06	5.4	-3.6		
Fe-Fe ₂	0.4	3.40	10.7	-8.0		
Fe-O _Z	4.7	4.11	11.7	-6.6		
Fe/ZSM5-17-s.c. (model 3:3)					0.25	0.12
Fe-O ₁	3.0	1.90	8.1	12.0		
Fe-O ₂	3.1	2.04	6.9	-7.2		
Fe-Fe ₁	1.6	3.03	2.0	-4.3		
Fe-Fe ₂	1.3	3.42	8.5	-8.5		
Fe-O _Z	4.8	4.18	11.2	-8.9		

The statistical significance of the fitted Fe-Fe₂ shell was confirmed by the comparison between the noise level present in the experimental data with the amplitude of the chi function produced by only this contribution (Fe-Fe₂, Fig. 13c).

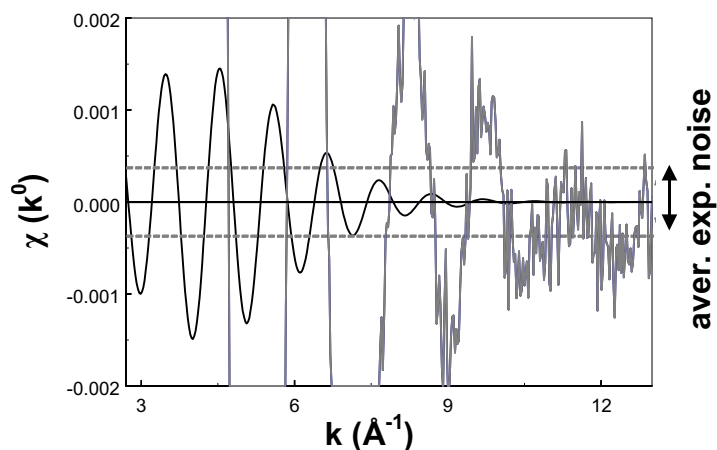


Figure 13c: Comparison between the average noise level in the experimental data of Fe/ZSM5-17-m.c. (see Fig. 13a) and the amplitude of the fitted Fe-Fe₂ contribution (see Table 6); fitted Fe-Fe₂ $\chi(k^0)$ (black solid line) and experimental Fe/ZSM5-17-m.c. $\chi(k^0)$ (gray solid line).

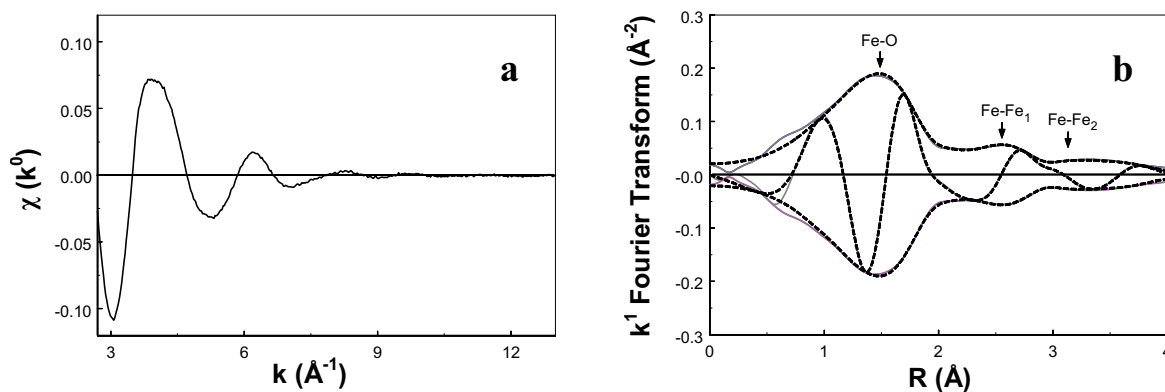


Figure 14: a) $\chi(k^0)$ experimental data of Fe/ZSM5-17-s.c., measured in He at 77 K; b) k^1 Fourier transformed experimental (gray solid line) and fitted (black dashed line, $1 < R(\text{\AA}) < 4$, $\Delta k = 2.7-13.0$) data of Fe/ZSM5-17-s.c., measured in He at 77 K.

The EXAFS data of the Fe/ZSM5-s.c. are displayed in Figure 14a. The k^1 Fourier transformation and the best total fit obtained are presented in Fig. 14b. The large Fe-O peak at 1.5 Å does not show any differences when compared to the corresponding one in the washed and the mild calcined samples. On the opposite, significant changes are visible in both the real and the imaginary part of the Fe-Fe shells. For an easier comparison the Fourier Transforms of the washed and of the differently calcined samples are presented together in Fig. 15.

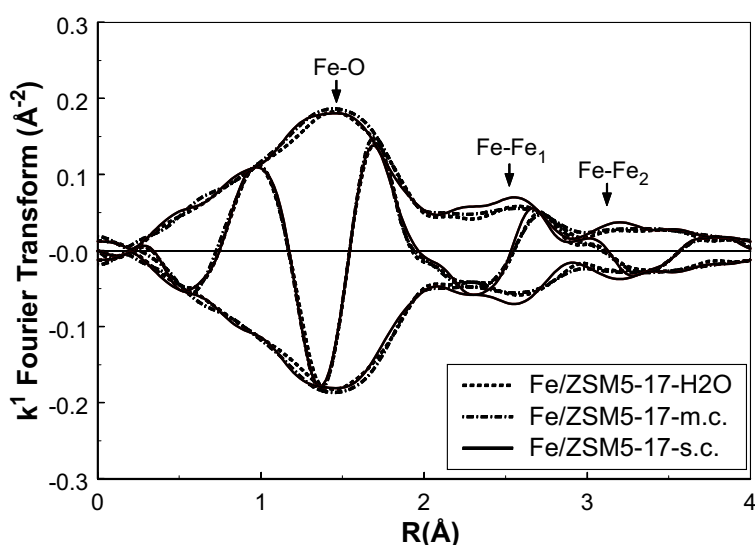


Figure 15: k^1 Fourier transformed experimental EXAFS data of Fe/ZSM5-17-H₂O, Fe/ZSM5-17-m.c. and Fe/ZSM5-17-s.c., measured in He at 77 K ($\Delta k=2.7-13.0$).

On the Fe/ZSM5 sample upon severe calcination an increase is clearly visible in the intensity of the real part of the Fe-Fe₁ shell, together with a minor shift of the imaginary part towards a shorter distance. At the same time, the contribution of the second Fe-Fe shell (Fe-Fe₂) becomes significantly better resolved and increased in intensity as well. The EXAFS coordination parameters for model 3:3 are collected in Table 6.

The increase of the Fe-Fe coordination numbers of both Fe-Fe shells after severe calcination is consistent with a significant formation of Fe clusters after severe calcination. Nevertheless, clear differences are still present in the local coordination of iron between the severely calcined sample and the hematite reference (Fig. 16).

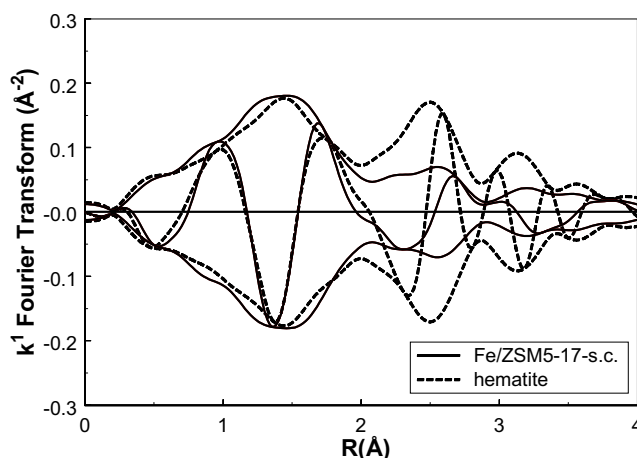


Figure 16: k^1 Fourier transformed experimental EXAFS data of Fe/ZSM5-17-s.c. and α -Fe₂O₃, measured in He at 77 K ($\Delta k=2.7-13.0$).

Discussion

Sublimation of FeCl₃

The EXAFS fit of the sample after FeCl₃ sublimation revealed that the majority of the Fe-species formed upon reaction with the Brønsted sites are mononuclear (Table 6) (21). They consist of isolated tetrahedral Fe³⁺, attached to the zeolite matrix via two oxygen atoms located at the same distance. The charge of iron is further balanced by two chlorine atoms. The detection of a minor Fe-Fe scattering (Fe-Fe, N=0.3), can be ascribed to the presence, already at this stage of the synthesis, of Fe-binuclear clusters or Fe-species with a higher nuclearity. The presence of such species was revealed by an *in situ* ESR study by Kucherov and Shelef on Fe/ZSM5 samples (obtained by sublimation) exceeding a Fe/Al ratio of 0.6 (23). Also the presence of weakly bound FeCl₃ located on the external surface of the zeolite can not be ruled out (21).

Washing

As already pointed out by Marturano *et al.* (21), washing was proved to be the key step for the formation of the binuclear Fe-complexes, proposed as the catalytically active phase in Fe/ZSM5 (1,2,12,18). It can be concluded from our work that during this step dramatic changes occur to the local environment of the Fe atoms. While the oxidation state of iron remained unchanged (Fe³⁺), as appears from the centroid position of the HR-XANES Fe K pre-edge (Table 4) and from the near edge region of the XAFS spectra (Fig. 10), the geometry turned from tetrahedral to octahedral. Since the integrated intensity of the pre-

edge peak of the Fe/ZSM5-17-H₂O sample is lower than that of the hematite reference, it is concluded that the octahedral configuration of iron in the Fe/ZSM5 after washing possesses a higher degree of symmetry than that in hematite (34). The high dispersion of the Fe phase is underlined by the complete absence of pre-edge spectral contributions centered above 7115.0 eV. Their presence, reported in the literature to increase with the degree of Fe(O,OH)₆-octahedral polymerization (ferrihydrite<goethite<hematite) (34,35), is, on the contrary, clearly visible in the pre-edge peak of the measured hematite (Figs. 8 and 9).

The removal of chlorine from the Fe local surrounding appeared clearly from the EXAFS results. The washing step must also be responsible for the displacement of part of the isolated mononuclear species and their subsequent re-stabilization to the Al of the framework to form Fe-binuclear clusters. This observation is in agreement with the partial regain of the intensity of the Brønsted Al-OH vibrations (Fig. 1). From the I.R. it can also be deduced that the formed binuclear iron species are not bound at the silanols position, since the Si-OH groups appeared to be completely restored after washing.

The Mössbauer spectra exclude the presence in our washed sample of a significant fraction of isolated mono-atomic Fe-species (Fig. 5a). The present of such species at this stage of the synthesis was suggested by Marturano *et al.* (21) in order to explain an EXAFS Fe-Fe coordination number lower than one (0.5) as found in the analysis of their EXAFS data. Our EXAFS data-analysis, on the contrary, shows a Fe-Fe coordination number of 1.0 (Table 5). The combination of the Mössbauer and EXAFS results obtained in this work proves that the coordination number of 1.0 found for the Fe-Fe shell is not the result of an average between mononuclear Fe-species and Fe-polycations.

The Mössbauer result, on the other hand, suggest a possible underestimation in the coordination number of the Fe-Fe₁ shell obtained by the EXAFS fit. Indeed, some agglomeration of Fe was revealed by the Mössbauer spectrum collected from the washed Fe/ZSM5 sample at 4.2 K (Fig. 5a, Tab. 3a) (51). The broad width of the sextet suggests the coexistence of Fe species with different nuclearity (average size of 2 nm). Since no Fe-Fe contribution could be fitted by EXAFS at high distances, typical of a three dimensional polymerization (56,57), it is concluded that the agglomerated Fe-containing phase must consist also of linear oligomers located in the zeolite micropores. The homogeneity of the distribution of iron within the zeolite crystals was confirmed by EELS (Figs. 3b and 4) and by HR-TEM (Fig. 2a). In particular, no gradient in the iron concentration was detected when approaching the crystal surface (note that the local concentration of iron measured by EELS was found to be consistent with the bulk ICP results) and no particles could be detected on the external surface of the zeolite.

The structure of the binuclear Fe-complexes formed upon washing can be determined by comparing the Fe-O and Fe-Fe coordination numbers and interatomic distances in Fe/ZSM5-17-H₂O with those of α -goethite and hematite, as obtained from XRD data (58,59) (see Table 7). As can be seen, the structural parameters obtained for Fe/ZSM5-17-H₂O with the 3:3 and the 2:2:2 fit models (Table 5) correspond to those of the closest Fe-Fe binuclear building block in α -goethite. In this unit, two iron atoms are symmetrically connected via two hydroxyl groups.

Table 7: Fe-O and Fe-Fe atomic distances and coordination numbers in α -goethite and hematite from X-ray diffraction data (57,58).

Shells	Closest Fe-Fe binuclear unit in α -goethite		α -goethite		hematite	
	R (Å)	C.N.	R (Å)	C.N.	R (Å)	C.N.
Fe-O ₁	1.95	3	1.95	3	1.96	3
Fe-O ₂	2.09	3	2.09	3	2.12	3
Fe-Fe ₁	3.02	1	3.02	2	2.95	4
Fe-Fe ₂	--	--	3.28	2	3.36	3
Fe-Fe ₃	--	--	3.46	4	3.74	7

The formation of highly dispersed binuclear complexes is coherent with the hydrolysis process known for FeCl₃ in aqueous solution. This starts via the formation of a hexaaqua ion [(Fe(OH₂)₆)³⁺], which is stable only in strongly acidic media ([H⁺ > 6M]) due to a strong tendency towards hydrolytic polymerization (56,57). At higher pH, a condition that is certainly encountered during the extensive washing of the zeolite, the formation of a dimer represents the first step prior to condensation to large polycations and possible precipitation as α -goethite or hematite (56,57,60-62). The extremely important role of the zeolitic support is indeed to prevent the thermodynamically favored iron condensation. This must be obtained by an immediate stabilization via the lattice charge of the nascent Fe binuclear complexes, which blocks their possible further migration and aggregation. A decisive role in this respect is most probably played also by the steric hindrance encountered by the iron species in the narrow micropores of the ZSM5. The question which still has to be answered

is whether the zeolite is able to prevent further migration and polymerization of the Fe binuclear complexes also during the subsequent calcination step.

Calcination

In order to investigate the stability of the Fe binuclear complexes two different calcination procedures were applied, *i.e.* a mild and a severe calcination. In both cases the final temperature (550°C) was maintained for three hours. While the severe calcination procedure reproduces conditions typical of a standard calcination, the mild calcination procedure was specially aimed to prevent metal clustering. A similar procedure was successfully applied by de Graaf. *et al.* in order to prevent agglomeration of Pt particles in zeolite Y (63). Mild calcination was obtained by coupling a high gas-flow with a moderate temperature ramp. As a result, the highest possible quantity of moisture was removed from the zeolite at relatively low temperature, strongly suppressing the migration of hydrolyzed species and the resulting clustering.

Since the XRD patterns recorded after both types of calcination were identical to the one measured from the parent H/ZSM5 support, it is concluded that no damage occurred to the framework of the zeolite during these treatments. This observation is supported by the combination of the Al-XAFS and the Al-NMR results. Al-NMR showed that in the parent support around 93% of the Al atoms were arranged in tetrahedral coordination into the zeolite framework (Fig. 6). This result was confirmed by the Al K XANES data, recorded from the same support (Fig. 7). Since no differences were visible between the Al K XANES spectrum of H-ZSM5-17 and Fe/ZSM5-17-s.c. (Fig. 7), it is concluded that no large formation of extra-framework (octahedral) aluminum occurred during the synthesis, not even upon application of the most severe calcination procedure. No significant changes were visible in the I.R. spectra of the Fe/ZSM5 upon calcination as well (Fig. 1). The intensity of the silanol and of the Al Brønsted signal appeared to be similar to that of the washed sample. This indicates that, even after calcination, a significant fraction of iron was still bound to the zeolite framework. Nevertheless, differences in the broadening of the silanol and of the Al Brønsted bands make a quantitative comparison between washed and calcined samples not possible.

While the above mentioned results underline the stability of the support during the synthesis and the pretreatment of the Fe/ZSM5 catalysts, the effects of the different calcination procedures on the agglomeration of iron appear very clearly from the results of the macro- and microscopic characterization techniques. In the Mössbauer spectra of the severely calcined sample (Fig. 5c), sextet lines are visible at all temperatures. This is a clear indication of the presence of large particles with a size distribution from 2 to over 10 nm.

The presence of this sextet, on the contrary, appeared to be significantly lower when the mild calcination was applied (Fig. 5b). The fact that for mild calcination the onset of the magnetically split components occurred only at 77 K accounts for a significantly smaller average dimension of the agglomerated phase. Furthermore, the very large width of these asymmetrically broadened sextet lines reflects the poor crystallinity of the agglomerated phase after mild calcination.

The differences in the abundance, degree of crystallinity and dimension between the Fe-containing particles of the two samples was confirmed by TEM (Figs. 2b, 2c, 2d). While on the severely calcined Fe/ZSM5 Fe-rich particles were easily detected (Fig. 2c), they were difficult to identify after mild calcination, even at the maximum possible magnification. On Fe/ZSM5-17-m.c. Fe-containing particles were very low in number and degree of crystallinity, appearing as few and poorly defined darker spots. Their richness in iron was confirmed by local EDX elemental analysis. For the few visible Fe-containing crystals on the mildly calcined sample the best match of the d-spacings was obtained with crystalline α -goethite and possibly hematite. On the severely calcined sample, together with α -goethite, hematite crystals were clearly visible (see also Figs. 3e, 3f and 4). This finding is coherent with the expected evolution of Fe metastable hydroxylated species. In the internal volume of the zeolite polymerization processes are hindered by both the unbalanced charge of the framework and the narrow dimensions of the zeolite pores. But, once iron is transported to the external surface, the agglomeration can proceed to the formation of the most thermodynamically stable structures, *i.e.* α -goethite and, finally, hematite (56,57,60-62,64).

Part of iron was removed from the internal volume of the zeolites to the external surface after calcination. This was confirmed by the EELS measurements (Figs. 3d, 3f and 4). While no significant change was measured in the micropore volume of the Fe/ZSM5 upon mild calcination, some regain in the internal volume was indeed detected after applying the severe procedure. The migration of iron towards the external surface of the crystals is clearly depicted in Fig. 3d. The edges of the crystal of the Fe/ZSM5-17-m.c. are clearly enriched in iron when compared to the internal region. Nevertheless, no clear aggregation in form of particles is detectable yet. On the severely calcined sample, on the other hand, large particles are visible.

HR-XANES demonstrated that the oxidation state and the geometry of the local coordination of iron did not change upon calcination (Fig. 9, Tab. 4). Independently of the calcination procedure, Fe is present in octahedra with an oxidation state of 3+. Some small tailing appeared in the Fe K-pre-edges after calcination at energies above 7115.0 eV. This

contribution, which is more pronounced in the severely calcined sample, is ascribed to the presence of three-dimensional polymerization of part of iron (34,35).

The Fourier Transform of the EXAFS data of Fe/ZSM5 after mild calcination appears to be similar to that of the sample after washing (Fig.15). This indicates that the agglomeration phenomena involved only a minor fraction of iron. An additional shell ($\downarrow\text{Fe-Fe}_2$) with a low coordination number ($N=0.4$) had to be introduced for optimizing the fitting of the Fe-Fe scattering. Contemporarily, the coordination number of the first iron shell ($\downarrow\text{Fe-Fe}_1$) appeared to be only slightly increased (+20%), when compared to the sample measured after washing. The increase in the Fe-Fe₁ shell, whose distance is typical of edge-sharing octahedrally coordinated iron neighbors, can be ascribed to the additional formation of linear oligomers. As can be seen from Table 7 this shell (Fe-Fe₁) is present in α -goethite with a coordination number of 2. Also the distance of the second iron shell in Fe/ZSM5-17-m.c. (Fe-Fe₂, 3.40 Å) appears to match that obtained by the average of the external shells in α -goethite (Fe-Fe₂ and Fe-Fe₃ in Table 7). These shells are due to the presence in the goethite structure of corner sharing octahedrally coordinated Fe units. The appearance of this second shell in the Fourier Transform of the mildly calcined Fe/ZSM5, therefore, can be attributed to the incipient formation of lowly agglomerated iron hydroxide particles, which can end up in the crystallization of α -goethite particles. It should be noted that the results of the fit are coherent with the presence of α -goethite crystallites revealed by HR-TEM. The small changes in coordination numbers of the Fe-Fe shells, nevertheless, suggest that a significant fraction of iron must still exist in the form of binuclear complexes. From the coordination number of the Fe-Fe shells (Table 6) binuclear clusters in Fe/ZSM5-17-m.c. are estimated to account for around 70% of the total iron amount. It should be noted, nevertheless, that this value appears to be overestimated, when compared with the results obtained by Mössbauer spectroscopy (Table 3b), which reveals that after mild calcination binuclear complexes can not account for more than 40% of iron.

Much more clear changes were revealed in the EXAFS Fourier Transform of the severely calcined sample (Fig. 15). The intensity of the two Fe-Fe shells appeared to be enhanced. This is reflected in the increment of the coordination numbers of both the Fe-Fe₁ and the Fe-Fe₂ shell to respectively 1.6 and 1.3 (Table 6). This simultaneous increase is the result of the formation of large α -goethite and hematite crystals, as was indeed detected by HR-TEM and EELS. These particles were formed at the expense of iron located in the zeolite channels. From the EXAFS fit the amount of binuclear Fe-clusters after the severe calcination is estimated to be around 40% of the total iron quantity. As can be seen in Fig. 16 the k^1 Fourier Transform of the Fe/ZSM5-17-s.c. is still very different from that of the hematite reference. This is ascribed to the very broad distribution in particle size and in the

low degree of crystallinity of the aggregated phases. Also for this sample a lower presence of Fe-binuclear species, when compared to the EXAFS results, is suggested by Mössbauer spectroscopy (less than 20% of iron).

While clear changes were revealed by EXAFS in the Fe-Fe coordination of the Fe/ZSM5 as a function of the calcination procedure, the Fe-O coordination remained unchanged (Table 6). This result underlines the similarity, under the experimental conditions applied, in the oxygen distribution around iron in the Fe binuclear complexes (prior to and after calcination) and in the building blocks of the agglomerated phase. All the Fe/ZSM5 samples (with the exception of the Fe/ZSM5-17-Cl) were pretreated with He at 30°C after being exposed to air. Humidity could have been responsible for rehydration of the Fe binuclear complexes in the calcined Fe/ZSM5, veiling differences with the washed sample. This could be the reason for the differences between the results obtained in this study and those presented on the calcined Fe/ZSM5 by Marturano *et al.* (21). In their EXAFS study a calcined Fe/ZSM5 sample was measured after flushing He at 400°C. The reactivity of oxygen in Fe/ZSM5 will be discussed by our group in detail elsewhere (65).

It should be noted that the results of the EXAFS fitting presented in this work for the sample Fe/ZSM5-17-s.c. (Table 6) are different from those presented by our group on the same sample in a previous report (19). Significant differences are present in the results of the fitting of both the Fe-O and the Fe-Fe contributions. The high-resolution XANES data of the severely calcined samples used in this study prove that under ambient conditions the local coordination of Fe is octahedral. The tetrahedral geometry found in the previous study could be the result of dehydration phenomena occurring during the pretreatment applied to Fe/ZSM5 samples prior to the XAFS measurement (He, 150°C (in Ref. 19) versus He, 30°C (in this study). The differences in the Fe-Fe fit, on the other hand, is clearly due to the underestimated R fit range ($1.0 < R(\text{Å}) < 3.0$) used in the previous study. As a consequence, the contribution of more distant iron, indeed present in the Fourier transformed signal at 3.2 Å, was overlooked. In this study the significantly improved quality of the EXAFS data allowed statistically more reliable fits in a wider R range $1.0 < R(\text{Å}) < 4.0$ by using up to five different shells.

The results presented in this study are summarized in a scheme presented in Figs. 17 a,b,c. The scheme combines the evolution along the synthesis of the Fe species, with a description of the migration and agglomeration phenomena occurring to iron at a macroscopic scale.

Sublimation of FeCl₃

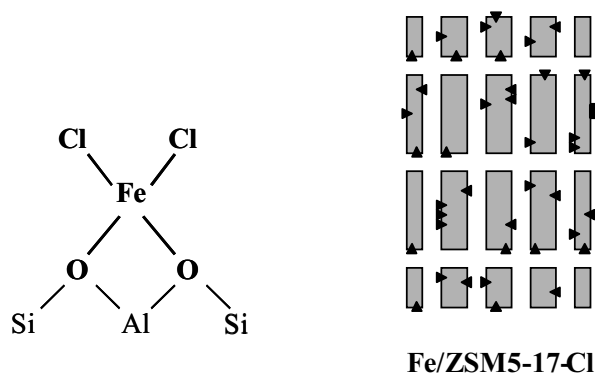


Figure 17a: Fe-species in over-exchanged Fe/ZSM5 after FeCl₃ sublimation: Fe-monomers at Al-Brønsted sites position (▼, see proposed structure); minor presence of Fe-linear oligomers (▼▼▼) and/or FeCl₃ (■).

Washing

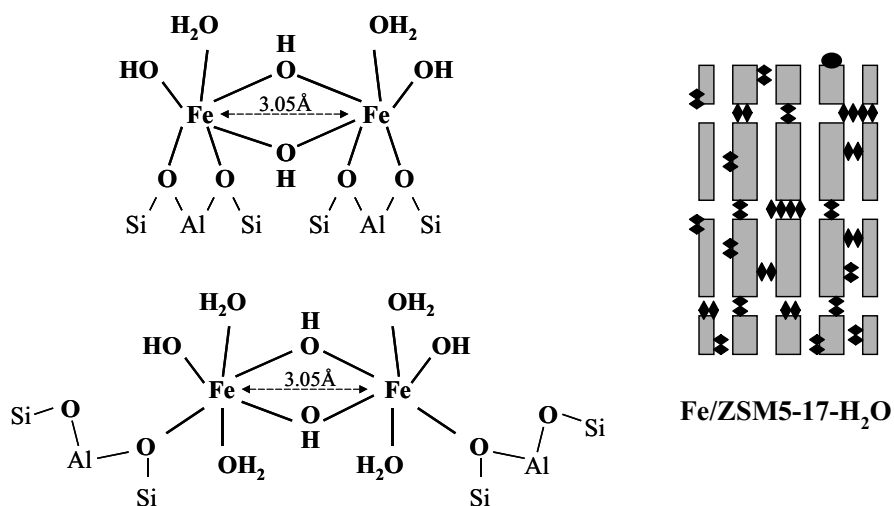
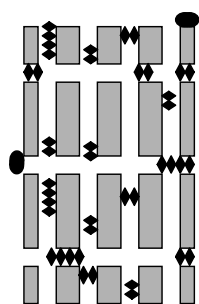
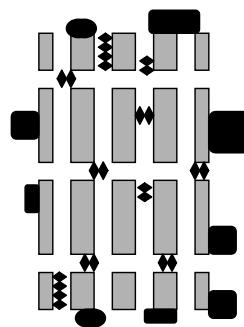


Figure 17b: Fe-species in over-exchanged Fe/ZSM5 after washing: binuclear Fe-oxo/hydroxo complexes (◆◆, see proposed structures); minor presence of linear Fe-oxo/hydroxo oligomers (◆◆◆◆) and amorphous Fe-oxidic nanoparticles (●).

Mild calcination vs. Severe calcination



Fe/ZSM5-17-m.c.



Fe/ZSM5-17-s.c.

Figure 17c: Fe-species in over-exchanged Fe/ZSM5 after different calcination procedures.

After mild calcination: binuclear Fe-oxo/hydroxo complexes (\blacklozenge); linear Fe-oxo/hydroxo oligomers ($\blacklozenge\blacklozenge\blacklozenge$); amorphous Fe-oxidic nanoparticles and infrequent goethite (possibly also hematite) crystallites (\bullet).

After severe calcination: hematite and α -goethite crystals (\blacksquare); Fe-oxidic amorphous nanoparticles (\bullet); linear Fe-oxo/hydroxo oligomers ($\blacklozenge\blacklozenge\blacklozenge$); binuclear Fe-oxo/hydroxo complexes (\blacklozenge).

Conclusions

After FeCl₃ CVD iron is stabilized by the ZSM5 matrix in the form of isolated mononuclear complexes located at the Brønsted sites position. These iron complexes consist of tetrahedrally coordinated Fe³⁺ bound to the framework via two oxygens and further surrounded by two chlorine atoms. The presence at this stage of a minor fraction of binuclear chlorinated Fe-complexes or Fe species with a higher nuclearity is suggested by EXAFS.

During the washing treatment mononuclear iron species are displaced and subsequently stabilized to the framework in the form of octahedrally coordinated binuclear Fe-complexes. The structure of the binuclear complexes, determined by EXAFS, resembles very closely that of the closest binuclear building blocks in α -goethite, *i.e.* they consist of

two edge-sharing octahedrally coordinated Fe atoms. The presence, after washing, of monomeric Fe-species is ruled out.

As expected, calcination results in aggregation of iron, removed from the Brønsted sites. Applying a severe calcination results in significant migration of iron to the external surface of the zeolite, where it further aggregates to form abundant and clearly visible α -goethite and hematite crystals. Oligomers and amorphous nano-particles are also formed within the zeolite micropores. The extent of this aggregation can nevertheless be limited by adequately tuning the conditions of the calcination.

Reference list

1. Chen, H.-Y., and Sachtler, W.M.H., *Catal. Today* **42**, 73 (1998).
2. Chen, H.-Y., Voskoboinikov, T., and Sachtler, W.M.H., *J. Catal.* **180**, 171 (1998).
3. Chen, H.-Y., Voskoboinikov, T., and Sachtler, W.M.H., *Catal. Today* **54**, 483 (1999).
4. Long, R.Q., and Yang, R.T., *J. Am. Chem. Soc.* **121**, 5595 (1999).
5. Ma, A.-Z., and Grünert, W., *Chem. Commun.* 71 (1999).
6. Sun, Q., Gao, Z.-H., Chen, H.-Y., and Sachtler, W.M.H., *J. Catal.* **201**, 89 (2001).
7. El-Malki, E.-M., van Santen, R.A., and Sachtler, W.M.H., *J. Catal.* **196**, 212 (2000).
8. Feng, X., and Hall, W.K., *J. Catal.* **166**, 368 (1997).
9. Kögel, M., Sandoval, V.H., Schwieger, W., Tissler, A., and Turek, T., *Catal. Lett.* **51**, 23 (1998).
10. Joyner, R., and Stockenhuber, M., *J. Phys. Chem. B* **103**, 5963 (1999).
11. Lobree, L.J., Hwang, I.-C., Reimer, J.A., and Bell, A.T., *J. Catal.* **186**, 242 (1999).
12. El-Malki, E.-M., van Santen, R.A., and Sachtler, W.M.H., *J. Catal.* **196**, 212 (2000).
13. Heinrich, F., Schmidt, C., Löffler, E., and Grünert, W., *Catal. Comm.* **2**, 317 (2001).
14. Kögel, M., Mönnig, R., Schwieger, W., Tissler, A., and Turek, T., *J. Catal.* **182**, 470 (1999)
15. Rauscher, M., Kesore, K., Mönnig, R., Schwieger, W., Tißler, A., and Turek, T., *Appl. Catal. A* **184**, 249 (1999).
16. Hall, W.K., Feng, X., Dumesic, J., and Watwe, R., *Catal. Lett.* **52**, 13 (1998).
17. Marturano, P., Kogelbauer, A., and Prins, R., *J. Catal.* **190**, 460 (2000).
18. Chen, H.-Y., El-Malki, E.-M., Wang, X., van Santen, R.A., and Sachtler, W.M.H., *J. Molec. Catal. A* **162**, 159 (2000).
19. Battiston, A.A., Bitter J.H., and Koningsberger, D.C., *Catal. Lett.* **66**, 75 (2000).
20. Marturano, P., Drozdová, L., Kogelbauer, A., and Prins, R., *J. Catal.* **192**, 236 (2000).

21. Marturano, P., Drozdová, L., Pirngruber, G.D., Kogelbauer, A., and Prins, R., *Phys. Chem. Chem. Phys.* **3**, 5585 (2001).
22. Voskoboinikov, T., Chen, H.-Y., and Sachtler, W.M.H., *J. Molec. Catal. A* **155**, 155 (2000).
23. Kucherov, A.V., and Shelef, M., *J. Catal* **195**, 106 (2000).
24. Jeanguillaume, C., and Colliex, C., *Ultramicroscopy* **28**, 252 (1989).
25. Colliex, C., Tencé, M., Lefèvre, E., Mory, C., Gu, H., Bouchet, D., and Jeanguillaume, C., *Mikrochim. Acta* **71**, 114 (1994).
26. van Bokhoven, J.A., Sambe, H., Ramaker, D.E., and Koningsberger, D.C., *J. Phys. Chem B* **103** (36), 7557 (1999).
27. van Bokhoven, J. A., van der Eerden, A. M. J., Smith, A. D., and Koningsberger, D. C., *J. Synchrotron Rad.*, **6**, 201 (1999).
28. van der Eerden, A. M. J., van Bokhoven, J. A., Smith, A, and Koningsberger, D.C. *Rev. Sci. Instrum.* **71-9**, 3260 (2000).
29. Sette, F., Ruocco, G., Krisch, M., Bergmann, U., Masciovecchio, C., Mazzacurati, V., Signorelli, G., and Verbeni, R., *Phys. Rev. Lett.* **75**, 850 (1995).
30. Hämmäläinen, K., Siddons, D.P., Hastings, J.B., and Berman, L.E., *Phys. Rev. Lett.* **67**, 2850 (1991).
31. de Groot, F.M.F., Pizzini, S., Fontaine, A., Hämmäläinen, K., Kao, C.C., and Hastings, J.B., *Phys. Rev. B* **51**, 1045 (1995).
32. Vaarkamp, M., Mojet, B.L., Modica, F.S., Miller, J.T., and Koningsberger, D.C., *J. Phys. Chem.* **99**, 16067 (1995).
33. Schroeder, S.L.M., *Adv. Spectroscopy* **26**, 1 (1998).
34. Wilke, M., Farges, F., Petit P.-E., Brown, G.E.Jr., and Martin, F., *Am. Miner.* **86**, 714 (2001).
35. Dräger, G., Frahm, R., Materlik G., and Brummer, O., *Phys. Stat. Sol. B* **146**, 287 (1988).
36. Vaarkamp, M., Linders, J.C., and Koningsberger, D.C., *Physica B*, **209** (1995).
37. Vaarkamp, M., Dring, I., Oldman, R.J., Stern, E.A., and Koningsberger, D.C., *Phys. Rev. B* **50**, 7872 (1994).
38. Koningsberger, D.C., Mojet, B.L., van Dorssen, G.E., and Ramaker, D.E., *Top. Catal.* **10**, 143 (2000).
39. Cook, J.W., and Sayers, D.E., *J. Appl. Phys.* **52**, 5024 (1981).
40. Iball, J., and Morgan, C.H., *Acta Cryst.* **23**, 239 (1967).
41. Ankudinov, A.L., and Rehr, J.J., *Phys. Rev. B* **56**, R1712 (1997).
42. Blake, R.L., Hessevick, R.E., Zoltai, T., and Finger, L.W., *Am. Miner.* **51**, 123 (1966).

43. Lind, M.D., *J. Chem. Phys.* **47** (3), 990 (1967).
44. Koningsberger, D.C., *Jpn. J. Appl. Phys.* **32**, 877 (1993).
45. Li, G.G., Bridges, F., and Booth C.H., *Phys. Rev. B* **52**, 6332 (1995).
46. Bordiga, S., Platero E.E., Arean, C.O., Lamberti, C., and Zecchina A., *J. Catal.* **137**, 179 (1992).
47. Woolery, G.L., Alemany, L.B., Dessau, R.M., and Chesler, A.W., *Zeolites* **6**, 14 (1986).
48. Kustov, L.M., Kazansky, V.B., Beran, S., Kubelkova, L., and Jiru, P., *J. Phys. Chem.* **91**, 5247 (1987).
49. Zecchina A., Bordiga S., Spoto, G., Scarano, D., Petrini D., Leofanti, G., Padovan M., and Otero Areàn, C.J., *J. Chem. Soc. Faraday Trans.* **88**, 2959 (1992).
50. "Powder Diffraction File 2000", International Centre for Diffraction data, USA, (2000).
51. Mørup, S., *Hyperfine Interactions* **60**, 959 (1990).
52. Engelhardt, G., and Michel, D., "High-Resolution Solid-State NMR of silicates and zeolites" Wiley, New York, (1987).
53. Bourgeat-Lami, E., Massiani, P., Di Renzo, F., Espiau, P., Fajula, F., and Des Courières, T., *Appl. Catal.* **72**, 139 (1991).
54. Heumann, D., Dräger, G., and Bocharov, S., *J. Physique IV*, **7C2**, 481, (1997).
55. Westre, T.E., Kennepohl, P., de Witt, J., Hedman, B., Hogson, K.O., and Solomon, E.I., *J. Am. Chem. Soc.* **119**, 6297 (1997).
56. Richens, D.T., "The chemistry of aqua ions", Wiley, New York, (1997).
57. Jolivet, J.-P., "Metal Oxide Chemistry and Synthesis", Wiley, New York, (2000).
58. Suzuki, S., Suzuki, T., Kimura, M., Takagi, Y., Shinoda, K., Tohji, K., and Waseda, Y., *App. Surf. Science* **169-170**, 109 (2001).
59. Rustad, J.R., Felmy, A.R., and Hay, B.P., *Geochim. Cosmochim. Acta* **90**, 1553 (1996).
60. Sylva, R.N., *Pure. Appl. Chem.* **22**, 115 (1972).
61. Flynn, C.M., *Chem Rev.* **84**, 31 (1984).
62. Cornell, L.M., Giovanoli, R., and Schneider, W., *J. Chem. Tech. Biotechnol.* **46**, 115 (1989).
63. de Graaf, J., van Dillen, A.J., de Jong, K.P., and Koningsberger, D.C., *J. Catal.* **203**, 307 (2001).
64. Music, S., Czakó-Nagy, I., Salaj-Obelic, I., and Ljubešić, N., *Mater. Lett.* **32**, 301 (1997).
65. Chapter 3 of this thesis; Battiston, A.A., Bitter, J.H., Heijboer, W.M., de Groot, F.M.F., and Koningsberger, D.C.; submitted to *J.Catal.*

Reactivity of the Fe-Binuclear Complexes in Over-Exchanged Fe/ZSM5, Studied by *In situ* XAFS Spectroscopy:

Heat Treatment in He and O₂

Abstract

The structure of the iron species in mildly calcined over-exchanged Fe/ZSM5, prepared by CVD of FeCl₃, was studied during heat treatments in He or O₂/He (50:50) by coupling *in situ* Fe K-edge HR-XANES and EXAFS. The majority of iron appears to be present as Fe-binuclear complexes. EXAFS shows that the closest Fe-O shell in the complexes can be described with a [HO-Fe-O-Fe-OH]²⁺ core. Heating to a moderate temperature (up to ~150°C) results in the desorption of water from the Fe coordination sphere, in He as well as in a O₂/He (50:50) mixture. The composition of the gas phase strongly influences the changes occurring to the binuclear complexes in the 150-350°C temperature range. Above 250°C in He a significant fraction of iron undergoes auto-reduction. This is accompanied by the removal of approximately one oxygen atom from the closest Fe-O shell, ascribable to the Fe-O-Fe bridging oxygen atom. The presence of oxygen in the gas phase (P_{O₂}=0.5 bar), on the contrary, suppresses the auto-reduction capability of the binuclear complexes by inhibiting the removal of the Fe-O-Fe bridging oxygen.

Introduction

Iron-exchanged ZSM5 has recently attracted considerable attention due to its ability to catalyze diverse selective oxidation reactions. Its activity has been demonstrated for the selective oxidation of benzene to phenol using N_2O (1-5), the catalytic decomposition of N_2O (6-9), and for the Selective Catalytic Reduction of nitrogen oxides using HydroCarbons (HC-SCR) (10-12).

While the catalytic properties of iron-exchanged ZSM5 are well established, a debate is open in the literature on the nature and the reactivity of the Fe-active phase. The discussion is complicated by the fact that diverse synthesis techniques are used, resulting in different Fe/ZSM5 materials. These differences concern: i) the way by which iron is loaded (synthesis or post-synthesis methods); ii) the chemical composition of the starting ZSM5 support (Si/Al ratio); iii) the amount of iron loaded; iv) the activation treatment applied to the obtained Fe/ZSM5 (calcination, activation *in vacuo* or steaming).

Fe-framework substituted ZSM5, activated by calcination *in vacuo* or by steaming at high temperature, has shown remarkable activity towards the selective oxidation of benzene to phenol by N_2O and towards the decomposition of N_2O (1-9). Studies by Ribera *et al.* (5) and Ramírez *et al.* (13), performed on Fe-framework substituted ZSM5, activated by steaming (~0.6 Fe weight %), have shown that during the activation treatment different Fe-species are formed. These species vary from isolated extra-framework Fe oxo-ions and oligonuclear oxo-iron complexes located in the zeolite channels to larger highly dispersed iron-oxide nanoparticles on the external surface of the zeolite. Experiments with 1,3,5-trimethylbenzene, too large to fit inside the zeolite pores, have demonstrated that the latter are not involved in the oxidation of benzene to phenol (5). This observation supports the idea that only highly dispersed Fe-species located within the zeolite channels are responsible for the peculiar selective oxidation properties of Fe/ZSM5. Panov and coworkers have ascribed the catalytic activity of this material to the presence of extra-framework binuclear iron species, located in the zeolite micropores and formed by extraction of iron from the zeolite matrix during the activation treatment. By reaction with N_2O these iron centers are believed to be capable of generating a specially reactive oxygen (1-4,14-16). This oxygen (called by the authors α -oxygen) is believed to be responsible for the oxidation of benzene to phenol already at room temperature.

Binuclear Fe oxo/hydroxo species located at the Brønsted sites position of the framework have been proposed to be the active phase also in Fe/ZSM5 prepared by the Chemical Vapor Deposition (CVD) of anhydrous $FeCl_3$ (7,10,11,17). Together with aqueous ion-exchange (18) and solid-state ion exchange (19-24), CVD of $FeCl_3$ belongs to the so-called post-synthesis loading techniques. With the CVD technique Fe is exchanged from the gas

phase at around 330°C for the H⁺ Brønsted sites of an acidic Al-ZSM5 support. Final steps in the synthesis are a washing procedure, followed by drying in air and calcination in oxygen (10,25). The as-obtained material presents major differences when compared to the activated Fe-framework substituted ZSM5, mentioned above. First, a significantly higher iron loading can be achieved (~4.5 Fe weight %, depending on the Si/Al ratio). Secondly, no significant damage occurs to the zeolite framework during the activation (calcination) (25). This indicates that the formation of active Fe-species does not require extraction of aluminum from the zeolite framework.

The identification of the active phase with binuclear Fe-oxo/hydroxo complexes in Fe/ZSM5 by FeCl₃ CVD is based on results obtained by H₂ and CO TPR, FTIR, EPR and isotopic exchange with ¹⁸O₂ (7,10,11,17,26). The binuclear Fe-complexes, with the proposed core-structure [HO-Fe-O-Fe-OH]²⁺, are believed to be responsible for the decomposition of N₂O (7) and for the selective reduction of NO by hydrocarbons in the presence of excess oxygen (10,11,26).

EXAFS studies performed by Marturano *et al.* (27,28) and by our group (25,29) have confirmed that, indeed, Fe-binuclear complexes are largely present in Fe/ZSM5 obtained by CVD. The structure of these binuclear complexes, after washing, resembles that of the closest Fe-binuclear building unit in α-goethite (25,28). In this unit two octahedrally coordinated iron atoms are symmetrically connected via two hydroxyl groups (30,31).

A major problem in determining a structure-activity relation for the active phase in Fe/ZSM5 is that for activated Fe-framework substituted ZSM5, as well as for Fe/ZSM5 prepared by FeCl₃ CVD, Fe-species (spectators) different than binuclear complexes are present (7,17,25,26). In particular, Fe-binuclear complexes can undergo agglomeration during calcination (25), finally resulting in the formation of catalytically inactive (3,10,24) goethite and hematite crystals on the external surface of the zeolite. However, as demonstrated in a previous study by our group (25), agglomeration of iron in Fe/ZSM5 obtained by CVD can be controlled by adequately tuning the conditions applied during calcination. Agglomeration of Fe-species can be significantly suppressed by applying a mild calcination procedure, obtained by coupling a moderate temperature ramp with a high gas flow-rate. The resulting mildly calcined Fe/ZSM5 is, therefore, the most suited material for establishing a structure-activity relation for Fe/ZSM5 synthesized by CVD.

The objective of this work is to study the reactivity of the Fe-species present in Fe/ZSM5 obtained by CVD of FeCl₃. The reactivity of oxygen is of particular interest since it represents the key-step for the decomposition of N₂O (7), as well as for the HC-SCR of NO (10,11,17,26). The oxidation state of iron and its local environment in a mildly calcined Fe/ZSM5 sample have been followed during heating treatments in He and O₂, by

combining the results of *in situ* EXAFS and High Resolution (HR)-XANES. The HR-XANES of the Fe K-edge, especially the pre-edge feature (related to $1s \rightarrow 3d$ metal electronic transitions (32-34)), provides detailed information on both the oxidation state of iron, as well as on the coordination geometry (35). This information can be used as input for the analysis of the EXAFS data. Furthermore, both HR-XANES and EXAFS benefit from the advantage of being applicable *in situ*, *i.e.* at reaction temperature and in the presence of reactants. Their combination is, therefore, a powerful tool for tracking structural changes occurring on iron during gas treatments and catalytic reactions. From the results obtained in this study a model will be proposed for the reactivity of the Fe-species present in Fe/ZSM5 during heating treatments in helium and oxygen. In a subsequent paper a structure-activity relation will be presented for the selective reduction of NO by hydrocarbons in the presence of excess oxygen (50).

Experimental

Preparation of the sample

Over-exchanged Fe/ZSM5 was prepared following the FeCl_3 CVD method proposed by Chen and Sachtler (10) and extensively described in our previous work (25). Particular attention was paid to calcination. The procedure applied (mild calcination) was identical to the one proposed in Ref. (25). The sample was heated under a He flow of 800 ml/min with a moderate temperature ramp ($0.5^\circ\text{C}/\text{min}$) to 200°C . At this temperature, 200 ml/min of O_2 were added to the He flow while, under the same temperature ramp, heating was continued to 550°C . After 3 hrs at 550°C , the temperature was decreased to 30°C . The resulting sample, stored in air, will be referred to as Fe/ZSM5.

Characterization

ICP, N₂ physisorption, XRD

The elemental composition of the starting H/ZSM5 support and of Fe/ZSM5 was determined by using Inductively Coupled Plasma emission spectroscopy (ICP). 0.10 g of the samples were mixed in a platinum cup together with 0.40 g of Li-tetraborate and 0.20 g of Li-metaborate, and heated to 925°C . This temperature was maintained for 1 hr. After cooling, the resulting soluble borate was dissolved in 330 ml HCl (1.0 M), diluted to 1000 ml with doubly deionized water, and analyzed.

The micropore volume of the acidic support and of Fe/ZSM5 (after washing and after calcination) was determined by N_2 physisorption, using a Micromeritics ASAP 2010, as

described in (25). N₂ physisorption data obtained on sample Fe/ZSM5 were corrected for the additional metal loading (~4.4 weight %) for comparison with the H/ZSM5 support. XRD diffractograms obtained from the acidic support and from the Fe/ZSM5 sample (after washing and after calcination) were compared to visualize possible lattice damage or formation of additional Fe-rich crystalline phases. X-Ray Diffraction patterns were recorded using a Nonius PDS 120 powder diffractometer. The radiation used was Co K α 1 ($\lambda=1.78897$ Å). Diffractograms were recorded for 24 hrs and averaged in order to optimize the signal-to-noise ratio.

Fe K-edge HR-XANES

High-Resolution X-ray Absorption Near Edge Spectroscopy (HR-XANES) was applied in order to study the oxidation state and the coordination geometry of Fe in Fe/ZSM5. This information was obtained by analyzing the features (centroid position and integrated intensity) of the Fe K pre-edge, located 15-20 eV before the main Fe K-edge crest. The HR-XANES measurements at the Fe K-edge were carried out at the undulator beamline ID16 at the ESRF (Grenoble, France). Details about the experimental set-up are given in (36) and in our previous paper (25).

HR-XANES data collection

Fe/ZSM5 was pressed into self-supporting wafers and placed in an *in situ* fluorescence cell (37) at 45° with respect to the beam. Spectra were recorded at 1 bar during heating treatments from 30 to 350°C (heating ramp of 3°C/min). The heating treatments were performed under different atmospheres, *i.e.* flowing He (100 ml/min) or a 50:50 He/O₂ flowing mixture (total flow=100 ml/min). The sample heated up in He, after 30 minutes stabilization (under flowing He) at 350°C, was flushed with a 50:50 He/H₂ mixture (total flow=100 ml/min, T=350°C) and measured after 15 minutes at the same conditions. Hematite was measured under static He at 30°C as internal reference.

HR-XANES data processing

The fluorescence Fe K XANES spectra were normalized by the average absorption intensity, calculated in the 7200-7300 eV region. In order to isolate the pre-edge feature, the contribution to the pre-edge of the main Fe K-edge was subtracted from the normalized XANES spectra. This contribution was calculated using a cubic spline function, obtained by interpolating the data several eVs before and after the pre-edge (35).

The recorded HR-XANES spectra revealed the presence of fluorescence saturation effects. This was revealed by comparing the maximum intensity of the isolated pre-edges of the normalized HR-XANES spectra measured in fluorescence with those measured (on the same samples) in transmission mode at beamline X1.1 at Hasylab (*vide infra*).

Nevertheless, numerical comparison showed that, as far as the pre-edge is concerned, it was possible to correct for the saturation effects by dividing the maximum intensity of the isolated fluorescence pre-edges by that of the corresponding pre-edges measured in transmission. This procedure was performed independently on the hematite reference and on sample Fe/ZSM5, measured at 30°C in He. The correction factor obtained for Fe/ZSM5 measured at 30°C in He was used to normalize also the pre-edge data of Fe/ZSM5 measured at higher temperatures and in different environments (He/O₂, He/H₂). The rightness of the correction applied was further confirmed by using the procedure outlined in Ref. (38), based on intensity dependent correction of the occurring saturation.

The characteristics of the isolated pre-edges, *i.e.* centroid position, and integrated intensity were calculated using the software Grams. Prior to calculations, the pre-edge of α -Fe₂O₃ (not shown here, see Ref. (25)) was deconvoluted into pseudo-Voigt components (50% Gaussian, 50% Lorentzian peaks shape). Contribution from components centered above 7115.0 eV was ignored (32,35). The estimated accuracy in the energy determination for the HR-XANES spectra presented in this study is ± 0.05 eV, while the error in the integrated intensity is $\pm 5\%$.

Fe K-edge XAFS

Fe K-edge XAFS was applied in order to study the Fe oxidation state and the local atomic environment around iron, *i.e.* number, distances and chemical nature of Fe-neighbors. The XAFS data were collected at the Wiggler station X1.1 of Hasylab (Hamburg, Germany). The experimental set-up is described in Ref. (25).

XAFS data-collection

Fe/ZSM5 was pressed to obtain self-supporting wafers, calculated to have an absorbency ($\mu \cdot x$) of 2.5, and placed in a controlled atmosphere cell. The cell is similar to the one used for the HR-XANES fluorescence measurements and is described in detail elsewhere (37). The samples were treated *in situ* under flowing He (50 ml/min) or under a 50:50 O₂/He mixture (total flow of 50 ml/min). They were heated under the mentioned flows to 120 or 350°C, applying a temperature ramp of 5°C/min. Spectra were recorded at working temperature (under flowing atmospheres) or, with the cell closed, after being cooled to 77 K. A list of the measurements performed on sample Fe/ZSM5, including information on pretreatments, measuring conditions, number of averaged scans and measurements codes, is given in Table 1. XANES spectra of hematite and Fe-titanate were also measured and used, respectively, as internal Fe^{III} and Fe^{II} references.

Table 1: List of XAFS spectra recorded from Fe/ZSM5: pretreatments and measuring conditions.

Pretreatments (flowing atmosphere)	Environ. conditions during measurement	Aver. scans	Measurements code
He, 15 min, 30°C	static He, 77 K	3	Fe/ZSM5-He 30°C/LN
↑He, 30 min at 120°C	static He, 77 K	3	Fe/ZSM5-He 120°C/LN
↑He, 30 min at 350°C	flowing He, 350°C	1	Fe/ZSM5-He 350°C (1 st)/350°C
↑He, 60 min at 350°C	flowing He, 350°C	1	Fe/ZSM5-He 350°C (2 nd)/350°C
↑He, 90 min at 350°C	flowing He, 350°C	1	Fe/ZSM5-He 350°C (3 rd)/350°C
↑He, 120 min at 350°C	static He, 77 K	3	Fe/ZSM5-He 350°C/LN
↑O ₂ /He, 60 min at 350°C	flowing O ₂ /He, 350°C	3	Fe/ZSM5-O ₂ 350°C/350°C
↑O ₂ /He, 120 min at 350°C	static O ₂ /He, 77 K	3	Fe/ZSM5-O ₂ 350°C/LN

↑= heating treatment (5°C/min)

XAFS data-processing

Extraction of the EXAFS data from the measured absorption spectra was performed with the XDAP code developed by Vaarkamp *et al.* (39). Three scans were recorded for each measurement and averaged. In case of significant differences between the three scans, spectra were analyzed separately (see Table 1, scans Fe/ZSM5-He 350°C (1st, 2nd, 3rd)/350°C). The pre-edge was subtracted using a modified Victoreen curve (40). The background was subtracted employing cubic spline routines with a continuously adjustable smooth parameter (41,42). Normalization was performed by dividing the data by the intensity of the absorption spectrum at 50 eV above the Fe K-edge.

EXAFS Fe-O, Fe-Fe references, data-analysis

The Fe-O reference used for the EXAFS data-analysis was created from experimental EXAFS data, obtained from ferric acetylacetonate (measured at L.N. temperature). The Fe-Fe phase shifts and backscattering amplitudes were calculated using the software FEFF7 (43). The theoretical Fe-Fe reference was calibrated on EXAFS data obtained from hematite at L.N. temperature, by fitting in R-space. The complete procedure followed for the creation and the calibration of the EXAFS Fe-O and the Fe-Fe references is reported in Ref. (25).

The EXAFS data-analysis was performed by applying multiple-shell fitting in R-space (41). The difference file technique was applied to resolve the different contributions in the EXAFS data. The EXAFS fits were checked by applying k^1 , k^2 and k^3 weightings. The number of independent fit parameters (N_{indp}) was determined by the equation:

$$N_{\text{indp}} = \frac{2\Delta k \Delta R}{\pi} + 2 \quad [1],$$

as outlined in the ‘Reports on Standard and Criteria in XAFS Spectroscopy’(44). Errors in the numerical values obtained by the EXAFS data analysis are estimated to be $\pm 10\%$ in the coordination number (N), $\pm 1\%$ in the distance (R), $\pm 5\%$ in the Debye Waller factor ($\Delta\sigma^2$) and $\pm 10\%$ in the inner potential correction (ΔE_0) (45).

Results

ICP, N₂ physisorption, XRD

Table 2 shows the elemental composition and the micropore volume of the parent H/ZSM5 support and of the Fe/ZSM5 sample after washing, and upon mild calcination.

Table 2: Elemental composition (ICP) and micropore volume (N₂ physisorption) of H/ZSM5 (starting support) and of Fe/ZSM5, after washing (Fe/ZSM5-w) and after washing followed by a mild calcination (Fe/ZSM5-w+mc).

Samples	Si/Al (atomic ratio)	Fe/Al (atomic ratio)	Micropore volume (cm ³ /g _{support})
H/ZSM5	17.0	0.0	0.15
Fe/ZSM5-w	17.4	1.0	0.12
Fe/ZSM5-w+mc	17.2	1.0	0.12

The Si/Al ratio in the starting support and in the obtained Fe/ZSM5 is, within the margin of error, the same. This result shows that no aluminum was leached out during the synthesis (25). The Fe/Al of 1.0 is a typical result of the FeCl₃ CVD technique, by which a complete exchange of Fe^{III} for the Brønsted protons of the support is obtained. It should nevertheless be noted that, as shown in previous works (21,25,27), partial removal of Fe from the Brønsted sites may occur during washing and calcination.

After the loading of iron, a decrease of around 20% was detected in the micropore volume of the ZSM5 support (Fe/ZSM5-w). No further changes were visible upon mild calcination. This shows that applying a mild calcination procedure does not result in significant removal of iron to the external surface of the zeolite. This observation was confirmed by HR-TEM measurements shown in Ref. (25).

X-ray diffractograms (not shown), collected after the subsequent steps of the Fe/ZSM5 synthesis, did not reveal any changes in the diffraction peaks. This indicates that no detectable damage to the ZSM5 framework is observed, nor the presence of additional Fe oxidic or oxo-hydroxidic crystalline phases.

Fe K-edge HR-XANES

Fig. 1 shows the normalized background subtracted high-resolution pre-edges isolated from the HR-XANES spectra of Fe/ZSM5, measured during the heat treatment in helium.

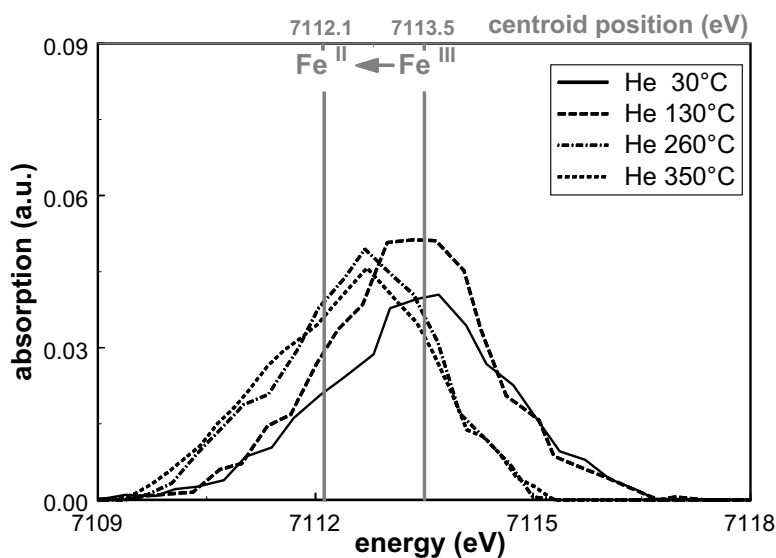


Figure 1: Normalized high-resolution background subtracted pre-edge spectra of Fe/ZSM5, measured during heat treatment in He (1 bar, 100 ml/min, heating ramp of 3°C/min).

By increasing the temperature from 30 to 130°C a clear enhancement was detected in the pre-edge intensity, while no significant shift was visible in the pre-edge position. An additional increase of the temperature to 260°C caused a shift of the pre-edge towards lower energy, accompanied by only a slight decrease in the maximum intensity and in the

area (integrated intensity) of the pre-edge. Reaching the final temperature of 350°C resulted in an additional minor shift towards lower energy, while no further changes were measured in the pre-edge area.

The characteristics (integrated intensity vs. centroid position) of the pre-edges of Fe/ZSM5, measured during the heat treatment in helium, are plotted in Fig. 2 with small black dots.

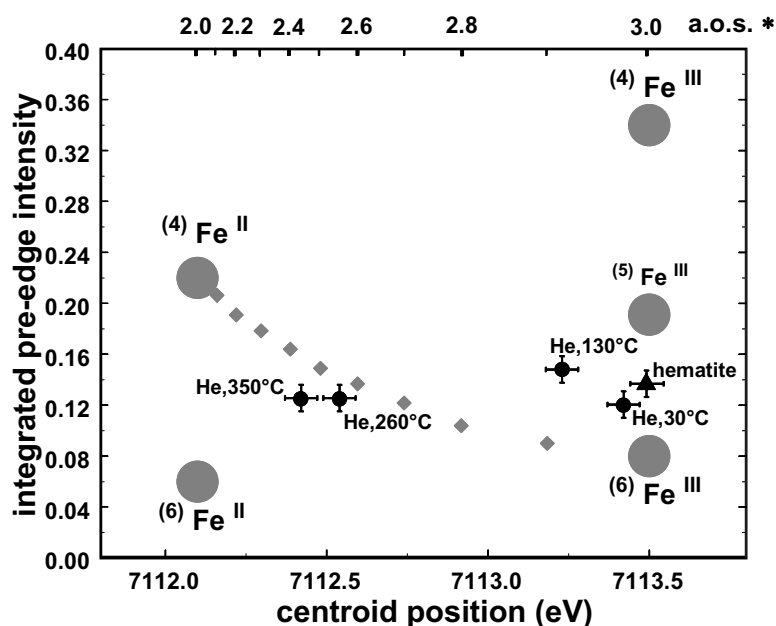


Figure 2: Summary of pre-edge characteristics (centroid position and integrated intensity) of Fe/ZSM5 (●), measured during heating treatment in He. Pre-edge characteristics of $(^6)\text{Fe}^{\text{III}}$, $(^5)\text{Fe}^{\text{III}}$, $(^4)\text{Fe}^{\text{III}}$, $(^6)\text{Fe}^{\text{II}}$, $(^4)\text{Fe}^{\text{II}}$ (●) and of $(^6)\text{Fe}^{\text{III}}/(^4)\text{Fe}^{\text{II}}$ binary mixtures (◆), obtained from the literature (35), are reported for comparison, together with the experimental pre-edge features of hematite (▲). The diagram does not consider $(^5)$ coordinated $\text{Fe}^{\text{II}}/\text{Fe}^{\text{III}}$ combinations, as well as ternary or more complex mixtures. * The average oxidation number (a.o.s) of the $(^6)\text{Fe}^{\text{III}}/(^4)\text{Fe}^{\text{II}}$ binary mixtures is reported in the upper x-axis against the corresponding energy of the centroid positions (lower x-axis).

This figure also gives the pre-edge features of well-defined Fe-crystalline materials, with known Fe oxidation state and coordination geometry. Here II and III give the Fe oxidation state, while the number between brackets in the upper script represents the number of oxygen neighboring atoms. Single-phase Fe compounds are indicated with large gray dots,

while binary mixtures of ⁶Fe^{III} / ⁴Fe^{II} are plotted with small gray lozenges. As a comparison, the results obtained for hematite measured in He at 30°C are also shown, depicted with a triangle.

The pre-edge features of the Fe-references have been obtained from the work of *Wilke et al.* (35). In their work the authors have shown that, irrespectively of the coordination geometry, the centroid position of Fe^{II} and Fe^{III} are separated by 1.4 ±0.1 eV, and are positioned at 7112.1 and 7113.5 eV, respectively. At a given oxidation state, the lowest pre-edge integrated intensity corresponds to the most centro-symmetric coordination of iron (⁶Fe). A decrease in symmetry, as well as in the number of coordinated neighbors (⁶Fe→⁴Fe), results in an increase of the pre-edge integrated intensity. The variation in pre-edge intensity is larger for Fe^{III} compounds.

The results of *Wilke et al.* obtained for binary mixtures of ⁶Fe^{III}/⁴Fe^{II} are important to understand the changes in the coordination geometry of Fe in Fe/ZSM5, as a function of the heat treatment in He. They have systematically varied the ⁶Fe^{III}/⁴Fe^{II} molar ratio of a binary mixture. In their XANES study they determined the centroid position and the integrated intensity of the pre-edge feature of the different mixtures. The average oxidation state (a.o.s) of the ⁶Fe^{III}/⁴Fe^{II} binary mixtures is given here in the upper x-axis as a function of the corresponding energy of the centroid positions (lower x-axis). It should be noted that the average red-ox state and integrated intensity of iron varies non-linearly with the pre-edge position. This phenomenon is caused by the different contributions to the pre-edge intensity from tetrahedrally and octahedrally coordinated Fe atoms.

By comparing the data obtained for Fe/ZSM-5 with those of the references, it can be concluded that iron in Fe/ZSM5 measured in He at 30°C is present as slightly distorted octahedrally coordinated Fe^{III}. Its oxidation state and coordination geometry appear, indeed, to be very similar to that of the hematite reference. By heating Fe/ZSM5 in He to 130°C an increase is visible in the pre-edge integrated intensity, while only a slight shift (-0.2 eV) of the centroid position is observed. The main effect of moderate heating in He is a decrease in symmetry or/and in the number of neighbors coordinated to iron, without a significant reduction in the average Fe oxidation state. A plausible interpretation for these results appears to be the incipient removal of water molecules from the coordination of iron.

An additional increase of the temperature to 260°C caused a clear shift of the pre-edge (-0.7 eV), together with only a slight decrease of its integrated intensity. As can be seen in Fig. 2, the features of the pre-edge at 260°C in He appear to be similar to that of a 50:50 ⁶Fe^{III}/⁴Fe^{II} mixture. Although only qualitative conclusions can be deduced, the results clearly show the onset, above 130°C, of reduction phenomena involving a considerable fraction of iron. The reduction is accompanied by an additional decrease in the average Fe

coordination-number. This can be ascribed to a further desorption of water and, coherently with the chemical reduction of iron, to removal of oxygen. The features of the pre-edge appear to be only slightly affected (additional slight reduction) by an increase of the temperature from 260°C to 350°C.

Fig. 3 shows the normalized high-resolution background subtracted pre-edges of Fe/ZSM5, measured during heating in oxygen from 30°C to 350°C ($O_2/He=50:50$). The pre-edge measured in He at 30°C is also given for comparison.

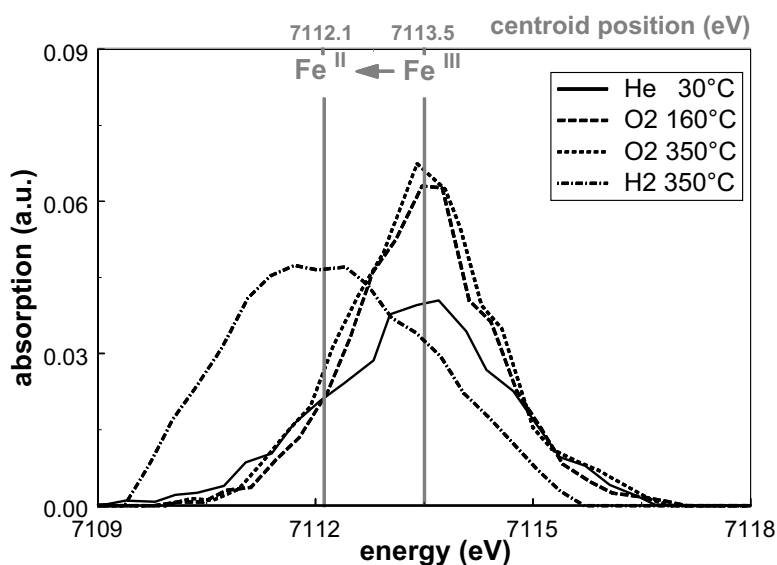


Figure 3: Normalized high-resolution background subtracted pre-edge spectra of Fe/ZSM5, measured during heat treatment (heating ramp of 3°C/min) in oxygen (1 bar, 100 ml/min, $O_2/He=50:50$), and measured in hydrogen (1 bar, 100 ml/min, $H_2/He=50:50$) at 350°C after heat treatment in He to 350°C (1 bar, 100 ml/min, heating ramp of 3°C/min).

Heating Fe/ZSM5 in oxygen to 160°C resulted in a strong increase in the pre-edge intensity. This increase is almost identical to that measured under He at 130°C (see Fig. 1). Increasing the temperature further to 350°C did not cause any major change with respect to both the pre-edge position and its intensity. These results are visualized in Fig. 4. Heating in the presence of oxygen caused a decrease in the centrosymmetry of Fe but did not result in chemical reduction of Fe. This can be ascribed to the removal of coordinated water molecules. As can be seen, the average Fe pre-edge features measured on Fe/ZSM5 in oxygen at 350°C resembles those of five-fold coordinated Fe^{III} .

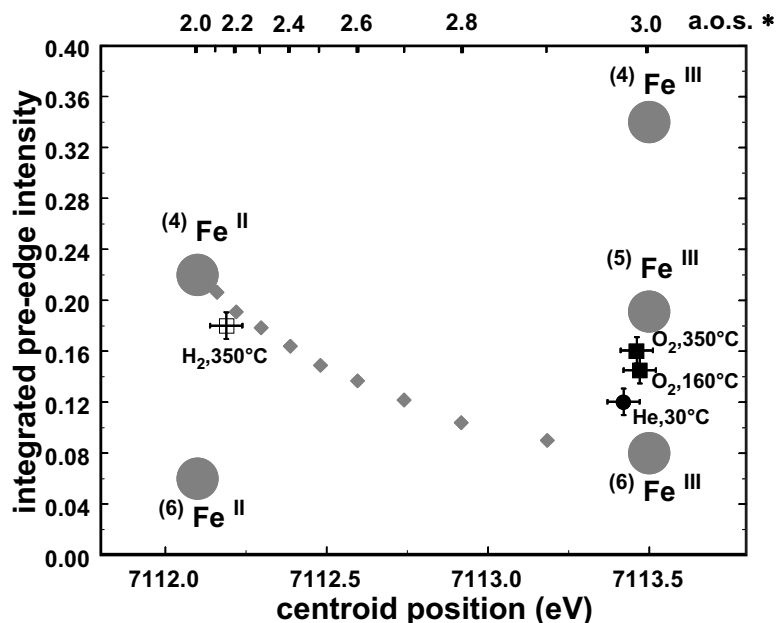


Figure 4: Summary of pre-edge characteristics of Fe/ZSM5 measured at 30°C in helium (●), during heat treatment in oxygen (■), and measured in hydrogen at 350°C (□) after heat treatment in He to 350°C. For details on Fe-references (35) see caption Fig. 2.

Completely different results were obtained on the Fe pre-edge measured in H₂ at 350°C, after preheating in He to the same temperature (see Fig. 3). The pre-edge is clearly shifted to lower energy (-1.3 eV, when compared to the reference sample) and its integrated intensity appears to be increased. The pre-edge characteristics in H₂ at 350°C are very close to that of tetrahedrally coordinated Fe^{II}, as depicted in Fig. 4. Thus, the reduction process affected almost all of the Fe atoms in sample Fe/ZSM5.

Fe K-edge XAFS

Heat treatment in He

The effects of the heating treatment in He on the oxidation state of iron are visualized in Fig. 5. The picture shows the XANES spectra of Fe/ZSM5, measured at liquid nitrogen temperature after treatment in He at 30°C, 120°C, and at 350°C (after 120 minutes stabilization). The XANES spectra of hematite and Fe-titanate are also reported, respectively as internal Fe^{III} and Fe^{II} references.

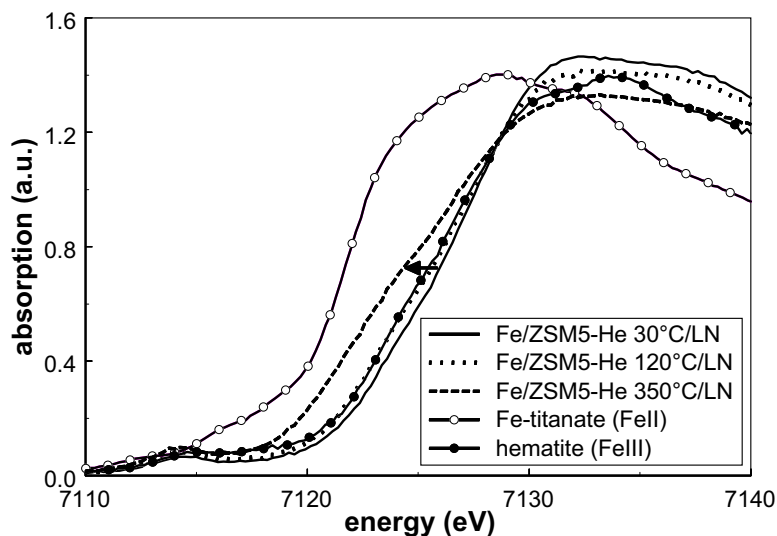


Figure 5: Normalized XANES spectra of Fe/ZSM5-He 30°C/LN (solid line), Fe/ZSM5-He 120°C/LN (dotted line), Fe/ZSM5-He 350°C/LN (dashed line). Normalized XANES spectra of hematite and Fe-titanate are also reported, respectively as internal Fe^{III} and Fe^{II} references.

As can be seen from the picture, the Fe K-edge position of Fe/ZSM5 at 30°C corresponds to that of hematite (Fe^{III}). Coherently with what observed by HR-XANES, heating to 120°C does not result in reduction of iron. A reduction is observed only upon heating in He to 350°C.

Fig. 6a shows the experimental EXAFS data (measured in He at 77 K) of Fe/ZSM5-He 30°C/LN (solid line), Fe/ZSM5-He 120°C/LN (dotted line) and Fe/ZSM5-He 350°C/LN (dashed line). Sample Fe/ZSM5-He 350°C/LN was measured after 120 min. stabilization in He at 350°C. Fig. 6a shows that both the EXAFS amplitude and the nodes in k-space are affected by the treatment in He, thus heating in He resulted in significant changes affecting the local environment of iron. These changes are also revealed in the corresponding Fourier Transforms of the experimental EXAFS data (Fig. 6b). Three main peaks are visible, centered respectively at around 1.5 Å (Fe-O, in the picture), 2.6 Å (Fe-Fe₁) and 3.1 Å (Fe-Fe₂). It can be seen that the largest changes occur after heating in He to temperatures higher than 120°C. Large changes can be observed in the Fe-O shells region in the range 1.0 < R < 2.0 Å. Also the Fe-Fe₁ shell is influenced.

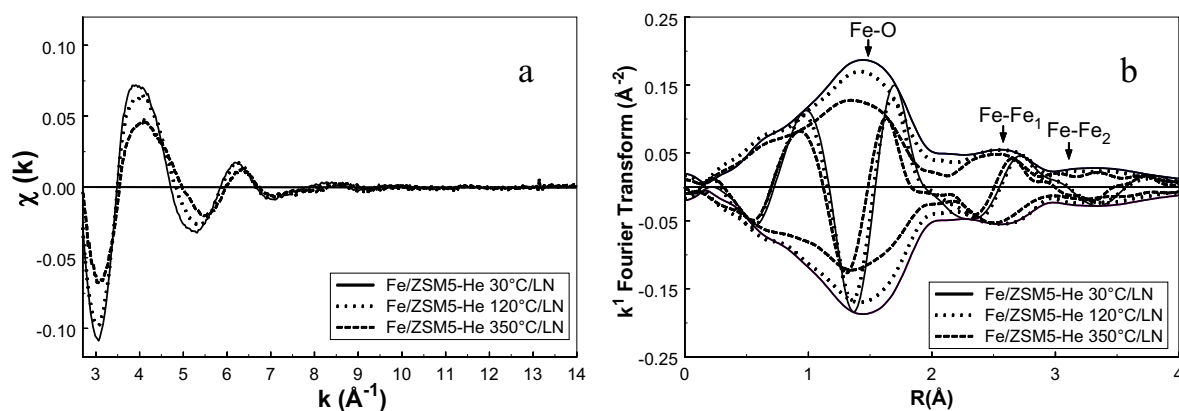


Figure 6: a) Experimental $\chi(k)$ data measured as a function of the heat treatment in He: Fe/ZSM5-He 30°C/LN (solid line), Fe/ZSM5-He 120°C/LN (dotted line), Fe/ZSM5-He 350°C/LN (dashed line); b) Fourier transform (k^1 , $\Delta k=2.7-13.2 \text{ \AA}^{-1}$) of EXAFS data of Fe/ZSM5-He 30°C/LN (solid line), Fe/ZSM5-He 120°C/LN (dotted line) and Fe/ZSM5-He 350°C/LN (dashed line). Sample Fe/ZSM5-He 350°C/LN, was measured after 120 min. stabilization in He at 350°C.

The EXAFS coordination parameters obtained by the R-space fitting procedure for sample Fe/ZSM5-He 30°C/LN are collected in Table 3. For the R-space fit the Fourier transform range was taken from 2.7 to 13.2 \AA^{-1} with a range in R-space from 0.7 to 4.2 \AA . The number of independent parameters was calculated to be $N_{\text{indp}} = 25.4$. Coherently with the results obtained by HR-XANES on Fe/ZSM5 measured at 30°C, the fit of the Fe-O contribution revealed the presence of six oxygen neighbors. A good quality fit could be obtained with two different oxygen distributions, *i.e.* by using two oxygen shells (model 3:3) or three oxygen shells (model 2:2:2). The total number of free fit parameters was 18 and 22, respectively. No significant difference was obtained in the statistical variance of the two fits. It should be noted that for both models the fits were optimized by including distant oxygen neighbors, attributed to the zeolite framework (Fe-O_z). No further implications for a structural model were derived from this Fe-O_z contribution, added to the fit in order to analyze more reliably shell Fe-Fe₂ (*vide infra*).

The second peak of the Fourier Transform (Fe-Fe₁) was fitted with a Fe-Fe shell at 3.05 \AA with a coordination number of 1.2. This shell is ascribed to the presence of binuclear Fe-complexes (25). The fact that the coordination number of this shell is higher than 1.0 and that an additional Fe-Fe₂ shell could be fitted at higher distance ($R=3.40 \text{ \AA}$, $N=0.4$), as

already discussed in Ref. (25), is the result of further agglomeration of a fraction of iron. From the EXAFS coordination numbers of the Fe-Fe shells, binuclear clusters in sample Fe/ZSM5 are estimated to account for at least 70% of the total iron (25).

Table 3: Coordination parameters obtained by R-space analysis (k^1 , $\Delta k=2.7-13.2 \text{ \AA}^{-1}$; $\Delta R= 0.7-4.2 \text{ \AA}$) of EXAFS data of Fe/ZSM5-He 30°C/LN.

Shells	N ($\pm 10\%$)	R (\AA) ($\pm 1\%$)	$\Delta\sigma^2$ (10^{-3} \AA^2) ($\pm 5\%$)	ΔE_0 (eV) ($\pm 10\%$)	k^1 -variance (%)	
					Im. part	Abs. part
Fe/ZSM5-He 30°C/LN (model 2:2:2)					0.46	0.41
Fe-O ₁	1.9	1.86	-3.9	0.5		
Fe-O ₂	2.0	1.97	-5.0	13.4		
Fe-O ₃	2.1	2.09	-1.0	-6.8		
Fe-Fe ₁	1.2	3.05	5.9	-3.2		
Fe-Fe ₂	0.4	3.40	14.2	-5.5		
Fe-O _Z	4.5	4.01	15.0	-5.0		
Fe/ZSM5-He 30°C/LN (model 3:3)					0.38	0.36
Fe-O ₁	3.0	1.90	9.6	12.0		
Fe-O ₂	3.1	2.04	4.3	-7.3		
Fe-Fe ₁	1.2	3.06	5.4	-3.6		
Fe-Fe ₂	0.4	3.40	10.7	-8.0		
Fe-O _Z	4.7	4.11	11.7	-6.6		
model (2:2:2): $N_{\text{indp}} = 25.4$; $N_{\text{free (fit)}} = 22$						
model (3:3): $N_{\text{indp}} = 25.4$; $N_{\text{free (fit)}} = 18$						

The quality of the R-space fit using the 2:2:2 model is demonstrated in Fig. 7 for the Fe/ZSM5 sample treated in He at 30°C RT and measured at L.N. temperature.

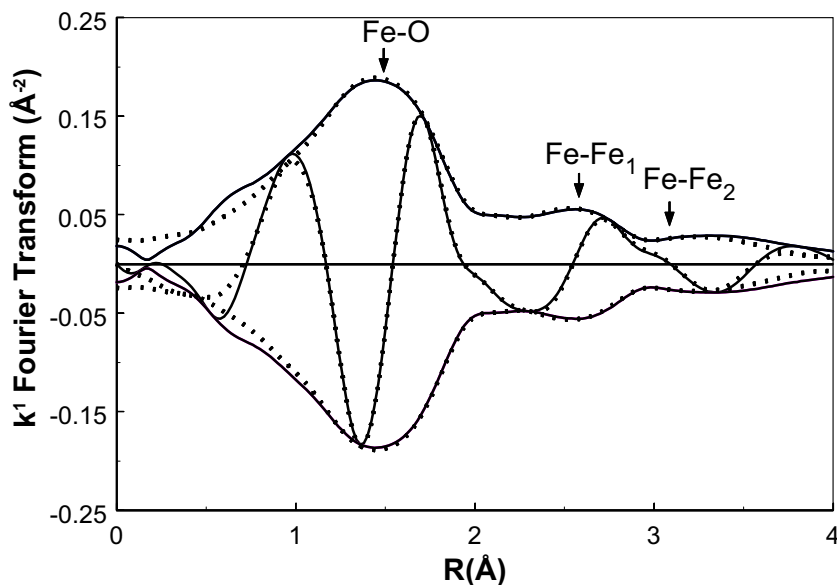


Figure 7: Fourier transform (k^1 , $\Delta k=2.7-13.2 \text{ \AA}^{-1}$) of EXAFS data of Fe/ZSM5-He 30°C/LN (solid line) and R-space fit (dotted line; $0.7 < R(\text{\AA}) < 4.2$; fit-model 2:2:2).

The results obtained during the heat treatments can be best described and understood in terms of the 2:2:2 model. The reactivity of the Fe/ZSM5 sample, using the 2:2:2 model, is visualized in changes in the number of oxygen neighbors in the Fe-O₁ and Fe-O₃ coordination.

The results of the R-space fits of measurements Fe/ZSM5-He 30°C/LN, Fe/ZSM5-He 120°C/LN and Fe/ZSM5-He 350°C/LN, using the 2:2:2 model, are summarized in Table 4. It can be seen that the coordination number of the Fe-O₃ coordination significantly decreases with increasing temperature from 2.1 (30°C) to 1.4 (120°) and to 0.9 (350°C). As a result, the imaginary part of the total Fe-O contribution appears to be shifted towards lower R (Fig. 7). Since the EXAFS analysis showed already a decrease in the coordination number of the Fe-O₃ shell at 120°C (Fe-oxidation state is III), the oxygen located in this shell can not be responsible for red-ox behavior of iron. The Fe-O₃ shell is therefore attributed to weakly bound oxygen, most probably of H₂O. Besides a further decrease in the oxygen coordination number, an increase in the disorder ($\Delta\sigma^2$) and a change in the inner potential value (ΔE_0) of the Fe-O₃ shell is observed when heating from 120 to 350°C. At the same time a small decrease is visible in the coordination number of the Fe-O₁ shell.

Table 4: Coordination parameters (model 2:2:2) obtained by R-space analysis (k^1 , $\Delta k=2.7-13.2 \text{ \AA}^{-1}$; $\Delta R=0.7-4.2 \text{ \AA}$) of EXAFS data of Fe/ZSM5-He 30°C/LN, Fe/ZSM5-He 120°C/LN and Fe/ZSM5-He 350°C/LN.

Shells	N ($\pm 10\%$)	R (\AA) ($\pm 1\%$)	$\Delta\sigma^2$ (10^{-3} \AA^2) ($\pm 5\%$)	ΔE_0 (eV) ($\pm 10\%$)	k^1 -variance (%)	
					Im. part	Abs. part
Fe/ZSM5-He 30°C/LN					0.46	0.41
Fe-O ₁	1.9	1.86	-3.9	0.5		
Fe-O ₂	2.0	1.97	-5.0	13.4		
Fe-O ₃	2.1	2.09	-1.0	-6.8		
Fe-Fe ₁	1.2	3.05	5.9	-3.2		
Fe-Fe ₂	0.4	3.40	14.2	-5.5		
Fe-O _Z	4.5	4.01	15.0	-5.0		
Fe/ZSM5-He 120°C/LN					0.49	0.37
Fe-O ₁	2.0	1.85	-3.9	0.5		
Fe-O ₂	2.0	1.97	-5.0	13.4		
Fe-O ₃	1.4	2.09	-2.2	-6.8		
Fe-Fe ₁	1.2	3.05	2.9	-3.2		
Fe-Fe ₂	0.4	3.40	14.2	-5.5		
Fe-O _Z	4.5	4.01	15.0	-5.0		
Fe/ZSM5-He 350°C/LN					0.58	0.55
Fe-O ₁	1.8	1.85	-3.5	-1.8		
Fe-O ₂	2.0	1.97	-4.3	12.6		
Fe-O ₃	0.9	2.08	2.2	-11.1		
Fe-Fe ₁	1.2	2.97	1.3	1.8		
Fe-Fe ₂	0.4	3.40	15.0	-5.5		
Fe-O _Z	3.2	3.99	15.0	-4.9		
$N_{\text{indp}} = 25.4$; $N_{\text{free (fit)}} = 22$						

The decrease of the oxygen coordination number of the Fe-O₃ shell as a function of the He treatment is visualized in Fig. 8. No changes are observed for the Fe-O₂ shell during the heat treatment in He.

Also a change in the distance of the Fe-Fe₁ is observed when heating from 120°C to 350°C, indicating a shortening in the Fe-Fe distance of the binuclear Fe-complexes (2.97 Å in He at 350°C). During the fitting process, the coordination number and distance of the Fe-Fe₂ shell were fixed to the values obtained for measurement Fe/ZSM5-He 30°C/LN (model 3:3). Fe-Fe₂ is a minor contribution and no important information was derived from this shell for the auto-reduction properties of the Fe/ZSM5 sample.

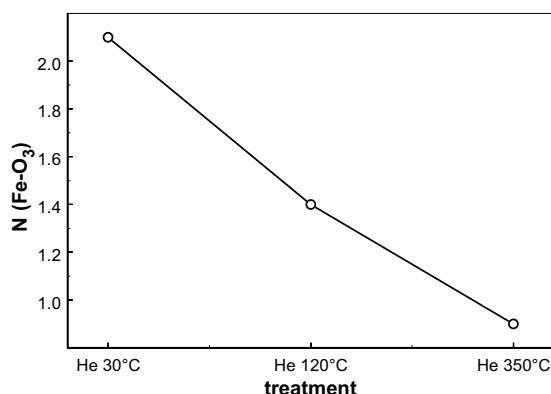


Figure 8: Average number of oxygen atoms in the Fe-O₃ coordination shell (model 2:2:2) as a function of heat treatment in He.

Stabilization in He at 350°C

The results presented above for the He treatment at 350°C were obtained after 120 minutes stabilization on stream and after cooling the Fe/ZSM5 sample to liquid nitrogen temperature. However, very important changes occurred during this stabilization period. The HR-XANES results (Fig. 2) already showed that, after reaching 350°C in He, the oxidation state of Fe is close to 2.4. The XANES spectra recorded *in situ* at 350°C are depicted in Fig. 9.

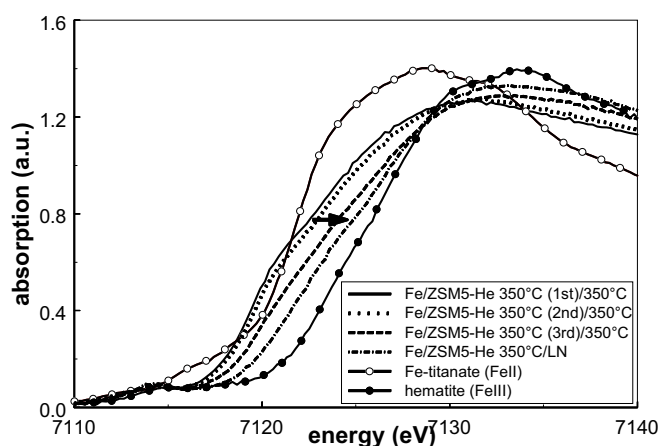


Figure 9: Normalized XANES spectra of Fe/ZSM5-He 350°C (1st)/350°C (solid line), Fe/ZSM5-He 350°C (2nd)/350°C (dotted line), Fe/ZSM5-He 350°C (3rd)/350°C (dashed line), and Fe/ZSM5-He 350°C/LN (dashed-dotted line). Normalized XANES spectra of hematite and Fe-titanate are also reported, as internal Fe^{III} and Fe^{II} references.

The figure shows a clear shift to lower energy of the edge position of spectrum Fe/ZSM5-He 350°C (1st)/350°C, recorded after 30 minutes stabilization. This confirms that heating Fe/ZSM5 in He to 350°C results in the reduction of a significant fraction of iron. However, the state of iron under He at 350°C appeared to be unstable. This is visible by tracking the shift of the edge position with time on stream (measurements 1st, 2nd and 3rd). A significant shift (+2.0 eV) occurred, showing an average re-oxidation of iron.

The effect of the re-oxidation process on the local structure of iron can be tracked by the analysis of the EXAFS data collected *in situ* in He at 350°C. The EXAFS spectra obtained respectively after 30, 60 and 90 minutes exposure to He are shown in Fig. 10a.

It can be seen that both the amplitude and the nodes of the EXAFS oscillations are changing as a function of the stabilization period.

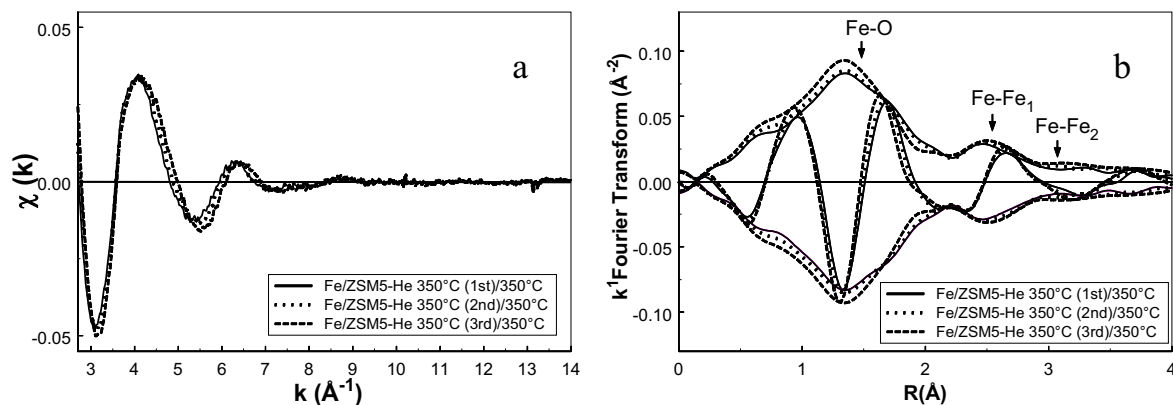


Figure 10: a) Experimental $\chi(k)$ data of Fe/ZSM5-He 350°C (1st)/350°C (solid line), Fe/ZSM5-He 350°C (2nd)/350°C (dotted line), Fe/ZSM5-He 350°C (3rd)/350°C (dashed line); b) Fourier transform (k^1 , $\Delta k=2.7-13.2 \text{ \AA}^{-1}$) of EXAFS data of Fe/ZSM5-He 350°C (1st)/350°C (solid line), Fe/ZSM5-He 350°C (2nd)/350°C (dotted line), Fe/ZSM5-He 350°C (3rd)/350°C (dashed line).

The corresponding Fourier transforms are presented in Fig. 10b. The Fe-O contribution shows an increase with time on stream of its maximum intensity (at around 1.4 \AA in the picture) accompanied by a contraction towards lower distance. No significant differences are visible, on the contrary, in the Fe-Fe contribution.

Table 5 shows the results of the EXAFS fit, performed on Fe/ZSM5 measured *in situ* at 350°C during the stabilization in He.

Table 5: Coordination parameters (model 2:2:2) obtained by R-space analysis (k^1 , $\Delta k=2.7-13.2 \text{ \AA}^{-1}$; $\Delta R=0.7-4.2 \text{ \AA}$) of EXAFS data of Fe/ZSM5-He 350°C (1st)/350°C, Fe/ZSM5-He 350°C (2nd)/350°C, Fe/ZSM5-He 350°C (3rd)/350°C and Fe/ZSM5-He 350°C/LN. $N_{\text{indp}}=25.4$; $N_{\text{free (fit)}}=22$.

Shells	N ($\pm 10\%$)	R (\AA) ($\pm 1\%$)	$\Delta\sigma^2$ (10^{-3} \AA^2) ($\pm 5\%$)	ΔE_0 (eV) ($\pm 10\%$)	k^1 -variance (%)	
					Im. part	Abs. part
Fe/ZSM5-He 350°C (1 st)/350°C					0.55	0.30
Fe-O ₁	1.2	1.88	2.6	-5.5		
Fe-O ₂	2.0	1.97	7.2	12.6		
Fe-O ₃	1.2	2.08	8.8	-9.3		
Fe-Fe ₁	1.1	2.99	13.0	0.4		
Fe-Fe ₂	0.4	3.40	17.2	0.1		
Fe-O _Z	1.6	4.09	15.0	-8.8		
Fe/ZSM5-He 350°C (2 nd)/350°C					0.67	0.39
Fe-O ₁	1.4	1.88	2.6	-5.5		
Fe-O ₂	2.0	1.97	7.2	12.6		
Fe-O ₃	1.1	2.08	8.8	-9.3		
Fe-Fe ₁	1.1	2.99	13.0	0.4		
Fe-Fe ₂	0.4	3.40	13.8	1.5		
Fe-O _Z	2.2	4.00	15.0	-7.2		
Fe/ZSM5-He 350°C (3 rd)/350°C					0.94	0.47
Fe-O ₁	1.7	1.89	1.9	-6.5		
Fe-O ₂	2.0	1.97	7.2	12.6		
Fe-O ₃	0.7	2.06	2.0	-8.7		
Fe-Fe ₁	1.2	2.97	12.5	-0.4		
Fe-Fe ₂	0.4	3.40	14.8	3.1		
Fe-O _Z	3.7	3.91	18.0	-2.2		
Fe/ZSM5-He 350°C/LN					0.58	0.55
Fe-O ₁	1.8	1.85	-3.5	-1.8		
Fe-O ₂	2.0	1.97	-4.3	12.6		
Fe-O ₃	0.9	2.08	2.2	-11.1		
Fe-Fe ₁	1.2	2.97	1.3	1.8		
Fe-Fe ₂	0.4	3.40	15.0	-5.5		
Fe-O _Z	3.2	3.99	15.0	-4.9		

The quality of the R-space fit of the EXAFS spectra collected at 350°C is demonstrated in Fig. 11 for measurement Fe/ZSM5-He 350°C(1st)/350°C.

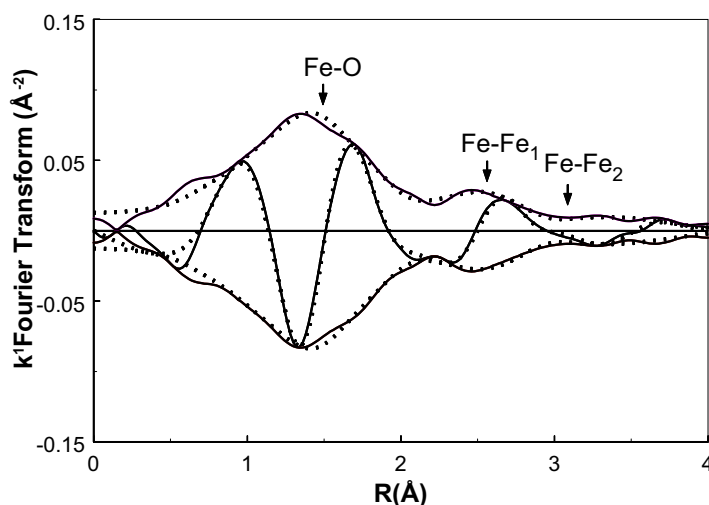


Figure 11: Fourier transform (k^1 , $\Delta k=2.7-13.2 \text{ \AA}^{-1}$) of EXAFS data of Fe/ZSM5-He 350°C (1st)/350°C (solid line) and R-space fit (dotted line; $0.7 < R(\text{\AA}) < 4.2$; fit-model 2:2:2).

The most significant changes with time on stream occurred in the coordination number of the Fe-O₁ shell. The coordination number increased from 1.2 (1st scan) to 1.7 (3rd scan). As already deduced from the XANES spectra (Fig. 9), this increase was accompanied by a corresponding partial re-oxidation of iron. The Fe-O₁ shell is therefore associated with the red-ox properties of the Fe-binuclear complexes. The decrease with time on stream of the coordination number of the Fe-O₃ shell, which was already shown not to be related to red-ox properties of iron (previous section), is most probably due to further desorption of water from the coordination sphere of iron. No differences were visible in the Fe-O₂ shell.

Heat treatment in O₂

The influence of the oxygen presence on the reducibility of iron during the heat treatment can be seen in Fig. 12, by comparing the XANES spectra of Fe/ZSM5-He 350°C (1st)/350°C and Fe/ZSM5-O₂ 350°C/350°C. As can be seen, the edge position of the sample heated in He (after 30 min. stabilization) appears to be close to the edge of Fe-titanate (Fe^{II}), while the edge position of Fe/ZSM5 heated in oxygen corresponds to that of the hematite reference (Fe^{III}). Thus, oxygen prevented the auto-reduction of iron.

The XAFS spectra in the presence of oxygen were measured *in situ* (Fe/ZSM5-O₂ 350°C/350°) and after cooling to 77 K (Fe/ZSM5-O₂ 350°C/LN). Differently from what observed under helium, the three EXAFS spectra recorded in oxygen at high temperature with increasing exposure time appeared to be identical, and were, therefore, averaged.

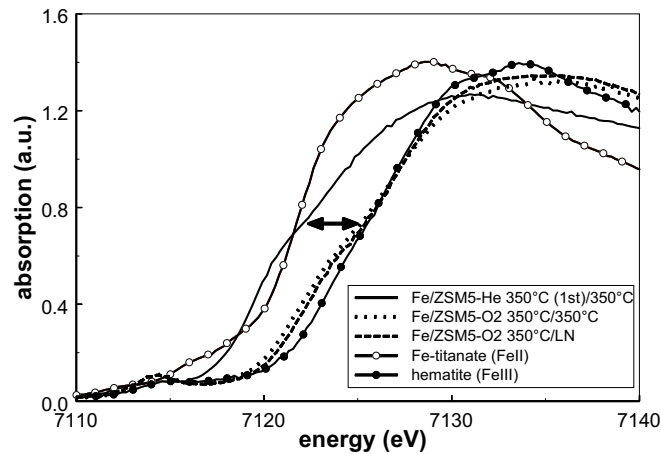


Figure 12: Normalized XANES spectra of Fe/ZSM5-He 350°C (1st)/350°C (solid line), Fe/ZSM5-O₂ 350°C/350°C (dotted line) and Fe/ZSM5-O₂ 350°C/LN (dashed line). Normalized XANES spectra of hematite and Fe-titanate are also reported, as internal Fe^{III} and Fe^{II} references.

Significant differences are visible when comparing the EXAFS functions of Fe/ZSM5 measured *in situ* at 350°C in oxygen, and in helium, after 30 min. stabilization (Fig. 13a). The corresponding Fourier Transforms, collected in Fig. 13b, show that these differences concern mainly the Fe-O coordination. In the presence of oxygen, the Fe-O peak appears significantly enhanced in intensity and shifted towards lower R.

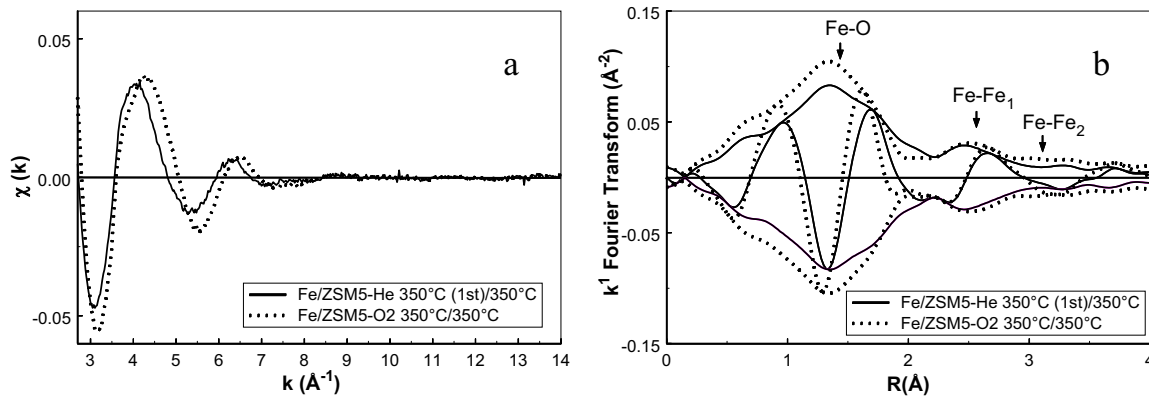


Figure 13: a) Experimental $\chi(k)$ data of Fe/ZSM5-He 350°C (1st)/350°C (solid line) and Fe/ZSM5-O₂ 350°C/350°C (dotted line); b) Fourier transform (k^1 , $\Delta k=2.7-13.2 \text{ \AA}^{-1}$) of EXAFS data of Fe/ZSM5-He 350°C (1st)/350°C (solid line) and Fe/ZSM5-O₂ 350°C/350°C (dotted line).

The quality of the fit for measurement Fe/ZSM5-O₂ 350°C/350°C is shown in Fig. 14.

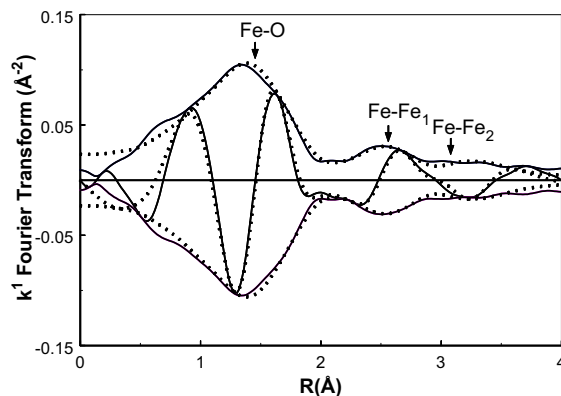


Figure 14: Fourier transform (k^1 , $\Delta k=2.7-13.2 \text{ \AA}^{-1}$) of EXAFS data of Fe/ZSM5-O₂ 350°C/350°C (solid line) and R-space fit (dotted line; $0.7 < R(\text{\AA}) < 4.2$; fit-model 2:2:2).

Table 6: Coordination parameters (model 2:2:2) obtained by R-space fit analysis ($\Delta k=2.7-13.2 \text{ \AA}^{-1}$; $\Delta R=0.7-4.2 \text{ \AA}$) of EXAFS data of Fe/ZSM5-O₂ 350°C/350°C and Fe/ZSM5-O₂ 350°C/LN.

Shells	N ($\pm 10\%$)	R (\AA) ($\pm 1\%$)	$\Delta\sigma^2$ (10^{-3} \AA^2) ($\pm 5\%$)	ΔE_0 (eV) ($\pm 10\%$)	k^1 -variance (%)	
					Im. part	Abs. part
Fe/ZSM5-O ₂ 350°C/350°C					1.26	0.50
Fe-O ₁	1.9	1.86	2.0	-2.5		
Fe-O ₂	2.0	1.99	5.0	13.0		
Fe-O ₃	1.0	2.02	1.6	-13.3		
Fe-Fe ₁	1.2	2.99	9.8	-1.6		
Fe-Fe ₂	0.4	3.40	15.1	-3.7		
Fe-O _Z	4.4	3.81	15.0	1.0		
Fe/ZSM5-O ₂ 350°C/LN					0.97	0.70
Fe-O ₁	2.0	1.85	-3.8	-4.3		
Fe-O ₂	2.0	1.97	-5.0	12.0		
Fe-O ₃	1.0	2.02	4.5	-6.6		
Fe-Fe ₁	1.2	2.96	2.4	2.0		
Fe-Fe ₂	0.4	3.40	15.0	0.0		
Fe-O _Z	3.8	3.91	15.0	-2.2		

$N_{\text{indp}} = 25.4$; $N_{\text{free (fit)}} = 22$

The structural parameters obtained by the analysis of the EXAFS spectra recorded in the presence of oxygen are collected in Table 6. Apart from differences in the Debye-Waller factors (temperature effects), the results of the fits (Fe/ZSM5-O₂ 350°C/350°C and Fe/ZSM5-O₂ 350°C/LN) coincide. The total Fe-O coordination number (around 5.0) appears to be consistent with the results obtained by HR-XANES (see Fig. 4, (O₂, 350°C)). When compared to the sample measured at 350° in He after 30 min. stabilization (see Table 5), a sharp increase was detected in the coordination number of shell Fe-O₁ (1.9 vs. 1.2 for Fe/ZSM5-He 350°C(1st)/350°C). The coordination number of shell Fe-O₃, on the contrary, appears only slightly decreased, probably as a result of further water desorption with time on stream (1.0 vs. 1.2, for Fe/ZSM5-He 350°C(1st)/350°C). The Fe-O₃ distance appears also to be slightly shortened. Also during the heating treatment in oxygen, the Fe-O₂ shell remained unaffected.

As shown by the results obtained during the heat treatments, changes in the oxidation state of iron are related to variations only in the Fe-O₁ coordination number. A coordination number of approximately 1 corresponds to an average Fe-oxidation state close to II. When the Fe-O₁ coordination number is increased to 2, Fe results to be completely oxidized (Fe^{III}). The changes in the Fe-O₁ coordination number, as a function of the different treatments, are visualized in Fig. 15.

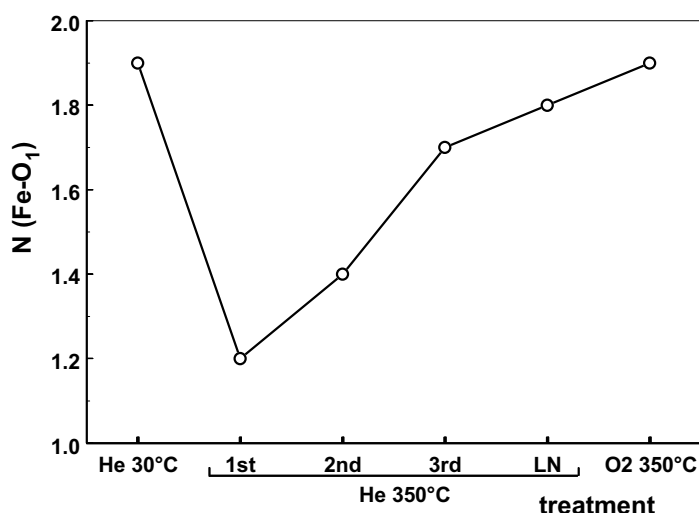


Figure 15: Number of oxygen atoms in the Fe-O₁ coordination shell (model 2:2:2) as a function of heat treatment in He, and in the presence of O₂.

As in the presence of helium, also the heat treatment in oxygen resulted in a shortening of the distance and in a decrease of the Debye-Waller factor of the Fe-Fe₁ shell (see for comparison Table 4, Fe/ZSM5-He 30°C\LN). No differences were detected, on the other hand, in the coordination numbers of the Fe-Fe shells, excluding Fe-Fe agglomeration phenomena during the treatment.

Discussion

Several studies performed on Fe/ZSM5, obtained by CVD or solid-state ion exchange of FeCl₃, have elucidated the evolution of iron along the different steps of the synthesis (7,10,11,21,25,28,46), *i.e.* loading of iron, washing, and calcination. Upon sublimation of FeCl₃, iron is exchanged for the H⁺ Brønsted protons of the zeolite in the form of isolated FeCl₂⁺ species (25,28,46). During the washing step, these species aggregate to form Fe-binuclear complexes, still bound to the framework aluminum (25,28). The structure of the Fe-binuclear species in washed Fe/ZSM5, determined by EXAFS, resembles that of the closest Fe-binuclear building unit in α -goethite (30,31), consisting of octahedrally coordinated Fe^{III} oxo/hydroxo-ions. A possible structure for the Fe-binuclear complexes, based on the similarity with the building blocks in α -goethite (30,31), was proposed in our previous study (25), and is depicted in Fig. 16.

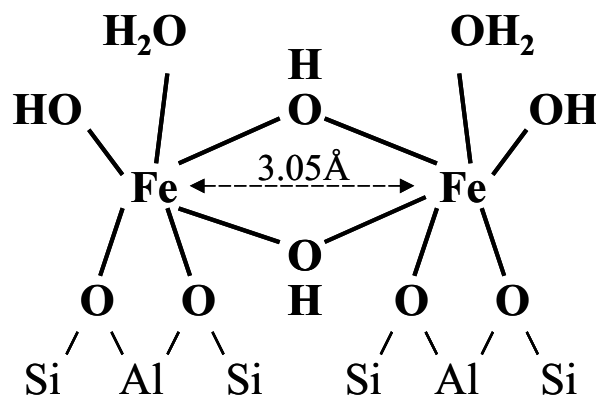


Figure 16: Proposed structure for the binuclear Fe-complexes in Fe/ZSM5, obtained by CVD of FeCl₃, upon washing.

In this model hydroxo-bridged Fe atoms are bound to the framework via two oxo-ions, and balance the lattice extra-charge of two aluminum atoms. The Fe-O coordination, coherently with EXAFS and HR-XANES results, showing that iron possesses an octahedral coordination, is further completed by adsorbed water and by a terminal hydroxyl group. A

similar model was presented by Marturano *et al.* (28), proposing a single oxo-bridge to the zeolite lattice.

The influence of calcination on the further evolution of the binuclear iron complexes was investigated in our previous work (25). We have found that, if the calcination procedure is carefully controlled (mild calcination procedure), agglomeration of the binuclear Fe-complexes towards inactive oxidic clusters can be significantly suppressed, although not completely. This finding, based on HR-TEM, EELS, Mössbauer, FTIR and EXAFS spectroscopy is confirmed by the results of the EXAFS analysis, presented in this work. Irrespectively to the different pretreatments applied (heating in He or O₂), two Fe-Fe shells could always be fitted, with a coordination number respectively of 1.2 and 0.4 (Tables 3-6). The closest Fe-Fe shell (Fe-Fe₁) is ascribed to the presence of binuclear Fe-complexes (25,28). The fact that the coordination number (N) of this shell is higher than 1.0 and that also a second Fe-Fe shell (Fe-Fe₂) could be fitted at a higher distance 3.40 Å (N=0.4), suggests that a fraction of iron possesses a higher degree of agglomeration than the binuclear complexes (25). Nevertheless, from the EXAFS coordination numbers of the Fe-Fe shells, binuclear clusters in mildly calcined Fe/ZSM5 are estimated to account for at least 70% of the total iron. It should nevertheless be noted that quantification by Mössbauer spectroscopy has shown that this number could be overestimated (25).

Binuclear iron complexes in mildly calcined Fe/ZSM5, pretreated in He at 30°C

While calcination is generally applied as an activation procedure for Fe/ZSM5 obtained by CVD of FeCl₃ (10-12,25), its influence on the local Fe-O coordination of the Fe-binuclear complexes, formed upon washing, has not been unraveled, yet. The features of the Fe K pre-edge of (mildly calcined) Fe/ZSM5 measured in He at 30°C (Fig. 2) show that iron has a slightly distorted octahedral coordination and an oxidation state of III (35). These results are confirmed by the position of the Fe K-edge (Fig. 5), which overlaps with that of the Fe^{III} hematite reference, and by the results of the EXAFS analysis (Table 3), showing the presence of six oxygen neighbors in the Fe-coordination sphere. The EXAFS data could be fitted with a symmetric oxygen distribution in two (model 3:3) or three (model 2:2:2) oxygen shells. A plausible structure for the binuclear Fe-complexes in mildly calcined Fe/ZSM5 after pretreatment in He at 30°C, arising from the EXAFS and the HR-XANES results, is depicted in Fig. 17 (oxygen atoms are labeled consistently with the 2:2:2 model in Table 3). This structure matches the model previously proposed in the literature (7,10,11,17) for the catalytically active phase in calcined Fe/ZSM5, *i.e.* a binuclear Fe-complex with the core-structure [HO-Fe-O-Fe-OH]²⁺. This model is based on experimental

evidences obtained by TPR, FTIR and ESR studies (10-12,17) and appears as a plausible evolution of the binuclear complexes formed upon washing.

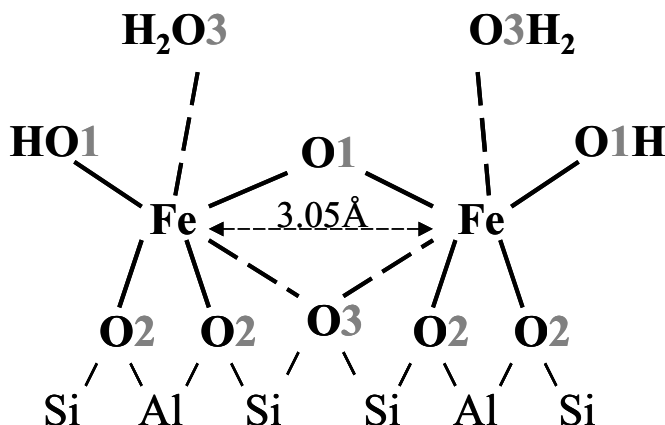


Figure 17: Proposed structure for the binuclear Fe-complexes in Fe/ZSM5, obtained by CVD of FeCl₃, upon mild calcination and treatment in He at 30°C.

The Fe-O-Fe bridging oxygen atom may result by the condensation at high temperature of two bridging hydroxyl groups with the desorption of a water molecule. A sufficient partial pressure of O₂ in the gas phase during calcination should prevent migration and desorption of the bridging oxygen.

In the model presented in Fig. 17, the two oxygen atoms located by the EXAFS analysis in the closest oxygen shell (Fe-O₁), are assigned respectively to a bridging oxygen atom and a hydroxyl group. The Fe-O₁ distance (1.86 Å) appears to be consistent with the average distance of a terminal OH group and a Fe-O-Fe bridging oxygen. Molecular modeling calculations performed on a binuclear [OH-Fe-O-Fe-OH]²⁺ model-complex, bound to the zeolite framework via two oxo-ions (47), have found for the terminal Fe-OH groups a distance of 1.88 Å and for the bridging Fe-O-Fe oxygen atom a Fe-O distance of 1.93 Å. Slightly shorter Fe-O distances are nevertheless reported in the literature for Fe-O-Fe oxo-bridges (around 1.85 Å) (48). EXAFS is therefore not able to discriminate between these two types of oxygen. Oxygen located in shell Fe-O₂ is ascribed to two bridging (Fe-O-Al) O-atoms, by which the iron atoms are stabilized to the zeolite lattice. Indeed, the Fe-O₂ distance of 1.97 Å is consistent with the average distance found for oxygen in the (Fe-O-Al) coordination of the mononuclear FeCl₂⁺ complexes formed upon CVD of FeCl₃ (25,28). In our previous work (25) we found a distance of 1.99 Å. Marturano *et al.* (28), though optimizing their EXAFS fit by introducing two separate Fe-O shells, found for the same Fe-O-Al coordination an average distance of 1.96 Å. Molecular modeling

calculations, mentioned above, found for the Fe-O-Al bridges an average Fe-O distance of 1.95 Å, thus consisting with the Fe-O₂ shell assignment. The most distant oxygen, located in shell Fe-O₃, is assigned to weakly bound oxygen as in adsorbed water. As discussed further, since upon heating to 350°C the C.N. of shell Fe-O₃ appeared to be reduced from 2 to only 1, oxygen atoms were not completely assigned to adsorbed water molecules. As depicted in Fig. 17 the second oxygen neighbor in Fe-O₃ was tentatively assigned to a Si-O-Si bridging oxygen of the zeolite framework.

Heat treatment in He (auto-reduction)

During heating in He different changes are revealed with increasing temperature in the Fe-O coordination of the Fe-binuclear complexes. Heating to 120°C results in an increase of the integrated intensity of the Fe K pre-edge (Figs. 1,2). This is the result of a decrease in the centrosymmetry of the coordination of the Fe atoms (35), caused by a lowering in the number of oxygen neighbors. The EXAFS fit reveals indeed a slight decrease, from 2.1 to 1.4, in the coordination number of the most distant Fe-O shell (Fe-O₃, Table 4). Shell Fe-O₃ therefore contains weakly bound oxygen, coherently with its elongated Fe-O bond. Since the decrease in the Fe-O₃ coordination number is not accompanied by a reduction in the oxidation state of iron, as revealed by the position of both the pre-edge centroid (Fig. 2) and the Fe K-edge (Fig. 5), removal of oxygen up to 120°C is ascribed exclusively to desorption of water, as depicted in Fig. 18.

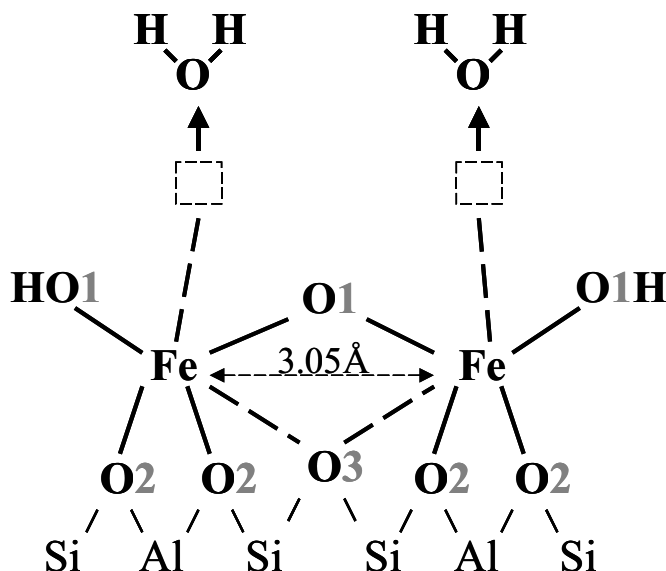


Figure 18: Influence of moderate heating (up to ~150°C) in He or O₂/He (50:50) on the binuclear Fe-complexes in mildly calcined Fe/ZSM5: desorption of water.

No further changes are revealed in the results of the EXAFS fit. In particular, as already mentioned, no changes were visible in the fit of the Fe-Fe coordination, excluding further agglomeration of iron during heating.

An additional increase of the temperature under flowing helium caused clear changes in the features of the Fe K pre-edge (Figs. 1 and 2), showing a clear reduction in the average oxidation state of iron. Indeed, the centroid position and the integrated intensity of Fe/ZSM5, already at 260°C, correspond to those of a reference 50:50 $^{6}\text{Fe}^{\text{III}/(4)}\text{Fe}^{\text{II}}$ physical mixture (35). A slight additional reduction was revealed at 350°C. The reduction is confirmed by the clear shift (~ 4.0 eV) to lower energy of the Fe K-edge (Fig. 9).

These results show that, at high temperature in He, oxygen must be activated and removed from the Fe-O coordination of the binuclear complexes. Auto-reduction phenomena associated to desorption of oxygen at high temperature are known in the literature for Fe/ZSM5 prepared by CVD or solid-state ion exchange of FeCl_3 . O_2 -TPD experiments performed by Voskoboinikov *et al.* (49) on Fe/ZSM5 obtained by CVD on ZSM5 supports with different Si/Al ratios, have shown that oxygen can be desorbed from Fe/ZSM5 by merely heating. Furthermore, the amount of oxygen released increases with decreasing Si/Al ratios. Lobree *et al.* (21) have come to the similar conclusions studying the auto-reducibility of iron in Fe/ZSM5 obtained by solid-state ion exchange. They found that, at a fixed Si/Al ratio (S.A.R. was 25 in their experiments), the auto-reducibility of iron can be strongly enhanced by increasing the iron loading, *i.e.* by reducing the average distance of the iron atoms in the zeolite channels. Kucherov and Shelef (46) reached an identical conclusion using EPR spectroscopy. Activation of oxygen should therefore be facilitated by the close interaction of Fe atoms as in case of Fe-binuclear clusters. The most suited candidate for the reactivity in He appears to be the bridging oxygen atom between the two Fe atoms. This hypothesis is supported by results obtained through $^{18}\text{O}_2$ isotopic exchange studies (26). The experiments, performed on Fe/ZSM5 obtained by CVD, have shown that at temperatures up to 450°C a R1 isotopic exchange mechanism prevails, *i.e.* molecular oxygen from the gas phase exchanges only one ^{18}O atom against a ^{16}O atom from the solid. On Fe/ZSM5 obtained via impregnation, on the contrary, where the presence of binuclear complexes have been demonstrated to be negligible (26), a R2 mechanism prevails, in which $^{18}\text{O}_2$ is exchanged in one step against two ^{16}O atoms.

The analysis of the Fe/ZSM5 EXAFS data recorded in He at 350°C (Fe/ZSM5-He 350°C (1st)) show that the reduction in the oxidation state of Fe is accompanied by a removal of oxygen from the closest Fe-O shell (Fe-O₁, Table 5). The coordination number of shell Fe-O₁ is reduced from 2.0 to 1.2, coherently with the removal of bridging Fe-O-Fe oxygen. Shell Fe-O₂ remains unmodified, confirming the correctness of its assignment to Fe-O-Al

bridges, while only a slight further decrease is revealed in shell Fe-O₃. This is probably the result of further desorption of water with time on stream. A slight contraction is also visible in the Fe-Fe interatomic distance. By comparison with the Fe-Fe distance measured after cooling to 77 K (Fe/ZSM5-He 350°C/LN, Table 4), the contraction can not be ascribed to temperature effects and is probably the result of a rearrangement of the complexes upon heating. From the body of the HR-XANES and EXAFS results, the most plausible structure for the binuclear complexes in He at 350°C, is depicted in Fig. 19.

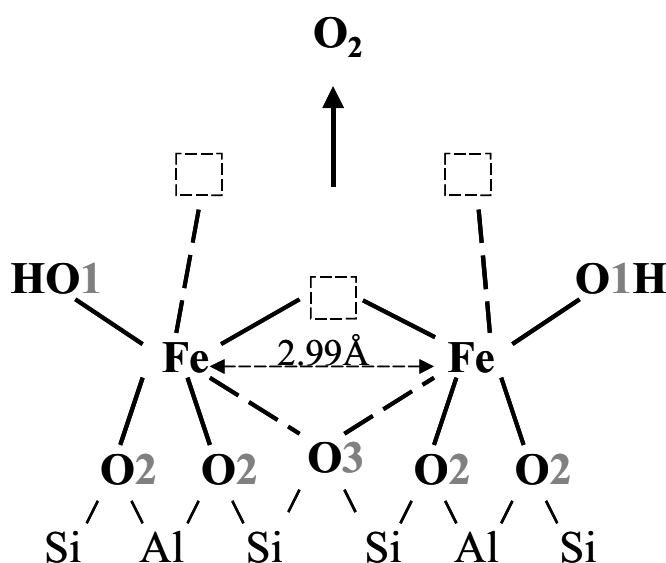


Figure 19: Proposed structure for the binuclear Fe-complexes upon heating in He to 350°C. Autoreduction of iron is ascribed to the removal of the Fe-O-Fe bridging oxygen atom.

At this stage of the treatment two vacancies have been created in the coordination of iron by the desorption of respectively a weakly bound water molecule (Fe-O₃) and bridging oxygen (Fe-O₁). A discussion still open in the literature concerns the possibility of liberating gaseous O₂ by spatially separated oxo-complexes such as [HO-Fe-O-Fe-OH]²⁺, having only one bridging oxygen atom. Voskoboinikov *et al.* (26) have suggested that such complexes might communicate with each other via the O₂⁻ ions of the zeolite. Neighboring Fe-O-Fe complexes, separated by a limited number of O₂⁻ ions of the support could disproportionate into one Fe-O-O-Fe and one Fe-□-Fe complex, where □ stands for a vacancy. Oxygen could be subsequently easily desorbed by the (generated) highly unstable peroxy-complex. Such a mechanism would require the existence of Fe-binuclear complexes bound to pairs of Al centered tetrahedra in close proximity with each other. This condition

could indeed be fulfilled by a significant fraction of the iron complexes in over-exchanged Fe/ZSM5 (Fe/Al=1) with a high Al/Si ratio.

Although a significant fraction of the Fe-binuclear complexes can undergo auto-reduction in He at relatively low temperature ($\sim 250^\circ\text{C}$), they appear to be highly unstable. This was revealed by the differences in the XAFS spectra recorded with time on stream at 350°C and at 77 K after 120 min. stabilization in He at 350°C . As can be seen in Fig. 9 the Fe K-edge appeared to be shifted stepwise to higher energy with exposure time, thus re-oxidation of iron took place during the measurements. The re-oxidation was accompanied by a re-increase in the coordination number of shell Fe-O₁ (Table 5). The remaining shells, on the contrary, remained virtually unchanged. This results confirm the previous observation that changes in the oxidation state of iron are related to only one oxygen atom in the closest Fe-O shell (Fe-O₁), most probably the Fe-O-Fe bridging atom. The reason for the re-oxidation with time on stream is still unclear. While He with a high purity was used (certified purity 5.0), additional oxygen traps were not added to the He line. It can therefore not be excluded that traces of oxygen from the gas phase might have partially reoxidized the Fe-complexes. Nevertheless, re-oxidation could also have been caused by oxygen released at high temperature from the zeolite, supporting the idea of Voskoboinikov et al. (26) of an easy oxygen exchangeability between the zeolite and the Fe-binuclear complexes.

Heat treatment in the presence of O₂

Up to a moderate temperature, the addition of oxygen to the helium flow does not cause significant changes to the coordination of iron. Heating Fe/ZSM5 to 160°C in oxygen results in an increase of the Fe K pre-edge intensity (Figs. 3 and 4) similar to that measured in He at 130°C (Figs. 1 and 2). As in the case of He, this is ascribed to desorption of water, coordinated to the binuclear complexes upon exposure of the Fe/ZSM5 sample to air. As expected, desorption of water is not influenced by the presence of oxygen (Fig. 18).

On the opposite, changes occurring to the binuclear complexes at higher temperature (from 130°C to 350°C) appeared to be strongly influenced by the presence of oxygen in the gas phase. As can be seen in Fig. 4, which collects the pre-edge features of Fe/ZSM5 heated in oxygen, the oxidation state of iron remained unchanged (Fe^{III}) up to 350°C . This is confirmed by the position of the Fe K-edge, which overlaps with that of the hematite reference (Fig. 12). These results show that the presence of oxygen in the gas phase ($P_{\text{O}_2}=0.5$ bar) suppresses the auto-reduction capability revealed by the binuclear complexes at the same temperature in He. The intensity of the Fe K pre-edge in oxygen at 350°C is similar to that of the five-fold coordinated Fe^{III} reference (Fig. 4) (35). Coherently, five oxygen neighbors have been identified by the EXAFS analysis (Table 6). As at 350°C in

helium, only one oxygen is located in the Fe-O₃ shell, in agreement with the removal of one water molecule during heating. The distance of the remaining oxygen in the Fe-O₃ shell appears to be slightly shortened, pointing to a stronger bond of the Fe to the zeolite Si-O-Si oxygen. Shell Fe-O₂, assigned to two oxygen atoms of Fe-O-Al bridges remained unchanged, consistently with the assignment. As can be seen also qualitatively, by comparing the k¹ Fourier Transforms depicted in Fig. 13b, the difference in the Fe-O coordination of the binuclear complexes at 350°C in the presence or absence of oxygen are localized at low R. The EXAFS analysis revealed indeed, that differently from the measurement in He at 350°C, in the presence of oxygen the coordination number of the Fe-O₁ shell remains two, as it was in Fe/ZSM5 measured in He at 30°C. This result confirms that the Fe^{II} ↔ Fe^{III} red-ox reversibility in the binuclear complexes is related to one oxygen atom located in shell Fe-O₁ (R=1.86Å). According to the model proposed by Chen *et al.* (10-12) this atom is assigned to a Fe-O-Fe bridging oxygen (Fig. 20). In the presence of a significant partial pressure of oxygen in the gas phase its removal (desorption) from the Fe-complexes appears to be inhibited.

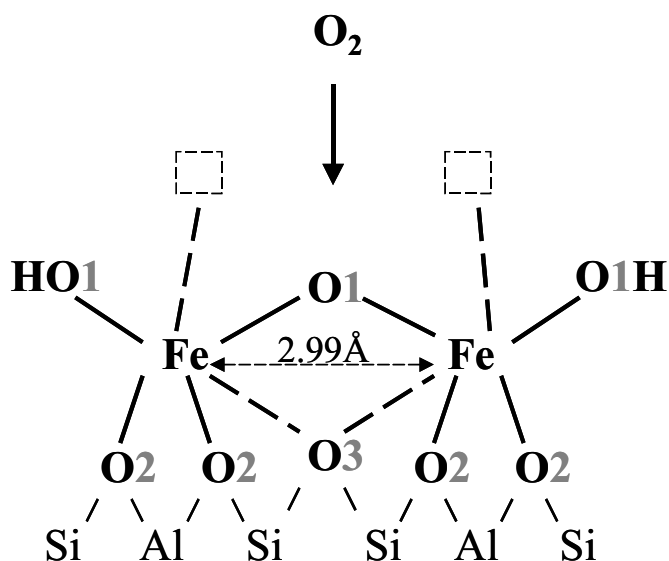


Figure 20: Proposed structure for the binuclear Fe-complexes upon heating to 350°C in O₂/He (50:50). The presence of oxygen in the gas phase inhibits the removal of the Fe-O-Fe bridging oxygen atom.

Conclusions

The analysis of the EXAFS and HR-XANES data obtained from mildly calcined Fe/ZSM5 shows that the majority of iron is present as Fe oxo/hydroxo binuclear complexes. The closest Fe-O coordination of the Fe-binuclear complexes can be described with a [HO-Fe-O-Fe-OH]²⁺ core.

Heat treatments to 350°C in He and in a 50:50 O₂/He mixture do not cause further agglomeration of iron. Heating to a moderate temperature (up to ~150°C) results in the desorption of water from the Fe coordination sphere. As expected, desorption of water is unaffected by the composition of the gas phase (He or a 50:50 O₂/He mixture).

On the contrary, the composition of the gas phase strongly influences the changes occurring to the binuclear complexes in the 150-350°C temperature range. By heating in He a significant fraction of iron is reduced (auto-reduction). This is accompanied by the removal of approximately one oxygen atom from the closest Fe-O shell, attributed to the Fe-O-Fe bridging oxygen atom. The reduced binuclear complexes appear to be highly unstable and undergo re-oxidation with time on stream.

The presence of oxygen in the gas phase (P_{O₂}=0.5 bar) suppresses the auto-reduction capability of the binuclear complexes by inhibiting the removal of the Fe-O-Fe bridging oxygen.

Reference list

1. Panov, G. I., Kharitonov, A., and Sobolev, V., *Appl. Catal.* **98**, 1 (1993).
2. Panov, G. I., Sobolev, V., Dubkov, K.A., Parmon, V.N., Ovanesyan, N.S., Shilov, A.E., and Shteinmann, A.A., *React. Kinet. Catal. Lett.* **61**, 251 (1997).
3. Panov, G.I., Uriarte, A.K., Rodkin, M.A., and Sobolev, V.I., *Catal. Today* **41**, 365 (1998).
4. Panov, G.I., *Cattech.* **4**, 18 (2000).
5. Ribera, A., Arends, I.W.C.E., de Vries, S., Pérez-Ramírez, J., and Sheldon, R.A., *J. Catal.* **195**, 287 (2000).
6. Kapteijn, F., Marbán, G., Rodríguez-Mirasol, J., and Moulijn, J.A., *J. Catal.* **167**, 256 (1997).
7. El-Malki, E.M., van Santen, R.A., and Sachtler, W.M.H., *J. Catal.* **196**, 212 (2000).
8. Pérez-Ramírez, J., Kapteijn F., Mul, G., and Moulijn, J.A., *Chem. Commun.* 693 (2001).
9. Pérez-Ramírez, J., Kapteijn F., Mul, G., and Moulijn, J.A., *Appl. Catal. B* **35**, 227 (2001).

10. Chen, H.-Y., and Sachtler, W.M.H., *Catal. Today* **42**, 73 (1998).
11. Chen, H.-Y., Voskoboinikov, T., and Sachtler, W.M.H., *J. Catal.* **180**, 171 (1998).
12. Chen, H.-Y., Voskoboinikov, T., and Sachtler, W.M.H., *Catal. Today* **54**, 483 (1999).
13. Pérez-Ramírez, J., Mul, G., Kapteijn, F., Moulijn, J.A., Overweg, A.R., Doménech, A., Ribera, A., and Arends, I.W.C.E., *J. Catal.* **207**, 113 (2002).
14. Ovanesyan, N.S., Shteinman, A.A., Sobolev, V.I., Dubkov, K.A., and Panov, G.I., *Kinet. Katal.* **39**, 863 (1998).
15. Rodkin, M.A., Sobolev, V.I., Dubkov, K.A., Watkins, N.H., and Panov, G.I., *Stud. Surf. Sci. Catal.* **130**, 875 (2000).
16. Dubkov, K.A., Ovanesyan, N.S., Shteinman, A.A., Starokon, E.V., and Panov, G.I., *J. Catal.* **207**, 341 (2002).
17. Chen, H.-Y., El-Malki, E.M., Wang, X., van Santen, R.A., and Sachtler, W.M.H., *J. Molec. Catal. A* **162**, 159 (2000).
18. Feng, X., and Hall, W.K., *J. Catal.* **166**, 368 (1997).
19. Kögel, M., Sandoval, V.H., Schwieger, W., Tissler, A., and Turek, T., *Catal. Lett.* **51**, 23 (1998).
20. Joyner, R., and Stockenhuber, M., *J. Phys. Chem. B* **103**, 5963 (1999).
21. Lobree, L.J., Hwang, I.-C., Reimer, J.A., and Bell, A.T., *J. Catal.* **186**, 242 (1999).
22. Wood, B.R., Reimer, J.A., and Bell, A.T., *J. Catal.* **209**, 151 (2002).
23. Heinrich, F., Schmidt, C., Löffler, E., and Grünert, W., *Catal. Commun.* **2**, 317 (2001).
24. Kögel, M., Mönnig, R., Schwieger, W., Tissler, A., and Turek, T., *J. Catal.* **182**, 470 (1999).
25. Chapter 2 of this thesis; Battiston, A.A., Bitter, J.H., de Groot, F.M.F., Overweg, A.R., Stephan, O., van Bokhoven, J.A., Kooyman, P.J., van der Spek, C., Vankó, G., and Koningsberger, D.C., submitted to *J. Catal.*
26. Voskoboinikov, T.V., Chen, H.-Y., and Sachtler, W.M.H., *J. Molec. Catal. A* **155**, 155 (2000).
27. Marturano, P., Drozdová, L., Kogelbauer, A., and Prins, R., *J. Catal.* **192**, 236 (2000).
28. Marturano, P., Drozdová, L., Pirngruber, G.D., Kogelbauer, A., and Prins, R., *Phys. Chem. Chem. Phys.* **3**, 5585 (2001).
29. Battiston, A.A., Bitter, J.H., and Koningsberger, D.C., *Catal. Lett.* **66**, 75 (2000).
30. Rustad, J.R., Felmy, A.R., and Hay, B.P., *Geochim. Cosmochim. Acta* **90**, 1553 (1996).
31. Suzuki, S., Suzuki, T., Kimura, M., Takagi, Y., Shinoda, K., Tohji, K., and Waseda, Y., *App. Surf. Science* **169-170**, 109 (2001).
32. Dräger, G., Frahm, R., Materlik, G., and Brummer, O., *Phys. Stat. Sol. B* **146**, 287 (1988).

33. Heumann, D., Dräger, G., and Bocharov, S., *J. Physique IV*, **7C2**, 481, (1997).
34. Westre, T.E., Kennepohl, P., de Witt, J., Hedman, B., Hogson, K.O., and Solomon, E.I., *J. Am. Chem. Soc.* **119**, 6297 (1997)
35. Wilke, M., Farges, F., Petit P.-E., Brown, G.E.Jr., and Martin, F., *Am. Miner.* **86**, 714 (2001).
36. Sette, F., Ruocco, G., Krisch, M., Bergmann, U., Masciovecchio, C., Mazzacurati, V., Signorelli, G., and Verbeni, R., *Phys. Rev. Lett.* **75**, 850 (1995).
37. Vaarkamp, M., Mojet, B.L., Modica, F.S., Miller, J.T., and Koningsberger, D.C., *J. Phys. Chem.* **99**, 16067 (1995).
38. Schroeder, S.L.M., *Adv. Spectroscopy* **26**, 1 (1998).
39. Vaarkamp, M., Linders, J.C., and Koningsberger, D.C., *Physica B*, **209** (1995).
40. Vaarkamp, M., Dring, I., Oldman, R.J., Stern, E.A., and Koningsberger, D.C., *Phys. Rev. B* **50**, 7872 (1994).
41. Koningsberger, D.C., Mojet, B.L., van Dorssen, G.E., and Ramaker, D.E., *Top. Catal.* **10**, 143 (2000).
42. Cook, J.W., and Sayers, D.E., *J. Appl. Phys.* **52**, 5024 (1981).
43. Ankudinov, A.L., and Rehr, J.J., *Phys. Rev. B* **56**, R1712 (1997).
44. Koningsberger, D.C., *Jpn. J. Appl. Phys.* **32**, 877 (1993).
45. Li, G.G., Bridges, F., and Booth C.H., *Phys. Rev. B* **52**, 6332 (1995).
46. Kucherov, A.V., and Shelef, M., *J. Catal.* **195**, 112 (2000).
47. Battiston, A.A., Bitter, J.H., De Romph, D., and Koningsberger, D.C.; in preparation.
48. Hsu, H.F., Dong, Y., Shu, L., Young, V.G.J., and Que, L.J., *J. Am. Chem. Soc.* **121**, 5230 (1999).
49. Voskoboinikov, T.V., Chen, H.-Y., and Sachtler, W.M.H., *Appl. Catal. B* **19**, 279 (1998).
50. Chapter 4 of this thesis; Battiston, A.A., Bitter, J.H., and Koningsberger, D.C., submitted to *J. Catal.*

Reactivity of the Fe-Binuclear Complexes in Over-Exchanged Fe/ZSM5, Studied by *In situ* XAFS Spectroscopy:

Selective Catalytic Reduction of NO with Isobutane

Abstract

In situ XAFS spectroscopy was applied in order to determine the active sites for the HC-SCR of NO_x in Fe/ZSM5, prepared by FeCl₃ sublimation. The number of (inactive) spectators in this catalyst was minimized by using a specially dedicated calcination procedure. The catalytic activity of Fe/ZSM5 during the collection of the XAFS data was monitored via chemiluminescence analysis of the gas outlet.

Binuclear Fe-complexes with a Fe-O-Fe core were found to be catalytic active species in this material. During heat treatment in He to 350°C the Fe-complexes undergo auto-reduction, ascribed to the removal of oxygen from Fe-O-Fe bridges (closest Fe-O coordination sphere) and the formation of Fe-□-Fe vacancies. Treatment with isobutane results in a further slight average reduction of iron, accompanied by an additional removal of oxygen from the Fe-O-Fe bridges. Fe in the binuclear complexes is readily oxidized when NO, NO+O₂ or a typical HC-SCR mixture (NO, i-C₄H₁₀, O₂) are fed to the Fe/ZSM5 catalyst. Re-oxidation is accompanied by filling of the Fe-□-Fe vacancies.

Under HC-SCR working conditions the average oxidation state of iron is 3+.

Introduction

Over-exchanged Fe/ZSM5, obtained by Chemical Vapor Deposition (CVD) of FeCl₃, has shown a remarkable activity for the decomposition of N₂O (1) and for the Selective Catalytic Reduction of nitrogen oxides using HydroCarbons (HC-SCR), even in the presence of water (2-5). Catalytic tests have demonstrated that the HC-SCR catalytic activity of Fe/ZSM5 depends on the concentration of oxygen and on the type of hydrocarbon employed in the feed. The highest N₂ yields have been obtained in the 2-10 vol% O₂ range by using n-butane or isobutane as reductant (3).

In order to unravel the HC-SCR reaction pathway on Fe/ZSM5, several studies have been performed by applying *in situ* FTIR spectroscopy (3,4,6). Intermediate adsorption species have been monitored while feeding (separately, or at the same time) typical HC-SCR reagents, *i.e.* NO, O₂ and i-C₄H₁₀ (or alternatively, a different alkane). Based on these results, and on catalytic tests performed with labeled reactants, a model for the HC-SCR reaction pathway has been proposed. According to this model, the first HC-SCR steps are believed to be the oxidation of NO by O₂ to form NO₂, which is then released to the gas-phase, and the formation of nitro (NO₂)⁻ and nitrate (NO₃)⁻ complexes. These (NO_y)⁻ complexes react further with the hydrocarbon, forming organic nitro- and nitroso-compounds. The nitro/nitroso deposits may evolve through different pathways, depending on the nature of the hydrocarbon. Independently on the type of hydrocarbon employed, the final step in the pathway is proposed to be the reaction of the organic compound with NO₂ from the gas phase, leading to the formation of a N-N bond and the desorption of N₂.

The active species responsible for the peculiar catalytic properties of over-exchanged Fe/ZSM5 are believed to consist of extra-framework binuclear Fe-oxo/hydroxo complexes, with a [OH-Fe-O-Fe-OH]²⁺ core (1-3,7,8), ligated to the Brønsted aluminum sites of the zeolite. Several spectroscopic studies have indeed demonstrated that binuclear Fe-oxo/hydroxo complexes are generated by the reaction of sublimated FeCl₃ with the Brønsted protons of the zeolite and by the subsequent hydrolysis processes occurring during washing (9-12). The Fe-binuclear species in washed Fe/ZSM5 consist of two octahedrally coordinated Fe^{III} oxo/hydroxo ions, with a structure similar that of the closest Fe-binuclear building unit in α-goethite (10,11).

The final treatment in the synthesis of Fe/ZSM5 is calcination. Calcination, applied to stabilize and activate the Fe-phase, is a delicate step for the further evolution of the Fe-binuclear complexes. Our group has shown that, if the calcination procedure is not carefully controlled, this treatment can result in the removal of a significant fraction of iron from the zeolite micropores, finally resulting in the formation of large catalytically inactive (8,13) goethite/hematite crystals (11). On the contrary, by adequately tuning the conditions

applied during calcination (11) a high concentration of Fe-binuclear species in Fe/ZSM5 can be preserved. The resulting material is therefore the best suited for characterizing structure and reactivity of the Fe-binuclear complexes, minimizing the interference of (inactive) spectators.

In a previous paper (14) we have studied the structure of the Fe-binuclear complexes in Fe/ZSM5, measured at 30°C in He, upon exposure to air. Furthermore, we have focused our attention on the changes occurring in the Fe-O coordination of the iron-complexes during heating treatments in He and in a He/O₂ (50:50) mixture. The results obtained, discussed in Ref. (14), are summarized in the model presented in Fig. 1.

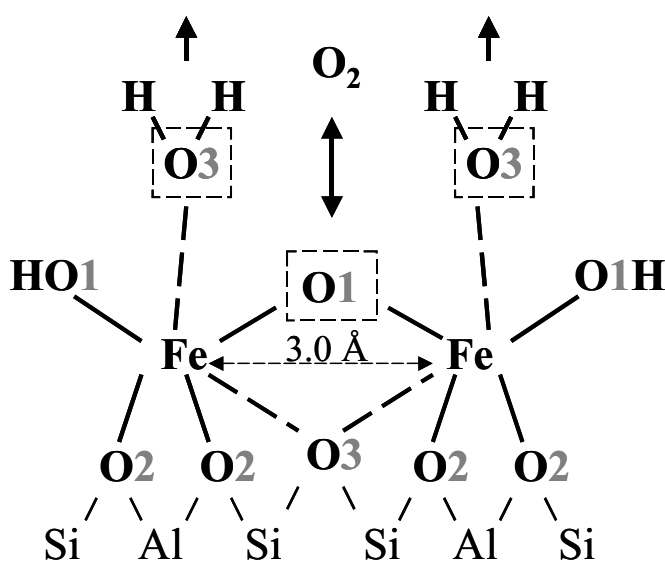


Figure 1: Proposed structure and reactivity of the binuclear oxo/hydroxo Fe-complexes in Fe/ZSM5, obtained by FeCl₃ CVD, during heat treatments to 350°C in helium and in the presence of oxygen (14).

Upon exposure to air, six Fe-O neighbors have been identified in the as-synthesized Fe/ZSM5. In the model proposed the oxygen atoms have been lumped together in three different Fe-O shells. The closest Fe-O shell (Fe-O₁, 1.85-1.89 Å) has been assigned to a terminal hydroxyl group and to an oxygen atom bridging the Fe ions, according to the [HO-Fe-O-Fe-OH]²⁺ core-model proposed by Chen and Sachtler (2). The Fe-O shell at intermediate distance (Fe-O₂, 1.97-1.99 Å) has been assigned to two oxygen atoms ligating the Fe atoms to the aluminum-centered tetrahedra of the zeolite (14). The most distant shell (Fe-O₃, 2.02-2.09 Å) has been attributed to an oxygen atom of the zeolite and to an adsorbed water molecule, respectively.

The assignment of the different Fe-O shells is based on the results obtained during the heat treatments. Heating Fe/ZSM5 to a moderate temperature (up to $\sim 150^\circ\text{C}$), in He as well as in the presence of O_2 , results in the removal of approximately one oxygen atom (O_3) from the most distant Fe-O shell. Since this is not accompanied by changes in the oxidation state of iron, the oxygen removal is consistent with desorption of weakly bound H_2O . The further evolution of the Fe-complexes at higher temperature ($\Delta T=150\text{-}350^\circ\text{C}$) is strongly influenced by the composition of the gas phase. In He a significant fraction of iron undergoes auto-reduction, a phenomenon already known in the literature for over-exchanged Fe/ZSM5 (9,13,15). This phenomenon coincides with the removal of only one oxygen atom (O_1) from the closest Fe-O shell. The most plausible interpretation appears to be the removal of the Fe-O-Fe bridging atom, as discussed in Ref. (14). The high reactivity of the bridging oxygen is claimed to be responsible for the capability of Fe/ZSM5 to oxidize NO to NO_2 and to decompose N_2O (1,8). Noticeably, the presence of oxygen in the gas phase completely suppresses both the reduction of iron and the removal of the Fe-O-Fe bridging oxygen. The core structure of the binuclear complexes at 350°C in oxygen ($P_{\text{O}_2} = 0.5$ bar) matches the model previously proposed by Chen and Sachtler (2).

In this paper the structure and the reactivity of the Fe-binuclear complexes in mildly calcined over-exchanged Fe/ZSM5 is determined under HC-SCR working conditions. This has been achieved by monitoring the local environment of the Fe-binuclear complexes at 350°C : i) in the presence of single HC-SCR reactants, *i.e.* NO, O_2 , or $i\text{-C}_4\text{H}_{10}$, fed separately and ii) during the HC-SCR reaction, *i.e.* in the contemporary presence of the three reactants. Information on the coordination geometry of Fe, obtained by the analysis of the Fe K-pre-edge features (centroid position and integrated intensity) has been used as input information for the fitting of the recorded EXAFS data. The catalytic activity of Fe/ZSM5 during the XAFS measurements has been monitored by analyzing the composition of the gas-phase via a NO_x chemiluminescence analyzer.

Experimental

Catalyst preparation

$\text{NH}_4/\text{ZSM5}$ (Si/Al=17.0, determined by ICP), obtained from Zeolyst, was converted into the acidic form by calcination in oxygen at 550°C for 3 h. The resulting H/ZSM5 was used as host for the synthesis of over-exchanged Fe/ZSM5, by applying the FeCl_3 Chemical Vapor Deposition technique (2). The procedure applied has been described in detail previously (11,14). First, anhydrous FeCl_3 was sublimated into the zeolite micropores. The sample was subsequently washed under stirring in doubly demineralized water for

hydrolyzation and removal of excess chlorine. After drying overnight at 70°C, the sample was calcined. The procedure applied (mild calcination) was identical to the one proposed in our previous work (11). The sample was heated under a He flow of 800 ml/min with a moderate temperature ramp (0.5°C/min) to 200°C. At this temperature, 200 ml/min of O₂ were added to the He flow while, under the same temperature ramp, heating was continued to 550°C. After 3 hrs at 550°C, the temperature was decreased to 30°C. The sample after calcination will be further denoted as Fe/ZSM5.

Catalytic testing

Fe/ZSM5 was tested for the selective catalytic reduction of NO with isobutane under Plug-Flow conditions. The catalyst (powder) was pressed, sieved to 90-212 µm, and charged in the reactor upon dilution with quartz. The sample was preheated to 350°C with a rate of 5°C/min under a He flow of 100 ml/min. The reaction feed was obtained by blending four flows, *i.e.* 1% NO/He, 1% i-C₄H₁₀/He, O₂ and He. Each flow-rate was regulated by a digital Brooks mass-flow controller. The resulting inlet composition was 2000 vppm NO, 2000 vppm i-C₄H₁₀, 3%vol. O₂, balance He, with an overall flow of 140 ml/min. Catalytic tests were performed using 100 or 20 mg catalyst. Based on an apparent zeolite density of 0.5 g/cm³, the calculated Gas Hourly Space Velocity (GHSV) was respectively 42000 and 210000 h⁻¹. The operating conditions applied during the activity tests are summarized in Table 1.

Table 1: Description of the reactor and of the operating conditions during the HC-SCR catalytic tests with isobutane on Fe/ZSM5.

Parameters description	Test 1	Test 2
Catalyst amount (Fe/ZSM5) (mg)	100	20
Quartz amount (g)	4.0	0.45
Sieve fraction (µm)	90-212	90-212
Reactor internal diameter (mm)	12	4
Total bed length (mm)	36	25
Total feed rate (cm ³ /min)	140	140
Calculated GHSV (h ⁻¹)	42000	210000
Feed composition (vol%): NO (0.2), i-C ₄ H ₁₀ (0.2), O ₂ (3.0), balance He.		

A Perkin Elmer Autosystem XL gas chromatograph equipped with a TCD detector was used to monitor the effluent N_2 , $i-C_4H_{10}$, N_2O , CO and CO_2 . The gases were separated using a Haysep Q and a Molsieve 13 X column (80-100 mesh). In order to be able to measure NO and NO_2 , a Thermo Environmental Instruments 42C NO_x chemiluminescence analyzer was connected in parallel with the gas chromatograph. The GC and the NO_x analyzer could be operated simultaneously. Catalytic data reported were measured after 60 min stabilization at each temperature.

***In situ* Fe K-edge XAFS**

XAFS data-collection

The XAFS data were collected at the Wiggler station X1.1 at Hasylab (Hamburg, Germany). The experimental set-up used is described in detail in Ref. (11). Fe/ZSM5 was pressed to obtain self-supporting wafers, calculated to have a total absorption (μ^*x) of 2.5, and placed in a controlled atmosphere cell (16). Spectra were recorded after specific pretreatments. The complete list of the XAFS measurements, including information on pretreatments, measuring conditions and sample codes, is collected in Table 2.

Table 2: List of XAFS spectra recorded from Fe/ZSM5: pretreatments and measuring conditions.

Pretreatments (flowing atmosphere)	Environ. conditions during measurement	Measurements code
↑; He, 30 min at 350°C	flowing He, 350°C	Fe/ZSM5-He 350/350
↑↑; O_2 /He, 60 min at 350°C	flowing O_2 /He, 350°C	Fe/ZSM5- O_2 350/350
↑; $i-C_4H_{10}$ /He, 60 min at 350°C	flowing $i-C_4H_{10}$ /He, 350°C	Fe/ZSM5- CH_x 350/350
↑; $i-C_4H_{10}$ /He, 90 min at 350°C	$i-C_4H_{10}$ /He, 77 K	Fe/ZSM5- CH_x 350/LN
↑; NO/He, 60 min at 350°C	flowing NO/He, 350°C	Fe/ZSM5-NO 350/350
↑; NO/He, 90 min at 350°C	NO/He, 77 K	Fe/ZSM5-NO 350/LN
↑; $NO+O_2$ /He, 60 min at 350°C	flowing $NO+O_2$ /He, 350°C	Fe/ZSM5- $NO+O_2$ 350/350
↑; $NO+O_2$ /He, 90 min at 350°C	$NO+O_2$ /He, 77 K	Fe/ZSM5- $NO+O_2$ 350/LN
↑; deNO/He, 60 min at 350°C	flowing deNO/He, 350°C	Fe/ZSM5-deNO 350/350
↑; deNO/He, 90 min at 350°C	deNO/He, 77 K	Fe/ZSM5-deNO 350/LN

↑ = heating treatment to 350°C (5°C/min) performed in He
 ↑↑ = heating treatment to 350°C (5°C/min) performed in O_2 /He

Fe/ZSM5 was heated to 350°C under 50 ml/min flowing He (with the exception of measurement Fe/ZSM5-O₂ 350/350, heated in the presence of oxygen). After 10 minutes stabilization at 350°C, specific gas mixtures were fed to the cell, while the temperature was maintained at 350°C. The composition of the different feeds is presented in Table 3.

Table 3: Inlet gas composition during *in situ* XAFS measurements of Fe/ZSM5.

Measurements code	Inlet gas composition (vol.%)
Fe/ZSM5-He 350/350	He (100)
Fe/ZSM5-O ₂ 350/350	O ₂ (50), balance He
Fe/ZSM5-CH _x 350/350	i-C ₄ H ₁₀ (0.2), balance He
Fe/ZSM5-NO 350/350	NO (0.2), balance He
Fe/ZSM5-NO+O ₂ 350/350	NO (0.2), O ₂ (5), balance He
Fe/ZSM5-deNO 350/350	NO (0.2), i-C ₄ H ₁₀ (0.2), O ₂ (5), balance He

After 30 min. on stream, three spectra were recorded *in situ* at 350°C. After closing the *in situ* cell and cooling to 77 K, three additional scans were recorded. XANES spectra of hematite and Fe-titanate were also measured, upon purging with He at RT and cooling to 77 K. They were used, respectively, as internal Fe^{III} and Fe^{II} references. The three scans recorded for each measurement were compared and averaged, with the exception of measurement Fe/ZSM5-He 350/350. As extensively discussed in Ref. (14), due to differences between the scans, caused by a partial re-oxidation of the sample with time on stream, the three spectra of this measurement were not averaged. In this case, only data from the first scan were used.

Analysis of the Fe K pre-edge

The oxidation state of iron was determined by the analysis of the centroid position of the background subtracted Fe-K pre-edge and by the position of the Fe-K absorption edge. In addition, information on the local coordination geometry of iron was derived from the analysis of the pre-edge centroid position and of the background subtracted pre-edge integrated intensity (17). The Fe K pre-edge was isolated from the XAFS spectra by using a cubic spline function, obtained by interpolating the data several eVs before and after the pre-edge (14,17). Centroid position and integrated intensity of the background-subtracted pre-edge were calculated with the software Grams. The estimated accuracy in the

determination of the centroid position is ± 0.1 eV. The error in the integrated intensity is approximately $\pm 5\%$.

XAFS data-processing

XAFS data were extracted from the measured absorption spectra by means of the XDAP code (18). The pre-edge was subtracted using a modified Victoreen curve (19). Background subtraction from the absorption XAFS spectra was performed by employing cubic spline routines, with a continuously adjustable smooth parameter (20,21). Normalization was performed by dividing the data by the intensity of the absorption spectrum at 50 eV above the Fe K-edge.

EXAFS data-analysis, phase-shifts, backscattering amplitudes

The local environment around iron, *i.e.* number and distances of Fe-neighboring atoms, was determined by EXAFS (20). The information on the coordination geometry of Fe, obtained from the analysis of the Fe K pre-edge, was used as input for the EXAFS analysis.

The Fe-O reference was obtained from experimental EXAFS data of ferric acetylacetonate. The procedure followed for the creation of the Fe-O reference file is described in Ref. (11). Fe-Fe phase shifts and backscattering amplitudes were calculated using the software FEFF7 (22). The Fe-Fe reference was calibrated on EXAFS data obtained from hematite at 77 K (11), by fitting in R-space. The crystallographic parameters used for the fit of the calibration reference (23,24) can be found in Ref. (11).

The EXAFS data-analysis was performed by applying multiple-shell fitting in R-space ($\Delta R = 0.7\text{-}4.2$ Å; $\Delta k = 2.7\text{-}13.2$ Å⁻¹). The difference file technique was applied together with phase-corrected Fourier Transforms to resolve the different contributions in the EXAFS data (20). The EXAFS fits were checked by applying k^1 , k^2 and k^3 weightings.

The number of independent fit parameters (N_{indp}) was determined as outlined in the 'Reports on Standard and Criteria in XAFS Spectroscopy' (25). For the measurements performed in this work it was calculated to be 25.4.

Errors in the numerical values obtained by the EXAFS data analysis are estimated to be $\pm 10\%$ in the coordination number (N), $\pm 1\%$ in the distance (R), $\pm 5\%$ in the Debye Waller factor ($\Delta\sigma^2$) and $\pm 10\%$ in the inner potential correction (ΔE_0) (26).

Catalytic activity during XAFS data-collection

In order to monitor the catalytic activity of Fe/ZSM5 during the collection of XAFS spectra Fe/ZSM5-NO 350/350, Fe/ZSM5-NO+O₂ 350/350 and Fe/ZSM5-deNO 350/350 (see Table 2), a Thermo Environmental Instruments 42C NO_x chemiluminescence analyzer was connected in parallel to the outlet of the cell. Concentration of NO and NO₂ were measured at a time interval of 1 minute, while recording the XAFS spectra. Stabilization of the NO

and NO₂ concentration in the outlet was obtained for all the three measurements within 60 min. from the beginning of the treatment.

Results

HC-SCR catalytic testing

The results of the catalytic test performed on Fe/ZSM5 for the selective catalytic reduction of NO with isobutane under excess oxygen at 42000 h⁻¹ GHSV are depicted in Fig. 2a. Feed composition and GHSV for this test were chosen in order to be able to compare our results to the ones already available in the literature (2). In agreement with those results, a maximum in the conversion of NO to N₂ was obtained at a temperature of about 360°C. The maximum N₂ yield was around 78%, confirming the high activity of Fe/ZSM5 towards the HC-SCR reaction, when using isobutane as reductant. Contemporarily, a considerable amount of CO (above 50% yield at maximum NO conversion) was formed, as a result of the incomplete i-C₄H₁₀ combustion. Both N₂O and NO₂ were absent from the products, the selectivity towards N₂ being complete in the whole temperature range.

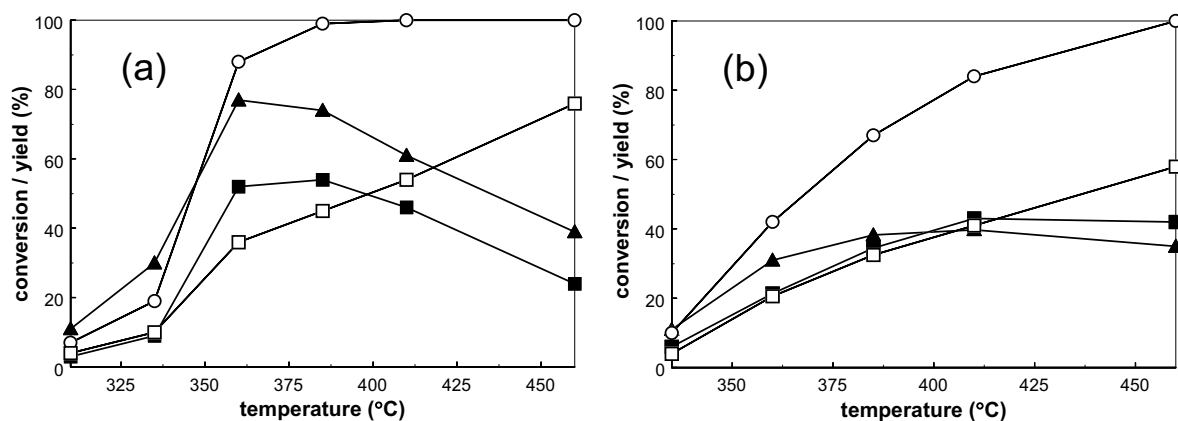


Figure 2: Selective catalytic reduction of NO by isobutane over Fe/ZSM5: (▲) N₂ yield, (○) i-C₄H₁₀ conversion, (■) i-C₄H₁₀ conversion to CO, (□) i-C₄H₁₀ conversion to CO₂. Inlet composition: 0.2% i-C₄H₁₀ + 0.2% NO + 3% O₂, balance He. Total flow rate = 140 cm³·min⁻¹. (a) GHSV = 42000 h⁻¹; (b) GHSV = 21000 h⁻¹. GHSV is based on an apparent zeolite density of 0.5 g·cm⁻³.

Reducing the residence time of the reactants (Fig. 2b, GHSV=21000 h⁻¹) caused a shift in the maximum N₂ yield towards higher temperature (to approximately 400°C). Nevertheless, even under this extreme flow-rate, the catalyst maintained a considerably high activity

(around 36% maximum N₂ yield), while no N-containing by-products were detected in the gas phase.

Heat treatment in He and O₂

The normalized XANES spectra of Fe/ZSM5 recorded at 350°C in He (Fe/ZSM5-He 350/350) (solid line) and in a 50:50 O₂/He mixture (Fe/ZSM5-O₂ 350/350) (dotted line) are presented in Fig. 3a. The corresponding background-subtracted pre-edges are depicted in the upper-left part of the figure. XANES spectra measured from Fe-titanate and hematite are reported as internal references.

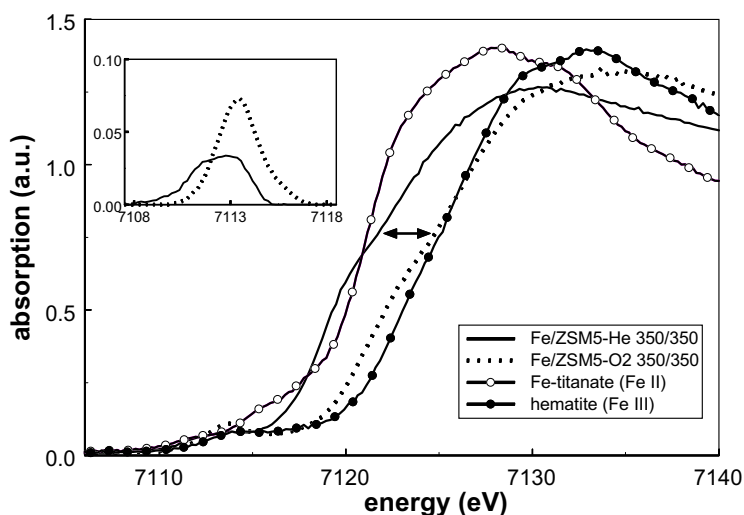


Figure 3a: Normalized XANES spectra and background subtracted pre-edges (enlarged in the upper-left part of the figure) of Fe/ZSM5-He 350/350 (solid line) and Fe/ZSM5-O₂ 350/350 (dotted line). Normalized XANES spectra of hematite and Fe-titanate are also reported, respectively as internal Fe^{III} and Fe^{II} references.

As can be seen, the position of the Fe/ZSM5 Fe K-edges are separated by approximately 4.0 eV. While the edge of the sample treated in oxygen corresponds to that of hematite (Fe^{III}), the edge of the sample measured in He appears to be close to that of Fe-titanate (Fe^{II}). The features of the pre-edges appear also to be different. The pre-edge measured in He is clearly shifted towards lower energy and displays a lower intensity.

Centroid position and integrated intensity of the pre-edge in Fe/ZSM5, measured upon the heat treatments, are plotted in Fig. 3b.

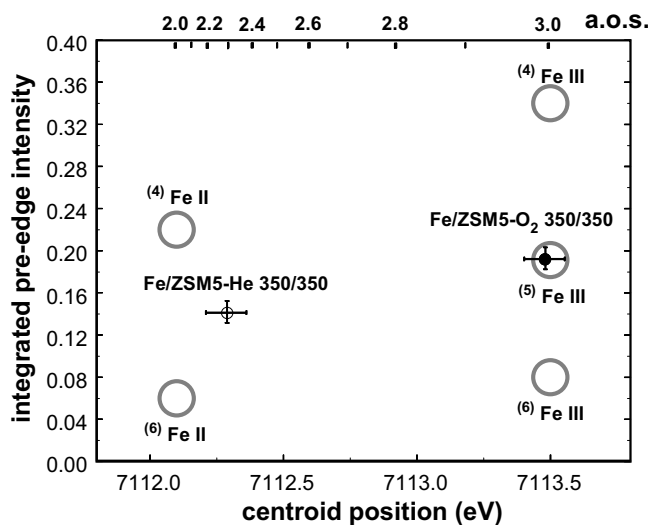


Figure 3b: Pre-edge characteristics (centroid position and integrated intensity) of Fe/ZSM5-He 350/350 (○) and Fe/ZSM5-O₂ 350/350 (●). Pre-edge characteristics of iron with known coordination and oxidation state (⁶Fe III, ⁵Fe III, ⁴Fe III, ⁶Fe II, ⁴Fe II: (○)), obtained from the literature (17), are reported for comparison.

In the same figure the Fe K pre-edge features of crystalline single-phase iron-containing references (large gray circles), obtained from the work of Wilke *et al.* (17), are reported for comparison. The Fe-references differ for oxidation state (II or III) and for coordination geometry (from perfectly octahedral (⁶) to perfectly tetrahedral (⁴)). The number in the upper brackets indicates the number of neighboring atoms in the Fe coordination sphere. In the upper x-axis of the figure the average oxidation state of iron (a.o.s) is plotted as a function of the pre-edge centroid energy (lower x-axis). This relation has been obtained by XAFS measurements on ⁶Fe^{III}/⁴Fe^{II} physical mixtures (17). By comparison with the references, it can be concluded that the average oxidation state of iron in Fe/ZSM5 measured at 350°C in He is close to +2.3. Although only qualitative conclusions can be derived by the present data (14), the average Fe-coordination in Fe/ZSM5 at 350°C in helium appears to be close to that of five-fold- or highly distorted tetrahedrally coordinated iron. Reduction of iron and oxygen removal from the Fe-coordination sphere, as already discussed in our previous work (14), is the result of auto-reduction phenomena occurring to Fe/ZSM5 during the heat treatment in the absence of oxygen. Iron in untreated Fe/ZSM5, indeed, is octahedrally coordinated, with an oxidation state of 3+ (11,14). The oxidation state of iron in Fe/ZSM5 measured in the presence of oxygen at 350°C is 3+. The Fe-coordination geometry corresponds to that of a five-fold coordinated reference. This shows that heating in oxygen

influences the Fe-O coordination, decreased from six (untreated sample, (14)) to five oxygen neighbors, but does not change the oxidation state of iron.

The differences in the Fe-O coordination sphere of Fe/ZSM5-He 350/350 and Fe/ZSM5-O₂ 350/350 can be visualized by comparing the Fourier transforms of their EXAFS data (Fig. 3c).

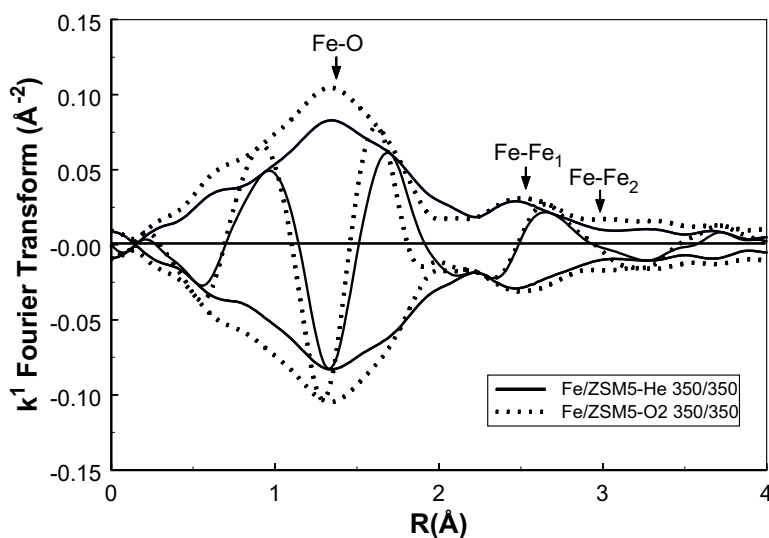


Figure 3c: Fourier transform (k^1 , $\Delta k=2.7-13.2 \text{ \AA}^{-1}$) of EXAFS data of Fe/ZSM5-He 350/350 (solid line) and Fe/ZSM5-O₂ 350/350 (dotted line).

The most distant peaks (Fe-Fe₁ and Fe-Fe₂) are due to Fe-Fe neighbors. As already discussed in our previous work (14), they are ascribed to the presence of binuclear Fe-complexes, together with a minor fraction of Fe-species with a higher Fe-Fe coordination. The main peak (Fe-O) is due to oxygen. As can be seen, this Fe-O peak in Fe/ZSM5-O₂ 350/350 displays a higher intensity (real part) than in Fe/ZSM5-He 350/350. Furthermore, the imaginary part appears to be clearly shifted towards lower distance. This indicates that in Fe/ZSM5-O₂ 350/350 additional oxygen is present, located at low R.

The coordination parameters obtained by R-space analysis of the EXAFS data are presented in Table 4. For the fit, a distribution of oxygen in three different sub-shells was chosen. The assignment of three different Fe-O sub-shells was based on the results obtained during the heat treatments (14). The model proposed for the evolution of the binuclear complexes upon the heat treatments has been shown in Fig. 1. Shell Fe-O₂, which remained unchanged, was ascribed to two oxygen atoms, anchoring the Fe atoms of the binuclear

complexes to the Al centered tetrahedra of the zeolite. The most distant O shell (Fe-O3) could be attributed to a semi-bridging oxygen from the zeolite. Shell Fe-O1 was attributed to a Fe-O-Fe bridging oxygen and to a terminal OH group.

Table 4: Coordination parameters obtained by R-space analysis (k^1 , $\Delta k=2.7-13.2 \text{ \AA}^{-1}$; $\Delta R= 0.7-4.2 \text{ \AA}$) of EXAFS data of Fe/ZSM5-He 350/350 and Fe/ZSM5-O₂ 350/350; $N_{\text{indp}}= 25.4$; $N_{\text{free (fit)}}= 22$.

Shells	N $\pm 10\%$	R (\AA) $\pm 1\%$	$\Delta\sigma^2$ (10^{-3} \AA^2) $\pm 5\%$	ΔE_0 (eV) $\pm 10\%$	k^1 -variance (%)	
					Im. part	Abs. part
Fe/ZSM5-He 350/350					0.55	0.30
Fe-O ₁	1.2	1.88	2.6	-5.5		
Fe-O ₂	2.0	1.97	7.2	12.6		
Fe-O ₃	1.2	2.08	8.8	-9.3		
Fe-Fe ₁	1.1	2.99	13.0	0.4		
Fe-Fe ₂	0.4	3.40	17.2	0.1		
Fe-O _Z	1.6	4.09	15.0	-8.8		
Fe/ZSM5-O ₂ 350/350					1.26	0.50
Fe-O ₁	1.9	1.86	2.0	-2.5		
Fe-O ₂	2.0	1.99	5.0	13.0		
Fe-O ₃	1.0	2.02	1.6	-13.3		
Fe-Fe ₁	1.2	2.99	9.8	-1.6		
Fe-Fe ₂	0.4	3.40	15.1	-3.7		
Fe-O _Z	4.4	3.81	15.0	1.0		

As can be seen from Table 4, the most significant differences in the fit-results for Fe/ZSM5-He 350/350 and Fe/ZSM5-O₂ 350/350 are in shell Fe-O₁. Approximately two oxygen atoms (1.9) are present for Fe/ZSM5-O₂ 350/350, while only 1.2 oxygen atoms are present for Fe/ZSM5-He 350/350. This difference can be explained by the removal of the bridging Fe-O-Fe oxygen, as a result of auto-reduction of iron at 350°C in He. The clear differences in the Fe-O₁ shell as a function of the gas-phase composition can also be visualized qualitatively in Fig. 3d, where, for both measurements, the EXAFS Fourier Transform of only contribution Fe-O₁ is plotted. As can be seen, the intensity of the shell in

He appears to be almost halved. The presence of O₂ in the gas phase inhibits removal of oxygen.

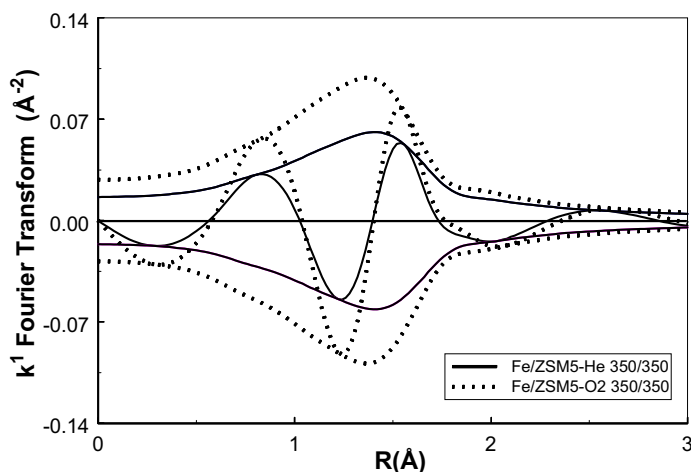


Figure 3d: Fourier transform of the Fe-O₁ contribution, obtained by R-space analysis (k^1 , $\Delta k=2.7-13.2 \text{ \AA}^{-1}$; $\Delta R=0.7-4.2 \text{ \AA}$) of EXAFS data of Fe/ZSM5-He 350/350 (solid line) and Fe/ZSM5-O₂ 350/350 (dotted line).

The XANES spectra, the pre-edge features and the EXAFS results of the heat treatments in He and O₂ will be used as reference for the analysis of the XAFS data obtained *in situ*, during the separate feeding of i-C₄H₁₀, NO, NO+O₂ and during the HC-SCR reaction with isobutane (see Tables 2 and 3).

Treatment with isobutane

The normalized XANES spectrum and the background-subtracted pre-edge of Fe/ZSM5 recorded at 350°C in the presence of isobutane (Fe/ZSM5-CH_x 350/350, dashed line) is presented in Fig. 4a. The XANES spectra and pre-edges of Fe/ZSM5-He 350/350 (solid line) and of Fe/ZSM5-O₂ 350/350 (dotted line) are also plotted, for comparison. Both the Fe-K edge and the pre-edge of Fe/ZSM5-CH_x 350/350 appear to be similar to those measured at 350°C in helium and only slightly shifted towards lower energy. This is ascribed to a minor additional reduction of Fe. The additional Fe reduction is confirmed by the analysis of the pre-edge features (Fig. 4b). The centroid position of Fe/ZSM5-CH_x 350/350 corresponds to an average iron oxidation state of 2.2.

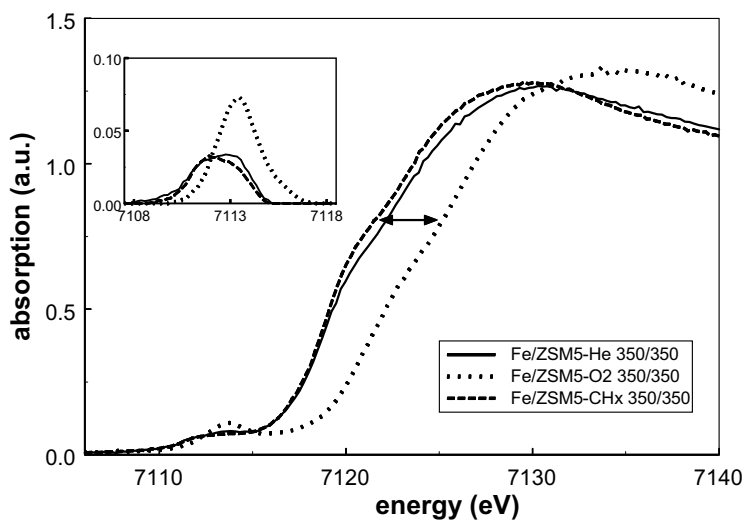


Figure 4a: Normalized XANES spectra and background subtracted pre-edges of Fe/ZSM5-CH_x 350/350 (dashed line), Fe/ZSM5-He 350/350 (solid line) Fe/ZSM5-O₂ 350/350 (dotted line).

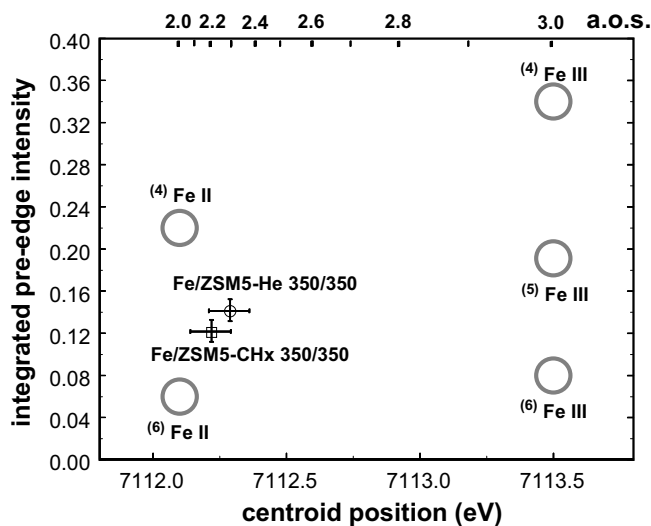


Figure 4b: Pre-edge characteristics (centroid position and integrated intensity) of Fe/ZSM5-CH_x 350/350 (□) and of Fe/ZSM5-He 350/350 (○). For details on Fe references, see caption Fig 3b.

In Fig. 4c the Fourier Transform of the EXAFS data of measurement Fe/ZSM5-CH_x-350/350 (dotted line) is compared to that of Fe/ZSM5-He 350/350 (solid line).

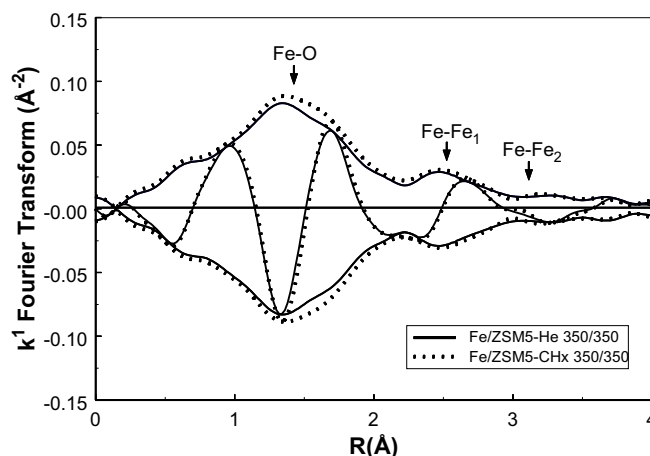


Figure 4c: Fourier transform (k^1 , $\Delta k=2.7-13.2 \text{ \AA}^{-1}$) of EXAFS data of Fe/ZSM5-CH_x 350/350 (dotted line) and Fe/ZSM5-He 350/350 (solid line).

Differences are visible only in the 1.3-2.0 Å R range, where the real part of the sample treated with isobutane appears to be slightly enhanced. No differences are visible in the Fe-Fe coordination, showing no further aggregation of iron during the treatment.

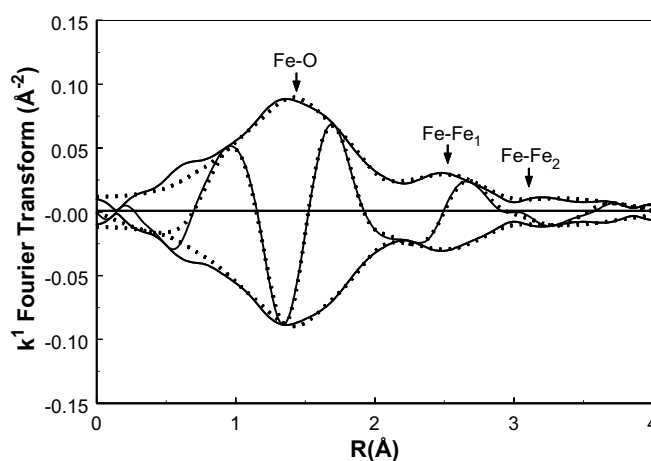


Figure 4d: Fourier transform (k^1 , $\Delta k=2.7-13.2 \text{ \AA}^{-1}$) of EXAFS data of Fe/ZSM5-CH_x 350/350 (solid line) and R-space fit (dotted line; $\Delta R=0.7-4.2 \text{ \AA}$).

The Fourier Transform of the EXAFS data of Fe/ZSM5-CH_x 350/350 (solid line) and the R-space fit (dotted line) are presented in Fig. 4d. It can be seen that the quality of the R-space fit is excellent.

The coordination parameters obtained by the R-space analysis of the EXAFS data of Fe/ZSM5-CH_x 350/350 are presented in Table 5.

Table 5: Coordination parameters obtained by R-space analysis (k^1 , $\Delta k=2.7-13.2 \text{ \AA}^{-1}$; $\Delta R= 0.7-4.2 \text{ \AA}$) of EXAFS data of Fe/ZSM5-CH_x 350/350, Fe/ZSM5-NO 350/350, Fe/ZSM5-NO+O₂ 350/350 and Fe/ZSM5-deNO 350/350; $N_{\text{indp}}= 25.4$; $N_{\text{free (fit)}}= 22$.

Shells	N ±10%	R (Å) ±1%	$\Delta\sigma^2$ (10^{-3} \AA^2) ±5%	ΔE_0 (eV) ±10%	k ¹ -variance (%)	
					Im. part	Abs. part
Fe/ZSM5-CH _x 350/350					0.36	0.27
Fe-O ₁	1.0	1.88	0.8	-5.5		
Fe-O ₂	2.0	1.97	8.4	12.6		
Fe-O ₃	1.4	2.08	5.7	-9.2		
Fe-Fe ₁	1.2	2.99	14.5	0.4		
Fe-Fe ₂	0.4	3.40	17.2	0.1		
Fe-O _Z	1.7	4.09	15.0	-8.8		
Fe/ZSM5-NO 350/350					1.18	0.45
Fe-O ₁	1.7	1.86	1.6	-1.5		
Fe-O ₂	2.0	1.99	8.5	9.5		
Fe-O ₃	1.0	2.02	0.5	-10.2		
Fe-Fe ₁	1.2	3.00	8.9	-2.7		
Fe-Fe ₂	0.4	3.40	15.0	-3.7		
Fe-O _Z	4.4	3.81	15.0	1.0		
Fe/ZSM5-NO+O ₂ 350/350					1.55	0.51
Fe-O ₁	2.0	1.86	1.0	-6.9		
Fe-O ₂	2.0	1.97	3.2	13.0		
Fe-O ₃	1.0	2.02	1.0	-6.0		
Fe-Fe ₁	1.2	2.96	10.5	1.9		
Fe-Fe ₂	0.4	3.40	15.0	0.1		
Fe-O _Z	4.1	3.91	15.0	-2.2		
Fe/ZSM5-deNO 350/350					1.37	0.60
Fe-O ₁	1.8	1.85	3.2	0.3		
Fe-O ₂	2.0	1.97	6.0	13.0		
Fe-O ₃	1.2	2.02	9.1	-12.1		
Fe-Fe ₁	1.2	2.97	9.5	-0.2		
Fe-Fe ₂	0.4	3.40	15.0	0.0		
Fe-O _Z	5.1	3.85	15.0	-0.4		

In Fig. 4e the Fourier Transform of shell Fe-O₁ is presented for measurements Fe/ZSM5-CH_x 350/350 (dashed line), Fe/ZSM5-He 350/350 (solid line) and Fe/ZSM5-O₂ 350/350 (dotted line).

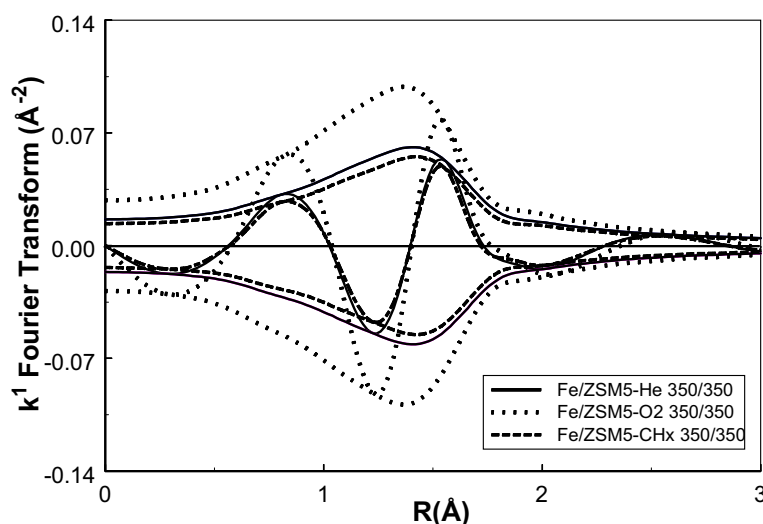


Figure 4e: Fourier transform of the Fe-O₁ contribution, obtained from the R-space analysis (k^1 , $\Delta k=2.7-13.2 \text{ \AA}^{-1}$; $\Delta R=0.7-4.2 \text{ \AA}$) of EXAFS data of Fe/ZSM5-CH_x 350/350 (dashed line), Fe/ZSM5-He 350/350 (solid line) and Fe/ZSM5-O₂ 350/350 (dotted line).

As expected, in Fe/ZSM5 measured under isobutane this shell is significantly less intense than in the presence of oxygen. The intensity of the shell appears to be slightly lower than in the sample measured under He. The results confirm the removal in a reducing atmosphere of oxygen ascribable to the Fe-O-Fe bridges. They also demonstrate that almost all reactive oxygen from the sample can be removed by merely heating. A slight increase is visible in the coordination number of shell Fe-O₃ (from 1.2 to 1.4) when comparing the fit results of Fe/ZSM5-He 350/350 (Table 4) with those of Fe/ZSM5-CH_x 350/350 (Table 5). Since EXAFS is not able to distinguish between light scattering atoms (in this study O, C, N), a precise assignment to the scattering neighbors is not possible. Nevertheless, it appears reasonable to ascribe the increase of the coordination number of shell Fe-O₃ to absorbed C-containing species.

Table 6 collects the coordination parameters of Fe/ZSM5, measured upon cooling the *in situ* cell to 77 K in the presence of the different reactants. A more severe increase in the coordination number of the Fe-O₃ shell (from N=1.4 to N=1.8), accompanied by a shift in

its distance (from 2.08 to 2.14 Å) was detected upon cooling the sample under isobutane to 77 K. This can be explained by a further adsorption of C-containing species from isobutane, occurred during the cooling process.

Table 6: Coordination parameters obtained by R-space analysis (k^1 , $\Delta k=2.7-13.2 \text{ \AA}^{-1}$; $\Delta R= 0.7-4.2 \text{ \AA}$) of EXAFS data of Fe/ZSM5-CH_x 350/LN, Fe/ZSM5-NO 350/LN, Fe/ZSM5-NO+O₂ 350/LN, Fe/ZSM5-deNO 350/LN; $N_{\text{indp}}= 25.4$; $N_{\text{free (fit)}}= 22$.

Shells	N ±10%	R (Å) ±1%	$\Delta\sigma^2$ (10^{-3} \AA^2) ±5%	ΔE_0 (eV) ±10%	k^1 -variance (%)	
					Im. part	Abs. part
Fe/ZSM5-CH _x 350/LN					0.45	0.22
Fe-O ₁	1.0	1.85	-1.4	-0.4		
Fe-O ₂	2.0	1.97	1.0	12.6		
Fe-O ₃	1.8	2.14	9.5	-12.5		
Fe-Fe ₁	1.2	2.99	3.8	1.1		
Fe-Fe ₂	0.4	3.40	15.1	-6.6		
Fe-O _Z	2.7	4.02	15.0	3.1		
Fe/ZSM5-NO 350/LN					0.88	0.52
Fe-O ₁	1.7	1.86	-3.5	-3.2		
Fe-O ₂	2.0	1.99	-3.8	9.7		
Fe-O ₃	1.2	2.09	8.7	-12.6		
Fe-Fe ₁	1.2	3.00	1.6	-0.4		
Fe-Fe ₂	0.4	3.40	15.0	-3.7		
Fe-O _Z	4.4	3.81	15.0	1.0		
Fe/ZSM5-NO+O ₂ 350/LN					0.66	0.30
Fe-O ₁	2.0	1.85	-4.0	-4.0		
Fe-O ₂	2.0	1.97	-5.0	13.0		
Fe-O ₃	1.2	2.05	-1.2	-6.2		
Fe-Fe ₁	1.2	2.98	3.1	2.0		
Fe-Fe ₂	0.4	3.40	15.0	0.0		
Fe-O _Z	4.2	3.91	15.0	-2.2		
Fe/ZSM5-deNO 350/LN					0.80	0.60
Fe-O ₁	2.0	1.85	-4.5	-0.7		
Fe-O ₂	2.0	1.97	-5.0	13.0		
Fe-O ₃	1.4	2.09	0.2	-6.3		
Fe-Fe ₁	1.2	3.02	3.2	-2.7		
Fe-Fe ₂	0.4	3.40	15.0	0.0		
Fe-O _Z	5.3	3.91	15.0	-2.2		

Treatment with NO and NO+O₂

The catalytic activity of Fe/ZSM5 measured while recording the XAFS spectra of Fe/ZSM5-NO 350/350 and Fe/ZSM5-NO+O₂ 350/350 is reported in Fig. 5.

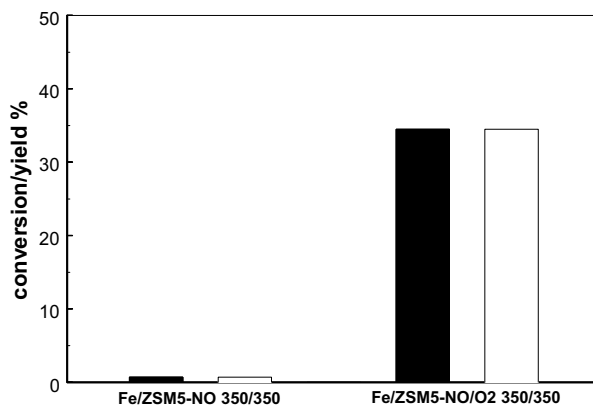


Figure 5: NO conversion (black bars) and NO₂ yield (white bars), as detected by NO_x chemiluminescence analysis of the gas outlet, during the *in situ* XAFS measurements Fe/ZSM5-NO 350/350 and Fe/ZSM5-NO+O₂ 350/350.

The black bars depict the conversion of NO, while the corresponding NO₂ yield is depicted in white. Mass-balance, calculated on nitrogen, showed that no measurable quantities of N₂ or N₂O were formed during the treatments. The concentration of the outlet gases reached a steady state after around 60 min. from the beginning of the treatments, and remained constant during the whole measurement. The delay in the stabilization is the result of back-mixing processes in the volume of the cell. As can be seen in Fig. 5 almost no activity was detected while flushing NO (2000 ppm) at 350°C over Fe/ZSM5. A NO₂ yield lower than 1% was measured. This could be the result of oxidation of NO by traces of oxygen in the gas phase but is most probably due to inaccuracy in the NO₂ measurement. Clear oxidation of NO, on the other hand, was detected when feeding NO (2000 ppm) to the sample in the presence of oxygen (5%). A NO₂ yield of approximately 35% was obtained, as a result of the catalytic oxidation of NO by Fe/ZSM5.

The normalized XANES spectrum and the background-subtracted pre-edge of Fe/ZSM5-NO 350/350 (dashed line) and of Fe/ZSM5-NO+O₂ 350/350 (dashed-dotted line) are presented in Fig. 6a. The XANES spectra and pre-edges of Fe/ZSM5-He 350/350 (solid line) and of Fe/ZSM5-O₂ 350/350 (dotted line) are included as references.

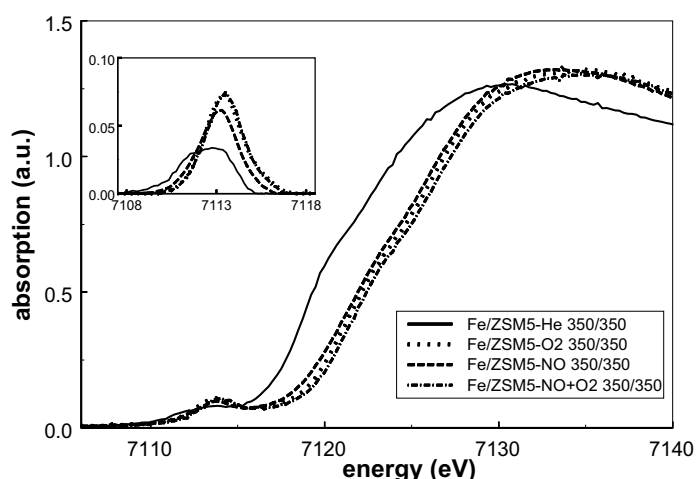


Figure 6a: Normalized XANES spectra and background subtracted pre-edges of Fe/ZSM5-NO 350/350 (dashed line), Fe/ZSM5-NO+O₂ 350/350 (dashed-dotted line), Fe/ZSM5-He 350/350 (solid line) and Fe/ZSM5-O₂ 350/350 (dotted line).

The Fe K-edge in the presence of NO and NO+O₂ appear to be positioned close to that measured in the presence of oxygen (Fe^{III}). They are separated by 0.4 eV, accounting for a slight average reduction of iron when NO was fed alone. No differences are visible when comparing the pre-edges of Fe/ZSM5-NO+O₂ 350/350 and Fe/ZSM5-O₂ 350/350. The pre-edge of Fe/ZSM5-NO 350/350, on the contrary, appears to be slightly less intense and shifted to lower energy. The pre-edge features are visualized in Fig. 6b.

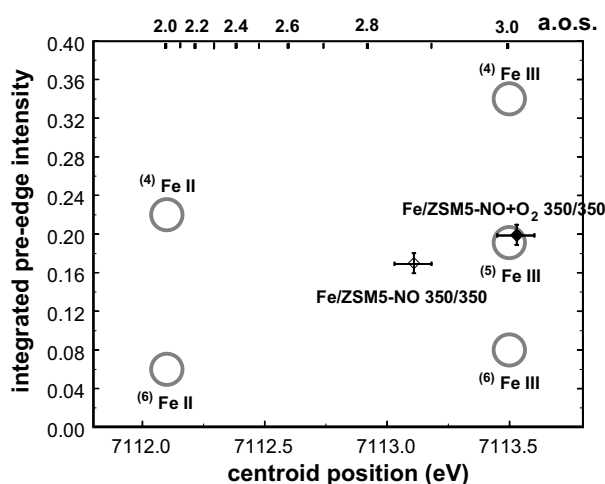


Figure 6b: Pre-edge characteristics (centroid position and integrated intensity) of Fe/ZSM5-NO 350/350 (◇) and Fe/ZSM5-NO+O₂ 350/350 (◆).

When NO is fed together with O₂, the features of iron in Fe/ZSM5 are typical of five-fold coordinated Fe^{III}. A similar coordination is measured in the absence of oxygen (Fe/ZSM5-NO 350/350), together with an average oxidation number of 2.8-2.9.

The Fourier Transform of the EXAFS data of Fe/ZSM5-NO 350/350 and Fe/ZSM5-NO+O₂ 350/350 are reported in Fig. 6c.

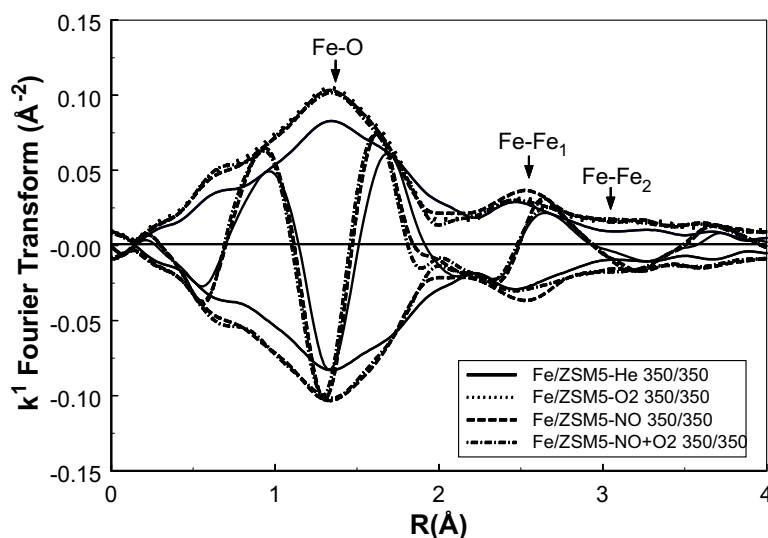


Figure 6c: Fourier transform (k^1 , $\Delta k=2.7-13.2 \text{ \AA}^{-1}$) of EXAFS data of Fe/ZSM5-NO 350/350 (dashed line), Fe/ZSM5-NO+O₂ 350/350 (dashed-dotted line), Fe/ZSM5-He 350/350 (solid line) and Fe/ZSM5-O₂ 350/350 (dotted line).

As can be seen, the total Fe-O coordination of both measurements overlaps with that of Fe/ZSM5-O₂ 350/350. The imaginary part of Fe/ZSM5-NO 350/350 in the R range 1.0-2.0 Å appears only slightly shifted to higher distance when compared to that of Fe/ZSM5-NO+O₂ 350/350. The structural parameters obtained by the analysis of the EXAFS data, measured at 350°C and LN temperature, have been presented in Table 5 and Table 6. Measurements Fe/ZSM5-NO 350/350 and Fe/ZSM5-NO+O₂ 350/350 show a total Fe-O coordination of 4.7 and 5.0, respectively. Differences between the two measurements are visible in the coordination number of the closest shell (Fe-O₁), showing the presence on average of 1.7 (Fe/ZSM5-NO 350/350) or 2.0 (Fe/ZSM5-NO+O₂ 350/350) neighbors. Similar coordination numbers have been obtained for the same measurements upon cooling to LN temperature.

The Fourier transforms of the EXAFS function of the closest Fe-O shell (Fe-O_1) are shown in Fig. 6d. Differences are visible between the intensities of the real part of the Fourier Transforms. The intensities are in the order $\text{Fe/ZSM5-NO } 350/350 < \text{Fe/ZSM5-O}_2 \text{ } 350/350 < \text{Fe/ZSM5-NO+O}_2 \text{ } 350/350$.

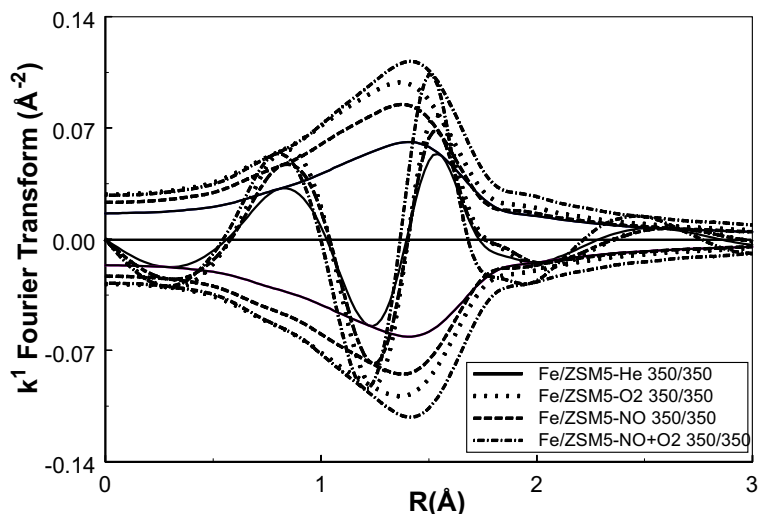


Figure 6d: Fourier transform of the Fe-O_1 contribution, obtained by R-space analysis (k^1 , $\Delta k=2.7\text{-}13.2 \text{ \AA}^{-1}$; $\Delta R=0.7\text{-}4.2 \text{ \AA}$) of EXAFS data of Fe/ZSM5-NO 350/350 (dashed line), Fe/ZSM5-NO+O₂ 350/350 (dashed-dotted line), Fe/ZSM5-He 350/350 (solid line) and Fe/ZSM5-O₂ 350/350 (dotted line).

SCR of NO with isobutane

The catalytic activity of the Fe/ZSM5 sample towards the HC-SCR reaction of NO with isobutane was monitored during the collection of the XAFS data of measurement Fe/ZSM5-deNO 350/350. A complete stabilization of the composition of the outlet gas was obtained upon approximately 60 minutes under reaction. The outlet composition remained stable during the recording of the XAFS spectra. The catalytic results are shown in Fig. 7. The conversion of NO is indicated by the black bar, while the NO₂ yield is depicted in white. The N₂ yield (gray bar) was calculated by mass-balance on nitrogen, by assuming no formation of N₂O. Indeed, as shown in Figs. 2a and 2b, N₂O is not a by-product of HC-SCR with isobutane on Fe/ZSM5. Furthermore, the reproducibility of the catalytic results

was confirmed by subsequent catalytic tests performed in the *in situ* XAFS cell, by measuring N_2 directly by gas chromatography.

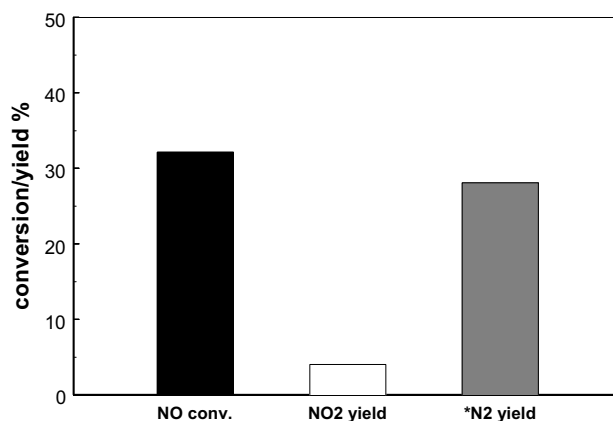


Figure 7: NO conversion (black bar), NO_2 yield (white bar) and N_2 yield (dark-gray bar), as detected by NO_x chemiluminescence analysis of the gas outlet, during *in situ* XAFS measurements of Fe/ZSM5-deNO 350/350. * N_2 yield is calculated from mass balance on nitrogen, assuming no formation of N-containing products different from NO and NO_2 .

As can be seen in Fig. 7, a NO conversion of 32% could be obtained. This result demonstrates that the XAFS spectra were obtained from the catalyst under deNO working conditions. Together with N_2 (28% yield) also the formation of a minor amount of NO_2 was detected (4% yield). Since NO_2 is not a by-product of the HC-SCR reaction catalyzed by Fe/ZSM5, its formation was most probably the result of oxidation of NO by oxygen, occurring on the stainless-steel walls of the cell or in the gas phase.

The normalized XANES spectrum and the background-subtracted pre-edge of Fe/ZSM5 recorded at 350°C during the SCR reaction of NO by isobutane (Fe/ZSM5-deNO 350/350, dashed line) is presented in Fig. 8a and compared with those of Fe/ZSM5-He 350/350 (solid line) and of Fe/ZSM5- O_2 350/350 (dotted line). The position of the Fe-K edge shows that the average oxidation state of iron in Fe/ZSM5 during reaction is 3+. The intensity of the pre-edge of Fe/ZSM5-deNO 350/350 appears to be lower than that measured at 350°C in oxygen. This can be ascribed to the presence of reaction intermediates in the coordination of iron.

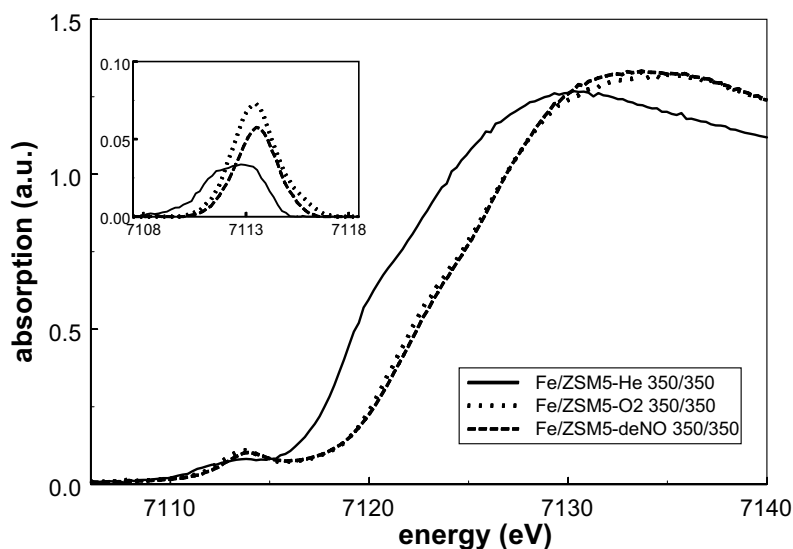


Figure 8a: Normalized XANES spectra and background subtracted pre-edges of Fe/ZSM5-deNO 350/350 (dashed line), Fe/ZSM5-He 350/350 (solid line) and Fe/ZSM5-O₂ 350/350 (dotted line).

The analysis of the pre-edge features, presented in Fig. 8b, confirms that the oxidation state of iron during reaction is 3+. The integrated pre-edge intensity is consistent with the presence on average of 5 to 6 neighboring atoms.

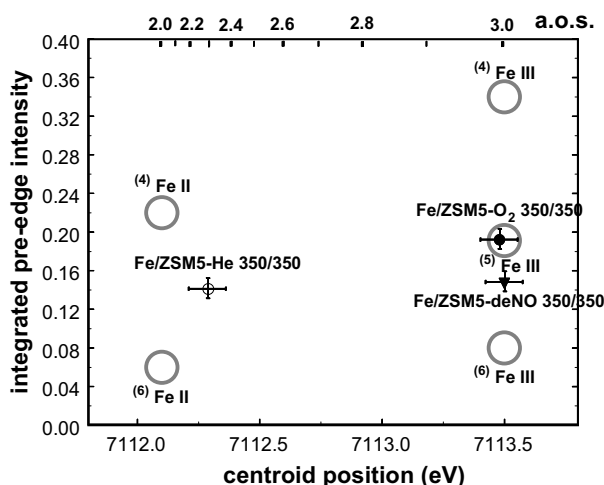


Figure 8b: Pre-edge characteristics (centroid position and integrated intensity) of Fe/ZSM5-deNO 350/350 (▼), Fe/ZSM5-He 350/350 (○) and Fe/ZSM5-O₂ 350/350 (●).

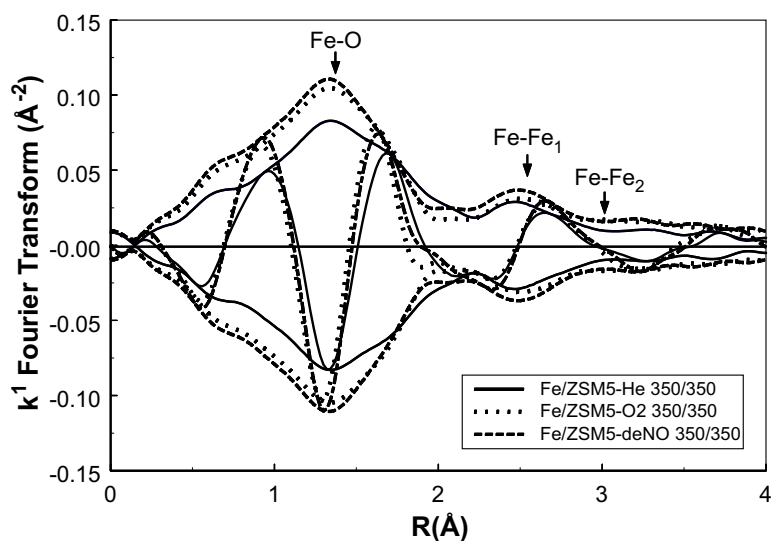


Figure 8c: Fourier transform (k^1 , $\Delta k=2.7-13.2 \text{ \AA}^{-1}$) of EXAFS data of Fe/ZSM5-deNO 350/350 (dashed line), Fe/ZSM5-He 350/350 (solid line) and Fe/ZSM5-O₂ 350/350 (dotted line).

The Fourier Transform of the EXAFS data of Fe/ZSM5-deNO 350/350 is shown in Fig. 8c. As in the case of separate feeding of NO or NO + O₂ (Fig. 6c), the Fourier transform appears similar to that of measurement Fe/ZSM5-O₂ 350/350. The EXAFS data-analysis (Table 5) shows that the coordination number of the Fe-O₁ shell is slightly reduced, from 2.0 to 1.8. The Fourier Transform of the EXAFS function of the Fe-O₁ contribution, plotted in Fig. 8d, shows indeed a slight decrease in the intensity of the real part.

This may indicate a slight removal of oxygen from the Fe-O-Fe bridges. Due to the contemporary presence of chemically different light scatterers, attribution to specific neighbors is not possible. It should furthermore be noted that the slight decrease in intensity in the Fe-O₁ contribution is not accompanied by a reduction of iron.

Cooling to LN temperature resulted in an average increase in the number of neighbors in the closest Fe-coordination (Fe/ZSM5-deNO 350/LN, Table 6), ascribed to further adsorption at low temperature. The coordination number of shell Fe-O₁ appeared to be slightly increased, from 1.8 to 2.0 neighbors. Also the coordination of shell Fe-O₃, previously attributed to adsorbed water (14) appeared to be enhanced (from 1.2 to 1.4). This may be the result of adsorption, upon cooling, of water produced during the HC-SCR reaction, but could as well be caused by the presence of C/N-containing reaction-intermediates.

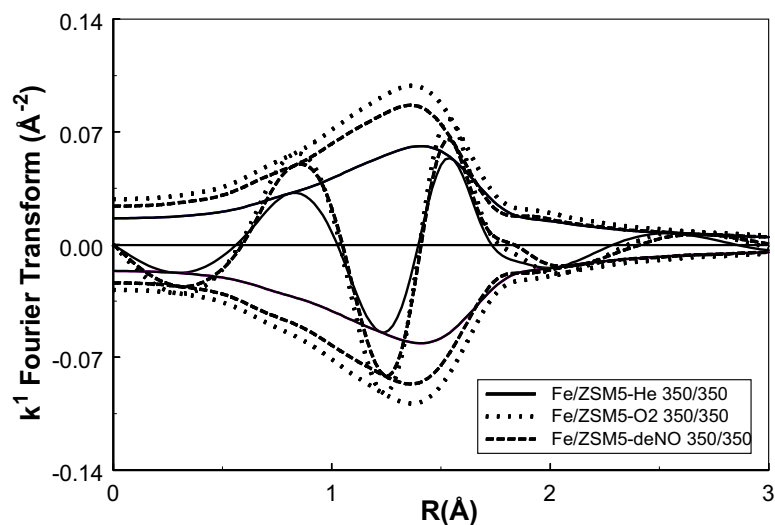


Figure 8d: Fourier transform of the Fe-O₁ contribution obtained by R-space analysis (k^1 , $\Delta k=2.7-13.2 \text{ \AA}^{-1}$; $\Delta R=0.7-4.2 \text{ \AA}$) of EXAFS data of Fe/ZSM5-deNO 350/350 (dashed line), Fe/ZSM5-He 350/350 (solid line) and Fe/ZSM5-O₂ 350/350 (dotted line).

Discussion

Catalytic activity of Fe/ZSM5 towards SCR of NO with isobutane

The catalytic tests performed on the Fe/ZSM5 sample, further used for the *in situ* XAFS characterization, confirm the high activity and selectivity of this catalyst for the selective catalytic reduction of NO to N₂ with isobutane (Figs. 2a and 2b). The performance of our sample appears to be identical to that shown by previous studies (2-5). A maximum N₂ yield can be obtained at around 360°C (around 78% at a GHSV of 42000h⁻¹), the selectivity towards N₂ being complete. Reducing the contact time of the reactants by five times (GHSV=210000 h⁻¹), does not result in a correspondent decrease in activity. Even under this extremely high flow-rate, Fe/ZSM5 still provides a N₂ yield of around 36% (Fig. 2b), coupled by a complete selectivity towards N₂. While these results appear very promising for practical applications of Fe/ZSM5, further tests are needed. In particular, the stability of the catalyst should be established under more realistic conditions, *i.e.* in the presence of water. As shown in our previous work (11), the presence of water at high temperature can be responsible for aggregation of iron and formation of unreactive hematite crystals on the external surface of the zeolite. This phenomenon could result in severe deactivation of the catalyst with time on stream.

Structure of the Fe-binuclear complexes and reactivity during heat treatment in He and O₂

XAFS spectroscopy allowed us to describe the structure of the Fe-binuclear complexes in Fe/ZSM5, prepared by sublimation of FeCl₃. This was achieved by studying a sample calcined with a controlled procedure, aimed at minimizing the formation of (inactive) spectators (11,14). It was also possible, as shown in a previous paper (14), to rationalize the reactivity of the Fe binuclear clusters during heat treatments in He and O₂ (see Fig. 1). The reactivity of oxygen in the complexes has been identified in the Fe-O₁ and Fe-O₃ shells located in the R range (1.85-1.89 Å) and (2.02-2.09 Å), respectively. Shell Fe-O₂ (1.97-1.99 Å), which remained unmodified during the treatments, has been ascribed to oxygen from the aluminum-centered tetrahedra, anchoring the Fe atoms to the framework of the zeolite. Removal of one oxygen atom from shell Fe-O₃ occurs already at low temperature (~150°C) and does not affect the oxidation state of iron. This has therefore been assigned to desorption of water. Shell Fe-O₁, on the contrary, appears to be affected only at higher temperatures (above 250°C) and is strongly influenced by the composition of the gas phase. Approximately one oxygen atom can be removed and only in the complete absence of oxygen from the gas-phase. Removal of this oxygen result in reduction of iron. The reactivity of this shell has been ascribed to the presence of highly reactive Fe-O-Fe bridges in the Fe binuclear complexes. This background information will be used as a basis for a further investigation of the active coordination site(s) of the binuclear Fe-complexes. The influence of the different reactants on these coordination sites will be discussed.

Treatment with isobutane

Fe/ZSM5 was treated with isobutane upon heating to 350° in He. The influence of isobutane on the Fe-binuclear complexes can therefore be tracked by comparing the results obtained by measurements Fe/ZSM5-CH_x 350/350 and Fe/ZSM5-He 350/350. The average oxidation state of iron for the two measurements appear similar, being respectively around 2.2 and 2.3 (Figs. 4a and 4b). It can therefore be concluded that treating with isobutane results in only a slight further reduction of iron, when compared to that caused by heating in He to 350°C (auto-reduction). Thus, the majority of reactive oxygen can be activated and desorbed from the Fe-binuclear complexes by merely heating. The slight increase in the reduction upon reaction with isobutane corresponds to a further removal of oxygen from the closest Fe-O shell (Fe-O₁), as shown by the decrease of its coordination number (from 1.2 in Fe/ZSM5-He 350/350 to 1.0 in Fe/ZSM5-CH_x 350/350, Tables 4 and 5). It is therefore ascribed to the extraction of oxygen from the Fe-O-Fe bridges. The slight decrease in the pre-edge intensity (Fig. 4b), together with the increase in the coordination number of shell

Fe-O₃, suggests the presence on iron of C-containing adsorbed species from isobutane. After cooling to LN temperature, the coordination number of shell Fe-O₃ increased significantly (Tables 5 and 6), as a result of further adsorption resulting from the cooling. The treatment in i-C₄H₁₀ did not cause any change in shell Fe-O₂, attributed to oxygen in Fe-O-Al bridges (see Fig. 1). This shows that the Fe-complexes remained firmly ligated to the zeolite framework. Indeed no increase was visible in the Fe-Fe coordination, demonstrating that no further aggregation phenomena of iron occurred during the treatment.

Treatment with NO and NO + O₂

The catalytic measurements performed during the collection of the XAFS spectra of Fe/ZSM5-NO 350/350 do not show any detectable activity for the catalytic decomposition of NO by Fe/ZSM5 (Fig. 5).

Flushing NO results in a clear increase in the oxidation state of iron, from 2.3 (Fe/ZSM5-He 350/350, Fig. 3b) to approximately 2.8-2.9 (Fig. 6b). The reason for the re-oxidation could be manifold. As shown in our previous work (14) reduced Fe binuclear complexes are highly unstable. Indeed, partial re-oxidation of the complexes was detected with time on stream under He. Voskoboynikov *et al.* (7) suggested the possibility of oxygen exchangeability between the Fe-complexes and the zeolite matrix. Re-oxidation could have therefore been caused by extraction of oxygen from the zeolite lattice. Traces of oxygen in the gas phase may also have been responsible for the re-oxidation. Indeed, as previously demonstrated (14), the oxygen vacancy between the two iron ions is readily regenerated by molecular oxygen from the gas phase. Nevertheless, oxidation by oxygen is not the only possible explanation. Fu *et al.* (27) have shown that NO can act as an oxidant in Fe/Y, where also the presence of Fe-binuclear complexes has been suggested. Lei *et al.* (28) have demonstrated that on [Cu-O-Cu]²⁺ ions in Cu/ZSM5 the same phenomenon occurs by the interaction of two NO molecules and the generation of one molecule of N₂O. The same pathway may occur on the Fe-binuclear complexes in Fe/ZSM5:

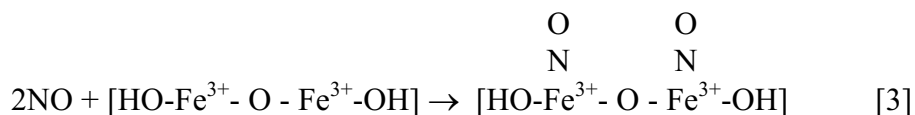
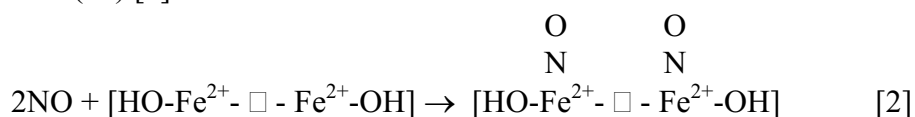


where \square stands for a vacancy. The N₂O formed, present in negligible concentration in the gas outlet, could not have been detected by our gas-analysis system.

Contemporarily with the re-oxidation of iron, an increase was visible in the number of O neighboring atoms in the Fe-O₁ shell (from 1.2 in Fe/ZSM5-He 350/350 to 1.7 in Fe/ZSM5-NO 350/350). When compared to the measurement performed in the presence of oxygen, the shell was not completely regenerated (1.7 neighbors for Fe/ZSM5-NO 350/350

against 1.9 for Fe/ZSM5-O₂ 350/350). As previously discussed, EXAFS is not able to distinguish between different light scattering atoms (O or N). The neighboring atoms in shell Fe-O₁ could therefore be attributed to oxygen (partial regeneration of Fe-O-Fe bridges) or to the presence of N-containing adsorbed species. Several FTIR studies have been performed to identify the species formed by the interaction of NO with the active sites of iron catalysts (3,4,6,8,13,29-33). Chen *et al.* (8), in particular, have studied the evolution of the N-containing adsorbed species generated by NO on over-exchanged Fe/ZSM5, obtained by chemical vapor deposition of FeCl₃. From their study different species have been identified as nitrosyl Feⁿ⁺(NO)_{1,2} and Feⁿ⁺(NO₂), the latter being formed with increasing time on stream.

These species, which tend to be formed more easily on reduced iron (Fe²⁺) [2], may exist as well on Fe³⁺(34) [3]:



Fe³⁺, as previously discussed, may have been generated by re-oxidation with oxygen, or by NO following pathway [1].

Together with the partial regeneration of the Fe-O-Fe bridges, via the pathway proposed by Lei *et al.* (28), nitrosyl species appear to be the most probable responsible for the changes affecting the closest coordination of iron (Fe-O₁) under NO at 350°C.

While Fe/ZSM5 is not able to decompose NO to N₂ and O₂, it is an active catalyst for the oxidation of NO to NO₂ in the presence of excess oxygen (see Fig. 5). The capability of Fe/ZSM5 to oxidize NO to NO₂ is well known. Catalytic tests performed by Chen *et al.* (8), using a feed composition similar to the one used in this work, showed a maximum conversion of NO to NO₂ of around 75% at 300°C under a GHSV of 42000 h⁻¹. As suggested by the authors, NO₂ is most likely formed by the reaction of NO with the bridging oxygen in Fe-O-Fe. The vacancy generated should be reoccupied by oxygen from the gas phase, or possibly by NO, following pathway [1]. FTIR studies (8,31) have shown that prevalently nitro (NO₂)⁻ and nitrate (NO₃)⁻ species are formed when NO and O₂ are fed together on Fe/ZSM5. Different pathways have been suggested for the formation of these species. Lobree *et al.* (31) have proposed, as the first step in this process, the formation of a super-oxide ion (O₂)⁻, generated by the reaction of O₂ with the Fe-complexes, followed by a

disproportionation of the iron atoms in the Fe-complexes, with the formation of a [HO-Fe²⁺] and a [O₂⁻-Fe³⁺-OH] group. Nitrate and nitro species should be formed by the subsequent reaction of NO and NO₂ from the gas phase, respectively with the [O₂⁻-Fe³⁺-OH] and the [HO-Fe²⁺] groups. Chen *et al.* (8) have proposed a different pathway, via the formation of a peroxy-bridge between the two Fe atoms in the complexes. The reaction of NO and NO₂ with the highly unstable peroxy-group would generate the nitro and nitrate species.

The immediate re-oxidation of iron (Fig. 6a) occurred upon contemporarily purging of NO and O₂ shows that, indeed, the Fe-binuclear complexes in Fe/ZSM5 are highly reactivity towards this mixture. The oxidation state of iron appears to be somewhat higher than that measured in the presence of NO alone. This observation, coupled with the increase in the coordination number of shell Fe-O₁, which appears almost identical to that measured in the presence of oxygen alone (Fe/ZSM5-O₂ 350/350), suggests a complete regeneration of the Fe-O-Fe bridges. The possible formation of highly unstable peroxy-bridges, suggested by Chen *et al.* (8) could not have been detected by the EXAFS set-up used in this study. It should be noted that the increment in the coordination number of shell Fe-O1 could also be assigned to the presence of absorbed nitro and nitrate species. A clear assignment with the present data is not possible.

As in the case of the treatment with isobutane and NO, also in the contemporary presence of NO and O₂ no significant changes were detected in shell Fe-O₂, attributed to oxygen binding the Fe-complexes to the zeolite framework, nor in the Fe-Fe coordination. It can be concluded that also in the presence of NO and NO+O₂ the binuclear complexes remained stably ligated to the framework and that no agglomeration of iron towards larger clusters occurred.

SCR of NO with isobutane

The activity of Fe/ZSM5 towards the selective catalytic reduction of NO to N₂ with isobutane was confirmed by the analysis of the outlet gases (Fig. 7), performed during the collection of the XAFS spectra Fe/ZSM5-deNO 350/350. The gas analysis shows that the XAFS spectra were recorded on Fe/ZSM5 under deNO working conditions.

As in the case of the treatments with NO or NO + O₂, changes occurring upon reaction with the HC-SCR mixture were identified in the closest Fe-O coordination sphere of the complexes. The coordination number of shell Fe-O1 (N=1.8) appeared to be significantly increased when compared to the sample heated in He (N=1.2). This was accompanied by a complete re-oxidation of iron (Fe³⁺). This result confirms that the active sites in the complexes for the selective reduction of NO are located in the oxygen vacancies formed

upon heating. Due to the inability of EXAFS to distinguish between light scatterers of different nature (C, N, O), it is not possible to assign the changes in the Fe-O1 coordination to an interaction with a specific reactant. As previously observed, the increase in the coordination number of shell Fe-O1 can in principle be ascribed to the regeneration of the Fe-O-Fe bridges, operated by O₂ or by NO/NO₂ from the gas phase, following pathway [2]. Nevertheless, the reaction pathway for the HC-SCR reaction, elucidated by Chen *et al.* (3,4) and Gao *et al.* (6), and presented in the Introduction section, shows that an extremely wide range of reaction intermediates may coexist on the binuclear Fe-complexes during reaction. The most plausible candidates consist of organic nitro- and nitroso-compounds. The presence during the SCR reaction of different adsorbed species in the coordination sphere of iron is confirmed by the lowered intensity of the Fe pre-edge, when compared to that measured in the presence of oxygen alone (Fig. 8b). The intensity of the pre-edge appears to be consistent with the presence of five to six atomic neighbors. Coherently, 5.0 neighbors were found by the EXAFS analysis. It should nevertheless be noted that, due to the extremely high static and dynamic disorder, originated by the different reaction intermediates, this number could be slightly underestimated. Indeed, upon cooling to 77 K, a slight increase was detected in the coordination number of shells Fe-O1 and Fe-O3. The increase in the coordination number of shell Fe-O3, in particular, could be attributed as well to adsorption at low temperature of water produced by combustion of isobutane during reaction.

Conclusions

The majority of iron in Fe/ZSM5 obtained by sublimation of FeCl₃, and calcined by using a special procedure aimed at minimizing the number of (inactive) Fe-spectators, consists of oxo/hydroxo binuclear Fe-complexes with a Fe-O-Fe core.

During heat treatment in He to 350°C the Fe-complexes undergo auto-reduction. This is ascribed to removal of oxygen from the Fe-O-Fe bridges (closest Fe-O coordination sphere), with the consequent formation of Fe-□-Fe vacancies.

The majority of reactive oxygen can be activated and desorbed from the Fe-binuclear complexes by merely heating. Treatment with isobutane results in only a further slight (average) reduction of iron, accompanied by an additional removal of oxygen from the Fe-O-Fe bridges.

The active sites of the Fe-complexes are located in the vacancies generated in the closest Fe-O coordination sphere by the oxygen desorption. Upon reaction with NO and NO + O₂, as well as during the HC-SCR reaction with isobutane, these vacancies are promptly

reoccupied and iron is oxidized. This can be ascribed to the adsorption of N- and C-containing species and/or by the regeneration of the Fe-O-Fe bridges in the complexes. The average oxidation state of iron measured on Fe/ZSM5 during the HC-SCR reaction is 3+.

Reference list

1. El-Malki, E.M., van Santen, R.A., and Sachtler, W.M.H., *J. Catal.* **196**, 212 (2000).
2. Chen, H.-Y., and Sachtler, W.M.H., *Catal. Today* **42**, 73 (1998).
3. Chen, H.-Y., Voskoboinikov, T., and Sachtler, W.M.H., *J. Catal.* **180**, 171 (1998).
4. Chen, H.-Y., Voskoboinikov, T., and Sachtler, W.M.H., *Catal. Today* **54**, 483 (1999).
5. Chen, H.-Y., Wang, X., and Sachtler, W.M.H., *Appl. Catal. A* **194-195**, 159 (2000).
6. Gao, Z.-X., Sun, Q., and Sachtler, W.M.H., *Appl. Catal. B* **33**, 9 (2001).
7. Voskoboinikov, T., Chen, H.-Y., and Sachtler, W.M.H., *J. Molec. Catal. A* **155**, 155 (2000).
8. Chen, H.-Y., El-Malki, E.M., Wang, X., van Santen, R.A., and Sachtler, W.M.H., *J. Molec. Catal. A* **162**, 159 (2000).
9. Kucherov, A.V., and Shelef, M., *J. Catal.* **195**, 112 (2000).
10. Marturano, P., Drozdová, L., Pirngruber, G.D., Kogelbauer, A., and Prins, R., *Phys. Chem. Chem. Phys.* **3**, 5585 (2001).
11. Chapter 2 of this thesis; Battiston, A.A., Bitter, J.H., de Groot, F.M.F., Overweg, A.R., Stephan, O., van Bokhoven, J.A., Kooyman, P.J., van der Spek, C., Vankó, G., and Koningsberger, D.C.; accepted for publication in *J. Catal.*.
12. Marturano, P., Drozdová, L., Kogelbauer, A., and Prins, R., *J. Catal.* **192**, 236 (2000).
13. Lobree, L.J., Hwang, I.-C., Reimer, J.A., and Bell, A.T., *J. Catal.* **186**, 242 (1999).
14. Chapter 3 of this thesis; Battiston, A.A., Bitter, J.H., Heijboer, W.M., de Groot, F.M.F., and Koningsberger, D.C., submitted to *J. Catal.*.
15. Voskoboinikov, T.V., Chen, H.-Y., and Sachtler, W.M.H., *Appl. Catal. B* **19**, 279 (1998).
16. Vaarkamp, M., Mojet, B.L., Modica, F.S., Miller, J.T., and Koningsberger, D.C., *J. Phys. Chem.* **99**, 16067 (1995).
17. Wilke, M., Farges, F., Petit P.-E., Brown, G.E.Jr., and Martin, F., *Am. Miner.* **86**, 714 (2001).
18. Vaarkamp, M., Linders, J.C., and Koningsberger, D.C., *Physica B*, **209** (1995).
19. Vaarkamp, M., Dring, I., Oldman, R.J., Stern, E.A., and Koningsberger, D.C., *Phys. Rev. B* **50**, 7872 (1994).

20. Koningsberger, D.C., Mojet, B.L., van Dorssen, G.E., and Ramaker, D.E., *Top. Catal.* **10**, 143 (2000).
21. Cook, J.W., and Sayers, D.E., *J. Appl. Phys.* **52**, 5024 (1981).
22. Ankudinov, A.L., and Rehr, J.J., *Phys. Rev. B* **56**, R1712 (1997).
23. Iball, J., and Morgan, C.H., *Acta Cryst.* **23**, 239 (1967).
24. Blake, R.L., Hessevick, R.E., Zoltai, T., and Finger, L.W., *Am. Miner.* **51**, 123 (1966).
25. Koningsberger, D.C., *Jpn. J. Appl. Phys.* **32**, 877 (1993).
26. Li, G.G., Bridges, F., and Booth C.H., *Phys. Rev. B* **52**, 6332 (1995).
27. Fu, C.M., Deeba, M., and Hall, W.K., *Ind. Eng. Chem. Prod. R&D* **19**, 299 (1990).
28. Lei, G.D., Adelman, B.J., Sárkány, J., and Sachtler, W.M.H., *Appl. Catal. B* **5**, 245 (1995).
29. Busca, G., Lorenzelli, V., *J. Catal.* **72**, 303 (1981).
30. Amiridis, M.D., Puglisi, F., Dumesic, J.A., Millman, W.S., and Topsøe, J., *J. Catal.* **142**, 572 (1993).
31. Lobree, L.J., Hwang, I.-C., Reimer, J.A., and Bell, A.T., *Catal. Lett.* **63**, 233 (1999).
32. Hadjiivanov, K., Knözinger, H., Tsynstskarski, B., and Dimitrov, L., *Catal. Lett.* **62**, 35 (1999).
33. Hadjiivanov, K., Saussey, J., Freysz, J.L., Lavalley, J.C., *Catal. Lett.* **52**, 103 (1998).
34. Segawa, K.-I., Chen, Y., Kubsh, J.E., Delgass, W.N., Dumesic, J.A., and Hall, W.K., *J. Catal.* **76** 112 (1982).

Accessibility of the Fe-Species in Over-Exchanged Fe/ZSM5, Prepared by Sublimation of FeCl₃

Abstract

Microscopic characterization by TEM, EELS and EXAFS, in combination with adsorption studies on a macroscopic scale using a TEOM, revealed that the accessibility of the micropores in over-exchanged Fe/ZSM5 prepared via FeCl₃ sublimation is retarded by the presence of Fe-species in the zeolite pores. As a result, the potentially active sites which are located deeply inside the zeolite crystal do not contribute significantly to the activity of the catalyst towards the selective catalytic reduction of NO by isobutane.

Introduction

Iron supported in ZSM5 has attracted a lot of interest due to its remarkable catalytic activity. It produces phenol from benzene and N_2O in a one step process (1-5). Furthermore, it is active in the catalytic decomposition of N_2O (6-11) and in the selective reduction of nitrogen monoxide (NO) to N_2 with hydrocarbons (HC-SCR), even in the presence of H_2O and SO_2 (12-14). The latter reaction is of significant importance for cleaning-up exhaust streams emerging from stationary and mobile sources powered by fossil fuels.

Different ways of preparing Fe/ZSM5 are put forward in literature. They can be classified in four groups, *i.e.* isomorphous substitution (15-19), ion-exchange in aqueous solution (20) or in solid phase (21-25), and sublimation of volatile $FeCl_3$ onto the zeolite matrix (12-14,26-31). For isomorphous substitution first the zeolite is prepared with iron embodied in the lattice. In a following step, iron can be partially extracted from the framework to the zeolite channels by means of a steaming or a calcination treatment *in vacuo* at high temperature (900°C). The resulting catalysts show high activity towards the decomposition of N_2O (7-10,11). However, the iron concentration, thus the concentration of active sites, is low in these materials (<0.5wt% of Fe). Higher loadings of iron can be obtained by ion-exchange in aqueous solution. Nevertheless, this method often results in the formation of large and catalytically inactive Fe-oxide clusters (12,32).

By using the $FeCl_3$ sublimation technique, Fe/ZSM5 samples with a high loading (over-exchanged Fe/ZSM5) and a high Fe dispersion can be prepared (12-14,26-31). Upon sublimation of $FeCl_3$ into the zeolite matrix, mononuclear $FeCl_2^+$ species are formed (30,31,33). By subsequent washing and calcination, a material can be obtained which is excellently suited for the HC-SCR reaction (13,14). The active phase in Fe/ZSM5 obtained by the sublimation technique is believed to consist of binuclear Fe-oxo/hydroxo species (12,13,26,27). These species have been proposed to have a structure similar to that of the Fe-core of the methane mono-oxygenase enzyme (MMO) (29) or of the closest binuclear building-blocks in oxo-hydroxides like goethite (30,31). In the literature the exact structure of the active Fe-phase is still a matter of debate.

In a previous study we have shown that the nature of the Fe-species in this material strongly depends on the calcination procedure applied (31). A mild calcination treatment, obtained by combining a high gas-flow rate with a low temperature ramp, results in a sample with a very high Fe dispersion. The Fe-species formed by this controlled procedure are for the majority binuclear and are located within the zeolite channels. A more severe calcination treatment, on the other hand, results in the migration and in the agglomeration

of a significant fraction of the binuclear complexes towards large Fe-(hydr)oxo clusters and crystalline goethite/hematite crystals on the external surface of the zeolite crystals.

In this study the catalytic activity of both samples for the HC-SCR of NO using isobutane is compared. The results show that the calcination procedure does not have any influence on the apparent catalytic activity. A combined microscopic and macroscopic characterization study has been performed to explain this result. First, microscopic characterization has been used in order to identify the nature of the different Fe-species in the samples and to study their evolution as a function of the calcination treatment. Subsequently, a macroscopic characterization, *i.e.* diffusion studies using a Tapered Element Oscillating Microbalance (TEOM) has been applied to determine the accessibility of the catalytically active sites. The TEOM results show that the Fe-species located deeply in the zeolites pores are not easily accessible for the reactants.

Experimental

Catalyst preparation

Fe/ZSM5 was prepared via the FeCl₃ sublimation technique (12). NH₄/ZSM5 (Si/Al=17), obtained from Zeolyst, was converted into the H⁺ form by calcination in an O₂ flow at 550°C for 3 hrs. In order to introduce iron in the zeolite, a special U-shaped reactor was constructed. In each leg of the reactor a porous frit and a Pyrex valve were mounted. 1.0 g of H/ZSM5 was loaded onto one of the frits and flushed overnight in He (40 ml/min) at 300°C. The temperature was then lowered to 30°C under the same He flow. The reactor was isolated, closing its inlet and outlet valves, and was moved to a glove bag, where 0.31 g of anhydrous FeCl₃ (98%, Acros Organics) were loaded on its second frit. The reactor was then reconnected to the He line and sublimation exchange was performed at a temperature of 330°C for 30 min. After the sublimation procedure, the sample was washed in 1000 ml doubly deionized H₂O for 30 minutes and dried overnight in air at 70°C. Half of the washed sample was calcined under flowing oxygen in a tubular oven at 550°C for 3 hrs, (ramp 10°C·min⁻¹); this sample will further be referred to as severely calcined Fe/ZSM5 (Fe/ZSM5-sc). For the calcination of the other half, a plug flow reactor was used. This sample was heated with a low temperature ramp (0.5 °C·min⁻¹) to 200°C under a He flow of 800 ml/min. At this temperature 200 ml/min of O₂ were added to the He flow, while, under the same ramp, 550°C were reached. This sample, also calcined at 550°C for three hours, will be called mildly calcined Fe/ZSM5 (Fe/ZSM5-mc).

Characterization and catalysis

N₂ physisorption

The micropore volume of the starting H/ZSM5 support and of the Fe/ZSM5 samples was determined by N₂ physisorption, using a Micromeritics ASAP 2010. The measurements were performed at 77 K, in the pressure range 0-1 bars, after de-gassing the samples *in vacuo* at 200°C for 16 hrs. N₂ physisorption data obtained on the Fe-loaded samples were corrected for the additional metal loading for comparison with the support.

Transmission Electron Microscopy

Imaging of the samples was obtained through High-Resolution Transmission Electron Microscopy (HR-TEM). For this purpose a Philips CM30UT electron microscope was used with a field-emission gun operated at 300 kV as the source of the electrons. Measurements were performed also with a Philips CM200FEG, operated at 200 kV. Samples were positioned on a carbon microgrid supported on copper by placing a few droplets of a suspension of ground sample in ethanol. The grid was dried in air.

Electron Energy Loss Spectroscopy/Scanning Transmission Electron Microscopy (EELS/STEM)

Spatial distribution and clustering of iron were monitored by Electron Energy Loss Spectroscopy (EELS), at the Fe L_{2,3}-edges and the O K-edge. EELS was coupled with Scanning Transmission Electron Microscopy (STEM). The data were recorded with a scanning transmission electron microscope VGHB501, equipped with a field-emission source and a parallel Gatan 666 EELS spectrometer. The data, recorded at the Fe L_{2,3} and at the O K-edges, were corrected by the corresponding elemental cross-over sections. To obtain information on the concentration of iron in the ZSM5 crystals, the Fe intensity was divided by that of oxygen. Data were analyzed by means of Savantic Spim Doctor 5.3 and Digital Micrograph 5.3 software.

XAFS spectroscopy

Fe K-edge XAFS was applied in order to study the local atomic environment around iron, *i.e.* number, distances and chemical nature of Fe-neighbors (34). The XAFS data were collected at the Wiggler station X1.1 at Hasylab (Hamburg). A description of the experimental set-up used can be found in Ref. (31).

The Fe/ZSM5 samples were pressed to obtain self-supporting wafers, calculated to have an absorbency (μ^*x) of 2.5, and placed in a controlled atmosphere cell (35). Spectra were recorded at liquid nitrogen temperature after flushing the cell with He at 30°C.

Extraction of the EXAFS data from the measured absorption spectra was performed with the XDAP code developed by Vaarkamp *et al.* (36). The procedure followed for processing and analyzing the XAFS data was described in detail elsewhere (31).

Catalytic measurements

Samples Fe/ZSM5-mc and Fe/ZSM5-sc were tested for the HC-SCR of NO, using isobutane as reductant. For the catalytic tests 20 mg of the samples (grain size 90-212 μm) were mixed with 450 mg quartz and were loaded into a tubular plug-flow reactor (i.d.=4 mm, total bed length=25 mm). The catalytic bed was heated to reaction temperature under flowing He ($100 \text{ ml}\cdot\text{min}^{-1}$). After 30 minutes stabilization in He, the feed gas stream, composed of 2000 vppm NO, 2000 vppm i-C₄H₁₀, 3 vol% O₂ and balance He (total flow=140 $\text{ml}\cdot\text{min}^{-1}$), was switched to the reactor. The temperature was varied in the 330-460°C range. Catalytic data were recorded after 1 hour on stream at each temperature. A Perkin Elmer Autosystem XL gas chromatograph, equipped with a TCD detector, was used to monitor the effluent N₂, i-C₄H₁₀, N₂O, CO and CO₂. NO and NO₂ were measured via a 42C Thermo Environmental Instruments NO_x chemiluminescence analyzer, connected in parallel with the gas chromatograph. The GC and the NO_x analyzer could be operated simultaneously.

n-hexane uptake experiments using a Tapered Element Oscillating Microbalance (TEOM)

Transient n-hexane uptake experiments were performed at 523 K at a total pressure of 1.3 bar. Prior to the uptake experiment, samples were dried *in situ* under N₂ at 623 K. The uptake measurements were performed in a Tapered Element Oscillating Microbalance (TEOM) reactor (Rupprecht & Pataschnick TEOM 1500 PMA), using 20 mg of catalyst, n-hexane flow of $0.078 \text{ mmol min}^{-1}$ and N₂ flow of 20 ml min^{-1} (N₂:nC₆ ratio=11 mol/mol). The n-hexane (Merck) was injected into the system using an HPLC pump (Shimadzu LC-10AD). The start of the uptake experiment ($t = 0$) was defined as the last data-point before the first mass change, as detected by the TEOM upon injection of n-hexane. All mass changes were corrected for gas density- and temperature-effects by performing blank runs over inert samples.

Results

Characterization and catalysis

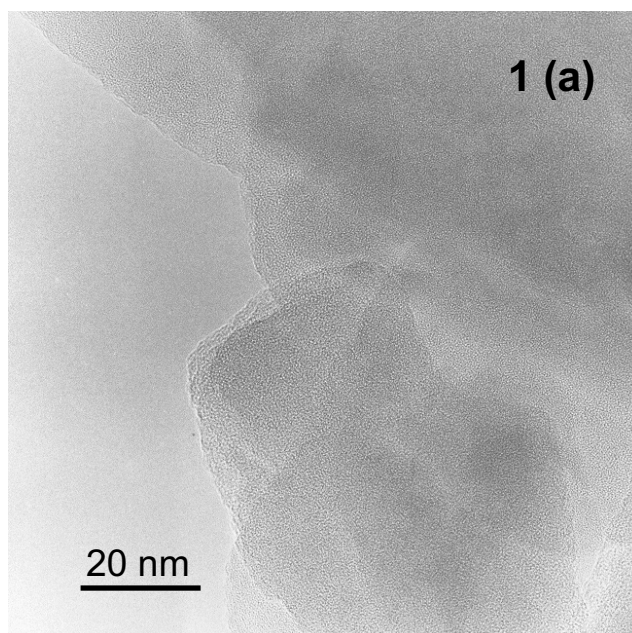
In order to evaluate the significance of the catalytic and n-hexane uptake results presented in this contribution it is indispensable to first draw attention to the characterization of the samples studied. A more extensive spectroscopic study can be found elsewhere (31).

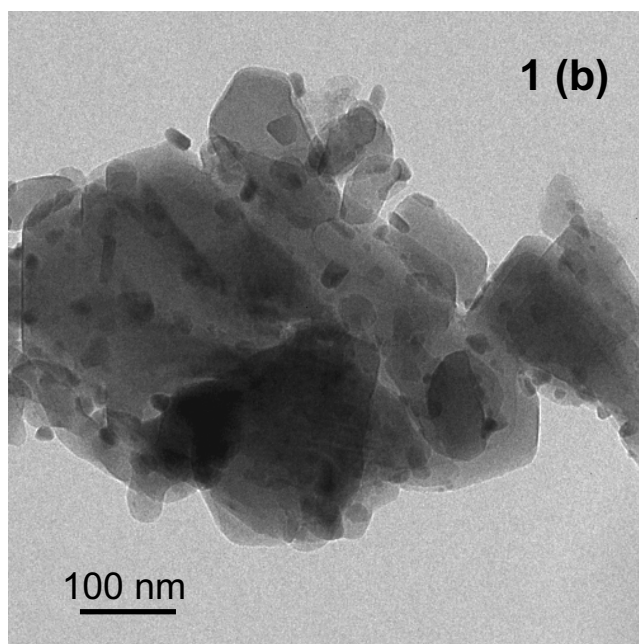
Table 1: Some characteristics of the materials used in this study.

	Si/Al* (atomic ratio)	Fe/Al* (atomic ratio)	Micropore volume (ml·g ⁻¹)	Mesopore area (m ² ·g ⁻¹)
H/ZSM5	17.0	0.0	0.15	57
Fe/ZSM5-mc	17.2	1.0	0.12	54
Fe/ZSM5-sc	17.2	1.0	0.13	44

* determined by ICP

In Table 1 some physico-chemical characteristics of H/ZSM5, and of Fe/ZSM5, subjected to the different calcination procedures, are presented. A small decrease (~20%) was observed in the micropore volume of the parent zeolite (H/ZSM5) after the introduction of iron and mild calcination (Fe/ZSM5-mc). Part of the micropore volume was restored in the case of a severe calcination (Fe/ZSM5-sc).

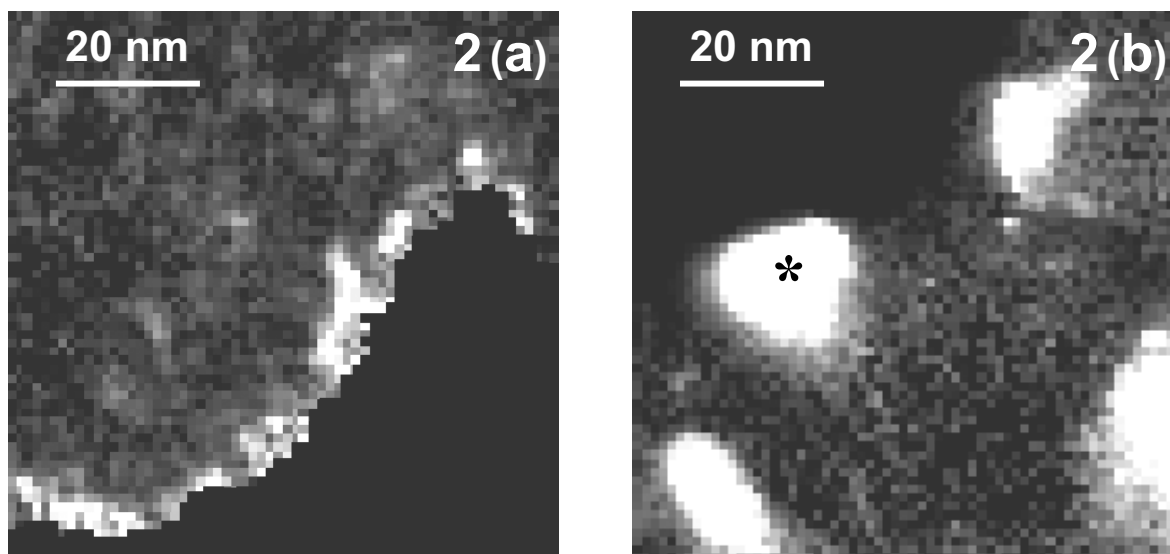




Figures 1: a) HR-TEM micrograph of Fe/ZSM5 upon mild calcination (Fe/ZSM5-mc); b) TEM micrograph (medium magnification) of Fe/ZSM5 upon severe calcination (Fe/ZSM5-sc).

The influence of the calcination procedure on the nature of the Fe-species in Fe/ZSM5 is visualized in Figures 1 by means of representative TEM micrographs. Figure 1a shows a micrograph of the mildly calcined sample. No significant presence of large Fe-containing clusters was revealed by HR-TEM. The presence of iron in the sample was confirmed by bulk elemental analysis (ICP, Table 1), as well as by EDX analysis, performed at a local scale. Iron must therefore be highly dispersed. On the contrary, the sample after severe calcination (Figure 1b) shows Fe-containing particles on the external surface of the ZSM5 crystals. The significantly higher Fe aggregation in the latter sample was confirmed by a Mössbauer study (31).

A more detailed picture of the distribution of iron in the samples was obtained by combining Scanning Transmission Electron Microscopy and Electron Energy Loss Spectroscopy (STEM-EELS). In Figures 2a and 2b two-dimensional maps of the Fe/O atomic ratio in the Fe/ZSM5 samples are shown. Data were collected in pixels from local sub-areas of 1.25·1.25 nm. The lighter the pixels in the figures, the higher the concentration of iron at that position. Due to the uniform distribution of oxygen in the ZSM5 matrix, the pictures represent the local Fe concentration.



Figures 2: 2D-EELS micrographs showing the Fe/O atomic ratio in Fe/ZSM5-mc (a) and Fe/ZSM5-sc (b). The lighter the area, the higher the Fe concentration.

Figure 2a shows that for the mildly calcined sample the iron concentration is enhanced near the edges of the crystals, although large Fe-oxidic particles are not formed yet, in agreement with the TEM results (see Figure 1). For the severely calcined sample, the large particles revealed by TEM could easily be detected also in the EELS experiment (Figure 2b). The white areas depict Fe-oxide particles located on the outer surface of the zeolite. In particular, the Fe/O ratio of the particle located in the center-left part of the picture, marked with an asterisk, could be established without interference of the underlying zeolite oxygen atoms. The Fe/O ratio in this large particle is 0.67, indicating that it consists of Fe_2O_3 .

The techniques mentioned above give information on the distribution of iron in the catalyst and on the chemical composition of the Fe-rich particles. However, they can not provide detailed information on the local atomic environment around iron. Such information was obtained by EXAFS (34). Details on the procedure applied for the generation of the Fe-O and Fe-Fe references and a more detailed discussion of the results obtained have been presented elsewhere (31). The most important structural parameters obtained with EXAFS on the mildly and severely calcined samples are collected in Table 2. As can be seen from the table, the Fe coordination number for the first Fe-Fe coordination shell (3.05 Å) in the mildly calcined sample is close to one. This indicates that the majority of iron is in a binuclear configuration. Since iron is surrounded by six oxygen atoms (the closest Fe-O coordination has been fitted by introducing three oxygen shells), it is assumed to be in an octahedral configuration. A second Fe-Fe shell was found at a higher distance (3.40 Å),

indicating some iron agglomeration. Nevertheless, the low coordination number of this second Fe-Fe shell (0.4) shows that agglomeration phenomena in Fe/ZSM5-mc involved only a minor fraction of iron.

Table 2 shows that increasing the severity of the calcination procedure (Fe/ZSM5-sc) leads to a clear increase in Fe-Fe coordination number in both the first and the second Fe-Fe shells. This result shows that, when a severe calcination is applied, a significant fraction of the Fe-binuclear octahedra undergoes aggregation.

Table 2: Average structural parameters of the Fe-species in Fe/ZSM5, determined by EXAFS. Analysis performed in R-space ($\Delta R=0.7-4.2$ Å; $\Delta k=2.7-13.2$ Å⁻¹).

Sample	Scatterer	Coordination number ±10%	Distance (Å) (±1%)
Fe/ZSM5-mc	O	1.9	1.86
	O	2.0	1.97
	O	2.1	2.09
	Fe	1.2	3.05
	Fe	0.4	3.40
	O	4.5	4.01
Fe/ZSM5-sc	O	2.0	1.86
	O	2.1	1.97
	O	1.8	2.09
	Fe	1.7	3.03
	Fe	1.3	3.42
	O	4.5	4.01

The results of the catalytic tests for the selective catalytic reduction of NO by isobutane, performed on the Fe/ZSM5 samples, are shown in Figure 3. Surprisingly, despite the significant difference in the Fe distribution (concentration of active binuclear species) in the mildly and severely calcined samples, the activity for HC-SCR was found to be the same.

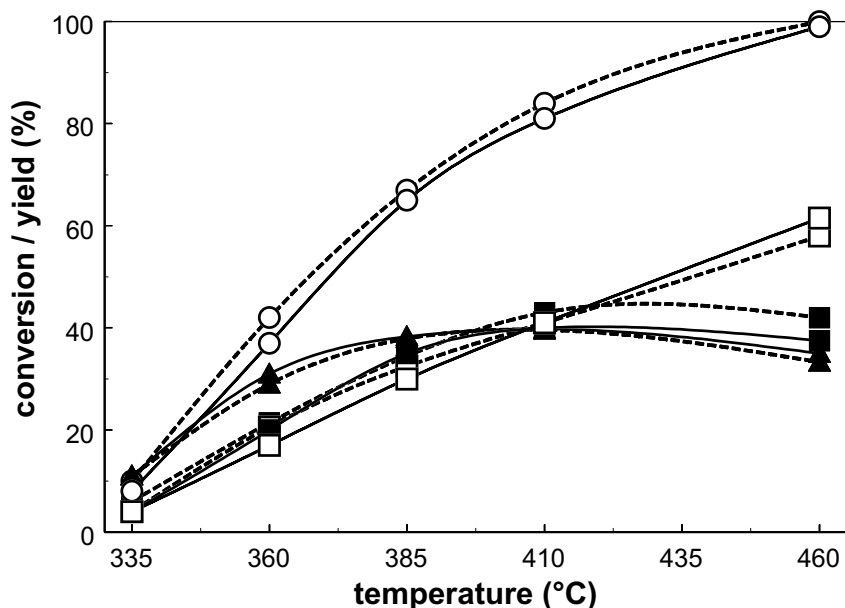


Figure 3: Catalytic activity towards the selective catalytic reduction of NO by isobutane of Fe/ZSM5-mc (dashed lines) and of Fe/ZSM5-sc (solid lines): (▲) N₂ yield, (○) i-C₄H₁₀ conversion, (■) i-C₄H₁₀ conversion to CO, (□) i-C₄H₁₀ conversion to CO₂. Inlet feed composition: 0.2% i-C₄H₁₀ + 0.2% NO + 3% O₂, balance He. GHSV = 21000 h⁻¹.

n-hexane uptake experiments (TEOM)

The parameters obtained from the EXAFS analysis (Table 2) indicate that the size of the Fe-binuclear clusters is comparable with that of the pores of the zeolite. Thus, the presence of these clusters might hamper the accessibility of the zeolite pores, especially for the isobutane molecule. This phenomenon could even be aggravated by the presence of agglomerated Fe-(hydr)oxo species trapped in the zeolite channels (linear polymerization of iron). In order to verify this hypothesis, the accessibility of the zeolite was studied by measuring the uptake of the probe molecule n-hexane, using a TEOM. Measurements were performed on the parent H/ZSM5 and Fe/ZSM5 samples after the different calcination treatments. Since the TEOM resembles a fixed bed reactor, it has the advantage that the uptake measurements can be performed under transient conditions and close to reaction temperature (523 K).

The experimental uptake curves for H/ZSM5, Fe/ZSM5-mc and Fe/ZSM5-sc are shown in Figure 4.

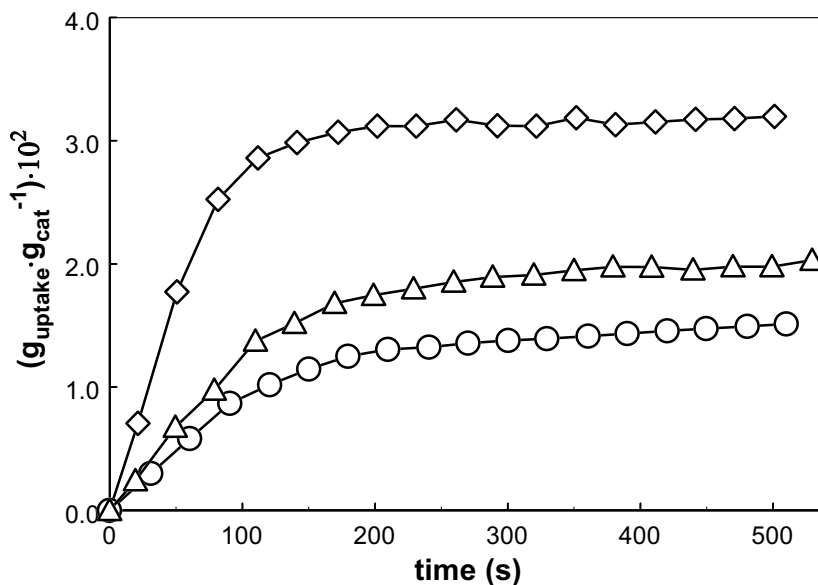


Figure 4: Experimental uptake curves of n-hexane over H/ZSM5 (\diamond), Fe/ZSM5-mc (\circ) and Fe/ZSM5-sc (Δ) ($T = 523 \text{ K}$, $P = 1.3 \text{ bar}$).

From this figure it is clear that the overall n-hexane uptake of the Fe/ZSM5 samples is lower than that of the parent H/ZSM5. Noticeably, the presence of iron decreases by $\sim 50\%$ the volume accessible for the probe molecule. Moreover, the initial slope of the uptake curves (uptake rate) is lower for the Fe-containing samples than for the parent H/ZSM5. Thus, the uptake of n-hexane is also retarded by the presence of Fe-species in the zeolite channels. For the parent H/ZSM5 the slope of the uptake curve becomes zero after 200 s, *i.e.* a steady state could be reached for this sample. On the opposite, for the Fe/ZSM5 samples no stable equilibrium could be detected up to 500 s. The initial fast uptake process (10-150 s) is followed by a further slow uptake (150-500 s). This becomes even clearer when the uptake of n-hexane is plotted as a function of the square root of time (Figure 5). For the parent H/ZSM5 a fast uptake is observed. The uptake rate (slope of the uptake curve) becomes zero with time on stream, indicating no net further uptake of n-hexane. For the Fe-containing samples the initial uptake rate is lower, when compared to that of the parent H/ZSM5. In addition, with time on stream, a slower uptake process is still occurring. Indeed, the slope of the uptake curves for the Fe/ZSM5 samples does not approach zero.

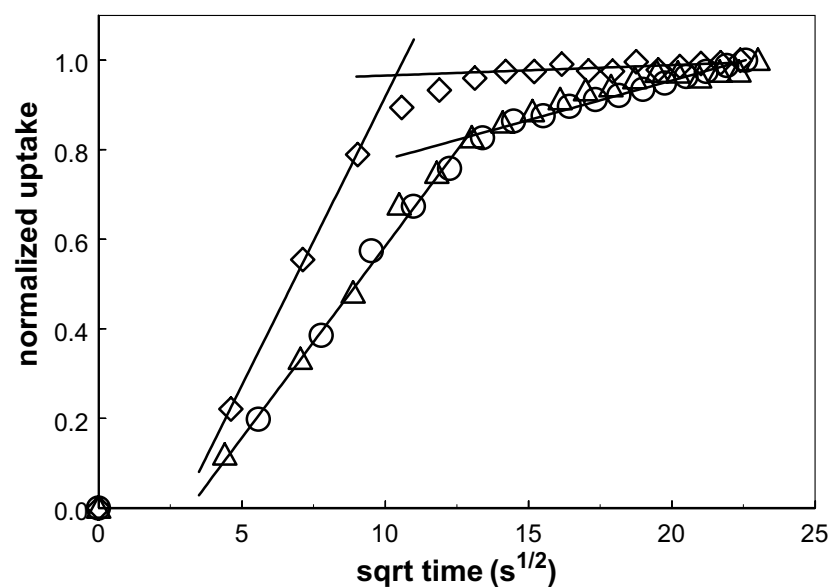


Figure 5: Normalized uptake curves of n-hexane over H/ZSM5 (\diamond), Fe/ZSM5-mc (\circ) and Fe/ZSM5-sc (Δ).

Discussion

The TEM/EELS results (Figs. 1 and 2) clearly show that the Fe-species present in Fe/ZSM5 agglomerate when subjected to a severe calcination procedure. From the EXAFS study, reported in Table 2, a more detailed picture of the evolution of iron as a function of the calcination treatment emerges. As previously discussed in Ref. (31), upon mild calcination the majority of the Fe-species in Fe/ZSM5 consist of binuclear Fe-clusters. In the clusters, iron is surrounded by six oxygen atoms (Table 2). The fitted distances resemble those of the Fe-O configuration of the closest Fe-binuclear building blocks in α -goethite. These data lead us to the conclusion that in the mildly calcined Fe/ZSM5 sample iron is present in isolated edge shared double Fe octahedra, similar to those encountered in the building units of lowly agglomerated oxo-hydroxide structures (31,37,38). Only a minority of these octahedra is aggregated into larger networks, as can be deduced by the presence of a second Fe-Fe shell at higher distance with an extremely low coordination number (0.4). On the contrary, when a severe calcination procedure is applied, the Fe-binuclear clusters tend to aggregate into catalytically inactive (12,32) Fe_2O_3 particles. This was shown by the

TEM/EELS micrographs and by the increase in coordination number of the Fe-Fe shells, as determined by EXAFS (Fe/ZSM5-sc).

Despite the clear differences in the degree of agglomeration of iron, Figure 3 shows that the catalytic behavior towards the selective catalytic reduction of NO with isobutane is similar for both the Fe-containing samples. Since the number of Fe-binuclear clusters, which are believed to be the catalytically active phase in this material, is significantly higher in the mildly calcined sample, the similar catalytic activity of the two samples indicates that during reaction intracrystalline diffusion might play a limiting role. Indeed, the size of the binuclear clusters is similar to that of the zeolite channels. Furthermore occlusion of the channels may also arise by the presence of polymeric Fe-(hydro)oxo within the channels (31).

In order to investigate to which extent the presence of iron might hamper the accessibility of the zeolite channels, we measured the uptake of n-hexane by a TEOM. Figure 4 clearly shows that the overall n-hexane uptake is significantly lower for the Fe-containing samples, when compared to that of the parent H/ZSM5. It must therefore be concluded that not all the space of the zeolite is accessible for the probe molecule after the introduction of iron. Since characterization of the samples by XRD and Al-NMR spectroscopy (31) showed that the zeolite structure of the Fe/ZSM5 samples remains intact, even upon applying a severe calcination procedure, the decrease in the volume accessible for n-hexane must be ascribed to the presence of the Fe-species occupying, and possibly blocking, part of the zeolite channels. Since the uptake for the severely calcined sample is higher than that of the mildly calcined one, the accessible space must be larger for the severely calcined sample. This is in agreement with the TEM/EELS experiments which show that more iron migrates to the surface of the zeolite during a severe calcination. It is important to note that the zeolite pores are only blocked for the relatively large n-hexane molecule. The smaller N₂ molecule can still access the entire pore system of the zeolite (Table 2). The slightly lower pore volumes for the Fe-containing samples is explained by the decrease in zeolite pore space due to the presence of the Fe-clusters.

For the parent H/ZSM5 a steady state with no net n-hexane uptake is reached after 200 s, as shown by the zero slope of the uptake curve. For both the Fe-containing samples, on the contrary, still a low but significant uptake occurs at longer times on stream. This could be explained either by a conversion of adsorbed n-hexane to coke or by a slow diffusion of n-hexane into difficult accessible voids in the zeolite. Since the adsorption process was found to be fully reversible, we conclude that coke formation did not occur and, thus, that part of the ZSM5 crystals must be difficult to access for n-hexane. Most likely the Fe-clusters

located in this part of the zeolite can not effectively take part to the catalytic action of the material.

This observation appears to be consistent with the catalytic performance displayed by the samples. Indeed, despite the clear difference in Fe dispersion and in the concentration of Fe catalytically active species, the samples show an identical activity for the HC-SCR of NO with isobutane. Since the n-hexane uptake rate for the Fe-containing samples is significantly lower than for the parent H/ZSM5, it is concluded that on both the Fe/ZSM5 samples mass transfer must be a limiting factor for catalysis, *i.e.* only a part of the intrinsically active Fe-species (binuclear complexes) are able to contribute effectively to the overall apparent HC-SCR catalytic activity. These complexes must be only the first few binuclear Fe-clusters encountered by the reactants entering the pores. For the mildly calcined sample these clusters might be located closer to the surface of the zeolite crystals, when compared to the severely calcined sample. A pictorial representation for the accessibility of the Fe-species in Fe/ZSM5, based on the results presented, is shown in Figure 6.

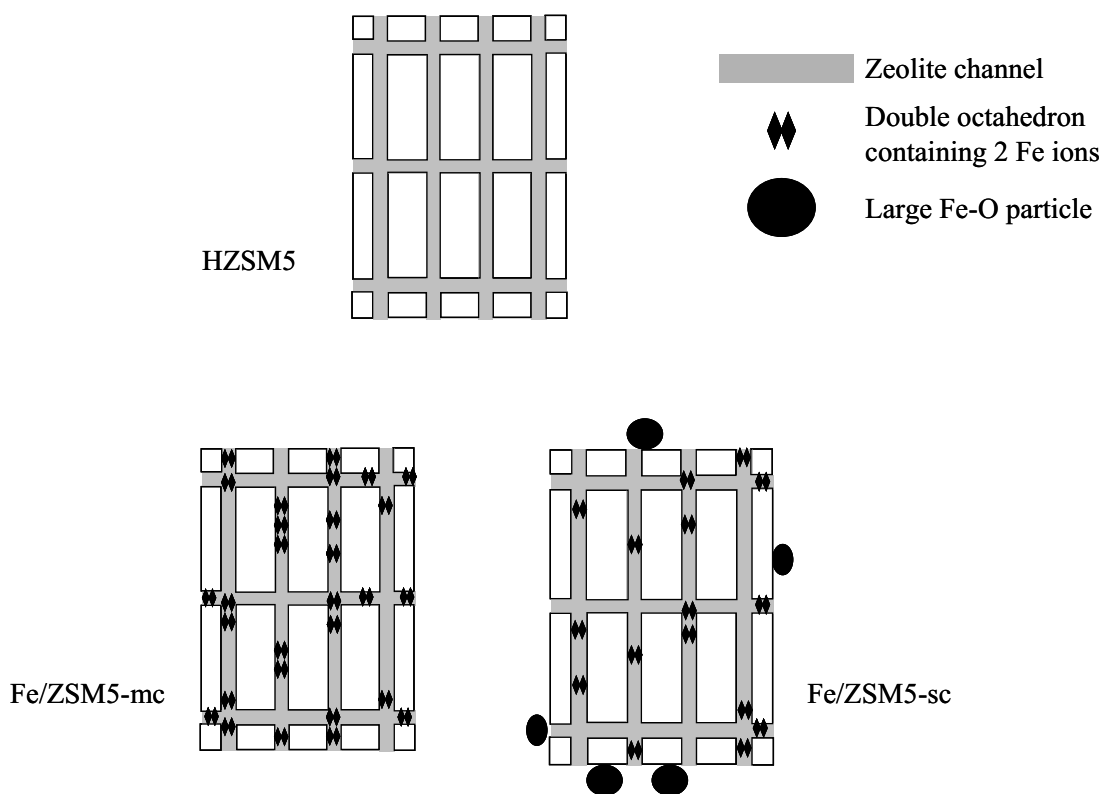


Figure 6: Pictorial representation of the accessibility of the Fe-active sites in mildly and severely calcined Fe/ZSM5.

Conclusions

Over-exchanged Fe/ZSM5 samples, subjected to two different calcination procedures (mild or severe), display the same catalytic activity towards the HC-SCR of NO using isobutane despite clear differences in Fe distribution and in the concentration of catalytically active species. The reason for this unexpected behavior was elucidated by performing uptake measurements with a Tapered Element Oscillating Microbalance (TEOM), using n-hexane as a probe molecule. The results show that for the two Fe/ZSM5 samples the uptake rate, as well as the total n-hexane uptake, are significantly lower than for the parent H/ZSM5. It is therefore concluded that in both samples the Fe-species block the micropores of ZSM5 for hydrocarbons uptake. As a result, only a part of the potentially active Fe-binuclear species are able to contribute effectively to the overall apparent HC-SCR catalytic activity. These species must be only the first few binuclear Fe-clusters encountered by the reactants entering the zeolite pores.

Reference list

1. Panov, G.I., Sheveleva, G.A., Kharitonov, A.S., Romannikov, V.N., and Vostrikova, L.A., *Appl. Catal. A: General* **82**, 31 (1992).
2. Panov, G.I., Uriarte, A.K., Rodkin, M.A., and Sobolev, V.I., *Catal. Today* **41**, 365 (1998).
3. Shepelev, S.S., and Ione, K.G., *React. Kinet. Catal. Lett.* **23**, 319 (1983).
4. Vereshchagin, S.N., Baikalova, L.I., and Anshits, A.G., *Izv. Akad. Nauk., Ser. Khim.* **8**, 1718 (1988).
5. Gubelmann M., and Tirel, P., Fr. Patent 2630735 (filed: May 2, 1988).
6. Sobolev V.I., Panov, G.I., Kharitonov, A.S., Romannikov, V.N., Volodin, A.M., and Kazimira G.I., *J. Catal.* **139**, 435 (1993).
7. Kapteijn, F., Marbán G., Rodríguez-Mirasol J., and Moulijn J.A., *Appl. Catal. B* **9**, 25 (1997).
8. Kögel, M., Mönnig, R., Schwieger, W., Tissler A., and Turek, T., *J. Catal.* **182**, 470 (1999).
9. Centi G., and Vanazza, F., *Catal. Today* **53**, 683 (1999).
10. Pérez-Ramírez J., Kapteijn F., Mul G., and Moulijn J.A., *Chem. Commun.* (no 693 (2001)).
11. Pérez-Ramírez J., Kapteijn F., Mul G., and Moulijn J.A., *Appl. Catal. B* **35**, 227 (2002).

12. Chen, H.-Y., and Sachtler, W.M.H., *Catal. Today* **42**, 73 (1998).
13. Chen, H.-Y., Voskoboinikov, T., and Sachtler, W.M.H., *J. Catal.* **180**, 171 (1998).
14. Chen, H.-Y., Voskoboinikov, T., and Sachtler, W.M.H., *Catal. Today* **54**, 483 (1999).
15. Ratnasamy, P., and Kumar, R., *Catal. Today* **9**, 328 (1991).
16. Bordiga, S., Buzzoni, R., Geobaldo, F., Lamberti, C., Giamello, E., Zecchina, A., Leofanti, G., Petrini, G., Tozzola, G., and Vlaic, G., *J. Catal.* **158**, 486 (1996).
17. Dubkov, K.A., Sobolev, V.I., and Panov G.I., *Kinet. Catal.* **39**, 72 (1998).
18. Lázár, K., Lejeune, G., Ahedi, R.K., Shevade, S.S., and Kotasthane, A.N., *J. Phys. Chem. B* **102**, 4865 (1998).
19. Pérez-Ramírez J., Kapteijn F., Mul G., and Moulijn J.A., Overweg, A.R., Doménech, A., Ribera A., and Arends, I.W.C.E., *J. Catal.* **207**, 113 (2002).
20. Feng, X., and Hall, W.K., *J. Catal.* **166**, 368 (1997).
21. Kögel, M., Sandoval, V.H., Schwieger, W., Tissler, A., and Turek, T., *Catal. Lett.* **51**, 23 (1998).
22. Joyner, R., and Stockenhuber, M., *J. Phys. Chem. B* **103**, 5963 (1999).
23. Lobree, L.J., Hwang, I.-C., Reimer, J.A., and Bell, A.T., *J. Catal.* **186**, 242 (1999).
24. El-Malki, E.-M., van Santen, R.A., and Sachtler, W.M.H., *J. Catal.* **196**, 212 (2000).
25. Heinrich, F., Schmidt, C., Löffler, E., and Grünert, W., *Catal. Commun.* **2**, 317 (2001).
26. El-Malki, E.-M., van Santen, R.A., and Sachtler, W.M.H., *J. Catal.* **196**, 212 (2000).
27. Chen, H.-Y., El-Malki, E.-M., Wang, X., van Santen, R.A., and Sachtler, W.M.H., *J. Molec. Catal. A* **162**, 159 (2000).
28. Battiston, A.A., Bitter J.H., and Koningsberger, D.C., *Catal Lett.* **66**, 75 (2000).
29. Marturano, P., Drozdová, L., Kogelbauer, A., and Prins, R., *J. Catal.* **192**, 236 (2000).
30. Marturano, P., Drozdová, L., Pirngruber, G.D., Kogelbauer, A., and Prins, R., *Phys. Chem. Chem. Phys.* **3**, 5585 (2001).
31. Chapter 2 of this thesis; Battiston, A.A., Bitter, J.H., de Groot, F.M.F., Overweg, A.R., Stephan, O., van Bokhoven, J.A., Kooyman, P.J., van der Spek, C., Vankó, G., and Koningsberger, D.C.; accepted for publication in *J. Catal.*
32. Hall, W.K., Feng, X., Dumesic, J., and Watwe, R., *Catal. Lett.* **52**, 13, (1998).
33. Kucherov, A.V., and Shelef, M., *J. Catal* **195**, 106 (2000).
34. Koningsberger, D.C., Mojet, B.L., van Dorssen, G.E., and Ramaker, D.E., *Top. Catal.* **10**, 143 (2000).
35. Vaarkamp, M., Mojet, B.L., Modica, F.S., Miller, J.T., and Koningsberger, D.C., *J. Phys. Chem.* **99**, 16067 (1995).
36. Vaarkamp, M., Linders, J.C., and Koningsberger, D.C., *Physica B*, **209** (1995).

37. Rustad, J.R., Felmy A.R., and Hay B. P., *Geochim. Cosmochim. Acta*, **60 (9)**, 1553 (1996).
38. Suzuki S., Suzuki T., Kimura M., Takagi, Y., Shinoda, K., Tohji, K., and Waseda, Y., *Appl. Surf. Science* **169-170**, 109 (2001).

Combining Pt/ZSM5 and Over-Exchanged Fe/ZSM5 for the Selective Catalytic Reduction of NO_x by Hydrocarbons: a Dual-Bed Configuration

Abstract

Pt/ZSM5, prepared by liquid ion-exchange from Pt(NH₃)₄(NO₃)₂, and Fe/ZSM5, obtained by sublimation of FeCl₃, have been combined and tested for the selective catalytic reduction of NO_x, using isobutane as probe reductant. Different reactor configurations have been explored, *i.e.* a single-bed (physical mixture of Fe/ZSM5 and Pt/ZSM5) and a dual-bed system with the two catalysts disposed in series (first Pt/ZSM5 and then Fe/ZSM5). Operating the two catalysts in a single bed (physical mixture) is not a practical solution since Pt catalyzes the direct oxidation of *i*-C₄H₁₀ to CO₂, with a detrimental effect on the overall selective reduction of NO_x. The dual bed configuration, on the contrary, is highly effective. Unreacted NO, and N₂O formed over Pt/ZSM5 in the first stage, can be converted to harmless N₂ over the second Fe/ZSM5 bed. The best results can be obtained with an intermediate additional injection of isobutane between the two catalytic beds, operated at 270°C (Pt/ZSM5) and at around 410°C (Fe/ZSM5), respectively. Under these conditions a N₂ yield of 90% was obtained with a complete suppression of CO and N₂O formation.

Introduction

Nitrogen oxides (NO, NO₂ and N₂O) are unwanted pollutants in the atmosphere (1,2). Their presence originates primarily from the end-pipe exhausts of stationary and mobile combustion systems (3).

Two technologies are nowadays largely applied for the reduction of NO_x emissions. The first one is the selective catalytic reduction of NO_x using ammonia (NH₃-SCR). The term selective refers to the ability of ammonia to preferably react with oxygen from the NO_x, instead of being oxidized by molecular oxygen (O₂) present in the streams to be treated. This technique is used for cleaning the emissions of stationary sources, like oil-, coal- and gas-fired power plants and industrial heaters (4-7). The second technique, is the so-called three way catalyst (TWC), applied to contemporarily reduce emissions of NO_x, CO and unburnt hydrocarbons, produced by (mobile) spark ignited gasoline engines. The catalyst, in this case, is not able to reduce the NO_x to N₂ in the presence of excess oxygen (lean conditions). Therefore, the air to fuel ratio supplied to the engine must be constantly controlled and kept around stoichiometric conditions (air/fuel weight ratio ~14.6).

Although these two technologies are efficient and well established, they present disadvantages. For the NH₃-SCR the drawbacks consist of relatively high costs of operation, problems related to the transport and storage of anhydrous ammonia, slips of unreacted ammonia to the atmosphere and possible plugging by ammonium sulfates, originated by the reaction of NH₃ with the sulfur-containing compounds present in the stream. The use of the TWC, on the other hand, appears to be in contrast with the demand for improved fuel economy, condition that can be fulfilled by engines operated under lean conditions, like diesel-powered ones.

A promising alternative to the above-mentioned clean-up techniques is the selective catalytic reduction of NO_x using hydrocarbons (HC-SCR). With the HC-SCR unburnt hydrocarbons present in the tail-pipe can be used, in combination with an eventual additional injection from an external source (as in the case of NH₃-SCR), to reduce the NO_x to N₂. This technique is applicable also in the presence of excess oxygen.

An extremely large number of catalytic materials have been investigated in the last decades towards the HC-SCR of NO_x (8,9). The most interesting results for practical applications have been obtained so far over Pt- and Fe-loaded zeolites. Platinum-containing zeolites, in particular Pt/ZSM5, show considerable activity at low temperature (200-300°C, depending on the reactant applied). Anyhow, they possess deficits as well. In particular, the selectivity towards N₂ is low, as N₂O is formed in comparable amounts during HC-SCR operation (10-14). This represents a major problem, since N₂O is a strong greenhouse gas and contributes to stratospheric ozone destruction.

The use of Fe has attracted highest attention in more recent years. In 1996 Feng and Hall reported for the first time on the exceptional activity and stability of Fe/ZSM5 towards the selective catalytic reduction of NO using isobutane as reductant (15,16). A N₂ yield of nearly 100% could be obtained in the temperature range 400-500°C at the relatively high gas hourly space velocity of 42000 h⁻¹. This high NO conversion could be maintained even in the presence of water (20 vol.%) and SO₂ (150 vppm). The catalyst was prepared by ion-exchange in aqueous solution from FeC₂O₄ (ferrous oxalate) under exclusion of air. While this synthesis technique showed problems in reproducibility (17,18), a superior method, consisting in subliming FeCl₃ into the cavities of an acidic H/ZSM5 support, was proposed two years later by Chen and Sachtler (19). Over the as-obtained Fe/ZSM5, at reaction conditions identical to those adopted by Feng and Hall, a NO conversion of approximately 75% could be obtained in the temperature range 350-400°C, with a complete selectivity towards N₂ (19,20). Similar performances could be achieved when using n-butane or propane as reductants (21). In the presence of 10 vol% of water the activity of the catalyst appeared to be almost unaffected. Fe/ZSM5 obtained by the FeCl₃ CVD technique has recently been demonstrated to be also active in the direct decomposition of N₂O (22). Major drawbacks of this catalyst, however, are the significant formation of CO during HC-SCR and the relatively high operating temperature (350-400°C).

A possible solution to overcome the problems encountered with both Pt- and Fe-catalysts is to combine them in a single catalytic-system. The goal is to obtain the highest possible NO_x conversion, contemporarily reducing emissions of N₂O and CO, typical undesired by-products of Pt and Fe, respectively.

The objective of this study is to monitor the possibility of combining Pt/ZSM5, obtained via liquid ion-exchange from Pt(NH₃)₄(NO₃)₂, and Fe/ZSM5, obtained by sublimation of FeCl₃, for the selective catalytic reduction of NO. i-C₄H₁₀ was used as probe reductant. Different reactor configurations have been tested, *i.e.* a single bed (physical mixture of Pt/ZSM5 and Fe/ZSM5), with the two catalyst operating at the same temperature, and a dual bed configuration, with the two catalyst disposed in series (first Pt and then Fe) and operating at different temperatures. It will be shown that, by applying a dual bed configuration, N₂O produced by Pt in the first stage can be decomposed/reduced over Fe/ZSM5 to harmless N₂ (deN₂O). By tuning the temperature of the second stage (Fe), also CO emissions can be minimized, with an overall increase in the N₂ yield. The best performance of the system can be achieved with an intermediate i-C₄H₁₀ injection between the two stages.

Experimental

Catalyst preparation

The list of the catalysts used in this study, together with their chemical composition, is presented in Table 1. All the samples were synthesized starting from acidic H/ZSM5 supports, obtained by calcination in O₂ at 550°C of NH₄/ZSM5 (Zeolyst).

Table 1: Some characteristics of the samples tested in this study.

Catalyst	*Si/Al ratio	*Fe/Al ratio	Metal (wt%)	Pretreatment	Sample code
Pt/ZSM5	17	--	†(Pt) 0.5	calcination	Pt-0.5-calc
				calcination followed by reduction	Pt-0.5-red
				autoreduction	Pt-0.5-autored
Pt/ZSM5	17	--	†(Pt) 0.1	autoreduction	Pt-0.1-autored
Fe/ZSM5	17	1.0	*(Fe) 4.4	calcination	Fe-17-4.4
Fe/ZSM5	30	1.8	*(Fe) 4.5	calcination	Fe-30-4.5
Fe/ZSM5	51	2.0	*(Fe) 3.0	calcination	Fe-51-3.0

* determined by ICP
† determined by XRF

Pt/ZSM5

Pt/ZSM5 samples were prepared by liquid ion-exchange (23). H/ZSM5 (5 g, Si/Al=17) was suspended under vigorously stirring in 1000 ml doubly demineralized water at 80°C. A solution of 0.5 g Pt(NH₃)₄(NO₃)₂ in 50 ml H₂O was prepared. For samples Pt-0.5 and Pt-0.1 (see Table 1) 5.0 and 1.0 ml of the solution, respectively, were diluted with additional 50 ml H₂O and were slowly dropped into the suspension (1 hr). The suspension was further maintained under stirring at 80°C for 24 hrs and subsequently filtered. The obtained Pt/ZSM5 samples were washed twice with H₂O, dried overnight at 80°C in air, pressed and sieved to 90-212 μm.

In order to evaluate the influence of different pretreatments on the catalytic activity of Pt/ZSM5, sample Pt-0.5 was divided into three parts (1.3 g each), which were subjected respectively to calcination, calcination followed by reduction, or auto-reduction. Sample Pt-0.1 was subjected solely to auto-reduction. The parameters describing the procedure

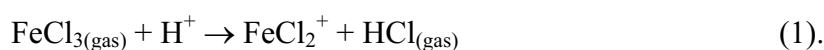
followed for the different pre-treatments of the Pt/ZSM5 catalysts are collected in Table 2. All the treatments were performed in a plug flow reactor (i.d.= 12 mm).

Table 2: Description of the parameters applied for the different pre-treatments of the Pt/ZSM5 samples used in this study.

Pretreatment	Catalyst amount (g)	Gas-flow composition (ml/min)	Temperature ramp (°C/min)	Max. temperature pretreatment (°C)
Calcination	1.3	20:80 O ₂ /Ar, (1000)	0.2	400 (3 hrs)
Reduction	1.3	H ₂ , (250)	5	400 (2 hrs)
Auto-reduction	1.3	Ar, (1000)	0.2	400 (3 hrs)
samples were cooled under Ar (100 ml/min, 5°C/min)				

Fe/ZSM5

Fe/ZSM5 was synthesized following the FeCl₃ sublimation technique (also referred to as chemical vapor deposition (CVD)), proposed by Chen and Sachtler (19). In order to study the influence of the Al content on the catalytic activity of the as-obtained Fe/ZSM5, three different Fe/ZSM5 samples were prepared, starting from H/ZSM5 batches with a Si/Al molar ratio of 17, 30 and 51 (see Table 1). A three-fold excess FeCl₃ was used, as the amount needed for a complete exchange versus the H⁺ Brønsted sites of the support, according to reaction (1):



The procedure applied during the synthesis has been extensively described in our previous works (24,25). Particular attention was paid to calcination, in order to minimize formation of catalytically inactive Fe₂O₃ clusters (24). The samples were heated under a He flow of 800 ml/min with a moderate temperature ramp (0.5°C/min) to 200°C. At this temperature, 200 ml/min of O₂ were added to the He flow while, under the same temperature ramp, heating was continued to 550°C. After 3 hrs at 550°C, the temperature was lowered to 30°C.

Catalyst characterization

Elemental composition of samples Pt-0.1 and Pt-0.5 was determined by XRF and ICP. Imaging of sample Pt-0.5 upon reduction (Pt-0.5-red) was obtained by TEM, using a Philips EM420 microscope, equipped with a field-emission gun operated at 120 kV.

Elemental analysis of the Fe/ZSM5 samples was performed by ICP.

Catalytic tests

System configuration

The different set-up configurations used in this study are presented in Fig.1.

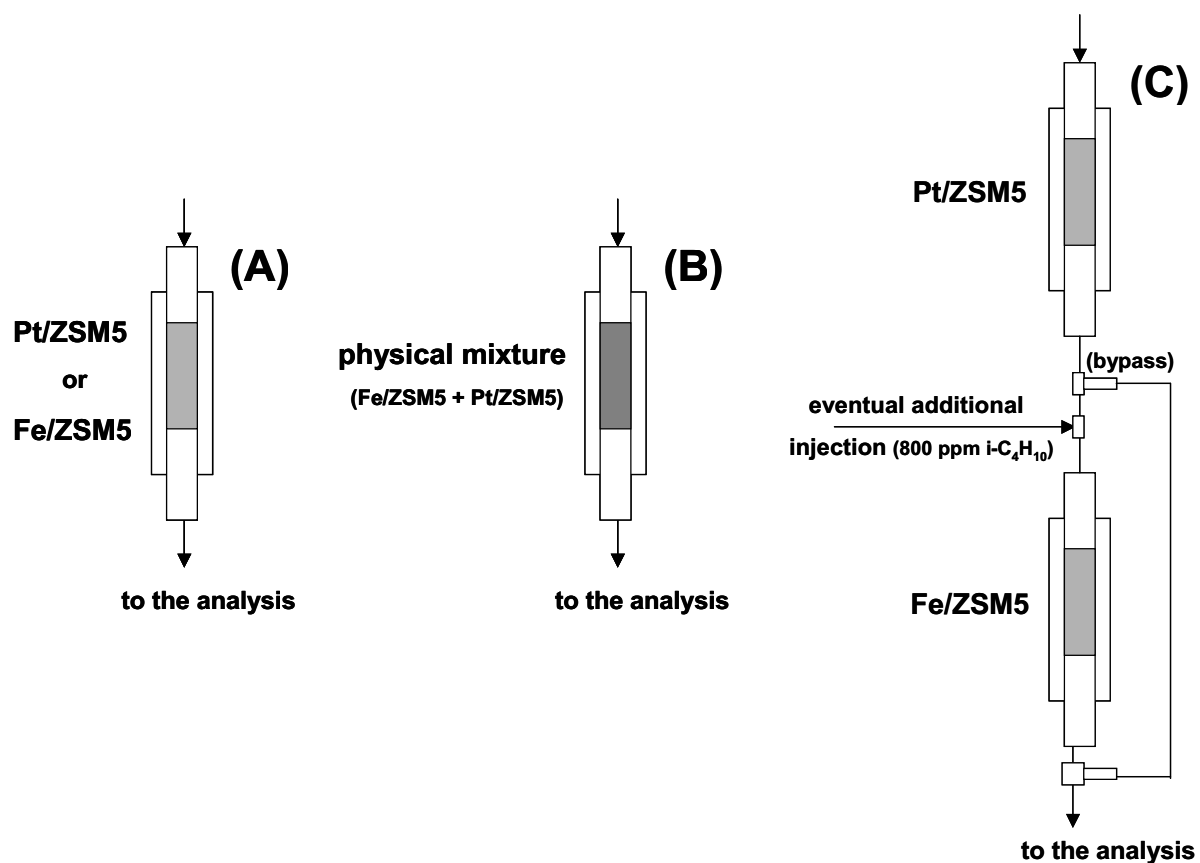


Figure 1: Reactor configurations adopted for the catalytic testing of Fe/ZSM5 and Pt/ZSM5 catalysts towards the selective catalytic reduction of NO (deNO) and N₂O (deN₂O) with isobutane: (A) single stage (Fe/ZSM5, tested for deNO or deN₂O; Pt/ZSM5, tested for deNO); (B) single stage (physical mixture of Fe/ZSM5 and Pt/ZSM5, tested for deNO); (C) two stages in series, operated at different temperatures, tested for deNO. First stage: Pt/ZSM5; second stage: Fe/ZSM5. Tests were performed also with an intermediate additional injection of isobutane between the two stages.

Catalytic activity measurements were carried out in a single quartz plug-flow reactor (single bed configuration, A or B), or in two identical quartz PFR reactors connected in series (dual bed configuration, C). A complete description of the catalytic tests performed is given in Table 3. Activity measurements were performed towards the selective catalytic reduction of NO (deNO) and towards the selective catalytic reduction of N₂O (deN₂O). For both reactions i-C₄H₁₀ was used as probe reductant.

Table 3: List of the catalytic tests performed in this study.

Single bed					
Process and catalyst	Samples	amount (mg)	SV (ml/g·h)	*GHSV (h ⁻¹)	reactor configuration (see Fig.1)
¹ deNO) Pt/ZSM5	Pt-0.5-calc	(100)	84000	42000	(A)
	Pt-0.5-red	(100)			
	Pt-0.5-autored	(100)			
¹ deNO) Fe/ZSM5	Fe-17-4.4	(100)	84000	42000	(A)
	Fe-30-4.5	(100)			
	Fe-51-3.0	(100)			
¹ deNO) Phys. Mixture	Fe-17-4.4	(100)	70000	35000	(B)
	+ Pt-0.1-autored	(20)			
² deN ₂ O) Fe/ZSM5	Fe-17-4.4	(100)	84000	42000	(A)
Dual bed					
Process and catalyst	Sample	amount (mg)	SV (ml/g·h)	*GHSV (h ⁻¹)	reactor configuration
³ deNO)					
1 st stage: Pt/ZSM5 +	Pt-0.5-autored	(100)	84000	42000	(C)
Inlet gas composition:					
¹ 2000 vppm NO, 2000 vppm i-C ₄ H ₁₀ , 3vol% O ₂ , balance He to 140 ml/min.					
² 2000 vppm N ₂ O, 2000 vppm i-C ₄ H ₁₀ , 3vol% O ₂ , balance He to 140 ml/min.					
³ 2000 vppm NO, 2000 vppm i-C ₄ H ₁₀ , 3vol% O ₂ , balance He to 140 ml/min; test performed also with additional injection of 800 vppm i-C ₄ H ₁₀ before the 2 nd bed (Fe/ZSM5).					
* Calculation based on an apparent zeolite density of 0.5 g/ml.					
† Calculated without taking into account additional injection of isobutane.					

Single bed (one stage)

Tests in a single bed were performed on Fe/ZSM5 and on Pt/ZSM5 samples, loaded separately (Fig. 1, (A)), and on a Fe/ZSM5:Pt/ZSM5 physical mixture (Fig. 1, (B)).

The Fe/ZSM5 samples, prepared through the identical synthesis route (CVD of FeCl₃) but from zeolitic supports with different Al concentration, were tested for the selective catalytic reduction of NO (deNO). Sample Fe-17-4.4 (the most rich in aluminum) was also tested for the deN₂O reaction.

Pt/ZSM5 samples (Pt-0.5), subjected to different pretreatments (see Table 3), were tested and compared solely for the deNO reaction.

The first experiment performed with the aim of monitoring the catalytic behavior of a Fe/Pt combination was the catalytic test of a Fe/ZSM5:Pt/ZSM5 physical mixture. For this test a 100:20 mixture (Fe-17-4.4:Pt-0.1-autored, weight ratio) was chosen and tested for the deNO reaction.

Dual bed (two stages)

The dual bed configuration (Fig. 1 (C)) was tested for the selective reduction of NO (deNO). This configuration was chosen in order to be able to operate Pt/ZSM5 and Fe/ZSM5 in series and at their respective optimal working temperature. The first stage was loaded with Pt/ZSM5 (Pt-0.5-autored). The optimal temperature window for Pt/ZSM5 (based on the maximum NO conversion) was obtained by the catalytic results of the Pt/ZSM5 single stage test for deNO. An additional fine-tuning was performed during the dual-bed experiments by varying the temperature of the first bed (Pt) in the 250-270°C temperature range. The second stage was loaded with Fe/ZSM5 (Fe-17-4.4). The temperature of the second bed was varied in a broader temperature range, *i.e.* between 310 and 385°C. Catalytic test were performed also upon injection of additional isobutane (800 vppm) between the two stages. In this case, the maximum temperature of the second bed (Fe) was raised up to 410°C. Conversion of the deNO feed was measured upon reaction on the first bed (using a by-pass) and upon reaction on both catalytic beds.

Catalytic bed preparation, mixing and analysis sections

Prior to measuring, samples were pressed and crushed to obtain a sieve fraction of 90-212 µm. Typically 100 mg of sample (with the exception of the deNO measurement performed over the Fe/Pt physical mixture (120 mg)) were mixed with 4.0 g of quartz, placed in the reactor, and heated under He (100 ml/min). Reacting mixtures were injected 30 minutes after the reaction temperature was reached.

The reaction feeds (deNO and deN₂O) were obtained by blending four flows, *i.e.* 1%vol. NO/He (or alternatively 1%vol. N₂O/He), 1%vol. i-C₄H₁₀/He, O₂ and He. Each flow-rate

was regulated by a digital Brooks mass-flow controller. The resulting inlet composition for the deNO tests was 2000 vppm NO, 2000 vppm i-C₄H₁₀, 3% vol O₂, balance He, with an overall flow of 140 ml/min. For the deN₂O tests NO was substituted by 2000 vppm N₂O. Based on an apparent zeolite density of 0.5 g/cm³, the calculated Gas Hourly Space Velocity (GHSV) in each stage was 42000 h⁻¹. For the test of the Fe/Pt physical mixture it was 35000 h⁻¹.

A Perkin Elmer Autosystem XL gas chromatograph equipped with a TCD detector was used to monitor the effluent N₂, i-C₄H₁₀, N₂O, CO and CO₂. The gases were separated using a Haysep Q and a Molsieve 13 X column (80-100 mesh). In order to be able to measure NO and NO₂, a Thermo Environmental Instruments 42C NO_x chemiluminescence analyzer was connected in parallel with the gas chromatograph. The GC and the NO_x analyzer could be operated simultaneously. Catalytic data reported were measured after 60 min. reaction at each temperature.

Results

Catalyst characterization

Pt/ZSM5

The chemical composition of the Pt/ZSM5 samples tested in this study is presented in Table 1.

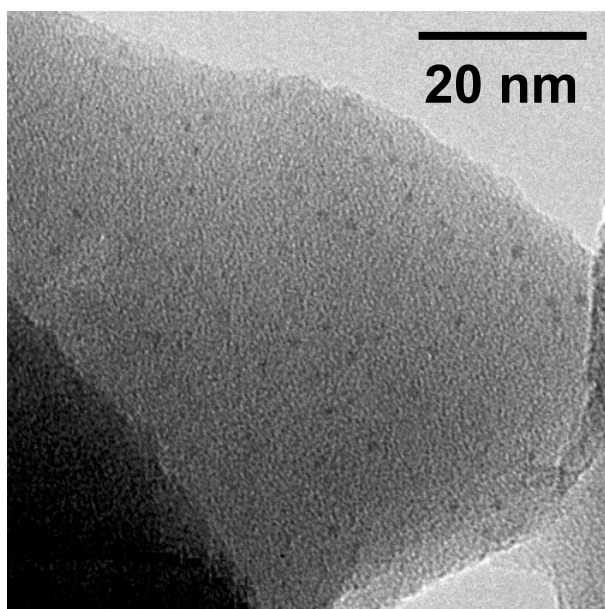


Figure 2: TEM micrograph of Pt-0.5-red.

Fig. 2 shows a representative TEM micrograph of sample Pt-0.5-red. As can be seen from the picture, Pt could be deposited on the ZSM5 support in the form of highly dispersed particles, with an average dimension, after reduction, of approximately 1-2 nm.

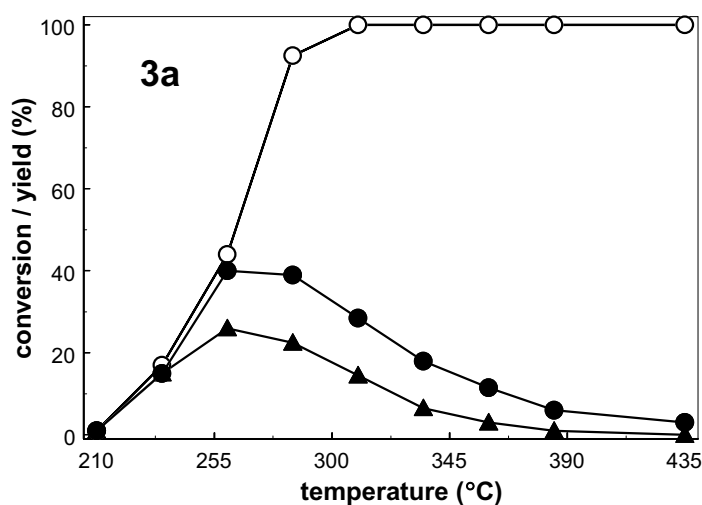
Fe/ZSM5

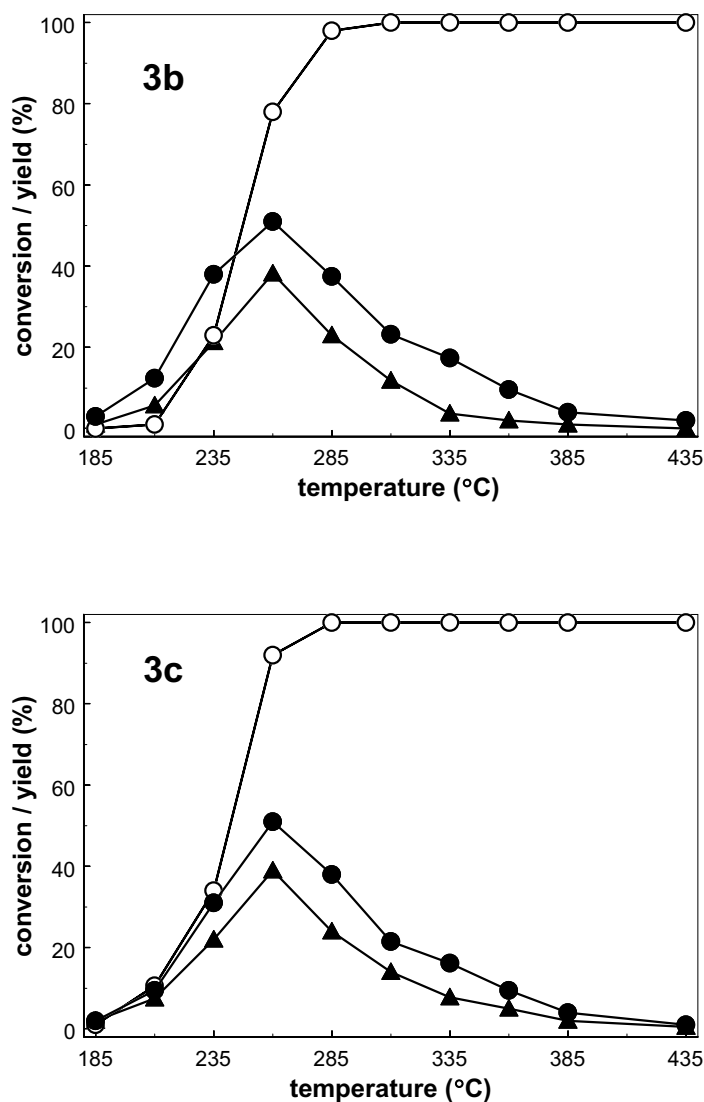
The chemical composition of the Fe/ZSM5 samples is shown in Table 1. As can be seen, a Fe/Al ratio of 1.0 was obtained from the H/ZSM5 support with the highest Al content (Fe-17-4.4). A higher Fe/Al ratio was obtained for the remaining samples. An extensive characterization of sample Fe-17-4.4 can be found in our previous study (24), where the evolution of the support and of the Fe-species along the different synthesis steps is presented.

Catalytic tests

Pt/ZSM5 (single bed)

The results of the catalytic tests towards the selective catalytic reduction of NO (deNO, single bed) of the Pt-0.5 series are presented in Figs 3a, b and c. Sample Pt-0.5-calc (Fig. 3a) shows a maximum NO conversion at around 260°C, corresponding to the isobutane light-off temperature. N₂ and N₂O are contemporarily formed by reduction of NO over the whole temperature range, N₂O being the primary product. CO₂ is the only oxidation-product of isobutane. Indeed, no traces of CO were detected, even at low temperature.





Figures 3: Selective Catalytic Reduction of NO (deNO) with isobutane over Pt-0.5-calc (3a), Pt-0.5-red (3b), Pt-0.5-autored (3c): N₂ yield (▲), N₂O yield (●), i-C₄H₁₀ conversion (O). Inlet composition: 2000 vppm i-C₄H₁₀, 2000 vppm NO, 3v% O₂, balance He; GHSV = 42000 h⁻¹. Reactor configuration (A), Fig. 1.

Similar catalytic features are shown by the Pt-0.5 catalyst upon reduction (Pt-0.5-red, Fig. 3b) or upon auto-reduction (Pt-0.5-autored, Fig. 3c). Also after the reductive treatments, Pt is responsible for the formation of large amounts of N₂O and for the complete oxidation of isobutane to CO₂. Nevertheless, on these samples the light-off of isobutane appears to be shifted towards lower temperature, when compared to that of the calcined sample (Fig. 4).

Contemporarily a clear increase is visible for the reduced and auto-reduced samples in the N_2 yield in the 210-260°C temperature range.

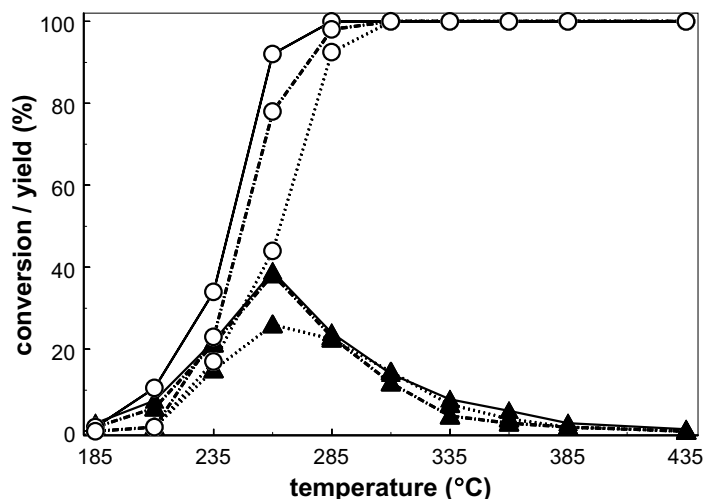
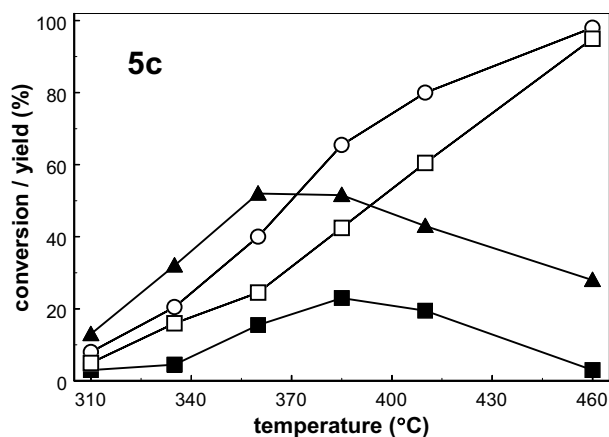
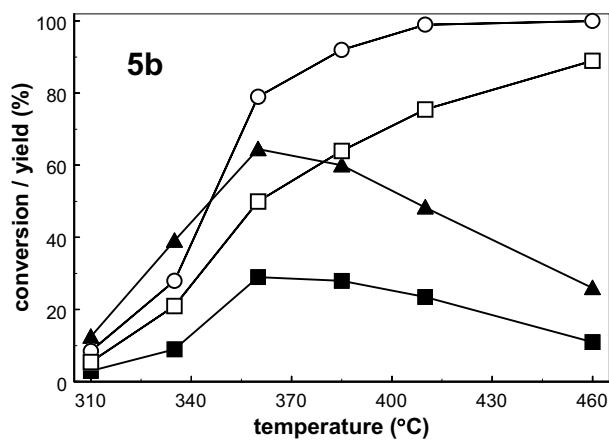
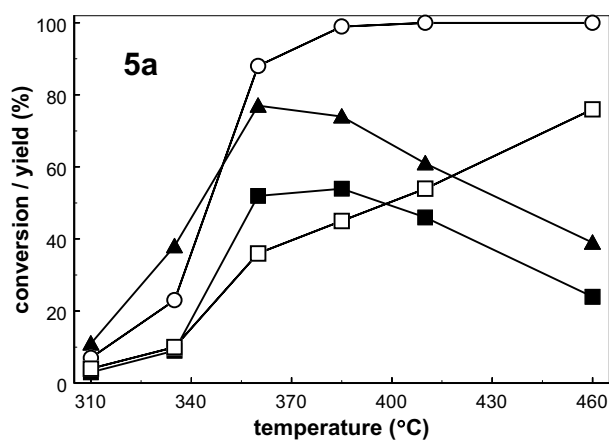


Figure 4: Effect of the pretreatment on the $i-C_4H_{10}$ conversion (○) and on the N_2 yield (▲), as obtained during the Selective Catalytic Reduction of NO (deNO) with isobutane over Pt/ZSM5: Pt-0.5-autored (solid line), Pt-0.5-red (dashed-dotted line), Pt-0.5-calc (dotted line).

Fe/ZSM5 (single bed)

The catalytic activity towards the deNO reaction of the Fe/ZSM5 samples (single bed) is presented in Figs. 5a, b and c.

Differently from Pt/ZSM5, Fe-containing catalysts show a complete selectivity to N_2 . In particular, no N_2O is formed as by-product during reaction. The maximum conversion of NO (N_2 yield) is obtained for all the samples at around 360°C, a significantly higher temperature than in the case of Pt/ZSM5 (+ 100°C). Combustion of isobutane to CO_2 is not complete. Indeed, reduction of NO to N_2 is accompanied by the formation of a significant amount of CO. This phenomenon was not observed on the Pt/ZSM5 catalysts. Yields of CO and N_2 show a typical volcano shape. This is the result of the direct oxidation of $i-C_4H_{10}$ to CO_2 , operated by O_2 from the gas-phase, and highly favored at high temperature (> 400°C).



Figures 5: Selective Catalytic Reduction of NO (deNO) with isobutane over Fe-17-4.4 (5a), Fe-30-4.5 (5b) and Fe-51-3.0 (5c): N₂ yield (▲), i-C₄H₁₀ conversion (○), CO yield (■) and CO₂ yield (□). Inlet composition: 2000 vppm i-C₄H₁₀, 2000 vppm NO, 3v% O₂, balance He; GHSV = 42000 h⁻¹. Reactor configuration (A), Fig. 1.

The catalytic results show that, on a weight basis, the most active Fe/ZSM5 sample for the selective reduction of NO to N₂ is the one with the highest Al content (Fe-17-4.4, Fig.6).

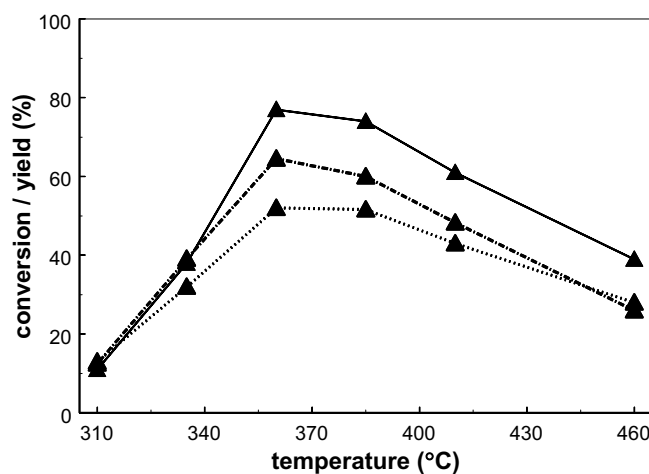


Figure 6: Effect of the Si/Al ratio on the N₂ yield (▲), as obtained during the Selective Catalytic Reduction of NO (deNO) with isobutane over Fe/ZSM5: Fe-17-4.4 (solid line), Fe-30-4.5 (dashed-dotted line), Fe-51-3.0 (dotted line).

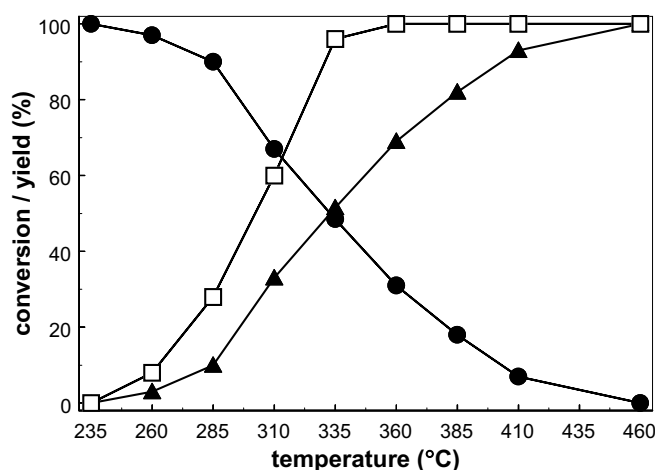


Figure 7: Selective Catalytic Reduction of N₂O (deN₂O) with isobutane over Fe-17-4.4: N₂ yield (▲), N₂O conversion (●) and CO₂ yield (□). Inlet composition: 2000 vppm i-C₄H₁₀, 2000 vppm N₂O, 3v% O₂, balance He; GHSV=42000 h⁻¹. Reactor configuration (A), Fig. 1.

Fig. 7 shows the catalytic activity of sample Fe-17-4.4 towards the selective catalytic reduction of N_2O (de N_2O). The N_2 yield in the de N_2O process displays a sigma-shaped profile, with a complete conversion of N_2O to N_2 obtained at approximately 460°C . Differently than in the deNO reaction, the N_2 yield during de N_2O is not limited by a maximum temperature. It can be noted from the picture that an increase in the conversion of N_2O can be obtained also upon complete consumption of $i\text{-C}_4\text{H}_{10}$ (360°C). This suggests that, at a sufficiently high temperature, Fe/ZSM5 is able to directly decompose N_2O to N_2 and O_2 .

Fe/ZSM5-Pt/ZSM5 physical mixture (single bed)

The first attempt to combine Pt/ZSM5 and Fe/ZSM5 for the selective reduction of NO was performed by using a physical mixture, with Fe/ZSM5 in large excess (Fe-17-4.4/Pt-0.1-autored = 100:20). The results of the catalytic test are shown in Fig. 8.

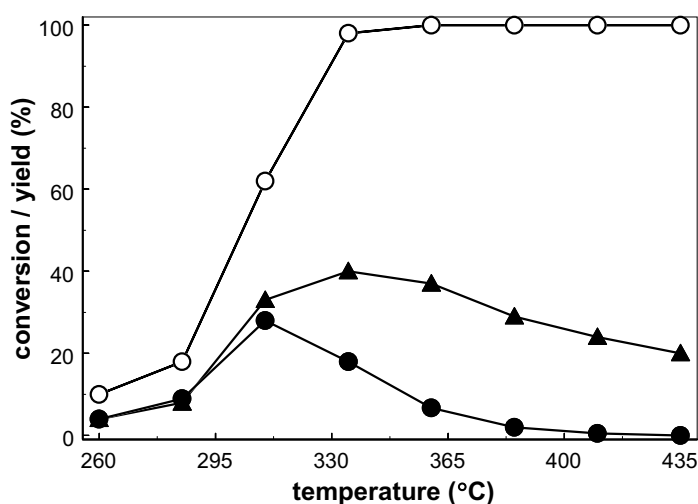


Figure 8: Selective Catalytic Reduction of NO (deNO) with isobutane over a Fe/ZSM5-Pt/ZSM5 physical mixture (100 mg Fe-17-4.4, 20 mg Pt-0.1-autored): N_2 yield (▲), N_2O yield (●) $i\text{-C}_4\text{H}_{10}$ conversion (○). Inlet composition: 2000 vppm $i\text{-C}_4\text{H}_{10}$, 2000 vppm NO, 3v% O_2 , balance He; GHSV = 35000 h^{-1} . Reactor configuration (B), Fig.1.

The catalytic behavior of the mixture shows features typical of both catalysts. The presence of Pt reduces the light-off temperature of $i\text{-C}_4\text{H}_{10}$, lowered from around 350°C (Fe-17-4.4 alone, Fig. 5a) to 300°C , and suppresses the formation of CO. Nevertheless, it is

responsible for the formation of undesired N_2O . In addition, no beneficial effect was visible in the maximum NO conversion. A side-effect of Pt at high temperature ($>300^\circ\text{C}$) is most probably to catalyze the direct oxidation of $i\text{-C}_4\text{H}_{10}$ and CO to CO_2 , with a detrimental effect on the overall selective reduction of NO to N_2 .

Pt/ZSM5-Fe/ZSM5 (dual bed configuration without intermediate injection of $i\text{-C}_4\text{H}_{10}$)

As shown by the results obtained on the physical mixture, the pre-requisite for effectively combining the catalytic properties of Fe/ZSM5 and Pt/ZSM5 for the selective catalytic reduction of NO is to operate the two catalysts at their corresponding optimal working temperature. This was obtained by adopting a dual bed configuration with the two catalysts operated in series (two stages). Pt/ZSM5 (Pt-0.5-autored) was loaded in the first stage and Fe/ZSM5 (Fe-17-4.4) in the second one. The results of the catalytic tests are shown in Figs. 9a, b, and c. The temperature of the first stage was maintained at 250°C (Fig.9a), 260°C (Fig. 9b) or 270°C (Fig. 9c), while the temperature of the second one was varied in the temperature range $310\text{--}385^\circ\text{C}$. Conversion of the deNO feed was measured upon reaction on the first bed and on both catalytic beds, in order to visualize the further effect of the Fe/ZSM5 bed. The first data-points (left part of the figures) show conversions and yields upon reaction over the first bed (Pt) alone. The remaining data were obtained upon reaction over both beds (Pt/ZSM5 + Fe/ZSM5).

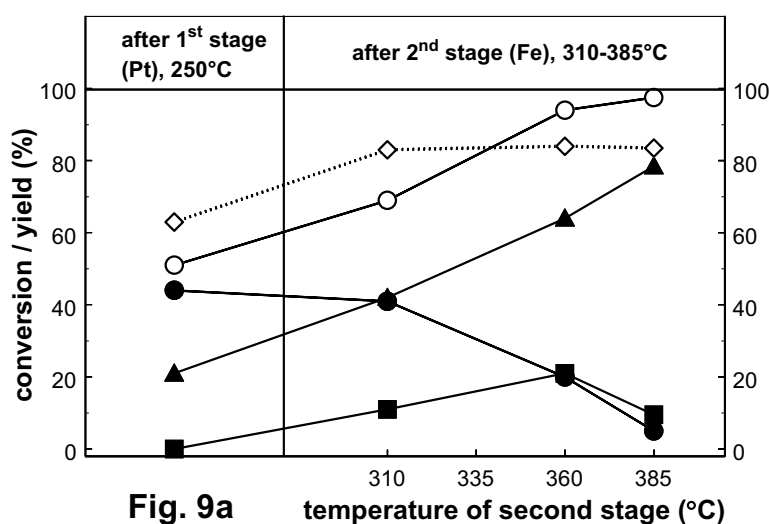
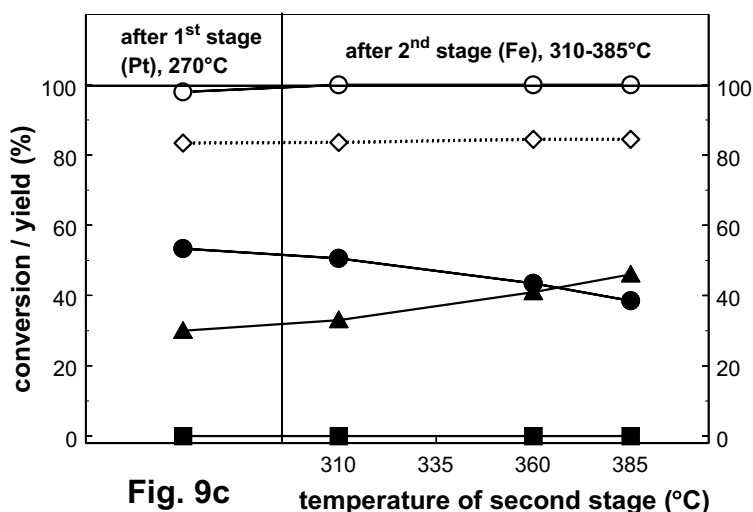
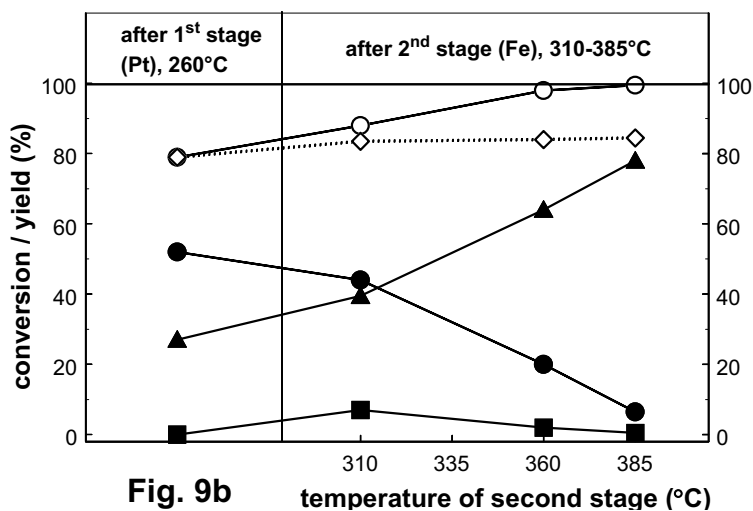


Fig. 9a



Figures 9: Selective Catalytic Reduction of NO (deNO) with isobutane over a Fe/ZSM5-Pt/ZSM5 dual bed system, without additional intermediate $\text{i-C}_4\text{H}_{10}$ injection (see reactor configuration (C), Fig.1): NO conversion (◇, dotted line), N_2 yield (▲), N_2O yield (●), $\text{i-C}_4\text{H}_{10}$ conversion (○), CO yield (■). Inlet composition: 2000 vppm $\text{i-C}_4\text{H}_{10}$, 2000 vppm NO, 3v% O_2 , balance He. The temperature of the first bed (100 mg Pt-0.5-autored) was maintained at 250°C (9a), 260°C (9b) or 270°C (9c), while the temperature of the second bed (100 mg Fe-17-4.4) was varied in the temperature range 310-385 °C.

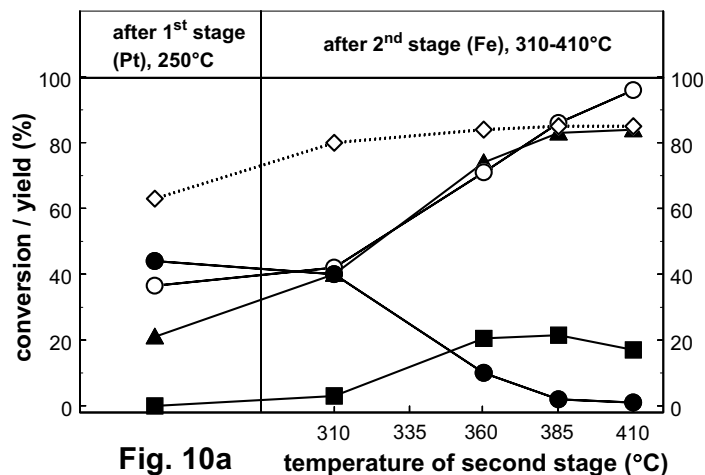
As can be seen from Fig. 9a, the fraction of unreacted $\text{i-C}_4\text{H}_{10}$ leaving the first (Pt) stage can be effectively used over the Fe/ZSM5 bed to obtain a further reduction to N_2 of both NO (deNO) and N_2O (de N_2O). At a temperature higher than 310°C the de N_2O reaction

prevails over the deNO process. Indeed, conversion of NO reaches its maximum already at 310°C, while the conversion of N₂O increases steadily up to the maximum temperature tested (385°C).

A similar behavior is shown in Fig. 9b. In this case, due to the increased temperature of the first (Pt) bed (260°C), less isobutane is available for the reduction of NO and N₂O to N₂ over Fe/ZSM5. Above 360°C, conversion of N₂O to N₂ appears to proceed also via direct decomposition. Decomposition of N₂O to N₂ is the only process occurring across the Fe-bed when no isobutane is left available. This situation is encountered when the Pt catalyst is operated at 270°C (Fig. 9c). In this case, no further removal of NO is possible, due to the inability of the Fe/ZSM5 to directly decompose NO to N₂ and O₂. The result is a significant decrease in the final N₂ yield, dropped from 80% (Figs. 9a and 9b, T = 385°C) to 50%. In the absence of a reductant the only possible solution to increase the N₂ yield would be a further increase in the temperature of the second bed, enhancing the N₂O decomposition rate.

Pt/ZSM5-Fe/ZSM5 (dual bed configuration with intermediate injection of i-C₄H₁₀)

In order to be able to operate the second bed at the lowest possible temperature contemporarily obtaining a high N₂ yield, isobutane must be available for the Fe/ZSM5 catalyst. A practical solution consists in injecting additional reductant between the two catalytic beds (see Fig. 1 (C)). The conversion plots obtained with intermediate isobutane injection are shown in Figs 10. Conversion of isobutane was calculated on the basis of the total amount of i-C₄H₁₀ introduced in the system (2800 vppm). Also in this experiment the temperature of the first stage was maintained at 250°C (Fig.10a), 260°C (Fig. 10b) or 270°C (Fig. 10c), while varying the temperature of the second one. The Fe/ZSM5 catalytic bed was tested up to 410°C.



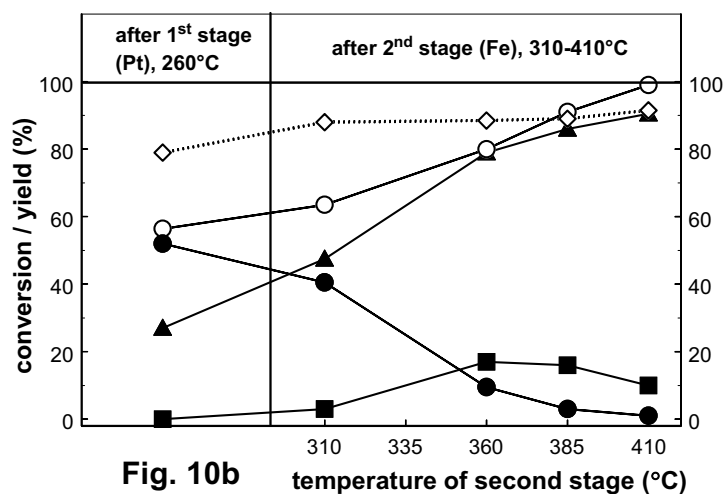


Fig. 10b

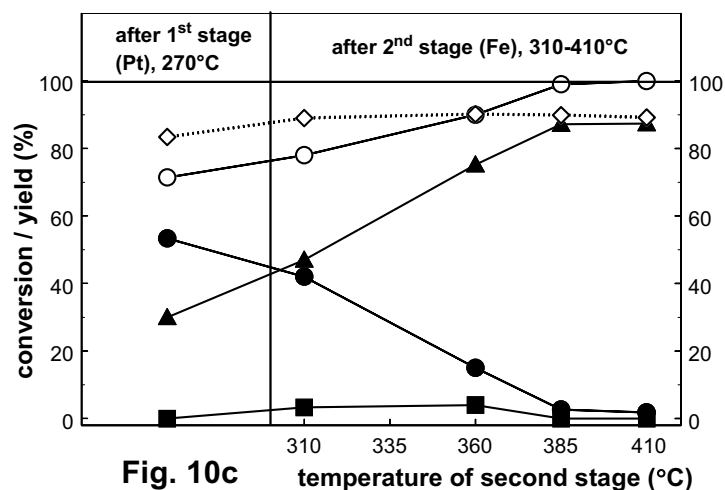


Fig. 10c

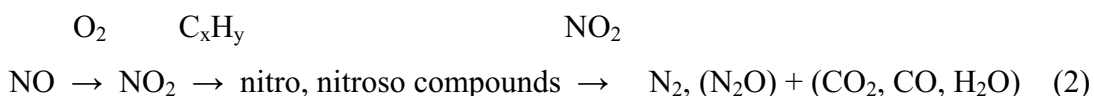
Figures 10: Selective Catalytic Reduction of NO (deNO) with isobutane over a Fe/ZSM5-Pt/ZSM5 dual bed system with additional intermediate $i\text{-C}_4\text{H}_{10}$ injection (see reactor configuration (C), Fig.1): NO conversion (\diamond , dotted line), N_2 yield (\blacktriangle), N_2O yield (\bullet), $i\text{-C}_4\text{H}_{10}$ conversion (\circ), CO yield (\blacksquare). Inlet composition: 2000 vppm $i\text{-C}_4\text{H}_{10}$ (additional 800 vppm $i\text{-C}_4\text{H}_{10}$ injected between the two stages), 2000 vppm NO, 3v% O_2 , balance He. The temperature of the first bed (100 mg Pt-0.5-autored) was maintained at 250°C (10a), 260°C (10b) or 270°C (10c), while the temperature of the second bed (100 mg Fe-17-4.4) was varied in the temperature range 310-410 °C.

The effect of the intermediate isobutane injection, when operating the first (Pt) bed at 250°C, can be seen by comparing Figs 9a and 10a. No significant increase can be obtained in the N_2 yield, nor in the overall NO conversion. Indeed, under these conditions sufficient

isobutane is already left available by the first bed (around 1000 ppm) and an additional injection is unnecessary. On the contrary, when the first catalytic bed is operated at 260°C (compare Figs. 9b and 10b), the added $i\text{-C}_4\text{H}_{10}$ can be effectively used by the Fe/ZSM5 catalyst to further reduce N_2O and part of the remaining NO coming from the first bed. Under the conditions tested a complete selectivity to N_2 can be obtained at 410°C, with an N_2 yield of 90%. In this case around 1000 ppm of CO are still present in the exhaust gases. The best results could be obtained when operating the Pt bed at 270°C (Fig. 10c). Under this conditions the only isobutane available for the Fe/ZSM5 bed is the one introduced by injection. As a result, formation of CO can be strongly limited, obtaining a complete combustion to CO_2 already at 385°C.

Discussion

Selective catalytic reduction of NO using hydrocarbons is a multi-step process. On most catalytic systems the first steps of the reaction consists in the oxidation of NO to NO_2 , with formation of adsorbed nitro (NO_2^-) and nitrate (NO_3^-) complexes. These complexes further react with hydrocarbons, forming organic nitro and nitroso compounds. The final step of the reaction consists in the reaction of the nitro and nitroso compounds with NO_2 from the gas phase, with the formation of a N-N bond and the release of N_2 (and N_2O) (20,21,26-29). The reaction pathway can be summarized as follows:



An ideal catalyst should be able to accelerate the entire reaction, avoiding formation of undesired by-products as N_2O and CO. Despite the large number of studies such material has not been found yet (9,29).

Pt/ZSM5, prepared by liquid ion-exchange, and Fe/ZSM5, obtained by sublimation of FeCl_3 , are among the most active catalysts for the selective catalytic reduction of NO using hydrocarbons. However, both catalysts have drawbacks for practical applications. For Pt/ZSM5 the major disadvantage is represented by its inability to selectively reduce NO to N_2 , as N_2O represents the major product from reduction under lean-conditions (10-14). For Fe/ZSM5, which couples an outstanding activity towards the selective reduction of NO with a complete selectivity towards N_2 (19-21), the drawback consists in the formation of large amounts of CO.

The idea of combining these two materials in a dual catalytic system for the selective reduction of NO using hydrocarbons arises from the ability of Fe-exchanged ZSM5

materials to catalyze also the direct decomposition of N₂O to N₂ and O₂ (22,30-32) and the reduction of N₂O by hydrocarbons (33). Fe/ZSM5 can be used for converting N₂O produced by Pt/ZSM5 to N₂ (deN₂O) via reduction or direct decomposition. Operating the Fe/ZSM5 catalyst at a sufficiently high temperature would also facilitate the complete combustion of the hydrocarbons to CO₂, suppressing release of CO.

In the first part of this study we have focused our attention on Pt/ZSM5 and Fe/ZSM5 separately, in order to select the best materials to be coupled. For Pt/ZSM5 the effect of different pre-treatments has been studied. As can be seen in Fig. 4 the most active material is obtained via a reduction (or auto-reduction) pre-treatment. In particular a higher N₂ yield can be obtained.

For the Fe/ZSM5 sample the influence of the Al content was investigated. The catalytic results for the selective catalytic reduction of NO show that the most active Fe/ZSM5 sample, on a weight basis, is the one synthesized from the H/ZSM5 support with the highest Al content (Fe-17-4.4, Fig.6). As discussed in previous studies (24,25) the most plausible candidates for the active phase in Fe/ZSM5 obtained by CVD of FeCl₃ consist of Fe binuclear oxo/hydroxo-complexes (19,20,22,34,35). The formation of such complexes requires the presence of two Al atoms in close proximity in the framework, condition that appears difficult to be fulfilled by ZSM5 supports with a low Al content. The decrease in catalytic activity with increasing Si/Al ratio can therefore be ascribed to a reduced presence of active phase (Fe-binuclear complexes) in the samples. Sample Fe-17-4.4, showing also a very high activity for the selective catalytic reduction of N₂O (Fig. 7) was therefore chosen to be combined with Pt/ZSM5.

Table 4: Catalytic performance of Pt/ZSM5-Fe/ZSM5 combinations towards the selective catalytic reduction of NO.

Configuration	Temperature (°C)	NO conversion (%)	N ₂ yield (%)	N ₂ O yield (%)	CO yield (%)
physical mixture	310	61	28	33	0
dual bed	260/385	84	78	6	1
dual bed with intermediate i-C ₄ H ₁₀ injection	270/410	90	88	2	0

The best results obtained by coupling Pt/ZSM5 and Fe/ZSM5 with the different system-configurations are collected in Table 4.

A Fe/ZSM5 and Pt/ZSM5 physical mixture was tried as first attempt. Operating the two catalyst at the same temperature in a single bed would be a preferred solution, mainly due to simplicity and economy of operation. Nevertheless, a physical mixture does not represent an effective solution (Table 4, Fig.8). Under such conditions the oxidative properties of Pt prevail, catalyzing the direct oxidation of $i\text{-C}_4\text{H}_{10}$ and CO to CO_2 . While, indeed, formation of CO can be suppressed, large amounts of N_2O are still produced. Furthermore, the overall conversion of NO is lowered when compared to that obtained on Fe/ZSM5 alone (Fig. 5a).

The results show the necessity of operating the two catalysts at their respective optimal working temperature. This was obtained by adopting a dual bed configuration with Pt/ZSM5 loaded in the first bed and Fe/ZSM5 in the second one. A similar configuration was tested with success by Pérez-Ramírez *et al.* (36) on catalytic materials different from the ones presented in this study. In their study the first catalytic bed consisted on a Pt-supported on carbon catalyst, while different materials were tested for the second (deN_2O) bed, *i.e.* mixed Co-Rh- and Co-Pd-La-oxides (derived from Al-hydrotalcites) and Fe/ZSM5 obtained by liquid ion-exchange from iron nitrate. While the Co-Rh mixed oxides showed higher activity in the decomposition of N_2O to N_2 and O_2 , the activity of Fe/ZSM5 was increased by the presence of a reductant (propene). It should be noted that Fe/ZSM5 prepared sublimation of FeCl_3 , tested in the current study, is a superior catalyst when compared to Fe/ZSM5 prepared by liquid ion-exchange for both the decomposition of N_2O (31) as for the selective catalytic reduction of NO (19,28). It therefore appears as a more appropriate candidate for practical applications.

The results obtained with the dual bed disposition (without intermediate injection of isobutane) show that Pt/ZSM5 and Fe/ZSM5 can be effectively coupled (Figs. 9a, 9b and 9c, Table 4). Unreacted NO, and N_2O formed over Pt/ZSM5 in the first stage, can be further converted to harmless N_2 over the second Fe/ZSM5 bed. Conversion of NO is possible only through selective reduction, thus, only if part of isobutane is left available for the second bed. This is clearly shown in Fig. 9c: when the Pt/ZSM5 bed is operated at 270°C (complete combustion of isobutane) Fe/ZSM5 is not able to further decompose NO to N_2 and O_2 . Conversion of N_2O , on the contrary, can proceed over Fe/ZSM5 via selective reduction (when isobutane is still available) as well as via direct decomposition. Decomposition of N_2O to N_2 is clearly shown in Fig. 9c. Reduction is certainly the preferred route, since it occurs faster. As a consequence a lower temperature is required by the second bed. A sufficiently high temperature is however necessary ($> 385^\circ\text{C}$) to obtain a complete oxidation of isobutane to CO_2 .

Provided that the Pt/ZSM5 bed is operated at a sufficient high temperature (260-270°C) an intermediate additional injection of isobutane has beneficial effects on the overall N₂ yield. Freshly injected isobutane can effectively reduce unreacted NO and N₂O, coming from the first catalytic bed, to N₂. This is shown by the results presented in Figs. 10b and 10c and Table 4. In this case, a somewhat higher temperature has to be maintained in the second bed (around 410°C) to completely oxidize CO to CO₂. The best results (around 90% N₂ yield, and almost zero CO and N₂O emissions), under the conditions tested, could be obtained with an intermediate injection of isobutane, operating the two catalytic beds respectively at 270°C (Pt/ZSM5) and 410°C (Fe/ZSM5).

The results shown appear to be promising. However, further experiments are required. In particular, the effectiveness of the system should be confirmed by durability tests, performed in the presence of additional water (10-20% vol) and at higher space velocities (GHSV of around 100000 h⁻¹).

Conclusions

Pt/ZSM5, obtained by liquid ion-exchange, and Fe/ZSM5, prepared through the FeCl₃ sublimation technique can be effectively coupled in a dual-bed catalytic system for the selective catalytic reduction of NO_x using isobutane as reductant.

The system consists of two catalytic beds connected in series, loaded respectively with Pt/ZSM5 (first stage) and Fe/ZSM5 (second stage) and working at different temperature. In the first stage (Pt/ZSM5) isobutane operates the reduction of NO to N₂ and N₂O. In the second bed (Fe/ZSM5) unreacted NO and N₂O formed over the Pt/ZSM5 catalyst can be further converted to harmless N₂.

Conversion of N₂O to N₂ over Fe/ZSM5 can occur via reduction or direct decomposition. Reduction is the preferred route since it can be accomplished at a lower temperature. The best results (90% N₂ yield) can be obtained by an intermediate additional injection of isobutane between the two catalytic beds. Provided that the two stages are operated at their optimal working temperatures (260-270°C for Pt/ZSM5 and around 410°C for Fe/ZSM5), a total selectivity to N₂ can be achieved, with a contemporarily suppression of CO and N₂O formation.

Reference list

1. Lomborg, B., "The Skeptical Environmentalist", Cambridge University Press, Cambridge, U.K., (2001).
2. Pârvulescu, V.I., Grange, P., and Delmon, B., *Catal. Today* **46**, 233 (1998).
3. Ertl, G., Knözinger, H., and Weitkamp, J., "Environmental Catalysis", Wiley-VCH Verlag, Weinheim, Germany, (1999).
4. Forzatti, P., *Appl. Catal. A* **222**, 221 (2001).
5. Bosch, H., and Janssen, F., *Catal. Today* **2**, 369 (1988).
6. Nakahjima, F., and Hamada, I., *Catal. Today* **29**, 109 (1996).
7. Matsuda, S., Kamo, T., Kato, A., and Nakajima, F., *Ind. Eng. Chem. Prod. Res. Develop.* **21**, 48, (1982).
8. Fritz, A., and Pitchon, V., *Appl. Cat. B* **13**, 1 (1997).
9. Traa, Y., Burger, B., and Weitkamp, J., *Micropor. Macropor. Mater.* **30**, 3 (1999).
10. Obuchi, A., Ohi, A., Nakamura, M., Ogata, A., Mizuno, K., and Ohuchi, H., *Appl. Catal. B* **2**, 71 (1993).
11. Iwamoto, M., Yahiro, H., Shin, H.K., Watanabe, M., Guo, J., Konno, M., Chikahisa, T., and Murayama, T., *Appl. Catal. B* **5**, L1-L5 (1994).
12. Captain, D.K., Roberts, K.L., and Amiridis, M.D., *Catal. Today* **42**, 93 (1998).
13. Xin, M., Hwang, I.C., and Woo, S.I., *Catal. Today* **38**, 187 (1997).
14. Bamwenda, G.R., Obuki, A., Ogata, A., Oi, J., Kushiya, S., and Mizuno, K. J., *Molec. Catal. A* **126**, 151 (1997).
15. Feng, X., and Hall, W.K., *Catal. Lett.* **41**, 45 (1996).
16. Feng, X., and Hall, W.K., *J. Catal.* **166**, 368 (1997).
17. Hall, W.K., Feng, X., Dumesic, J., and Watwe, R., *Catal. Lett.* **52**, 13 (1998).
18. Marturano, P., Kogelbauer, A., and Prins, R., *J. Catal.* **190**, 460 (2000).
19. Chen, H.-Y., and Sachtler, W.M.H., *Catal. Today* **42**, 73 (1998).
20. Chen, H.-Y., Voskoboinikov, T., and Sachtler, W.M.H., *J. Catal.* **180**, 171 (1998).
21. Chen, H.-Y., Voskoboinikov, T., and Sachtler, W.M.H., *Catal. Today* **54**, 483 (1999).
22. El-Malki, E.-M., van Santen, R.A., and Sachtler, W.M.H., *J. Catal.* **196**, 212 (2000).
23. de Graaf, J., van Dillen, J., de Jong, K.P., and Koningsberger, D.C., *J. Catal.* **203**, 307 (2001).
24. Chapter 2 of this thesis; Battiston, A.A., Bitter, J.H., de Groot, F.M.F., Overweg, A.R., Stephan, O., van Bokhoven, J.A., Kooyman, P.J., van der Spek, C., Vankó, G., and Koningsberger, D.C.; accepted for publication in *J. Catal.*.
25. Chapter 3 of this thesis; Battiston, A.A., Bitter, J.H., Heijboer, W.M., de Groot, F.M.F., and Koningsberger, D.C.; submitted to *J. Catal.*.

26. Yokohama, C., and Misono, M., *J. Catal.* **150**, 9 (1994).
27. Nishizaka, Y., and Misono, M., *J. Catal.* **160**, 95 (1996).
28. Gao, Z.-X., Sun, Q., and Sachtler, W.M.H., *Appl. Catal. B* **33**, 9 (2001).
29. Misono, M., *Cattech*, june (1998).
30. Kapteijn, F., Marbán, G., Rodríguez-Mirasol, J., Moulijn, J.A., *J. Catal.* **167**, 256 (1997).
31. Pérez-Ramírez, J., Kapteijn, F., Mul, G., and Moulijn, J.A., *Chem. Commun.* 693 (2001).
32. Pérez-Ramírez, J., Kapteijn, F., Mul, G., and Moulijn, J.A., *Appl. Catal. B* **35**, 227 (2001).
33. Kögel, M., Mönnig, R., Schwieger, W., Tissler, A., and Turek, T., *J. Catal.* **182**, 470 (1999).
34. Chen, H.-Y., El-Malki, E.-M., Wang, X., van Santen, R.A., and Sachtler, W.M.H., *J. Molec. Catal. A* **162**, 159 (2000).
35. Marturano, P., Drozdová, L., Pirngruber, G.D., Kogelbauer, A., and Prins, R., *Phys. Chem. Chem. Phys.* **3**, 5585 (2001).
36. Pérez-Ramírez, J., García-Cortés, J.M., Kapteijn, F., Illán-Gómez, M.J., Ribera, A., Salinas-Martínez de Lecea, C., and Moulijn, J.A., *Appl. Catal. B* **25**, 191 (2000).

Summary

An extremely large number of catalytic materials have been tested in the last decades towards the Selective Catalytic Reduction of NO_x by Hydrocarbons (HC-SCR). Among these catalysts, Fe/ZSM5, obtained by sublimation of FeCl_3 (also referred to as FeCl_3 chemical vapor deposition (CVD) technique), has shown outstanding properties, *i.e.* high activity and stability, even in the presence of water. It has also displayed a remarkable activity for the decomposition of N_2O to N_2 and O_2 . While the catalytic properties of this material are well established, several questions remain unanswered. They concern the structure and the reactivity of the catalytically active Fe-species, the contribution of the different synthesis steps to their formation, and the accessibility of the Fe-species for the reactants during catalysis. The work presented in this thesis has provided important insights in finding answers to these questions.

In **Chapter 2** the evolution of iron and of the zeolitic support in Fe/ZSM5 prepared by the FeCl_3 CVD technique was studied along the different synthesis steps.

Several relevant characterization techniques (EXAFS, HR-XANES, ^{57}Fe Mössbauer spectroscopy, EELS, HR-TEM, XRD, N_2 physisorption and FTIR spectroscopy) were applied in order to correlate the changes occurring in the local environment of the Fe atoms with migration and aggregation phenomena of iron at micro- and macroscopic scale. In addition, ^{27}Al NMR spectroscopy was used in combination with Al K-XAFS to monitor the local coordination of Al in the support.

During the first synthesis step (sublimation of FeCl_3) Fe is introduced in the zeolite mainly in the form of isolated mononuclear Fe-species, located at the Brønsted sites position. These iron complexes consist of tetrahedrally coordinated Fe^{3+} , bound to the framework via two oxygen atoms and further surrounded by two chlorine atoms.

The washing step is responsible for the formation of octahedrally coordinated binuclear Fe-complexes. The structure of the Fe-binuclear complexes, determined by EXAFS, resembles that of the closest binuclear building blocks in α -goethite, consisting of two edge-sharing

octahedrally coordinated Fe atoms. After washing, the presence of monomeric Fe-species is ruled out.

Calcination represents a very delicate step for the further evolution of iron. During this treatment Fe-complexes can be detached from the support and can migrate towards the external surface of the zeolite, leading to the formation of Fe-oligomers, amorphous oxidic nano-particles, and goethite/hematite crystals. A significant fraction of iron is indeed involved in this degenerative process upon application of a 'severe' calcination procedure. Nevertheless, agglomeration of Fe can be strongly suppressed by adequately tuning the conditions of the calcination. By applying a newly introduced 'mild' procedure (obtained by combining a moderate temperature ramp with a high gas flow rate) it is possible to obtain a material in which a very high concentration of binuclear Fe-complexes can be maintained.

Independently on the calcination procedure applied, no significant damage occurs to the framework of the zeolite, Al remaining tetrahedrally coordinated in the lattice.

Chapter 3 aims at investigating the reactivity of oxygen in the binuclear Fe-species present in mildly calcined Fe/ZSM5. Activation of oxygen is of primary importance for the decomposition of N₂O, as well as for the HC-SCR of NO. The study presented in this chapter was performed by coupling *in situ* Fe K-edge HR-XANES and EXAFS. Information on the coordination geometry of Fe, obtained by the pre-edge feature of the Fe K-edge (HR-XANES), was used as input for the analysis of the EXAFS data. The reactivity of the complexes was monitored during heat treatments to 350°C in He or O₂.

The results showed that, upon exposure to air, the majority of iron in mildly calcined Fe/ZSM5 is present as Fe-oxo/hydroxo binuclear complexes with an octahedral configuration. The closest Fe-O coordination of the Fe-binuclear complexes can be described with a [HO-Fe-O-Fe-OH]²⁺ core.

Heating to a moderate temperature (up to ~150°C), in He as in O₂, causes desorption of water from the Fe coordination sphere but does not affect the oxidation state of iron. Increasing the temperature of the heat treatment in He (above 250°C) results in further removal of oxygen and in the auto-reduction of the majority of iron. This is ascribed to the extraction of the Fe-O-Fe bridging oxygen from the core of the complexes, resulting in the formation of Fe-□-Fe vacancies. Noticeably, this phenomenon is suppressed when the heating treatment is performed in the presence of oxygen in the gas phase.

A detailed model structure for the reactivity of oxygen in the complexes is proposed and discussed in the chapter.

The results obtained in Chapter 3 were used as basis to investigate the structure and the reactivity under HC-SCR working conditions of the Fe-binuclear complexes in mildly calcined over-exchanged Fe/ZSM5 (**Chapter 4**). The aim was to determine the active coordination-sites in the binuclear complexes for the HC-SCR reaction of NO. The local environment of iron in the catalyst was studied by *in situ* XAFS spectroscopy. Measurements were performed at 350°C in the presence of single HC-SCR reagents (NO, O₂, or i-C₄H₁₀) and during the HC-SCR reaction, *i.e.* in the contemporary presence of the three reactants. The catalytic activity of Fe/ZSM5 during the XAFS measurements was monitored by analyzing the composition of the gas-phase via a NO_x chemiluminescence analyzer. The results suggest that the active sites in the complexes for the selective reduction of NO are located in the vacancies generated in the closest Fe-O coordination sphere by desorption of oxygen (Chapter 3). Upon reaction with NO, NO + O₂, as well as during HC-SCR operation, the vacancies generated during the heat treatment are promptly reoccupied and iron is re-oxidized. Coherently with the reaction pathway proposed in the literature for the HC-SCR reaction, this can be ascribed to the adsorption of N- and C-containing species and/or by the regeneration of the Fe-O-Fe bridges in the complexes. The easy exchangeability of oxygen in the complexes appears to be the key-step for their peculiar catalytic properties.

In **Chapter 5** it will be shown that Fe/ZSM5 samples subjected to different calcination procedures (mild or severe), despite the difference in Fe-distribution and in the concentration of catalytically active species, display the same catalytic activity towards the HC-SCR of NO, using isobutane as reductant. This finding indicates that during reaction intra-crystalline diffusion might play a limiting role. Indeed, the size of the binuclear clusters is similar to that of the zeolite channels. Furthermore occlusion of the channels may also arise by the presence of polymeric Fe-(hydro)oxo species.

In order to investigate to which extent the presence of iron might hamper the accessibility of the zeolite channels, uptake of n-hexane was measured, using a Tapered Element Oscillating Microbalance (TEOM), for the parent zeolite (H/ZSM5) and for the two Fe/ZSM5 samples. The results showed that for the two Fe/ZSM5 samples the n-hexane uptake rate, as well as the total n-hexane uptake are significantly lower than for the parent H/ZSM5. It is therefore concluded that the accessibility of the catalytic active Fe-species is retarded by the presence of iron in the zeolite pores. As a result, only a part of the potentially active Fe-binuclear species are able to contribute effectively to the overall apparent HC-SCR catalytic activity. These species might be only the first few binuclear Fe-clusters encountered by the reactants entering the zeolite pores.

Although Fe/ZSM5 obtained by CVD of FeCl₃ displays excellent catalytic properties for the selective catalytic reduction of NO_x using hydrocarbons, it presents the main disadvantage of producing large amounts of CO. In **Chapter 6** an explorative study is presented aiming at minimizing this inconvenience. The solution adopted was to couple Fe/ZSM5 with Pt/ZSM5, obtained via liquid ion-exchange from Pt(NH₃)₄(NO₃)₂. Pt/ZSM5 is an active material for HC-SCR, with significantly better oxidizing properties than Fe/ZSM5. For this reason it displays also a low selectivity to N₂ when used as HC-SCR catalyst, as N₂O is formed in comparable amount. Considering the high activity of Fe/ZSM5 towards the decomposition and the selective reduction of N₂O to N₂, combining these materials appears as an attractive solution.

In this study different reactor configurations have been explored, *i.e.* a single-bed (physical mixture of Fe/ZSM5 and Pt/ZSM5) and a dual-bed system with the two catalysts disposed in series (first Pt/ZSM5 and then Fe/ZSM5). It will be shown that while operating the two catalysts in a single bed (physical mixture) is not a practical solution (Pt catalyzes the direct oxidation of i-C₄H₁₀ and CO to CO₂, with a detrimental effect on the overall selective reduction of NO_x), adopting a dual bed configuration is highly effective. Unreacted NO, and N₂O formed over Pt/ZSM5 in the first stage, can be effectively converted to harmless N₂ over the second Fe/ZSM5 bed. The best results can be obtained with an intermediate additional injection of isobutane between the two catalytic beds, operated respectively at 270°C (Pt/ZSM5) and at around 410°C (Fe/ZSM5). Under the experimental conditions tested, a N₂ yield of 90% was obtained, with a complete suppression in CO and N₂O formation.

Samenvatting

In de afgelopen jaren is een zeer groot aantal katalytische materialen getest voor de selectieve katalytische reductie van NO_x door Koolwaterstoffen (HC-SCR). Onder deze katalysatoren vertoonde Fe/ZSM5, verkregen door sublimatie van FeCl_3 (ook wel FeCl_3 Chemical Vapor Deposition (CVD) techniek genaamd) uitzonderlijke eigenschappen, d.w.z. een hoge activiteit en stabiliteit, zelfs in de aanwezigheid van water. Het vertoonde bovendien een opvallende activiteit voor de decompositie van N_2O naar N_2 en O_2 . Hoewel de katalytische eigenschappen van dit materiaal goed zijn beschreven, blijven veel vragen onbeantwoord. Deze betreffen de structuur en de reactiviteit van de katalytisch actieve Fe-verbindingen, de bijdrage van de verschillende synthesestappen die tot hun vorming leiden, en de bereikbaarheid van de Fe-verbindingen door de reactanten gedurende katalyse. Het onderzoek dat in deze dissertatie beschreven is, heeft belangrijke inzichten geleverd voor beantwoording van deze vragen.

Hoofdstuk 2 beschrijft de veranderingen in ijzer en zeoliet drager in Fe/ZSM5, welke werd bereid door de FeCl_3 CVD techniek, gedurende de verschillende stappen van de synthese. Diverse relevante onderzoekstechnieken (EXAFS, HR-XANES, ^{57}Fe Mössbauer spectroscopie, EELS, HR-TEM, XRD, N_2 fysisorptie en FTIR spectroscopie) zijn toegepast om de veranderingen vast te stellen die tijdens de synthese plaatsvonden in de directe omgeving van Fe, zowel op micro- als op macroscopische schaal. ^{27}Al NMR spectroscopie is gebruikt in combinatie met Al K-XAFS om de locale coördinatie van Al atomen in de zeoliet te bestuderen. Tijdens de eerste stap van de synthese (sublimatie van FeCl_3) werd ijzer afgezet in de vorm van geïsoleerde mononucleaire Fe-verbindingen op de Brønsted-zure plaatsen van de zeoliet. Deze verbindingen bestaan uit tetraëdrisch gecoördineerd Fe^{3+} , gebonden aan het zeolietrooster door middel van twee zuurstofatomen. Verder zijn er twee chlooratomen gecoördineerd aan het ijzer.

Wassen met water zorgt voor de vorming van octaëdrisch omringde binucleaire ijzer-complexen welke lijken op de bouwstenen van α -goethiet d.w.z. een dubbele octaëder welke met een zijde gedeeld wordt; in het centrum van elke octaëder bevindt zich ijzer ion. Na wassing zijn alle monomere Fe-verbindingen verdwenen. Calcinatie is een delicate stap voor de verdere ontwikkeling van ijzer. Gedurende deze behandeling kunnen Fe-complexen zich losmaken van het zeolietrooster en zich bewegen naar het buitenoppervlak, hetgeen leidt tot de vorming van Fe-oligomeren, amorf oxide nano-deeltjes en goethiet/hematiet kristallen. Een significant deel van het ijzer is betrokken bij dit proces wanneer een zware

calcinatieprocedure gebruikt wordt. Niettemin kan clustering van ijzer voorkomen worden door een gunstige calcinatieprocedure te gebruiken. Door een nieuwe ontwikkelde ‘milde’ procedure toe te passen (verkregen door de combinatie van een lage opwarmingsnelheid en een hoge gasstroom) is het mogelijk een materiaal te verkrijgen waarin een hoge concentratie van binucleaire Fe-complexen is te handhaven. Onafhankelijk van de calcinatieprocedure blijkt dat zich geen significante schade voordoet aan de structuur van de zeoliet. Aluminium blijft tetraëdrisch gecoördineerd in het zeolietrooster.

Hoofdstuk 3 betreft het onderzoek naar de reactiviteit van zuurstof in de binucleaire Fe-complexen in Fe/ZSM5 verkregen na een milde calcinatie. Activering van zuurstof in de ijzerclusters is cruciaal voor de ontleding van N₂O, evenals voor HC-SCR van NO. De studie die in dit hoofdstuk is beschreven, is uitgevoerd door koppeling van *in situ* Fe-K edge HR-XANES en EXAFS. Informatie over de geometrische coördinatie van Fe werd verkregen door de analyse van de pre-edge in de Fe K-edge (HR-XANES). Deze informatie is gebruikt voor de analyse van de EXAFS-gegevens.

De reactiviteit van de Fe-complexen is geanalyseerd tijdens warmte-behandelingen in He of O₂ tot 350°C. Na blootstelling aan lucht is de meerderheid van ijzer in het mild gecalcineerd Fe/ZSM5 aanwezig als binucleaire oxo/hydroxo Fe-complexen met een octaëdrische configuratie. De eerste Fe-O coördinatieschil in de complexen is representatief voor [HO-Fe-O-Fe-OH]²⁺ kern.

Verwarming van het monster tot 150°C in He of in O₂, veroorzaakt de desorptie van water van de Fe-complexen maar tast de oxidatietoestand van het ijzer niet aan. Verhoging van de temperatuur boven 250°C in He resulteert in verwijdering van zuurstof en in de autoreductie van de meerderheid van het ijzer. Dit is toe te schrijven aan de verwijdering van de bruggende zuurstoffen in de Fe-O-Fe kern van de complexen. Dit resulteert in de vorming van Fe-□-Fe vacatures. Dit verschijnsel treedt niet op als de warmte-behandeling wordt uitgevoerd in de aanwezigheid van zuurstof in de gasfase. Een gedetailleerde modelstructuur van de reactiviteit van zuurstof in de Fe-complexen is uitgewerkt en besproken in het betreffende hoofdstuk.

De verkregen resultaten uit hoofdstuk 3 hebben als basis gediend voor het onderzoek naar de structuur en reactiviteit van de Fe-binucleaire complexen in het mild gecalcineerd Fe/ZSM5 onder HC-SCR condities (**hoofdstuk 4**). Doel was de bepaling van de actieve sites in de Fe-binucleaire complexen bij de HC-SCR reactie van NO. De directe omgeving van ijzer in de katalysator is bestudeerd met *in situ* XAFS-spectroscopie. De metingen zijn uitgevoerd in de aanwezigheid van afzonderlijke HC-SCR reactanten (NO, O₂, of i-C₄H₁₀)

en gedurende de HC-SCR reactie, *d.w.z.* in de gelijktijdige aanwezigheid van drie reactanten. De katalytische activiteit van Fe/ZSM5 tijdens de XAFS metingen werd gevolgd door de hoeveelheid NO_x in de gasfase te bepalen met een chemiluminiscentie analysator. Op basis van de resultaten werd geconcludeerd dat de actieve site van de Fe-complexen voor de selectieve reductie van NO een gecreëerde vacature in de eerste Fe-O coördinatieschil is. Bij reacties met NO, $\text{NO}+\text{O}_2$ als ook tijdens HC-SCR-werking, worden de vacatures die gegenereerd waren tijdens de warmtebehandeling direct weer ingenomen en is ijzer weer geoxideerd. Gebaseerd op een voorgesteld reactiemechanisme uit de literatuur voor de HC-SCR-reactie, kan dit worden toegeschreven aan de adsorptie van N- en C-bevattende verbindingen en/of door herintroductie van zuurstof. De gemakkelijke uitwisseling van zuurstof in de complexen lijkt een sleutelrol te spelen bij de bijzondere katalytische eigenschappen van Fe/ZSM5.

In **hoofdstuk 5** is beschreven dat Fe/ZSM5 monsters die een verschillende calcinatie procedure (mild of zwaar) hebben ondergaan, ondanks een verschil in Fe-distributie en in concentratie van katalytische actieve complexen, dezelfde katalytische activiteit vertonen ten opzichte van de HC-SCR van NO door isobutaan. Dit geeft aan dat intra-kristallijne diffusie van reactanten tijdens de reactie een beperkende rol zou kunnen spelen. De afmeting van de Fe-binucleaire clusters is gelijk aan die van de kanalen van de zeoliet. Bovendien zou afsluiting van de kanalen ook kunnen optreden bij de aanwezigheid van polymerische Fe-oxo/hydroxo species. Om te onderzoeken in welke mate de aanwezigheid van ijzer de toegankelijkheid van zeolietkanalen belemmert, is de opname van n-hexaan gemeten met gebruik van een *Tapered Element Oscillating Microbalance* (TEOM), bij de oorspronkelijke zeoliet (H/ZSM5) en bij de twee Fe/ZSM5-monsters. De resultaten laten zien dat voor de twee Fe/ZSM5 monsters zowel de n-hexaan opnamesnelheid als de totale n-hexaan opname significant lager zijn dan bij de oorspronkelijke H/ZSM5. Conclusie is derhalve dat de bereikbaarheid van de katalytisch actieve Fe-complexen vertraagd wordt door de aanwezigheid van ijzer in de zeolietporiën. Consequentie is dat slechts een deel van de potentieel actieve Fe-binucleaire deeltjes in staat is om een effectieve bijdrage te leveren aan de HC-SCR activiteit. Dit zouden alleen de binucleaire Fe-complexen in het eerste gedeelte van de zeolietkanalen kunnen zijn.

Hoewel Fe/ZSM5 verkregen door CVD uit FeCl_3 uitstekende katalytische eigenschappen vertoont voor de katalytische reductie van NO_x door koolwaterstoffen, heeft het een belangrijk nadeel: de grote hoeveelheid CO die tijdens de reactie geproduceerd wordt.

In **hoofdstuk 6** wordt een exploratief onderzoek beschreven met als doel dit nadeel te beperken. De voorgestelde oplossing is de koppeling van Fe/ZSM5 met Pt/ZSM5,

verkregen via ionenuitwisseling van $\text{Pt}(\text{NH}_3)_4(\text{NO}_3)_2$ vanuit een waterige oplossing. Pt/ZSM5 is actief voor HC-SCR met significant beter oxiderende eigenschappen dan Fe/ZSM5. Daarom laat het een lage selectiviteit naar N_2 zien als het gebruikt wordt als HC-SCR-katalysator door de vorming van N_2O in een vergelijkbare hoeveelheid. Gezien de hoge activiteit van Fe/ZSM5 voor zowel de selectieve reductie van N_2O als de directe decompositie van N_2O naar N_2 en O_2 , lijkt de combinatie van deze materialen een aantrekkelijke oplossing.

In dit onderzoek zijn verschillende reactor-configuraties onderzocht, namelijk een *single-bed* (fysisch mengsel van Fe/ZSM5 en Pt/ZSM5) en een *dual-bed* systeem waarbij de twee katalysatoren achtereen geplaatst zijn (eerst Pt/ZSM5 en dan Fe/ZSM5). Betoogd wordt dat, een *single-bed* oplossing niet afdoende werkt (Pt katalyseert de directe oxidatie van $i\text{-C}_4\text{H}_{10}$ en CO naar CO_2 , met een nadelig effect op de selectieve reductie van NO_x), terwijl een *dual-bed* configuratie zeer effectief is. Niet-gereageerde NO en N_2O gevormd over Pt/ZSM5 in het eerste bed kunnen doeltreffend worden geconverteerd tot N_2 in het tweede, Fe/ZSM5, bed. De beste resultaten worden behaald met een extra injectie van isobutaan tussen de twee katalytische bedden. Het eerste bed (Pt/ZSM5) wordt bij voorkeur gebruikt bij 270 °C en het tweede (Fe/ZSM5) rond 410 °C. Onder deze omstandigheden werd een N_2 opbrengst van 90% verkregen bij een volledige onderdrukking van CO en N_2O vorming.

List of Publications and Presentations

Publications:

- A.A. Battiston, J.H. Bitter, F.M.F. de Groot, A.R. Overweg, O. Stephan, J.A. van Bokhoven, P.J. Kooyman, C. van der Spek, G. Vankó and D.C. Koningsberger, 'Evolution of Fe-Species During the Synthesis of Over-exchanged Fe/ZSM5 Obtained by Chemical Vapor Deposition of FeCl₃'. Chapter 2 of this thesis.
Journal of Catalysis, accepted (2002).
- A.A. Battiston, J.H. Bitter, W.M. Heijboer, F.M.F. de Groot and D.C. Koningsberger, 'Reactivity of Fe-Binuclear Complexes in Over-exchanged Fe/ZSM5, Studied by *In situ* XAFS Spectroscopy. Part 1: Heat Treatment in He and O₂'. Chapter 3 of this thesis.
Journal of Catalysis, submitted (2002).
- A.A. Battiston, J.H. Bitter and D.C. Koningsberger, 'Reactivity of Fe-Binuclear Complexes in Over-exchanged Fe/ZSM5, Studied by *In situ* XAFS Spectroscopy. Part 2: Selective Catalytic Reduction of NO with Isobutane'. Chapter 4 of this thesis.
Journal of Catalysis, submitted (2002).
- A.A. Battiston, G.L. Bezemer, J.H. Bitter and D.C. Koningsberger, 'Combining Pt/ZSM5 and Fe/ZSM5 Obtained by Sublimation of FeCl₃ for the Selective Catalytic Reduction of NO_x: a Dual-Bed Configuration'. Chapter 6 of this thesis.
Applied Catalysis B: Environmental, submitted (2002).
- A.A. Battiston, D. de Romph, J.H. Bitter and D.C. Koningsberger, 'The Influence of the Si/Al Ratio on the Formation of the Fe-Binuclear Complexes in Over-exchanged Fe/ZSM5'.
In preparation.
- A.A. Battiston, J.H. Bitter and D.C. Koningsberger, 'Structure/Reactivity Correlation in Fe/ZSM5 for deNO_x Applications: *In situ* XAFS Characterization and Catalysis'.
Studies in Surface Science and Catalysis 135, 12-O-02 (2001).
- A.A. Battiston, J.H. Bitter and D.C. Koningsberger, 'XAFS Characterization of the Binuclear Iron-Complex in Over-exchanged Fe/ZSM5 - Structure and Reactivity'.
Catalysis Letters 66, 75 (2000).
- J.H. Bitter, A.A. Battiston, S. van Donk, K.P. de Jong and D.C. Koningsberger, 'Accessibility of the Fe-Species in Fe/ZSM5 Prepared via Sublimation of FeCl₃'. Chapter 5 of this thesis.
Microporous and Mesoporous Materials, submitted (2002).
- W.M. Heijboer, F.M.F. de Groot, A.A. Battiston, A. Knop-Gericke, M. Hävecker, R. Mayer, H. Bluhm, R. Schlögl, B.M. Weckhuysen and D.C. Koningsberger, '*In situ* Soft X-ray Absorption of Over-exchanged Fe/ZSM5'.
Journal of Physical Chemistry B, submitted (2002).

- W.M. Heijboer, F.M.F. de Groot, A.A. Battiston, A. Knop-Gericke, M. Hävecker, H. Bluhm, B.M. Weckhuysen and D.C. Koningsberger, 'The Influence of the Calcination Procedure on the auto-reducibility of iron in Over-exchanged Fe/ZSM5: an *In situ* Soft X-ray Absorption Study', **In preparation.**
- M.H. Groothaert, J.A. van Bokhoven, A.A. Battiston, B.M. Weckhuysen, and R.A. Schoonheydt, 'Identification of Bis(μ -oxo)dicopper in Cu-ZSM-5 and its Role in the NO Decomposition Cycle: A Combined Kinetic, UV-vis-NIR, EPR and *In situ* XAFS Study'. **Journal of American Chemistry Society, submitted (2002).**
- M.H. Groothaert, K. Lievens, J.A. van Bokhoven, A.A. Battiston, B.M. Weckhuysen, K. Pierloot and R.A. Schoonheydt, 'Bis(μ -oxo)dicopper as Key Intermediate in the Catalytic Decomposition of Nitric Oxide'. **To be submitted.**

Oral presentations:

- A.A. Battiston, J.H. Bitter and D.C. Koningsberger, 'Iron-Species in Over-exchanged Fe/ZSM5 for deNO_x applications: the Evolution and the Influence on Catalysis'. **3rd Netherlands' Catalysis and Chemistry Conference, Noordwijkerhout, The Netherlands, March 2002.**
- A.A. Battiston, S. van Donk, J.H. Bitter, K.P. de Jong and D.C. Koningsberger, 'Evolution of the Fe-species in Fe/ZSM5 for deNO_x Applications: Influence on Catalysis'. **NRSCC Workshop – Probing Catalytic Events, Utrecht, The Netherlands, October 2001.**
- A.A. Battiston, J.H. Bitter and D.C. Koningsberger, 'Structure/Reactivity Correlation in Fe/ZSM5 for deNO_x Applications: *In situ* XAFS Characterization and Catalysis'. **13th International Zeolite Conference, Montpellier, France, July 2001.**
- A.A. Battiston, J.H. Bitter, D.C. Koningsberger 'On the Structure of the Binuclear Fe-complexes in Over-exchanged Fe/ZSM5: XAFS Spectroscopy and Force Field Calculations.' **17th North American Catalysis Society Meeting, Toronto, Ontario, Canada, June 2001.**
- A.A. Battiston, J.H. Bitter and D.C. Koningsberger, 'Structure/Reactivity Correlation in Fe/ZSM5 for deNO_x Applications: *In situ* XAFS Characterization and Catalysis'. **2nd Netherlands' Catalysis and Chemistry Conference, Noordwijkerhout, The Netherlands, March 2001.**
- A.A. Battiston, J.H. Bitter and D.C. Koningsberger, 'Towards the Determination of the Active Sites in Over-exchanged Fe/ZSM5 for deNO_x Applications'. **Hamburger Synchrotron users pre-meeting, Hamburg, Germany, January 2001.**

- A.A. Battiston, J.H. Bitter, and D.C. Koningsberger, 'XAFS Characterization of the Binuclear Fe-complex in Over-exchanged Fe/ZSM5 - Structure and Reactivity'.
CW studiegroep Kristal- en structuuronderzoek congres, Lunteren, The Netherlands, March 2000.
- J.H. Bitter, A.A. Battiston, S. van Donk, K.P. de Jong and D.C. Koningsberger, 'Accessibility of the Binuclear Iron-species in Over-exchanged Fe/ZSM5 Prepared by Chemical Vapor Deposition of FeCl₃'.
Russian-Dutch Catalysis Meeting, Novosibirsk, Russia, June 2002.
- J.H. Bitter, A.A. Battiston and D.C. Koningsberger, 'Evolution of Iron in Over-exchanged Fe/ZSM5 During Pretreatment'.
Europacat V, Limerick, Ireland, September 2001.
- F.M.F. de Groot, W.M. Heijboer, A.A. Battiston, P. Glatzel and U. Bergmann, 'Selective X-ray Absorption Fine Structure'.
17th North American Catalysis Society Meeting, Toronto, Ontario, Canada, June 2001.

Poster presentations:

- A.A. Battiston, J.H. Bitter and D.C. Koningsberger, 'Structure of Active Iron-complexes in Over-exchanged Fe/ZSM5 Catalysts for HC-SCR Applications'.
1st Netherlands' Catalysis and Chemistry Conference, Noordwijkerhout, The Netherlands, January 2000.
- A.A. Battiston, J.H. Bitter, D.C. Koningsberger, 'Development of New Catalysts for Nitrogen Oxides Removal from Diesel Exhaust and Flue Gases by Hydrocarbons (HC-SCR)'.
EU summerschool on Surface Science and Catalysis, Dronten, The Netherlands, August 1999.
- J.H. Bitter, A.A. Battiston, S. van Donk, K.P. de Jong and D.C. Koningsberger, 'Accessibility of the Binuclear Fe-species in Over-exchanged Fe/ZSM5 Prepared by Chemical Vapor Deposition of FeCl₃'.
2nd FEZA Conference, Taormina-Giardini Naxos, Italy, September 2002.
- G.L. Bezemer, A.A. Battiston, J.H. Bitter and D.C. Koningsberger, 'Selective Catalytic Reduction of NO_x through Pt/ZSM5 and Over-exchanged Fe/ZSM5: a Dual Bed Configuration'.
3rd Netherlands' Catalysis and Chemistry Conference, Noordwijkerhout, March 2002.
- W.M. Heijboer, A. Knop-Gericke, A.A. Battiston, D.C. Koningsberger and F.M.F. de Groot, 'Soft X-ray Absorption Spectroscopy of Fe/ZSM5'.
3rd Netherlands' Catalysis and Chemistry Conference, Noordwijkerhout, March 2002.

Acknowledgements

This book is the result of the work I've carried out with the help of many other people, from the Netherlands and from abroad. I wish to express to all of you my sincere gratitude for all you have done.

Diek, my promoter, first of all, thank you for the possibility you offered me. Discussing with you has always been stimulating, your contribution to the EXAFS data analysis indispensable. I admire the energy you put in your work and I'm trying to figure out what you are going to do when (next June) your duty at the Department will come to its end. Writing your book won't be enough. Will you start a new Department in your house in France?

Harry, co-promoter, if you would not have gone to a conference in Florence in the summer of 1997 and moved to the Catalysis Department in Utrecht I would have never written this thesis. So, thank you... and the coincidence in life. We shared a lot of pleasant and exciting time together, in the department, at synchrotrons and congresses. I very much appreciated your daily supervision and our scientific discussions. I hope you will be proud of your first PhD student. Thank you.

Frank, although you were not officially involved in my PhD project you have provided an important contribution to my research. You have also given me the possibility of collaborating with many people from all over the world. I want to thank you for all you have done. I had a great time with you in Chicago, Hamburg, Paris, Berlin and, of course, Utrecht.

Dennis, my first student. You've done a great job. I still feel guilty for the many hours you had to spend all alone with Annie, busy with our force field calculations. Thank you, also for producing the picture depicted on the cover of my thesis. See you in Amsterdam.

Leendert, now it is your turn to carry out a research project. I'm confident you will do a great job. And I'm already curious about your results. Thank you for the enthusiasm and for your commitment. Not many students would have had so much patience with our gas chromatograph. I hope our paper will soon be accepted.

Kees, my last student. You started working with me at the very end of my project. A lot of ideas still to be tested, a very little time left. You finished up all the measurements, contemporarily interpreting the results and playing guitar. Thank you, Kees. Your CD is really good! You have one more fan.

Moniek and Sander, it has been a pleasure to have you as office-mates for these years. Thank you for the pleasant atmosphere we always shared. I'm sorry that in the last months I could not provide you with freshly prepared coffee in the morning, as I used to. You know, I was busy with these pages. I wish you all the best.

Frans, thank you for your warm welcome in Utrecht. You made me feel a little bit at home.

Sander, thank you for performing the TEOM measurements and analyzing the data. Krijn and Harry, thank you for your contribution to the interpretation of the results. Harry, thanks for writing the draft of Chapter 5 and for all the revision work.

Jeroen, thanks a lot for the NMR and XAFS measurements and for the comments on Chapter 2. The skiing season is approaching, be prepared. Here in the Netherlands I have to comfort myself with an ice-skating course. I wish you all the best in Zürich.

Marijke, it has been a real pleasure to work with you. I want to thank you for the fruitful collaboration we had and for your kind acknowledgement in your thesis.

Arian, thank you for the Mössbauer experiments you've performed in Delft. I hope to see you soon. Already at the next Filmfestival in Rotterdam?

Patricia, Cor, we have spent some time together looking for Fe-containing particles. Thank you for your patience and for the beautiful TEM pictures.

Gyorgy, I hope that not all the experiments you are leading at ESRF cost you so much energy and time as the one we did (HR-XANES). I want to thank you once again for your invaluable help. What about a visit to Amsterdam?

Odile, thanks to you and your group in Orsay for performing the STEM/EELS experiments and for the support provided during the data-analysis.

Axel, Michael, Ralph, Willem and Frank, thank you for the Soft X-rays experiments performed at Bessy. Due to the lack of time, the results could not be included in my thesis. They will be presented in the dissertation of Willem.

Pieter and Uwe, I had a very pleasant time with you in Chicago. Thank you.

I want to thank the whole Catalysis Department for the support received in these years. First of all, the people who helped me to perform the XAFS experiments: Michiel, Harry, Jan, Tijmen, Jeroen, Jules, Moniek, Ad v. d. E., Gerbrand, Laurens, Daphne and Willem. Jan, I'm still looking for the catalytically active phase in the salami-based bread-supported catalysts. No answer, yet. I'm getting obsessed! Do you have a project on this?

Evert, I'm very grateful for your technical support. Without your help my deNO_x set-up would have probably endangered a lot of people. And I would have never found the material for the *in situ* XAFS measurements to be performed at the synchrotrons.

Wim and all the people of the 'glasblazerij', thank you for making and repairing all my quartz reactors. I'm always been impressed by your ability, and by your kindness.

Viktor and Henk, thank you for building the electronics of my set-up. It never failed. Thank you also for letting me work a couple of weeks at your Apple computer for analyzing the EELS data.

Many thanks to Thea and Fred, for wisely monitoring my budget and for the technical support, to Marjan, for the XRD training and for the SEM work, and to Ad M., for the last BET measurements.

Dymph and Monique, thanks to you there is always a nice atmosphere in the secretariate. No wonder that so many of us like to frequent it. Thank you both for your help.

I also want to thank the people of the AD-department, Jan den Boesterd, Ingrid van Rooijen en Aloys Lurvink, for the nice posters and for so carefully preparing the cover of this thesis.

John, you are not here anymore. Thank you for your commitment and your funny games.

I miss you.

Annelies, you are a great friend. And the teacher everybody's dreaming of. I doubt that Tozzi will ever come to play in Utrecht (why should he, with Amsterdam so nearby?) but, no matter where, I hope one day we'll be singing with him 'Scoiattolo impaurito ti scaldai...'. It will really be a great day. Grazie, Annelies.

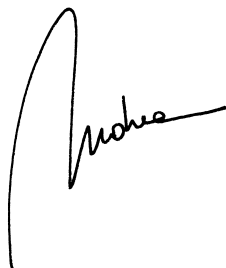
Silvia, Alessandro, Federica, it's always great to see you, even for a short time. Silvia, sorellina, how many things are happening. Time's running, and Federica will be able to read these lines sooner than we think. I wish you all the best, piccola.

Dear mum, dear dad. I bring your love and your desires with me, wherever I am. You can find them also in these pages. They are dedicated to you.

Giovanna, we have so many plans.

What's coming next? I'm so curious.

I kiss you, gently...

A handwritten signature in black ink, appearing to read 'Monique'. The signature is written in a cursive style with a large, sweeping initial 'M'.

Curriculum Vitae

Andrea Battiston was born on November 13, 1970 in Milan, Italy. In 1989 he received his secondary school diploma (Classical Studies) from Liceo Ginnasio Statale G. Berchet in Milan. After secondary school he studied Chemical Engineering at the Politecnico di Milano, with specialization in Industrial Chemistry, from which he graduated (Master's Degree) in April 1998. His graduation project, performed under the supervision of Dr. P. Gronchi and Prof. R. Del Rosso, dealt with the development of Ni-based catalysts for the carbon dioxide reforming of methane. His MA thesis was awarded a special mention by the Italian Interdivisional Catalysis Group. In August 1998 he moved to Utrecht University, Department of Inorganic Chemistry and Catalysis (Utrecht, The Netherlands) to start his PhD training under the supervision of Prof. D.C. Koningsberger and Dr. J.H. Bitter. His research topics covered characterization and development of Fe- and Pt-based catalysts for the selective catalytic reduction of NO_x by hydrocarbons. Most of the results obtained during his PhD project are presented in this thesis.

